PREFERENTIAL OXIDATION (PROX) OF CARBON MONOXIDE (CO) IN HYDROGEN RICH STREAM OVER COPPER SUPPORTED ON COBALT BASED CATALYSTS

By

TSOKE CHOENE CLEMENT

DISSERTATION

Submitted in fulfilment of the requirements for the degree of

MASTER OF SCIENCE

in

CHEMISTRY

in the

FACULTY OF SCIENCE AND AGRICULTURE

(School of Physical and Mineral Sciences)

at the

UNIVERSITY OF LIMPOPO

SUPERVISOR: Prof T. Magadzu

CO-SUPERVISORS: Dr R. Mhlaba

DR J. Moma (Wits)

2024

DEDICATION

I devote this study to global energy industries in service of mankind.

DECLARATION

I Tsoke Choene Clement hereby declare that PREFERENTIAL OXIDATION (PROX) OF CARBON MONOXIDE (CO) IN HYDROGEN RICH STREAM OVER COPPER SUPPORTED ON COBALT BASED CATALYSTS, is my own work and it was performed, evaluated, and written by myself under the supervision of Prof T. Magadzu, Dr R. Mhlaba and Dr J. Moma (Wits). I further declare that this study has not been previously submitted by anyone for any degree or whatsoever at any institution, university, nor college, and all the data and information reviewed from the literature have been fully acknowledged by means of proper references and citations.

Tsok

13 September 2024

Signature. **Date.**

ACKNOWLEDGEMENTS

The completion of this research project by myself would have been a very hard task. Therefore, I would like to express my sincere gratitude and thankful sentiments to my supervisor Prof T. Magadzu and my two co-supervisors, Dr R. Mhlaba from the Department of Chemistry at the University of Limpopo (UL) as well as Dr J. Moma from the University of Witwatersrand (Wits), for their unwavering support, whom without their guidance and quality assurances, this project would have been a complete catastrophe. I would further love to take the whole day if I may and appreciate the financial support from National Research Foundation (NRF) for ensuring that the tuition fees, meals, devices, and accommodations mustn’t be an obstacle to one’s determination for science and research, in service of human society. I fully acknowledge the UL Department of Chemistry for study areas, and every individual, colleague or peer who played part in developing, guiding, and concocting us to be ready for this huge journey in the field of chemical research. Lastly, I would love to thank my wonderful mother, Ms Tsoke M. Elizabeth, my one and only brother, Dr G. Tsoke, my family and friends for their persistent support, constant encouragement and advice. To not quit, and to embrace life with its challenges along the route to “finding solutions for South Africa”.

PRESENTATIONS

1. CC Tsoke, T Magadzu, R Mhlaba, J Moma ‘’Surfactants assisted hydrothermal and reflux in CuO_x/Co_3O_4 catalysts synthesis for hydrogen purification in fuel cell application’’ 13th FSA Postgraduate Research Day, 20-22 September 2023, at Bolivia Lodge, Polokwane.
2. CC Tsoke, T Magadzu, R Mhlaba, J Moma ‘’Surfactants/polymer assisted hydrothermal and reflux in CuO_x/Co_3O_4 catalysts synthesis for hydrogen purification in fuel cell application’’ SACI NORTH SECTION Young Chemists Symposium, 13 October 2023, at the University of Limpopo
3. CC Tsoke, T Magadzu, R Mhlaba, J Moma ‘’ Effects of preparation method as well as the addition of CuO_x species on Co_3O_4 towards preferential oxidation of CO in H_2 rich stream’’ 4th Gauteng Catalysis Forum, University of Johannesburg, 04 April 2024.

ABSTRACT

The use of hydrogen (H_2) fuel as an alternative source of energy for transportation and residential applications has recently increased. Polymer electrolyte membrane fuel cells (PEMFCs) use hydrogen produced from steam reformer and water gas shift as source of energy. The presence of trace amount (~0.5 – 2 vol.%) of carbon monoxide (CO) lower the efficiency of the fuel cells which prefers CO less than 10 ppm. Preferential oxidation of carbon monoxide (CO(PROX)) is a preferred method for the reduction of CO and a suitable catalyst with less selectivity to hydrogen species is required for this process. Transition metal oxide catalysts, such as CuO_x, Co_3O_4, CeO_2, ZrO_2, MnO_x etc are used for CO(PrOx) reaction. However, it still a challenge to prepared highly stable CO(PrOx) catalysts that can oxidize CO with minimal selectivity to H_2, especially in the presence of moisture and CO_2 in the feed stream.

The study reports various catalysts based on CuO_x and CeO_2 supported on Co_3O_4 catalysts, prepared by facile hydrothermal and reflux assisted precipitation and/or co-precipitation methods. The catalysts were prepared in the presence of surfactant/polymer (CTAB/PVP) mixture and used for CO(PrOx) reaction. The structural features of the synthesised catalysts were investigated by FTIR, XRD, SEM, BET, TEM, H_2-TPR and TGA-DTA analysis. The presence of Co^{3+} and Co^{2+} stretching vibrations in all the prepared samples was revealed by the FTIR analysis and arose from Co_3O_4 phase, as confirmed by XRD spectroscopy. CO(PrOx) data showed that the introduction of CeO_2 to Co_3O_4(Hyd) and Co_3O_4(Ref) catalysts by either hydrothermal or reflux route slightly increased the catalytic activity with temperature in dry CO(PrOx). The CuO_x dopant on the other hand drastically increased the catalytic performance of Co_3O_4 catalyst as compared to CeO_2, with 5 wt.% CuO_x being an optimum load in both methods. However, doping CuO_x by reflux to obtain 5 wt.% CuO_x /Co_3O_4(Ref) catalyst, had enormous positive influence on CO(PrOx) activity, archiving almost 94% CO Conversion at 40 °C, while 5 wt.% CuO_x /Co_3O_4(Hyd) achieved 74% CO conversion. The 5 wt.% CuO_x /Co_3O_4(Ref) catalyst consists of CuO_x species substituted within the Co_3O_4 framework, which increased the metal-support interactions and featured a smaller crystallite size, high surface area (S_{BET} = 64.9 m^2/g) and large pore size distribution. While the 5 wt.% CuO_x /Co_3O_4(Hyd) counter catalyst showed just 57.6 m^2/g S_{BET} and had relatively small pore sizes. The CO oxidation as a function of temperature in moisture saturated feed gas showed negative effects over the as prepared catalyst's sample. When tested for stability in moisture environment, the 5 wt.% CuO_x /Co_3O_4(Ref) catalyst demonstrated relatively good stability over time on stream, as compared to the 5 wt.% CuO_x/Co_3O_4(Hyd) counterpart. Co-feeding 15 vol.% CO_2 into the reactor stream demonstrated a negative influence on the catalytic stability over 5 wt.% CuO_x /Co_3O_4(Hyd) catalyst, where's 5 wt.% CuO_x /Co_3O_4(Ref) catalyst still showed a good CO conversion.

Introduction of CeO_2 on the optimized bimetallic 5 wt.% CuO_x/Co_3O_4 catalysts by similar preparation procedures to obtain a ternary catalyst resulted in a low CO(PrOx) performance, due to lowered surface area and morphology alterations as probed by the BET and SEM analysis. The ternary samples had a highly coarsened surface, with a high degree of irregularity. Under reflux method, the pore volume was also reduced dramatically upon CeO_2 addition due to blockage by agglomerated nanoparticle (TEM evident). As a result, the stability in CO_2 environment over 5 wt.% CuO_x/Co_3O_4(Ref) catalyst was tremendously decreased. However, the % CO_2 selectivity in these hash conditions (CO_2 and H_2O) over 5 wt.% CuO_x /Co_3O_4(Ref) and 5 wt.% CuO_x /Co_3O_4(Hyd) catalyst was improved upon ceria addition, ascertaining the role of CeO_2 in moisture and CO_2 resisting catalyst development.

Table of Contents

LIST OF FIGURES

LIST OF TABLES

LIST OF ABBREVIATIONS AND SYMBOLS

CO(PrOx)	Preferential Oxidation of Carbon Monoxide
PEMFCs	Polymer electrolyte membrane fuel cells
FTIR	Fourier transform infrared spectroscopy
BET	Brunnauer-Emmet-Teller
SEM	Scanning electron microscopy
TGA	Thermogravimetric analysis
TEM	Transmission electron microscopy
FTS	Fischer Tropsch synthesis
FWHM	Full width at half maximum
NPs	Nanoparticles
GC	Gas chromatography
TCD	Thermal conductivity detector
CNTs	Carbon nanotubes
XPS	X-ray photoelectron spectroscopy
XRD	X-ray diffraction
PXRD	Powdered X-ray diffraction
SAED	Selected area electron diffraction
Wt.%	Weight percentage (usually for solids)
Vol.%	Volume percentage (for gases)
WGS	Water gas shift
WGR	Water gas shift reaction
RWGR	Reverse water gas shift reaction

HRTEM	High resolution transmission electron microscopy
MSIn	Metal support interaction
MSIc	Metal support interface
MLIc	Metal ligand interface
H_2-TPR	Hydrogen temperature programmed reduction
TPR	Temperature programmed reduction
CTAB	Cetyltrimethylammonium bromide
PVP	Polyvinylpyrrolidone
DEG	Diethyleneglycol
PEG	Polyethyleneglycol
CAs	Capping agents
GHG	Greenhouse gases
CFP	Carbon footprint
FFs	Fossil fuels
CECs	Carbon Emitting Compounds
SR	Steam Reforming
DRM	Dry reforming of methanol
O_L	Lattice oxygen
OR	Ostwald ripening
O_V	Oxygen vacancy
SD	Sodium dodecanoate
NMs	Nano materials
GHSV	Gas hourly space velocity
h	hour

t	time
$\Delta H_{(298\ K)}$	Change in enthalpy at room temperature
ΔH^{o}	Standard enthalpy change (at STP)
E_a	Activation energy/Activation energy barrier
RLS	Rate limiting step
T	Temperature
d_s	d spacing (or interplanar distance)
D_{xal}	Crystallite size

CHAPTER 1

1. INTRODUCTION

1.1. Background

Anthropogenic emissions of greenhouse gases (GHGs) from industrial technologies used in the world today for various processes such as energy production, catalytic refining of unburned automotive gases, constructions, demolitions and mining segment, are detrimental to our spherical globe [1-3]. The major GHGs emitted include CO_2, SO_2 and NO_x [2]. However, there is almost 1% annual increase in other global GHGs, such as CH_4 and N_2O, accompanied by ~12-17% deforestation induced GHGs and 1.5-3 billion tons of carbon released into the atmosphere, from agricultural sectors [1]. A study by Shakoor *et al.*, [1], outlined that such activities could result in extreme climate changes and adverse environmental risks, which can cause diseases, thus threatening the livelihoods of the twenty-first century. Today, the utilization of carbon emitting compounds (CECs) such as fossil fuels (i.e., coal, crude oil etc.,) and biomass, is still high and is expected to account for ~75% of total energy production in 2050 [4]. Approximately 50% of these energy sources will satisfy the transportation demands in the year 2040, according to *International Energy Outlook* 2018 [5]. These predictions hasten the demand to abate utilization of CECs. Nonetheless, the ground-breaking pioneering of combustion and steam-turbine engines powered by fossil fuels was indeed a breakthrough during that time of human history. To date these processes of generating energy are concomitant with GHGs, and therefore no longer appreciated. It has been known to man for thousands of years (thanks to native combustion reaction), that there is enormous amount of energy stored within the chemical bonds of several chemical substances, such as hydrogen molecule (H_2), ammonia (NH_3) and various organic compounds (e.g., CH_4) [6]. However, an equipment which could utilize these chemical fuels to generate electricity and power more efficiently and cleaner, remained a mystery.

In 1839, the Welsh scientist William Robert Grove, invented the first fuel cell battery, after realizing that the electrochemical reaction between H_2 and O_2 molecules generate an electrical current [3]. Etymology was not in Grove’s vocabulary, so the term ‘fuel cell’ was coined by two other British chemists later after Grove’s foundations. Ludwig Mond and Charles Langer, obtain a current density of about 20 Am^{-2} at a voltage of 0.73 V, using coal as a fuel source. Since then, tremendous modifications have been made to fuel cell devices, to optimize their energy throughput, with an alkaline fuel cell managing to generate approximately 15 Kw of power, paving new opportunities in the field of fuel cell technology, attracting various big companies including the mighty NASA, for aerospace missions at late 1950s [3].

A fuel cell is an electrochemical device that converts energy stored within a chemical substance, such as H_2, into electrical energy and they are classified based on the electrolytes and the fuel they use. These includes solid oxide fuel cell (SOFC), molten carbonate fuel cell (MCFC), phosphoric acid fuel cell (PAFC), polymer electrolyte (or proton exchange) membrane fuel cell (PEMFCs) etc. PEMFCs is one of the best fuel cell devices ever built, using just platinum-catalysed electrodes and water based acidic polymer membranes as an electrolyte. It has advantages that not only surpass many fuel cell technologies but are also the milestone in modern energy generation. As a result of utilising the lightest element on earth (H_2 molecule) as a fuel; PEMFCs devices are much lighter, and easier to refuel on-site, compared to traditional batteries making them easy to implement on a large scale [7]. Conventional energy sources, such as ‘heavy’ lead acid batteries, pose potential risks of acid leakage and corrosion susceptibilities, whereas the ‘light’ PEMFCs use corrosion resistance metals like Pt. PEMFCs offer benefits, such as high energy density, rapidity in start-up and operational simplicity, with just water (H_2O) and heat as the byproducts, thus has zero carbon emissions [7-9]. Nonetheless, there are still few challenges limiting practical applications of PEMFCs technology, and to date, these challenges are unresolved. For example, the utilization of expensive and scarce platinum group metals (PGMs) and noble metals such as gold to purify H_2, are one amongst several other obstacles drawing back the success of fuel cell civilization [10-13]. Thus, the study investigates the effective usage of cheaper metal oxide catalysts in H_2 refinement by preferential oxidation of carbon monoxide, CO(PrOx), for PEMFCs technology.

1.2. Problem statement

Relying entirely on pure H_2 as a fuel, which is normally generated from conventional steam reforming (SR)-water gas shift (WGS) coupled processes [14], PEMFCs suffers one of the major critical obstruction brought by constituent gaseous byproduct found along H_2 fuel, i.e., the residual carbon monoxide (CO) gas. In real time, a typical WGS reformate gas mixture consists of nearly 40-75 vol.% H_2, ~0.5-2 vol.% CO, ~ 10 vol.% H_2O and ~15-20 vol.% CO_2 [15]. The most crucial reported problem in the literature is the inevitable production of trace amount of CO gas during H_2 production. This is noticeable also after harsh catalytic WGS reaction (see Figure 1.1), which is dedicated to further reduce trace amount of CO and increase the H_2 concentration. However, there is still CO that remains (>10 ppm), which is above the tolerance amount for PEMFCs. This harms the anode by binding strongly on Pt catalyst and blocks the H_2 adsorption, which lead to low fuel cell efficiency (i.e., 'current generation') [16, 17].

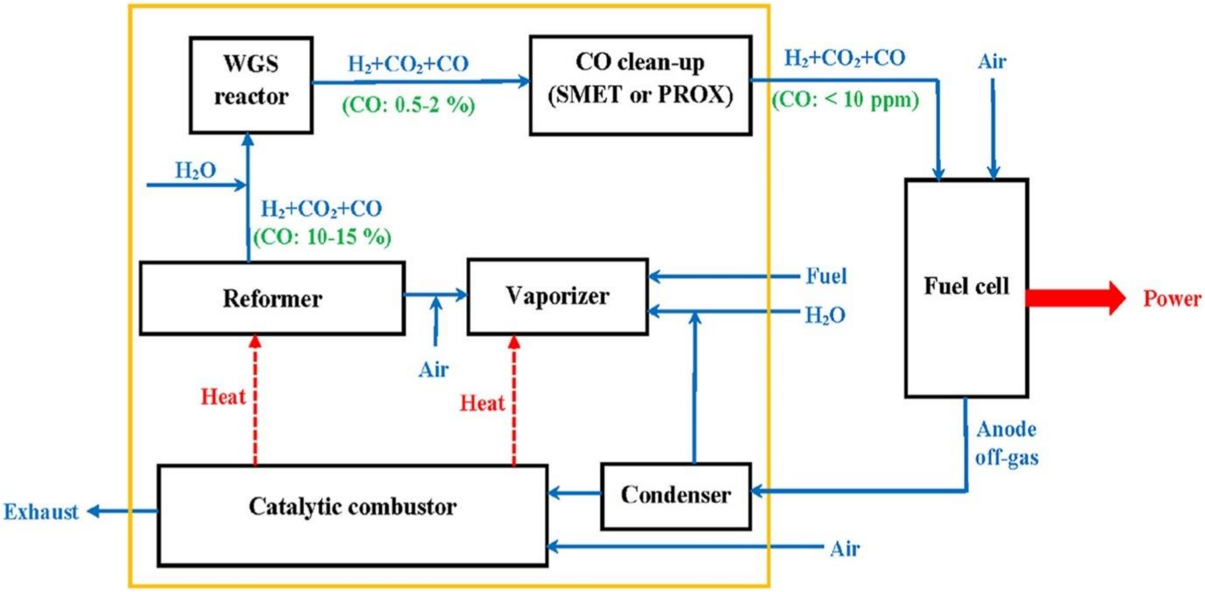

Figure 1.1 Schematic illustration of a fuel cell flow diagram and WGS H_2 refinement from hydrocarbon's reformates [23].

Furthermore, Qi *et al.,* [17], also reported that not only CO damages the Pt anode but also prone to poison the cathode electrode of the fuel cell, and the performance inhibition is more pronounced in cathodic poisoning than in direct anodic exterminations. Therefore, the concentration of CO in such reformate gases should be reduced to less than 10 ppm for optimum PEMFCs efficiency, and this is still a big challenge that delays the success of fuel cell technology [18-22]. Numerous heterogenous catalysts have been proposed for H_2 purification, particularly for selectivity yearnings, envisaging to specifically oxidize CO gas in H_2 rich stream, with minimal H_2 oxidation in the process. There are several catalytic methods that are normally recommended for CO removal from an impure H_2. These include membrane separation, pressure swing adsorption (PSA), selective CO methanation as well as water gas shift (WGS) reaction [19-21]. Xing *et al.*, [12], demonstrated that $NiCl_x/CeO_2$ catalysts had the best performance, featured high space velocity and water resistivity, and were able to maintain CO content of ~20 ppm during methanation process, as compared to expensive 0.7 & 3 wt % Ru/Al_2O_3 counterparts. Although the results were remarkable, the CO methanation is a parasitic process because it consumes viable H_2 required for PEMFCs, therefore impractical [25].

Preferential oxidation of CO(PrOx) has attracted considerable attention and is regarded as the best alternative route to ideally pick and specifically remove CO, particularly from WGS reformate, which contains other gaseous substances such as CO_2, H_2O and H_2. CO(PrOx) is said to be an extremely fast, direct, highly efficient, low costly and much practical process to abate CO in H_2 rich stream [23-24]. The CO(PrOx) process is achieved by deploying catalytic materials that can convert CO molecules into CO_2 at fuel cells operating temperatures (80-100 °C).

Several catalysts have been used over the past decades for CO(PrOx) reactions. Among these catalysts, include noble-metal based catalysts such as platinum group metals (PGMs) (i.e., Pd, Pt, Ru, Os, Rh and Ir) and precious metal catalysts like Ag & Au [25-28]. Sedmak and Hoˇ [31], reported that some of these noble metal catalysts (i.e., Pt, Pd, Ru and Rh supported on Al_2O_3) are only active at higher temperatures (150~200 °C) and their selectivity becomes compromised. The CO(PrOx) is normally set to operate between temperatures of around 200 °C (outlet temperature of upstream WGS) to 80 °C (Inlet temperature of downstream PEMFCs) [32], and most noble metals show deactivation at maximum temperature operation. These including the costs and rareness of precious metals limits their application in CO removal. Cao *et al.*, [32], further stated that the exothermic nature concomitant with CO(PrOx) reaction could lead to temperature variations within the reactor bed, accenting how important it is to design catalysts that can operate over a wide temperature window, and this is still a hard task in CO(PrOx) catalysis. Furthermore, it has remained a challenge to prepare a catalyst that can selectively oxidize CO in H_2 rich stream with good stability, when moisture and CO_2 are present in the gas reactor. CO_2 and moisture can block the active sites of the catalysts during CO(PrOx). In addition, CO_2 can react with excess H_2 promoting reverse water gas shift (RWGS) reaction, introducing CO that must be removed [21, 25].

1.3. Motivation

With an increase in worldwide population, high risks of our planet to CFP and new technology innovations, such as the design of aerospace ships and satellites aiming to take life to other planets and spaces, the need for green and sustainable energy is forever mounting. As described, the world is facing one of the worst devastating pandemics comparable to the mighty 'Ebola'. To date, the utilization of CECs such as, biomass, coal, crude oil and petroleum derivatives is still high, and is expected to account for almost three quarters of the total energy production in 2050, most of which shall satisfy the transportation demands as a results of industrialization and urbanization [4, 5].

The study is driven by the present and future need of renewable energy resources that are environmentally non-threatening and pollution friendly, such as PEMFCs, which shows a remarkably innocuous stationary (e.g., households electricity) and mobile (e.g., transportation) energy applications [3, 22]. This integrates to the development of cheap, active and highly stable catalysts which can purify H_2 fuel from WGS reformates and be able to convert a large amount of PEMFCs poisoning CO (~99.99% conversion) at a wide temperature window [21]. Transition 'non-noble' metal-oxide catalysts, such as cobalt oxide (Co_3O_4), manganese oxide (MnO_x), copper oxide (CuO_x), ceria (CeO_2), magnesia (MgO) and iron oxide (FeO_x) show a great potential in CO(PrOx) reaction [11, 33-37]. They also show catalytic activity so comparable to that of expensive noble metal catalysts [31], at both economic and industrial scale. They have a long-held status for being much cheaper, durable and abundant with high rate of CO conversion and are of great milestone materials for PEMFCs application [38-40]. In Zhao *et al's* work [41], superior activity of CeO_2/Co_3O_4-MnO_2/CeO_2 catalyst during CO(PrOx) reaction is ascribed to higher reducibility, high dispersion, unique porous structure, and strong interaction between Co_3O_4-MnO_2 and CeO_2 interfacial sites. Lendzion-Bieluń *et al.*, [42], have also notice that the synergistic effect of cobalt doped CuO/CeO_2 was correlated to better dispersion and reducibility of copper oxide, in the presence of cobalt metal additive. In addition to low costs of these types of catalysts, they also show great stability and activity owing to their synergistic effect during CO(PrOx) reaction [34, 41, 42].

Copper-cobalt composite oxide (CuO-Co_3O_4) supported on CeO_2 was reported to circumvent other unwanted reactions during CO oxidation, including RWGS and H_2 oxidation, thereby indirectly boosting CO(PrOx) [43]. The Co_3O_4 also strengthen the synergistic effect between Cu and Ce, increasing the interfacial site density and promote the release of lattice oxygen as well as formation of oxygen vacancies, which all drives the CO(PrOx) catalytic activity [43, 44]. Thus, the study envisages supported CuO-CeO_2 on cobalt-based catalyst prepared by co-precipitation assisted hydrothermal and reflux methods, for selective oxidation of CO in H_2 rich stream with good stability in the presence of moisture and CO_2 at PEMFs operating temperature.

1.4. Research purpose

1.4.1. Aim

The aim of the study is to develop CuO_x-CeO_2/Co_3O_4 catalyst for preferential oxidation of CO gas in H_2 rich stream at PEMFs operating temperature range.

1.4.2. Objectives

The objectives of the study are to:

i. prepare Co_3O_4 catalyst by reflux and hydrothermal assisted precipitation method.
ii. co-precipitate various amount of CuO_x and CeO_2 on cobalt oxide following a similar hydrothermal and or reflux procedure.
iii. incorporate different amounts of CeO_2 on the best CuO_x/Co_3O_4 catalysts by the same techniques.
iv. characterise the developed catalysts using techniques such as: X-ray diffraction (XRD), hydrogen-temperature programmed reduction (H_2-TPR), transmission electron microscopy (TEM) coupled with selective area electron diffraction (SAED) technique, scanning electron microscopy (SEM), Brunauer-Emmett-Teller (BET) isotherm, thermogravimetric analysis (TGA), Fourier

transform infrared (FTIR) spectroscopy and X-ray photoelectron spectroscopy (XPS).

v. investigate the catalytic activity, effective oxidation state of copper, effects of moisture, stability, and selectivity of the as-prepared catalysts in CO(PrOx) at temperature range of 40-200 ^oC.

1.5. SCIENTIFIC CONTRIBUTION

Embarking on a great journey in catalysis for green energy and production through hydrogen (H_2), the study will help develop catalysts needed to remove CO contaminating H_2 fuel, allowing the PEMFCs devices (for both stationery and transportation purposes) to operate at their maximum performance without adverse CO poisoning. The study will also provide some chemical strategies needed to optimise hydrogen purification and utilisation by catalysis of solid metal oxides, for sustainable and clean energy provision. This will eventually lead to healthier environment, tolerable climate changes, better economy, affordable energy, and pollution free habitats for every living organism. The outcome of this study shall be presented at local and national conferences. Parts of the research outcome will be published in a peer review Journals.

1.6. ETHICAL CLEARANCE

As the scope of this research doesn’t expands to the lives and ethics of any living organism, no ethical clearance is required.

1.7. STUDY OUTLINE

The dissertation consists of few important headlines that covers the scope and rational of the overall study. Introduction begins as chapter 1, where we reveal from the study background, historical view, and development, how fuel cells have spun the whole scientific community and paved a great journey in the field of chemical science, which recently had evolved into catalysis, specifically for production and refinement of industrial raw materials, that are of green energy applications, particularly hydrogen (H_2). Chapter 2 covers the literature review in which detailed research and discoveries on related subjects or data are unpacked, allowing versatile updates on the previous as well as recent findings, as a useful preparation plan to accomplish the goal of this study. The experimental techniques are discussed in chapter 3 and rationales as to why one catalysts preparation method was chosen over the other are clearly described. As part of the results (chapter 4), we reveal a powerful strategy to synthesise active CO(PrOx) nano catalysts, based on a highly active mesoporous Co_3O_4 spinel nano host, doped with copper (CuO_x) and ceria (CeO_2) nano crystals. The study also proposed a novel detailed 'organic type' of reaction mechanism and actual surface chemistry involved in CO(PrOx) reaction, in terms of electron dynamics at the molecular level, a new perspective on understanding catalytic oxidation mechanism of CO gas. Chapter 5 carries the study's general conclusion, which uses the findings of this work to address the question of the aim, recommending new strategies to completely mitigate the level of CO in H_2 fuel for PEMFCs application.

1.8. REFERENCES

[1] A. Shakoor, F. Ashraf, S. Shakoor, A. Mustafa, A. Rehman, and M. M. Altaf, “Biogeochemical transformation of greenhouse gas emissions from terrestrial to atmospheric environment and potential feedback to climate forcing,” Environmental Science and Pollution Research, vol. 27, no. 31, pp. 38513–38536, 2020.

[2] S. Kumar, “Attribution of health care expense to principal pollutants in green house gas emission: a panel data analysis of us states synthesis of ethical issues in credit derivatives view project attribution of health care expense to principal pollutants in green h,” Academy of Accounting and Finance Studies Jornal., vol. 26, no. 6, 2022.

[3] U. Lucia, “Overview on fuel cells,” Renewable and Sustainable Energy Reviews, vol. 30, pp. 164–169, 2014.

[4] E. L. V. Eriksson and E. M. A. Gray, “Optimization and integration of hybrid renewable energy hydrogen fuel cell energy systems – A critical review,” Applied Energy, vol. 202, pp. 348–364, 2017.

[5] D. Martínez del Monte, A. J. Vizcaíno, J. Dufour, and C. Martos, “Effect of K, Co and Mo addition in Fe-based catalysts for aviation biofuels production by Fischer-Tropsch synthesis,” Fuel Processing Technology, vol. 194, no. June, p. 106102, 2019.

[6] W. S. Chai, Y. Bao, P. Jin, G. Tang, and L. Zhou, “A review on ammonia, ammonia-hydrogen and ammonia-methane fuels,” Renewable and Sustainable Energy Reviews, vol. 147, p. 111254, Sep. 2021.

[7] W. R. W. Daud, R. E. Rosli, E. H. Majlan, S. A. A. Hamid, R. Mohamed, and T. Husaini, “PEM fuel cell system control: A review,” Renewable Energy, vol. 113, 2pp. 620–638, 2017.

[8] X. Lü, X. Miao, W. Liu, and J. Lü, “Extension control strategy of a single converter for hybrid PEMFC/battery power source,” Applied Thermal Engineering, vol. 128, pp. 887–897, 2018.

[9] C. Zhang, Y. Qiu, J. Chen, Y. Li, Z. Liu, Y. Liu, J. Zhang and C.S. Hwa, “A

comprehensive review of electrochemical hybrid power supply systems and intelligent energy managements for unmanned aerial vehicles in public services," Energy AI, vol. 9, no. June, p. 100175, 2022.

[10] Y. Chen, J. Lin, and X. Wang, "Noble-metal based single-atom catalysts for the water-gas shift reaction," Chemical Communications, vol. 58, no. 2, pp. 208–222, 2022.

[11] R. Mu, Q. Fu, X. Guo, X. Xu, D. Tan, and X. Bao, "A comparative study in structure and reactivity of 'FeO_x-on-Pt' and 'NiO_x -on-Pt' catalysts," Science China Chemistry., vol. 58, no. 1, pp. 162–168, 2015.

[12] S. Xing, H. Su, M. Yang, H. Gong, S. Ban, C. Zhao and H. Wang, "Experimental optimization analysis on operating conditions of CO removal process from hydrogen-rich reformate," International Journal of Hydrogen Energy, vol. 48, no. 64, pp.25216-25230. 2023.

[13] V. D. B. C. Dasireddy, J. Valand, and B. Likozar, "PROX reaction of CO in $H_2/H_2O/CO_2$ Water–Gas Shift (WGS) feedstocks over Cu–Mn/Al_2O_3 and Cu–Ni/Al_2O_3 catalysts for fuel cell applications," Renewable Energy, vol. 116, pp. 75–87, Feb. 2018.

[14] T. L. Levalley, A. R. Richard, and M. Fan, "ScienceDirect The progress in water gas shift and steam reforming hydrogen production technologies-A review," International Journal of Hydrogen, vol. 39, no. 30, pp. 16983–17000, 2014.

[15] M. V. Konishcheva, D. I. Potemkin, P. V. Snytnikov, O. A. Stonkus, V. D. Belyaev, and V. A. Sobyanin, "The insights into chlorine doping effect on performance of ceria supported nickel catalysts for selective CO methanation," Applied Catalysis B: Environmental, vol. 221, no. September 2017, pp. 413–421, 2018.

[16] D. Gu, C.J. Jia, H. Bongard, B. Spliethoff, C. Weidenthaler, W. Schmidt and F. Schüth, "Ordered mesoporous Cu–Ce–O catalysts for CO preferential oxidation in H_2 -rich gases: Influence of copper content and pretreatment conditions," Applied Catalysis B: Environmental, vol. 152–153, pp. 11–18, 2014.

[17] Z. Qi, C. He, and A. Kaufman, "Effect of CO in the anode fuel on the performance

of PEM fuel cell cathode," Journal of Power Sources, vol. 111, no. 2, pp. 239–247, 2002.

[18] N. Bion, F. Epron, M. Moreno, F. Mariño, and D. Duprez, "Preferential oxidation of carbon monoxide in the presence of hydrogen (PROX) over noble metals and transition metal oxides: Advantages and drawbacks," Topics in Catalysis, vol. 51, no. 1–4, pp. 76–88, 2008.

[19] E. D. Park, D. Lee, and H. C. Lee, "Recent progress in selective CO removal in a H_2-rich stream," Catalysis today, vol. 139, no. 4, pp. 280–290, 2009.

[20] H. C. Lee and D. H. Kim, "Kinetics of CO and H_2 oxidation over CuO-CeO_2 catalyst in H_2 mixtures with CO_2 and H_2O," Catalysis today, vol. 132, no. 1–4, pp. 109–116, 2008.

[21] T. M. Nyathi, N. Fischer, A. P. E. York, and M. Claeys, "Environment-Dependent Catalytic Performance and Phase Stability of Co_3O_4 in the Preferential Oxidation of Carbon Monoxide Studied in Situ," ACS Catalysis, vol. 10, no. 20, pp. 11892–11911, 2020.

[22] Y. Zhang, H. Liang, X. Y. Gao, and Y. Liu, "Three-dimensionally ordered macro-porous CuO-CeO_2 used for preferential oxidation of carbon monoxide in hydrogen-rich gases," Catalysis communication, vol. 10, no. 10, pp. 1432–1436, 2009.

[23] S. Sahebdelfar and M. T. Ravanchi, "Carbon monoxide clean-up of the reformate gas for PEM fuel cell applications: A conceptual review," International Journal of Hydrogen Energy, vol. 48, no. 64, pp.24709-24729, 2022.

[24] J. Saavedra, T. Whittaker, Z. Chen, C. J. Pursell, R. M. Rioux, and B. D. Chandler, "Controlling activity and selectivity using water in the Au-catalysed preferential oxidation of CO in H_2," Nature Chemistry, vol. 8, no. 6, pp. 584–589, 2016.

[25] P. Garbis, C. Kern, and A. Jess, "Kinetics and reactor design aspects of selective methanation of CO over a Ru/γ-Al_2O_3 catalyst in CO_2/H_2 rich gases," Energies, vol. 12, no. 3, pp. 1–15, 2019.

[26] P. Jing, X. Gong, B. Liu, and J. Zhang, "Recent advances in synergistic effect

promoted catalysts for preferential oxidation of carbon monoxide," Catalysis Science & Technology, vol. 10, no. 4, pp.919-934, 2020.

[27] G. Xiang, J. Huo, and Z. Liu, “Understanding and application of metal – support interactions in catalysts for CO-PROX,” Physical Chemistry Chemical Physics, vol.24, no. 31, pp. 18454–18468, 2022.

[28] C. H. Tu, A. Q. Wang, M. Y. Zheng, X. D. Wang, and T. Zhang, “Factors influencing the catalytic activity of SBA-15-supported copper nanoparticles in CO oxidation,” Applied Catalysis: General, vol. 297, no. 1, pp. 40–47, Jan. 2006.

[29] Y. Chen, J. Lin, and X. Wang, “Noble-metal based single-atom catalysts for the water-gas shift reaction,” Chemical Communications, vol. 58, no. 2, pp. 208–222, 2021.

[30] S. Kandoi, A. A. Gokhale, L. C. Grabow, J. A. Dumesic, and M. Mavrikakis, “Why Au and Cu are more selective than Pt for preferential oxidation of CO at low temperature,” Catalysis Letters, vol. 93, no. 1–2, pp. 93–100, 2004.

[31] G. Sedmak and S. Hoˇ, “Kinetics of selective CO oxidation in excess of H_2 over the nanostructured $Cu_{0.1}Ce_{0.9}O_{2-y}$ catalyst,” vol. 213, pp. 135–150, 2003.

[32] J. Cao, X. Zhang, X. Ou, T. Liu, T. Xing, Z. Li, X. Zhou, H. Yan, Y. Liu, X. Feng and Y. Tuo, “Reactant adsorption modulation by Fe and K in Pt catalyst for highly effective CO preferential oxidation in practical conditions,” Chemical Engineering Jouirnal, vol. 444, no. March, p. 136661, 2022.

[33] G. Marbán and A. B. Fuertes, “Highly active and selective CuO_x/CeO_2 catalyst prepared by a single-step citrate method for preferential oxidation of carbon monoxide,” Applied Catalysis B: Environmental, vol. 57, no. 1, pp. 43–53, 2005.

[34] S. Dey and G. C. Dhal, “The catalytic activity of cobalt nanoparticles for low-temperature oxidation of carbon monoxide,” Material Today Chemistry, vol. 14, p. 100198, 2019.

[35] C. Xu, S. Li, Y. Zhang, Y. Li, and J. Zhou, “ScienceDirect Synthesis of CuOx-CeO_2 catalyst with high-density interfaces for selective oxidation of CO in H_2 -rich stream,” International Journal of Hydrogen Energy, vol. 44, no. 8, pp. 4156–4166, 2018.

[36] U. S. Mohanty, M. Ali, M. R. Azhar, A. Al-Yaseri, A. Keshavarz, and S. Iglauer, “Current advances in syngas (CO + H_2) production through bi-reforming of methane using various catalysts: A review,” International Journal Hydrogen Energy, vol. 46, no. 65, pp. 32809–32845, 2021.

[37] Z. Zhang, Y. Tian, W. Zhao, P. Wu, J. Zhang, L. Zheng, T. Ding and X. Li, “Hydroxyl promoted preferential and total oxidation of CO over ε-MnO_2 catalyst,” Catalysis Today, vol. 355, pp. 214–221, Sep. 2020.

[38] M. Konsolakis, M. Sgourakis, and S. A. C. Carabineiro, “Applied Surface Science Surface and redox properties of cobalt–ceria binary oxides : On the effect of Co content and pretreatment conditions,” Applied Surface Science, vol. 341, pp. 48–54, 2015.

[39] V. D. B. C. Dasireddy, “Cu-Mn-O nano-particle/nano-sheet spinel-type materials as catalysts in methanol steam reforming (MSR) and preferential oxidation (PROX) reaction for purified hydrogen production,” vol. 182, 2022.

[40] M. I. Fadlalla, T. M. Nyathi, and M. Claeys, “Magnesium as a Methanation Suppressor for Iron- and Cobalt-Based Oxide Catalysts during the Preferential Oxidation,” vol.12, no. 2, p.118, 2022.

[41] Z. Zhao, T. Bao, Y. Li, X. Min, D. Zhao, and T. Muhammad, “The supported CeO_2/Co_3O_4-MnO_2/CeO_2 catalyst on activated carbon prepared by a successive-loading approach with superior catalytic activity and selectivity for CO preferential oxidation in H_2-rich stream,” Catalysis Communication, vol. 48, pp. 24–28, 2014.

[42] Z. Lendzion-Bieluń, M. M. Bettahar, S. Monteverdi, D. Moszyński, and U. Narkiewicz, “Effect of cobalt on the activity of CuO/CeO_2 catalyst for the selective oxidation of CO,” Catalysis Letters, vol. 134, no. 3–4, pp. 196–203, 2010.

[43] S. Malwadkar, P. Bera, and C. V. V Satyanarayana, “Influence of cobalt on performance of Cu-CeO_2 catalysts for preferential oxidation of CO,” vol. 38, pp. 941–950, 2020.

[44] H. Park, E.J. Lee, H. Woo, D. Yoon, C.H. Kim, C.H. Jung, K.B. Lee and K.Y. Lee, “Enhanced hydrothermal durability of Co_3O_4@CuO–CeO_2 Core-Shell catalyst for carbon monoxide and propylene oxidation,” Applied Surface Science, vol. 606, no. June, p. 154916, 2022.

CHAPTER 2

---

2. LITERATURE REVIEW

2.1. INTRODUCTION

Since the dawn of humanity, carbon based and non-renewable fossil fuels, including ‘black gold’ (crude oil), coal and natural gas had dominated the whole world energy supply till to date [1]. High consumption of these limited resources due to an exponential population growth will eventually result in energy depletion. These may lead to many environmental problems such as air pollution and adverse climate changes, which threatens the ecological sustainability, social progress, economic development and most importantly, human health [1-3]. Proton exchange or polymer electrolytes membrane fuel cells (PEMFCs) developments and its applications are of great importance in satisfying the modern human lifestyle’s. These needs include amongst others transportation and energy supply for households, as well as of clean environmental impact. PEMFCs device utilize a renewable, versatile, and non-polluting H_2 gas as a fuel, which has a higher gravimetric energy density compared to other fuel cells. In addition it is light, high energy efficiency, with rapid start-up due to thin cell’s structures and operate for a long period of time (due to the solid electrolytes); hence it is applicable to automobile and transportations [1, 2, 4, 5]. Throughout its entire development, the PEMFCs cell and its efficiency have always been confronted by trace amount of CO in hydrogen rich feed gas. The strong adsorption affinity of CO on the Pt anode is one of its intrinsic chemical properties that governs the poisoning effect of the anode, and reduction of the efficiency of the fuel cells [6-8]. Carbon monoxide is inevitably obtained as a byproduct during H_2 production by either steam reforming or partial oxidation of renewable fuels (such as bioethanol) and/or hydrocarbons (such as CH_4); followed by low temperature water gas shift (WGS) reaction [2, 7, 9, 10]. The final stage, WGS reaction, however, still contains trace amount of CO (0.5 – 2.0 Vol.%) as part of the reactant-product mixture at the outlet, and must be removed to the CO concentration tolerated by the PEMFCs, which is less than 10 ppm according to Nyathi *et al.*, [11].

Preferential oxidation of CO (CO(PrOx)) in hydrogen rich stream ideally ensures that the level of CO entering a fuel cell compartment from the WGS outlet is below the tolerable levels (< 10 ppm). An effective CO(PrOx) catalyst should have high selectivity towards CO oxidation, low cost in preparation, and should be able to work in moisture and CO_2 environment [7, 11, 12]. Thus, there is still a need to develop a highly active and selective CO (PrOx) catalysts. Economic drawbacks and mineral scarcity in different parts of the world had limited the utilisation of expensive noble metal catalysts, such as ruthenium based [12–14] and gold based [15-17] as CO(PrOx) catalysts. Recently, transition metal oxides-based catalysts such as CuO, CeO_2, Co_3O_4, MnO_x, and ZrO_2 have been proposed. These metal oxides have shown good catalytic performances towards CO(PrOx) over appreciable temperature window [18–21].

Cobalt (Co_3O_4) based catalysts are one of the best transition metal oxides for low temperature CO oxidation. Its catalytic performance is known to be strongly affected extrinsically by the amount of a dopant or support component, pretreatment conditions as well as the preparation method [19, 22]. For example, Zhen *et al.*, [24], prepared $Co_3O_4@CeO_2$ catalysts by reflux assisted soft-assembly method, using hexamethylene triamine (HMT) as structure control agent. The team noticed that the catalytic activity of bear Co_3O_4 catalysts in CO oxidation was enhanced by the addition of CeO_2. Reduction-oxidation pretreatment of Co_3O_4/ZrO_2 catalysts have demonstrated an improvement on the catalytic performance in CO(PrOx) catalysis [20]. The oxidative pretreatment of cobalt-ceria binary oxide catalysts has shown to preferentially expose cerium cations on the catalyst's surface, whereas the reductive pretreatment results in uniformly distributed ceria and cobalt species. These in turn facilitates the formation of oxygen vacancies through Co^{3+}/Co^{2+} and Ce^{3+}/Ce^{4+} redox synergy, and hence the CO(PrOx) performance [25]. The effects of preparation method towards catalyst morphology, which in turn dictates the types of the exposed crystal facets and thus the concentration of low coordinated active metal centre on the surface, is also of important concern in catalysts design [25, 26]. Different shaped catalysts including cubes [24, 28], nanorods [28, 29], nano mesh [31], nanoflakes [32] etc., shows different catalytic activities. These is because different crystal planes expose different amount of metal cations on the surface. For example, the {111} planes terminated by Co_3O_4 octahedra decorated nanocrystals are said to be rich in Co^{2+} [33], while the {100} in Co_3O_4 cubes are rich in Co^{3+} [33, 34]. The Co^{3+} is believed to be an active site for CO sorption during catalytic oxidation, while the oxide (O^{2-}) in the Co_3O_4 structure serve as a powerful oxidant for CO oxidation, and gets replenished by the gas feed oxygen (O_2) via Co^{2+} centre, in a Mars Van Krevelen (MvK) mechanism [19, 33, 35]. Such autotuning redox capability between the Co^{2+}/Co^{3+} as well as the preferential termination of octahedrally coordinated metal centre (Co^{3+}) by spinel crystal, attributes to good catalytic performance of Co_3O_4 based catalysts. Thus, the specific active metal centre on the surface, formation of oxygen vacancies and activation of molecular gas feed O_2 species are directly dictated by the preparation method, which in turn determines the catalytic performance. Nonstoichiometric CuO (i.e., CuO_x) is also reported as an important ingredient in CO(PrOx) catalysts due to its affinity towards CO as a result of copper-carbonyl (Cu^+-CO) intermediate, thus improves both the catalytic selectivity and activity [7, 36, 37]. Most reported catalyst based on CuO doped CeO_2, suffer from selectivity loss at high temperature above 120 °C [38, 39].

2.2. POLYMER ELECTROLYTE MEMBRANE FUEL CELLS (PEMFCs)

Tremendous attention received by PEMFCs technology is forever escalating, as studies and research aiming to optimize it evolves with time. PEMFCs is considered the most valuable and benign way to produce energy for both mobile and stationary applications [1-2]. It operates at low temperatures, has a high power generation, starts rapidly and produces no pollution during operation [43]. The ideally pure H_2 gas component is fed directly into the fuel cell, where it gets oxidized to H^+ and electrons (e^-) on the Pt anode (supported on a high surface area material) according to the following balanced chemical equation:

$$2H_2 \rightarrow 4H^+ + 4e^- \qquad (1)$$

The produced protons (H^+) are highly permeable to the water-based acidic polymer membrane (electrolyte) and thus passes through, while the impermeable electrons travel through the external circuit to the cathode, and gets reduced to water molecules (biproduct) using oxygen as an oxidizing agent [2-4]. The equation below depicts this cathodic process.

$$4H^+ + O_2 + 4e^- \rightarrow 2H_2O \qquad (2)$$

The overall reaction is:

$$2H_2 + O_2 \rightarrow 2H_2O \qquad (3)$$

The current produced during e^- migration can then be used to do valuable work, such as car engine start-up, motor rotation, electrical cooker and can have many applications in many electrical gadgets (see Figure 2.1). The storage and transportation of H_2 gas is an important topic/subject of concern in PEMFCs applications. It is for this reason that hydrogen rich gas produced from biomass and fossil fuel is fed directly into the fuel cells on board [45]. H_2 is normally produced in large scale (but low purity) via steam reforming of hydrocarbons followed by water gas shift reaction (WGSR), which still contains small amount of poisonous CO [1, 7-8]. To reduce CO further and increase the level of H_2 purity, additional reactor, the CO(PrOx) reactor, is thus incorporated [4, 9-10]. A good CO(PrOx) catalyst should ideally catalyse CO oxidation between PEMFCs operating temperatures (80 – 100 °C) to a low temperature window of a WGS reaction (200 °C), with good stability in such WGS conditions (i.e., in H_2-rich gas contaminated with CO_2 and moisture atmosphere) [5-6].

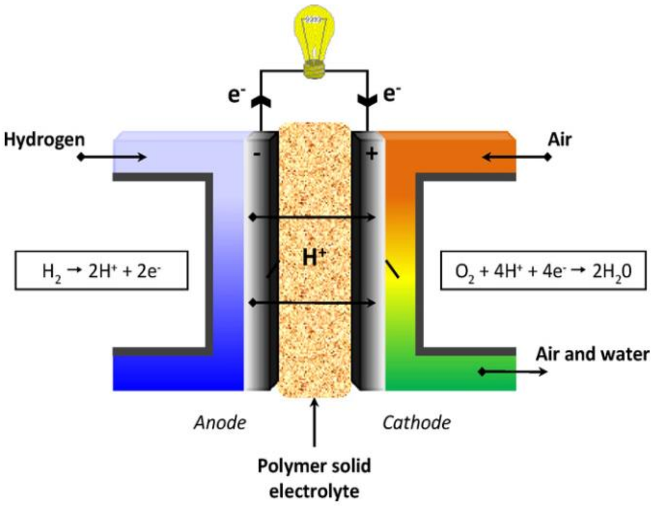

Figure 2.1 Schematic illustration of a PEMFCs device and vital chemical reactions (in boxes) [49].

2.3. STEAM REFORMING OF HYDROCARBONS FOLLOWED BY WATER GAS SHIFT (WGS) REACTION

It should be understood that the CO(PrOx) reactor is usually experimented as an intermediate between the PEMFCs and the WGS reactor, which is connected with an upstream steam reformer [48]. This on-board engineering set-up is a crucial, effective, and most affordable way to remove trace level of CO gas from excess H_2; which could make it to the PEMFCs, blocking the H_2 dissociative adsorption sites on the Pt anode, and thus tempers with performance of the device [44].

2.3.1. Industrial steam reforming (SR) of hydrocarbons

As the name infers, the process converts a mixture of steam ($H_2O_{(g)}$) and hydrocarbons (usually natural gas, CH_4, and sometimes CH_3OH) into H_2 and carbon oxides products, at higher temperatures (very endothermic) in the presence of a catalyst [1, 12-13]. Methane (CH_4) SR is the most common way to produce bulk H_2 at industrial scale, for PEMFCs applications and/or for ammonia production, since CH_4 (even CH_3OH) contains higher amount of hydrogen to carbon ratio [26]. The equations below depict two concomitant reactions of methane and steam during hydrogen production, one producing CO (equation (4)) and the other produces CO_2 gas (equation (5)).

$$CH_{4(g)} + H_2O_{(g)} \rightarrow 3H_{2(g)} + CO_{(g)} \qquad \Delta H_{(298\ K)} = +\ 206.1\ kJ/mol \qquad (4)$$

$$CH_{4(g)} + H_2O_{(g)} \rightarrow 4H_{2(g)} + CO_{2(g)} \qquad \Delta H_{(298\ K)} = +\ 165\ kJ/mol \qquad (5)$$

The two chemical reactions can occur simultaneously in a gas reactor during methane SR. The reactions takes place at extremely high temperatures (at around 700-1000 ^oC) and pressures (3-25 bar) on a suitable catalysts such as Ni supported on CeO_2, MgO, ZrO_2 and MgO-Al_2O_3 [52]. These rigorous reaction conditions are crucial to facilitate the endothermic nature of C-H covalent bond's disruption of the CH_4 gas molecule to produce H_2. In a typical SR reactor system, CO gas found alongside the reformates is then selectively combined with water in the second reactor chamber and therefore, converted into CO_2 and more hydrogen gas, via industrial water gas shift reaction (WGSR) as discussed in the following subsection.

2.3.2. Water gas shift reaction (WGSR)

Discovered in 1780 by Italian physicist, Felice Fontana [10, 16], WGSR remains one of the most industrial vital reactions for production or enrichment of H_2 from CO and H_2O mixture. The produced H_2 can be used to produce ammonia (for fertilizers) and methanol (for antigens and gasoline additives) [12, 17], or fed directly into the PEMFCs. WGSR has also found significance applications in converting natural resources (biomass, coal & natural gas) into valuable hydrocarbon fuel (e.g., paraffin

& olefins) in associated technologies such as Fischer Tropsch synthesis (FTS), as deployed greatly at Sasol and other related companies [55].

As a first step following SR (and partial oxidation of hydrocarbons), dedicated to remove CO from impure H_2 prior to CO(PrOx), WGSR selectively converts a mixture of CO and H_2O into more hydrogen and releases less carbon dioxide gas [10, 17-18]. WGSR is normally conducted as a two-stage process. The first one involves higher temperature catalysis (at around 310-450 ^oC) on chromium-oxide supported iron-oxide (Ferrochrome catalysts), and the second stage tangles low temperature (~200 ^oC) regime, using copper based catalysts, managing to lower CO concentration level to ~ 0.1-0.3 % [47]. The reaction is mildly exothermic with the following chemical equation:

$$CO_{(g)} + H_2O_{(g)} \leftrightarrow H_{2(g)} + CO_{2(g)} \quad \Delta H_{(298\ K\ (forward\ rxn))} = -41.09\ kJ/mol \qquad (6)$$

These reaction is thermodynamically favoured at lower temperatures and kinetically enhanced at elevated temperatures [8, 19], which is why two stage reactor system is efficient.

WGSR is sporadically observed as a side reaction in many catalytic reactions such as CO(PrOx). Using in situ XRD and magnetometer profiles systematically under CO(PrOx), Nyathi *et al.*, [11], evaluated bear Co_3O_4 nanoparticles and observed the reduction of octahedrally coordinated Co^{3+} cationic species in the Co_3O_4 spinel structure to CoO and Co^0, due to the presence of H_2 in fed gas. This reduced state of cobalt favoured WGSR at higher temperatures but only in the absence of CO_2, which otherwise would have shifted the reaction (equation 6) to the left (reverse water gas shift (RWGSR)), obeying Le Chatelier's principles. The team also noticed that co-feeding CO_2 had no effect on the Co_3O_4 phase stability and reducibility but led to unwanted reverse water gas shift reaction (RWGSR) and CO_2 methanation, which consume valuable H_2 needed for PEMFCs. Malwadkar *et al.*, [8], studied the influence of cobalt on Cu-CeO_2 catalytic performance for CO(PrOx) reaction and found that the RWGSR was suppressed by loading cobalt onto the Cu-CeO_2 catalyst, preserving H_2, which would have been diminished by CO_2 as reported by Nyathi *et al*'s group [11]. This also show the importance of a metal-support system in selectivity of a chemical reaction.

Despite their vast application in largescale production of H_2, catalytic SR followed by WGSR yield small carbon oxide products (CO_2 and CO) thereby contributing less to

GHGs emissions. As reviewed, SR-WGSR processes use cheaper metal oxide catalysts (Fe, Cr, Cu, Ni/MgO etc), which features high catalytic activity, recoverability, abundancy, and non-toxicity. Therefore it remains a landmark processes for production of largescale H_2 fuel at both the economic and industrial level, and are still used in the world today [57]. These processes (SR-WGSR) are also referred to as the 'grey' method of hydrogen production because of the methane used and their concomitant release of GHG (CO_2) without capture. On the other hand, we have the 'green' hydrogen production, which involves electrochemical process (i.e., the water electrolysis), powered by renewables (solar & wind, see Figure 2.2). These energy sources are not dependable, are highly intermittent, and extremely fluctuating. This means more useless costs in building unserviceable solar panels and wind turbines. Hence industrial companies still value conventional steam reforming followed by WGSR as the best way to produce H_2 (i.e., grey method).

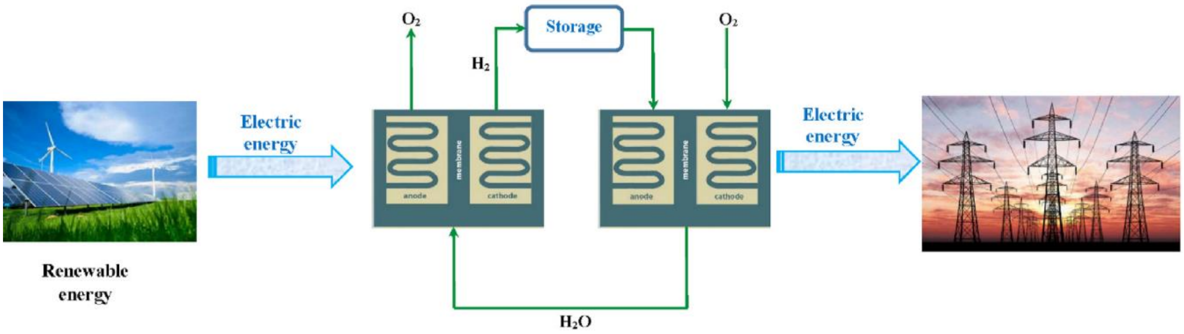

Figure 2.2 Schematic illustration of ideal 'green' H_2 production and economy [51].

The performance of the catalyst is a function of its selectivity and catalytic activity. These factors depend on metal oxidation states, catalyst phase stability, degree of crystallinity, reducibility, robustness, and other factors [20, 22-25]. For a structure sensitive reaction such as catalysis and corrosion; textural control and structural properties plays a key role in the dynamics of a chemical reaction [60]. Trace level of unconverted CO molecules from WGSR must be oxidized further to CO_2 before the gas is introduced to PEMFCs, via a special reactor intermediate called the CO(PrOx) reactor. Research approaches and attempts by computational, experimental, and theoretical models to understand physicochemical properties of solid nanomaterials, particularly exploitation of suitable catalysts for CO removal in delivering clean H_2 for

PEMFCs, is still an ongoing challenge in nano catalysis. Some prepared catalytic materials for CO(PrOx) reaction and work undertaken by several researchers in the literature, are rationalized in the sections below.

2.4. PREFERENTIAL OXIDATION OF CARBON MONOXIDE (CO(PrOx) ON VARIOUS METAL CATALYSTS

Although, WGSR plays a key role in CO removal and H_2 enrichment, sometimes even a small amount of CO (100 ppm) makes it through to the other side with H_2 as a mixture of syngas products, consisting of higher amount H_2 to CO ratio (75 vol.% H_2 : 2-0.5 vol.% CO) [14, 20]. This CO must be abated to concentration <10 ppm, which corresponds to 99.999% CO conversion in H_2 rich stream [11]. As described, CO(PrOx) is identified as the most accurate, affordable, and cost-effective way of removing trace level of CO in the reformate gases. The competitive nature of oxidation reaction between the two reactants, H_2 and CO, on a certain catalyst was already known and frequently reported in the literature. Hence an ingenious approach in catalyst synthesis for effective removal of CO in hydrogen rich stream, is absolutely engineering the catalyst for selectivity purposes [20, 21, 27]. Single metal and supported metal phase catalysts are remarkable materials in oxidation catalysis [28-30], but have several discrepancies which are rationalised in the following subsections.

2.4.1. Single atom catalysts in CO(PrOx)

Single atom catalyst system received little interest recently in catalytic oxidation of CO. With Au and Pt known to be an active standalone catalyst for CO(PrOx) reaction but are not promising for practical applications. Pt and Au are easily deactivated by carbonates (CO_3^-) and hydroxyl (OH^-) species, which are usually inevitable in CO_2 and H_2O fed gas found in realistic CO(PrOx) conditions [8]. Again, sintering processes, which could leads to catalysts deactivation has been reported as one of the major challenge in ‘single atom’ noble metal catalysts, especially in WGS simulated gas feed environment [51]. These however, can be avoided by supporting such active single metal atoms on a support component [51].

2.4.2. Supported metal catalysts in CO(PrOx)

Modifications has been made over the past decades by chemists to single atom catalysts system to stabilize and enhance their catalytic activity. Increasing catalytic activity by increasing surface area of an active nanoparticle through mobilisation on a high surface area support materials such as carbon nanotubes (CNTs) [65], alumina (Al_2O_3) [66], silica (SiO_2) [67], ceria (CeO_2) [33, 34]; is indeed a shrewd and competent way to synthesize and optimise the structural and chemical properties of a catalyst material. An oxide support can either be reducible or non-reducible.

2.4.2.1. Metal catalysts supported on non-reducible oxides.

Alumina (such as γ-Al_2O_3) and Silica (SiO_2), have quite remarkable large surface area compared to most metal oxide. Studies have shown that this surface area can be accessed in the form of pores in the material's hollow cavity or externally on the surface [27-29]. Applications of these materials individually or in combination (as in zeolites) for material support or catalysts are forever escalating, owing to this unique property. Ma *et al*., [71], hydrothermally synthesised Pd-based catalyst supported on a porous micro spherical Al_2O_3 as well as on Zirconia (ZrO_2). The Al_2O_3 supported catalysts (Pd-Al_2O_3) with a whopping surface area of 196 m^2/g was reported, with just 16 m^2/g for Pd-ZrO_2. Furthermore, Pd-Al_2O_3 possessed an excellent activity and CO_2 yield in ethyl acetate degradation, and volatile organic compounds (VOCs) oxidation with a turnover frequency (TOF) of ~ 7.76×10^{-3} s^{-1} at 160 °C, under a gas hourly space velocity (GHSV) of 50 000 h^{-1}. The catalyst had a long-term stability (50 h) in both the dry and the humid condition.

Xu *et al*., [67], also compared Ni/Al_2O_3 and Ni/SiO_2 catalyst in their performance towards dry reforming of methanol and found that Ni/SiO_2 had exceptional activity but poor stability (deactivated after 15 h, due to weak metal-support interaction). The nickel species was present as large nanoparticle around the SiO_2 island and promoted coking reaction, which deactivated the catalyst at higher temperatures (~800 °C). These was evident by large decrease is specific surface area of these nano material from 162.6 to 59.9 m^2/g, from fresh to spent catalyst, respectively. The low activity of Ni/Al_2O_3 catalyst arise from strong metal-support interaction which might have led to a decrease in the active phase component. However, the catalyst was stable on stream for about 50 h. The surface area of the fresh and spent Ni/Al_2O_3 catalyst were

159.3 and 152.1 m^2/g, respectively. Both Al_2O_3 and SiO_2 had higher surface area than other metal oxide supports (such as ZrO_2; ~16 m^2/g, [71]).

The Al_2O_3 and SiO_2 are thermochemically stable, recoverable, cheaper and have controllable surface acidity [72]. They also seem to offer the best surface area to volume ratio however, they suffer one major ‘chemical/electronic’ drawback. From catalytic oxidation perspective, it is very much beneficial when a support component participates in an actual chemical reaction rather than just offering a room to play. Zeolites and its major constituent, Al_2O_3 and SiO_2, are chemically inert, at least at lower temperatures (<100 ^oC), due to low content of O_2 adsorbed. This prevents them to donate their lattice oxygen (O_L) to the catalytic reaction and replenish themselves back with gas feed oxygen in the process, hence non-reducible [73]. The donation of O_L (i.e., O^{2-}) by a metal support also creates the oxygen vacancies, which can accommodate and activate atmospheric oxygen (O_2), a crucial step for re-oxidizing a reduced metal phase during reaction mechanism, thereby allowing gas feed O_2 to participate in the oxidation reaction [42, 43]. Another study by Cui *et al.*, [76], reported that O_L favours CO(PrOx) by participating in the rate limiting step (RLS) of this reaction, with a minimum apparent activation energy barrier of ~0.61 eV on $SrCoO_3$-(100) plane. Furthermore, during catalytic hydrogen spill over phenomenon, the mobility of charged species such as H^+/e^- is not feasible on non-reducible metal oxide support like alumina and silica, over which hydrogen radical induces a covalent bond, yielding undesired kinetics for migration [72]. Therefore, such electronic pitfall of non-reducible metal oxides limits their practical application in energy and catalysis, including CO(PrOx).

2.4.2.2. Metal catalysts supported on reducible metal oxides.

On the other hand, metal oxides that are reducible such as CeO_2, Co_3O_4, FeO_x and MnO_x are honoured in catalysis, because they can promote catalytic reactions by donating O_L and can also serve as great transportation media or support components in catalysts design [73]. Isolated Pt atom anchored on FeO_x framework possessed a higher catalytic CO conversion, due to the reduced adsorption energy and activation barriers for CO by the partially vacant 5d orbitals of the positively charged Pt atom supported on reducible FeO_x nanoparticles (DFT evident) [73]. Although Pt is active, it is expensive and sporadic while abundant and biocompatible FeO_x is unstable and prone to adopt different structures in different atmospheric environment, with $FeO_{(1-x)}$ and $FeO_{(2-x)}$ in a reducing and oxidizing environment respectively, with the latter being a deactivated form [77]. The study demonstrated that such polymorphism is not possible in $NiO_{(1-x)}$ supported on Pt substrate, over which the stabilization effect of active phase by the Pt correlates to variability of oxidation state of the oxide [77]. A study by Dey *et al.*, [78], showed that pure Fe_2O_3 can provide CO adsorption site and activates oxygen at FeO_x interface but cannot reach the ideal performance in CO(PrOx) reaction and doping this materials with metals like Cu, result in Cu-Fe solid solution with larger surface area escorted by synergistic benefits. Recently, a spinel type $MnCoO_x$ catalyst derived from layered hydroxide, with abundant $Co_{oct}^{3+}–O^{2–}–Mn_{oct}^{4+}$ active sites (has mobile oxide) have reported to completely oxidize CO in H_2-rich stream over a wide temperature window (80-100 °C) [79].

2.4.2.2.1. Copper oxide supported on reducible CeO_2 and or Co_3O_4 catalysts for CO(PrOx) reactions

Copper on a highly reducible ceria catalyst has long been known as the best couple for CO(PrOx) but almost every active catalyst suffers from concomitant undesired H_2 oxidation. This was reported in one of the early studies by Gamarra *et al.*, [80], which showed that Cu-Ce catalysts prepared by co-precipitation-microemulsion technique resulted in a high activity for both CO and H_2 oxidation (less selective). This was attributed to the presence of Cu species in both the surface and bulk of ceria, which facilitated oxygen vacancy formation ($Ce^{4+} + O^{2-} \rightarrow Cu^{2+} + O_V$) via substitutional defect. The O_V generated from ceria by a dopant is still another interesting property diversifying ceria's application and unsurprisingly, $CuO-CeO_2$ based system are still regarded as suitable material for CO(PrOx), regardless of their minimal H_2 oxidation susceptibilities. Copper also attracted considerable attention due to its chemical properties with multiple oxidation states (Cu^0, Cu^+ and Cu^{2+}) and had also been used in many industrial processes, such as methanol synthesis from CO_2 and/or hydrogenation [81]. In CO(PrOx) catalysis, Cu^+/Cu^{2+} redox couple drives the reaction, with a monovalent copper species (Cu^+) believed to be an active site for adsorption of CO molecules [29, 35, 41-42]. A study reported by Jing *et al.*, [73], revealed that CuO achieved maximum distribution on the {100} crystal planes of CeO_2 nanotubes and interacted strongly with the support, enhancing the CO_2 selectivity. Synthesis of CuO_x-

CeO_2 based catalyst with abundant Cu-Ce interfacial active sites and strong metal support interaction (MSIn) through a facile approach, is still an open challenge in nano catalysis. However, special reagents and their utilisation as nanoparticle nucleation controllers or modifiers are investigated each day to meet CO(PrOx) catalyst' ideal requirements.

Xu *et al.*, [82], had recently developed CuO_x-CeO_2 based catalysts via co-precipitation technique using $(CH_4)_6N_4$ (as both a base and a capping agent) as well as citric acid (as morphology directing agent). The resulting catalyst maintain 100% CO conversion at temperatures of ~95 °C to 235 °C. This was attributed to preservation of an active Cu^+ phase by a strong Cu-Ce interaction, which supressed formation of Cu^0 from this active component. Other reducible metal oxides that can offer O_L including MnO_x Co_3O_4, and TiO_2 also received considerable attention. Singh *et al.*, [84], employed a sonochemical method to fabricate Cu/Co_3O_4 catalyst and found that the catalytic activity was enhanced by the ability of Co_3O_4 to provide O_L to the oxidation reaction, as well as facile $Co^{3+} \leftrightarrow Co^{2+}$ intra-redox behaviour. The 3 wt.% Cu/Co_3O_4 catalyst remained active with stable CO conversion even at methanation susceptible temperatures (200 °C), due to Cu insertion into the Co_3O_4 structure, which favoured strong CO chemisorption rather than CH_4 chemisorption. On the other hand, the ability of cobalt to provide O_L might has been facilitated by the intrinsic low Co-O bond order/energy, which is another main chemical reason why cobalt has attracted so much attention in CO(PrOx) reaction [20]. However, cobalt, especially the Co_3O_4 phase can easily form electrophilic/basic oxygen species (O_2^-/O^-) on its surface [60], which can react with CO to form carbonates species (usually at high temperatures, >160 °C), which has low desorption kinetics compared to plausible bicarbonates counterparts, thereby blocking the active sites [22, 44-45].

These synergic interactions and advantages of bimetallic system especially with reducible supports, had indeed limited single atom catalyst's application in CO(PrOx). Recently, ternary-metallic as well as tetra-metallic catalytic systems were explored in greater details to improve the catalytic performance of many reported catalytic materials. Malwadkar *et al.*, [8], synthesised ternary catalysts system of general formular $(CuO)_{1-x}(Co_3O_4)_{x/3}$-$(CeO_2)_{2.5}$ via coprecipitation reaction, as to figure out the influence of Co on Cu-CeO_2 catalytic performance in CO(PrOx) operations. The catalysts with x = 0.75 had the best activity and selectivity, which were owed to multiple oxidation states (i.e., Co (ii & iii), Cu (i & ii) & Ce (iii & iv): XPS evident) of these metals on the interfacial sites, synergistically boosting the CO oxidation reaction. However, Cu and Co combined (i.e., x = 0.15-1) on ceria stimulated methanation reaction at 175 °C, marking a serious limitation of their developed material and therefore improvements in ternary systems are still recommended. Quaternary-metallic systems are also of great interest. For instance, Zhao *et al.*, [86], reported a four metal oxides system composing of $CeO_2/Co_3O_4-MnO_2/CeO_2$, which had a very high activity that correlated with higher reducibility, well dispersion, unique pores, and stronger interface between $Co_3O_4-MnO_2$ and CeO_2. Table 2.1 give a summary of some of the metal oxides catalysts used for CO(PrOx) reaction and their optimum activity temperature (T_{max}) and selectivity based on the preparation methods.

Table 2.1 Catalysts activity and selectivity results in dry CO(PrOx) catalysis over some reported metal oxide such as copper, ceria, and cobalt based catalysts.

Catalysts	**Preparation method**	**T_{max} (°C)**	**Maximum Conversion (%)**	**%CO_2 selectivity**	**Ref**
$Cu_xCe_{1-x}O_2$	Co-precipitation	100 °C	100	100	[2]
5 wt.% $Cu-CeO_2$	Hydrothermal	65 °C	100	100	[7]
15 wt.% $Co_3O_4-CeO_2$	Freeze-dried (support)/wet impregnation.	140 °C	92	50	[10]
Co_3O_4/ZrO_2(P)	Precipitation (support)/sonication-assisted impregnation	180	100	59	[20]
8Co-1Ce-1Mn	Co-precipitation	80	100	98 %	[21]
$Co_3O_4-CuCoO_2$	Hydrothermal	100	99	100	[31]
$5CuO/(0.3)Co_3O_4-CeO_2$	Templating-precipitation	120	100	95	[39]

Amongst the catalysts illustrated in Table 2.1, the catalysts prepared by hydrothermal method seem to give good CO(PrOx) results. Effects of preparation methods are discussed in detail in section 2.9. Nevertheless, adjustments are still made, and new methods are investigated each day to tune and optimize the CO(PrOx) performance of these promising materials. However, only few studies focused on how actual fed gas components inexorably in realistic CO(PrOx) reactor such as CO_2 and H_2O, affect the activity, selectivity, and most importantly, the stability of the catalysts. The CO(PrOx) performances over these catalysts meet the ideal PEMFCs requirements in dry conditions as shown in the Table 2.1. However, the catalysts should also work in the presence of moisture and CO_2 in the stream, and this is still a challenge, especially so with a good stability.

2.5. EFFECT OF co-FED GASES (CO_2 and H_2O) ON CATALYTIC PERFORMANCE IN CO(PrOx)

With total oxidation (TOX) included, many studies are conducting CO(PrOx) in dry conditions (i.e., without CO_2 and H_2O). Studies in a dry condition alone just provides vital understanding of the catalytic performance only, which has nothing to do with catalytic stability in these two gases, a vital criterion that must be met by a CO(PrOx) catalyst to be accepted for PEMFCs applications [9, 30, 46-47]. Therefore, a catalyst must be investigated towards CO(PrOx) efficiency and stability in the presence of CO_2 and H_2O for industrial applications and commercialization, as these two major gases are associated with processes that are used to produce H_2, such as SR (see, equation 4 and 5) and WGSR (equation 6), and have also been found to exist in real time combustion reactions, including CO oxidation in H_2 rich stream [11, 13].

To rule out, traditional noble metal catalysts such as gold (Au), are active and selective in CO(PrOx) at low temperatures (~100 °C) but prone to CO_2 poisoning, and selectivity losses as temperature increases [88], limiting their application even further. However, even recently promising candidates such as copper, ceria and cobalt behave strangely in moist and CO_2 environment. When studying the influence of cobalt on Cu-Ce based catalyst, Malwadkar *et al.*, [8], noticed a RWGSR catalysed by Co^0 species at higher temperature (>175 °C) when 22.83% CO_2 was fed into the reactor. Nyathi *et al.*, [11], also found similar results over Co_3O_4 catalysts. The reducibility of Co_3O_4 catalyst was not affected however, methanation as well as RWGSR took place over the Co^0 phase in CO_2 environment.

Gawade *et al*., [89], had previously prepared variants of CoO_x by precipitation method and doped these CoO_x species on CeO_2 nanoparticles via wet impregnation technique. At low temperatures (<150 °C), the catalysts had activity that was proportional to cobalt loading under dry CO(PrOx) conditions. Only the catalysts with higher cobalt loading (10 wt.%) was boosted for CO_2 and H_2O tolerance and assisted WGS in humid conditions, relative to other counterparts (1 & 2 wt.%). Depending on several factors such as the preparation methods as well as pre-treatment conditions, either CoO or Co_3O_4 could dominate in CoO_x phase. The CoO catalysts are somewhat active but deactivate easily in the presence of H_2O and CO_2 [88]. On the other hand, phase stability, activity, and reaction specificity of Co_3O_4 are also compromised in such conditions [11]. Several studies showed that H_2O can affect CO(PrOx) in several ways including, (1) blockage of active site (i.e., occupation of coordinatively unsaturated metal centre by H_2O molecules) (2) WGS/RWGSR equilibria disturbance (3) formation of less active CO-H_2O complex etc., [21, 47, 49-51]. Consequences of (1) and (2) are usually more conspicuous in CO(PrOx) and H_2O catalytic deactivation is more pronounced than that induced by CO_2 [6]. Cwele *et al*., [6], noticed a decrease in activity and an increase in selectivity (72-80%) over $Ce_{0.9}Co_{0.1}O_{2-\delta}$ towards CO(PrOx) reaction. However, the introduction of CO_2 and moisture in the feed resulted in a decrease in catalytic activity, due to the blockage of an active sites by surface adsorbed H_2O molecules as well as the competitive effect between CO_2 and CO for the active site. The degree of deactivation was reduced when copper was doped into the catalyst with the CO_2 and H_2O tolerance being proportional to copper loading. However, metal doping is not the only considered route to enhance water tolerance in the literature.

Fascinated by the fact that the electronegativity and the radius of nitrogen (which are 3.04 and 0.171 nm, respectively) are close to that of oxygen atom (3.171 and 0.140 nm, respectively), Yin *et al*., [91], developed oxygen vacancy rich nitrogen doped cobalt N-Co_3O_4 nanosheets via simple urea assisted method in a closed system (i.e., crucible and a lid on). The N-Co_3O_4 catalysts possessed large number of oxygen vacancies, high specific surface area (52,4 m^2/g) and pore volume, compared to the pristine Co_3O_4 and its analogous counterpart, which was synthesised in an open system (without a lid). The N-Co_3O_4 catalyst was stable for the entire 65 h in 3.0 vol.% H_2O at 130 °C. Nitrogen played a key role in accelerating the depletion rate of surface -OH group on Co_3O_4 core, caused by H_2O feed gas. Studies suggest that catalytic pathways of -OH involve the formation of thermodynamically unstable bicarbonate HCO_3^- intermediates upon reaction of CO with this surface -OH group (hence 'depletes' [91]), which then spontaneously decomposes as CO_2 and desorb at a faster rate than CO_2 formed by carbonates (CO_3^{2-}) pathway [22, 44]. This was also confirmed by Zhang *et al.*, [85], on -OH group enriched ε-MnO_2 catalysts, prepared by acid washing. This surface enriched -OH groups readily reacted with CO forming bicarbonate (HCO_3^-), a thermally unstable intermediate that provided CO_2 desorption sites.

These findings advise that, despite its long-whispered reputation for being bad in catalysis, H_2O can also play a significant role in the overall CO(PrOx) reaction and only few studies had reported on this tranquillity brought by 'pseudo-innocent' H_2O molecules. Recently, Ngema *et al.*, [20], observed an increase in O_2 to CO_2 selectivity (57 → 80%) on pre-treated Co_3O_4-ZrO_2 in WGSR simulated gas feed stream, achieving 100 and 80% CO conversion in 4 & 7 vol.% of H_2O respectively, at temperature of 180 °C (GHSV; 16 000 mL h^{-1} g_{cat}^{-1}). The good activity of the catalyst was ascribed to surface adsorbed water molecule monolayer, which prevented further formation of more water species by H_2 combustion, while exposing active sites for CO oxidation and CO_2 desorption. However, the catalyst deactivated in the presence of CO_2, attributed to the pre-treatment conditions which led to considerable number of basic sites (activated oxygen species) that are likely to form carbonates (CO_3^{2-}) species. This usually blocks the active vicinities of a catalyst, because of slow desorption kinetics of CO_3^{2-} intermediates from the surface.

Surface energetics can also dictate the effect of WGSR simulated feed gas. Gawade *et al.*, [89], deciphered this phenomenon by preparing CoO_x/CeO_2 nano catalysts, using precipitation (for support)/impregnation technique. The team observed that the activation energy, E_a, of H_2 is much greater than that of CO, suggesting that H_2 oxidation becomes more significant at higher temperatures. The E_a of CO and H_2 were inversely proportional to cobalt loading on all catalysts prepared, showing how cobalt plays a significant role in lowering the energy needed for CO(PrOx) reaction. With cobalt influencing the E_a (thus the kinetics) and copper stabilizing cobalt-ceria based catalyst in H_2O and CO_2 as reported by Cwele *et al.,* [6], this study proposes to combine these three metals (copper-ceria-cobalt) in one catalyst, driven by such properties. However, a great challenge now will be to obtain appropriate loading but this time not only for one active phase, as done by the two reporters (Cwele *et al.,* [6], and Gawade *et al.,* [89]), rather for two envisaged active metal phase, copper and ceria supported on cobalt. The metal load seems to have a great impact on the resulting catalysts. Indeed, the effect of metal loading was of a centricity in nano catalysis, and knowledge about metal loading in designing nano composites for CO(PrOX) application is shared intensively in the literature.

2.6. EFFECT OF METAL LOADING IN CO(PrOx) REACTIONS

Most heterogenous catalysts are semiconductors. Semiconducting oxides (including sulphides) also called defect or extrinsic semiconductors, display unique colour, conductivity, magnetism and catalytic properties due to their deviation from their normal precise stoichiometry [92]. The internal defects (i.e., Schottky and Frenkel defects) correlate to thermal disturbance within a crystalline solid as they are heated, and the external defects are associated with the addition of a dopant or impurities (or particle irradiation of the crystal) [93]. The former's defects benefits will be irrelevant at low temperature CO(PrOx) conditions. The latter is more prominent in altering the surface concentration of oxygen vacancy, with the aim of maintaining electroneutrality deviated by the dopant introduction [63, 64]. External defects can catalyse reversal surface reactions, including CO(PrOx), even without heat or at relatively low temperatures [93]. Of course, the degree of surface alteration depends on the concentration of the dopant introduced, and in terms of vacancies within a certain crystal, one pronounced affected structural parameter is the surface area. Surface reactions are influenced by many properties of the catalyst, with surface area being the most prominent factor and have been reported to be linked directly to the amount of metal dopant when designing a catalyst. For instance, Pojanavaraphan *et al.*, [17], reported that the optimum particle size of 21 nm of 3 wt.% Au/CeO_2-ZrO_2 catalyst resulted in an increase in surface area than the 5 wt.% counterpart, which showed Au agglomeration, and thus a reduced surface area.

Although it is logical and supported by the studies, that particle sizes and surface area are affected by metal content, other structural properties also find themselves in similar susceptibilities. Guo *et al.,* [30], synthesized $Cu_xCe_{1-x}O_2$ nanorods of various Cu composition (3, 5, 7, 11, 15, wt.% Cu/Ce) using a simple co-precipitation method. The team reported that appropriate amount of Cu that enriched the lattice distortion, oxygen mobility, oxygen vacancy concentration, thereby promoting the CO(PrOx) performance was 7 and 11 wt.% (i.e., 7 and 11 wt.% Cu/Ce-(rod) catalysts). These two catalysts also demonstrated strong metal support interactions, which carried out higher temperature CO reaction at the metal support interphase. However, high metal loading of 15 wt.% Cu/Ce -(rod) counterpart result in the formation of bulk CuO_x species sized between 40-50 nm (HRTEM evident), due to agglomeration of CuO nanoparticles. This catalyst showed a tremendous decrease in CO conversion from 100 % at 85 °C to 65% at 145 °C during preferential oxidation of CO in H_2 rich stream [30].

Electronic properties such as redox behaviour elucidated and driven by metal support interaction, is also a key parameter in many oxidation reactions and depend highly on metal loading. Cwele *et al*., [6], used urea assisted solution combustion method to study the effect of Cu additives on the performance of cobalt substituted ceria catalyst towards CO(PrOx) reaction. Their developed $Ce_{0.85}Cu_{0.05}Co_{0.10}O_{(2-\delta)}$ composite catalyst had increased reducibility and improved catalytic activity than its opponents. The reaction profiles and kinetics studies showed that H_2 and CO oxidation takes place on the same site without copper content, and independently when copper is doped in the support matrix as solid solution, making copper a suitable dopant in enhancing cobalt-ceria selectivity. The study has also showed that moisture and CO_2 tolerance increases as copper content was increased [6]. On the other hand, Papavasiliou *et al*., [45], achieved a higher CO conversion with 5 wt.% Cu supported on mesoporous crystalline TiO_2 as compared to 2 and 10 wt.% Cu/TiO_2 counter catalysts. The high activity (80% CO conversion at 150 °C) was ascribed to finely dispersed and easily reducible copper oxide nanoparticles. However, achieving an appropriate metal loading is an empirical phenomenon and usually experimented by varying the amount (wt.%) of dopant, hence will always remain a drawback at economic point of view.

Nonetheless, sometimes the economic drawbacks (including those of using expensive PGMs) is the last issue when designing a catalyst, since the overall goal is to influence the efficiency, optimize the catalytic activity, selectivity and most importantly to prepare a catalytic material of high stability during operation on stream. An expensive catalyst that can work for years is better than a cheap catalyst that must be replaced frequently. When talking about dopants, it is very crucial to emphasis on those that bring positive feedback which are called promoters, and they are sometimes supplemented to the catalysts to reduce catalytic deactivation and increase reducibility, among other benefits [61-62]. Since promoters are also dopants, the amount of loading of a promoter plays an equally important role when designing a catalyst. Promoters are classified into two major classes (electronic and or structural) and have greater influence on the overall catalytic activity.

2.7. INFLUENCE OF A PROMOTER ON A CATALYTIC ACTIVITY

Promoters (also called activators) are chemical substances classified based on their electronic or structural induction effect on a catalyst, to encourage its activity without themselves being involved directly in catalysis, and have been used to optimize heterogenous catalysts as early as 1920, till to date [67-70]. One popular catalytic promotion is the addition of alkali/alkaline metals to ammonia (NH_3) synthesis catalysts in Haber-Bosch process [70-72]. Such alkali promoter have also been utilized for CO(PrOx) catalyst's modifications [101]. The promoters could either alter the catalyst structurally or electronically.

2.7.1. Structural modifying promoters

Many non-reducible metal oxides such as Al_2O_3 and CaO are exceptional structural modifiers (or promoters), which have a serious implication on the textural parameters such as surface area and surface stabilisation during operation [70, 72]. The alumina usually exists as a thin layer of Al_2O_3 phase or segregates as both Al_2O_3 and a spinel $FeAl_2O_4$, and impedes the sintering process of activated iron in magnetite catalysts for ammonia production [100]. However, promoter distribution depends on the crystal structure of the host. For example, alumina dispersion in magnetite ($FeAl_2O_4$) differs from that of wuestite ($Fe_{1-x}O$) due to different crystal structures of the materials, and for alumina supported wuestite, reduced surface reconstruction is feasible allowing regeneration of the active sites and improved activity. On the other hand, CaO improves mechanical strength and thermal stability of the iron catalyst, while also making sure that it lasts longer [98].

Dongil *et al*., [101], reported that incorporation of alkali metals such as Na, Li, Cs & K increase the CO(PrOx) activity by decreasing the crystal size of ceria, which leads to increase in oxygen mobility by a large proportion of defects in doped Cu-CeO_2/CNTs catalyst, with potassium (K) doped catalyst being the most active component. The potassium doped catalysts had strong Cu-Ce interaction relative to its counterparts with caesium (Cs) doped catalysts, exhibiting the worst activity. However, alkali metals are generally known to be highly unstable in water and with catalysts dedicated to function or catalyse the reaction in humid environment, this could go sideways, and this was never addressed in the paper. Nonetheless, a major product of alkali metal reaction with water involves -OH moiety or group, which have shown to have catalytic value in CO(PrOx) reaction [44-45]. Therefore, a smart design might involve a surface modification by promoters that will favour -OH species, and metal oxide such as cobalt oxide (CoO) have shown to do so [20]. Hence having this candidate in a catalyst could be more beneficial.

2.7.2. Electrical modifying promoters

As in CO oxidation, ammonia production from molecular H_2 and atmospheric N_2 requires a large input of energy, owing to a great bond energy needed to overcome the nitrogen triple bond (~945 kJ/mol) [99], which is why most ammonia producing catalysts require some ‘promotion’. Catalytic promotion or activation by electronic promoters such as K_2O and alkaline earth metals, is another promotional mechanism in which an electron is donated from a promoter to the antibonding molecular orbitals of N_2 via a transitional metal, thereby weakening the N_2 triple bond [71-73]. A recent study by Ronduda *et al.,* [98], illustrated the success in ammonia synthesis catalyst by barium oxide promoted cobalt catalyst. The study attributed the activity to electron donation from the BaO promoter to N_2 molecule through cobalt. Furthermore, nitrogen binds more strongly to the dipole vicinities induced by electron transfer from the promoter (such as potassium) to the catalyst (such as iron core) i.e., the $Fe^{\delta-}$ - $K^{\delta+}$ environment [98].

Since N_2 and CO are slightly similar in their chemical structures, characterised by their linear geometry with triple bond between the atoms making up the molecule. A similar promotional mechanism induced by promoter in ammonia production could also assist in CO(PrOx) reaction i.e., via electron donation to the antibonding molecular orbital of

CO from the promoter through a transitional metal [71, 102]. But alkaline metals wouldn't be the first option since realistic CO(PrOx) can take place in WGS simulated gas feed (contains water), which might lead to formation of alkaline metal hydroxides, which are solids at normal conditions and can sinter or block the active sites. Alkaline earth metals exist in a fixed +2 oxidation state and therefore lack reducibility which can limit their ability to store and release oxygen; an important chemical aspect required for oxidative catalyst. On the other hand, transitional metal oxide promoters can be beneficial and studies on these candidates as potential CO(PrOx) activators are reported frequently but the mode of action or the chemistry they deploy to promote the activity is less reported as compared to alkaline/alkali earth metal.

Antonio *et al.*, [102], 'promoted' the activity of CeO_2 supported CuO by doping isovalent, aliovalent and variable valent cationic species and studied their CO(PrOx) activity in H_2O and CO_2 stream. The study showed that doping isovalent cation species such as Zr^{4+} into the ceria framework increased the oxygen storage capacity (OSC) through extrinsic oxygen vacancies. These facilitated the oxygen mobility by enhancing the Ce^{3+}/Ce^{4+} redox process, reaching above 95% CO conversion between 140-115 ^{o}C. This remarkable indorsed catalyst contained as little amount of copper as 6 wt.%, and still gave such outstanding results. Aliovalent doping (such as by, La^{3+}) enhanced catalytic activity via intrinsic oxygen vacancy formation. Variable valence state cations formed from Tb and Pr atoms (coexisting as both the M^{3+}/M^{4+}) facilitated both the intrinsic and extrinsic oxygen vacancy formation, and therefore increases oxygen mobility and storage capacity. The pitfall of this catalyst, however, is the nightmare brought upon by the detrimental effect of both H_2O and CO_2 co-feed gases, which had a negative effect on the overall catalytic proficiency.

Many researchers honour ceria as a support, due to its vast advantages such as OSC. However, recent approach suggested that supporting $CuO-CeO_2$ based catalyst using a suitable cationic species such as Mn and Fe, could allow lower ceria dosage, decrease its particle size, increasing the catalytic activity and stability by inducing a strong Cu-Ce interaction [101].

Since cobalt and these cationic species (3d elements) have the same outermost energy level with cobalt having one extra electron in this subshell (relative to Fe), we predict that supporting CuO_x-CeO_2 on cobalt can aid even further in activity. This could result because of high electron density which might facilitate electron donation [99], from the promoter specifically to the CO pie antibonding orbitals, lowering its energy barrier to break C≡O triple bond in H_2 rich stream, thereby determining the catalytic selectivity. Just like cerium oxide fluorite structure, Co_3O_4 spinel structure can self-generate the O_V, due to weakly bound oxygen species in the form of Co^{3+}-O- Co^{2+}, which is quite reactive [102]. Additionally, the activation energy barrier of the promoted catalytic system is lowered by an electride (i.e., electron as a counter anion) support, due to low work function and high electron density that facilitate electron donation [99]. Activation energy barriers are linked directly to the rate of chemical reaction by Arrhenius theory; therefore, a promoter will have a serious impact on the overall kinetics of the CO(PrOx) and thus the corresponding mechanism.

2.8. REACTION KINETICS AND MECHANISMS INVOLVED IN CO(PrOx)

A higher oxidation rate of CO conversion is a basic ideal necessity (adding to selectivity and activity) for those catalysts dedicated for CO(PrOx) reaction [103]. PEMFCs requires a constant supply of H_2 which implies a need for quick removal and fast purification of WGS reformate mixture, and this is a responsibility of CO(PrOx) catalysts. The CO(PrOx) oxidation is assumed to follow competitive Langmuir-Hinshelwood mechanism (CO & O_2 adsorb on the same active site); whereas some authors propose the Eley-Rideal mechanisms (gas phase CO directly react with adsorbed O_2, or verse versa). However, in catalyst systems in which an active phase is supported or promoted on reducible material, the catalytic reaction is thought to be via two step processes premised by Mars and Van Krevelen, at around 1954 [104]. This occurs when an adsorbing species such as CO stick on the surface of the metal catalyst, where it gets activated by chemisorption, and therefore obstructs the lattice oxygen to form CO_2, creating oxygen vacancy (O_V) in the process. The O_V is quickly replenished by gas phase oxygen to regenerate the active catalytic phase [1, 36, 72-73].

When considering the rates (kinetics), structure specific factors such as concentration of the active sites (function of the pre-exponential factor, A) as well as the activation energy, E_a, are important parameters and are highly affected by the shape and size of metal nanoparticle. Change in E_a at various temperature as modelled by the Arrhenius rate equation can signify several factors, such as change in morphology (due to defects, dopants, or low coordination edges) of a nanoparticle, and this can have significant consequence on the catalytic activity in the overall CO(PrOx) catalysis [60]. Sedmak and Hoˇ [103], fabricated nanostructured $Cu_{0.1}Ce_{0.9}O_{(2-y)}$ catalyst using sol gel method, aiming for simulated realistic CO(PrOx) reactor conditions. The catalyst had 100% selectivity over temperature range 45-90 °C. In this temperature range, the kinetics of the reaction was found to follow the redox mechanism represented by the Mars and Krevelen (MvK) type of reaction. Kinetics parameters showed that the activation energy was 57.2 and 60.2 kJ/mol for CO oxidation step and for reoxidation step, respectively. The value was not far from that obtained by Woods *et al.,* [106], who obtained E_a of 52 kJ/mol for CO oxidation on Co/CeO_2 nanoparticle (H_2 oxidation had E_a = 74 kJ/mol). The E_a values for CO oxidations differs by a magnitude of just ~5.2 kJ/mol and this could be attributed to several factors, such as type of material used (i.e., copper and cobalt as active phase in Sedmak *et al*'s [103], and Woods *et al's* [106], work respectively), method of preparation, chemical precursors used etc. Nonetheless, their results still confirm the selectivity brought by the catalyst active site as a function of E_a between CO and H_2 oxidation. The H_2 oxidation as reviewed, is favoured at higher reaction temperatures. The reaction rate of 2.7 x 10^{-6} mol/g.cat.s (at 90 °C, 0.01 bar CO partial pressure and O_2 stoichiometric partial pressure) was also reported [104], which agree with the modified Langmuir-Hinshelwood mechanism. Although, low temperature oxidation was seen to be facilitated by lattice oxygen, implying favourable Mars-van Krevelen mechanism. These observations were not in agreement with the paper reported by Zasada *et al.,* [34], which revealed that suprafacial (favour Langmuir-Hinshelwood) Co-O_{ads} oxygen species are more active (E_a = 0.83 eV) than the intrafacial Co-$O_{surface}$ surface site (E_a = 1.11 eV) in CH_4 oxidation, on the (100) faceted Co_3O_4 spinel crystal planes, prepared hydrothermally method (at 180 °C for ~5 h). This could suggest that different reactants (CO & CH_4 in this case) can take different pathways or mechanisms for a similar reaction (oxidation) on the same catalyst, but oxidation depends on the surface species. Ngema *et al.*, [20], suggested that lattice oxygens are beneficial at high temperature and adsorbed oxygen species such as O_2^- & O^- catalyse low temperature CO(PrOx).

The conundrum of whether these two mechanisms, compete, coexist, or occur sequentially, is still a debatable subject in the family of catalysis, and efforts must be made to settle this issue. Many studies focused on popular molecular modelling techniques such as density functional theories, *ab initio* atomistic thermodynamics, kinetic modelling, and many other conventional approaches to gain sight into these mechanisms. A recent and novel study on isotopes, particularly the temperature-programmed surface reaction (TPSR) of CO(PrOx) reaction using $^{18}O_2$ as an oxidant, by Hudy *et al.,* [105], proposed the combination of Mars-van Krevelen and Langmuir-Hinshelwood/ Eley-Rideal mechanism, over bare Co_3O_4 and mixed cobalt spinel $M_xCo_{(3-x)}O_4$; M = Cr, Fe, Mn, Ni, Cu & Zn) catalysts. By deploying organic chemistry knowledge on the surface of the catalysts, atomic and ion interactions as well as electron dynamics of metal oxide with precise bonding geometries and stoichiometry, mechanisms of CO oxidation and thus the kinetics could be understood. This work also provides such wonderful models to understand the nature and the mechanism of CO(PrOx) reaction, and this was never done before.

In biological systems, the Michaelis-Menten kinetics dictate the mechanism of an enzyme catalysed reaction [107]. Like enzymes, a catalyst that is highly selective/preferential for specific reagents or reaction is a luxury in many industrial catalytic applications, and achieving selectivity artificially in the laboratory is very much a challenge than in nature, in which a precise control of a protein/enzyme synthesis, folding and aggregation (analogous to crystal growth in nanoparticle synthesis) is accomplished precisely by the DNA. Nano-catalysis integrates both the benefit of homogenous and heterogenous catalysis such as selectivity and recovery respectively [108]. Thus, for a chemical process such as CO(PrOx) reaction, a nanomaterial must be precisely controlled during synthesis (i.e., temperatures, pressures, composition, and pH monitoring), chemically/structurally stabilized during the reaction/operation, and must be specifically developed for specific purpose. All these implies that the recipe (method of preparation) has a major impact on the prepared catalyst.

2.9. EFFECT OF SYNTHESIS PROCEDURES ON METAL NANOPARTICLES.

Catalysts synthesis methods influence the resulting chemical and physical behaviour in terms of structural, textural and redox properties through metal dispersion, homogeneity, size and shape of crystallites/particle, as well as the degree of metal-support interactions, all with an independent influence on the catalytic activity [14, 77-79]. But all desired wishes for a great experimental method in nanoparticle synthesis is cost effectiveness, simplicity in operational terms, low toxicity, biocompatible, environmentally friendly, and quick to fabricate.

Afandi *et al.*, [109], investigated the effect of hydrothermal (H), sol-gel (S), co-precipitation (C) and impregnation synthesis procedures on Ni-Ce/fCNTs catalytic activity, for CO_2 reforming of CH_4. The Ni-Ce/fCNTs-(H) catalyst had superior catalytic activity, converting 92 and 96% of CH_4 and CO_2, respectively at 800 °C and showed stable activity for 30 h on stream, with a constant syngas production of H_2/CO ratio = 0.91. The catalysts activity decreased with the following order: Ni-Ce/fCNTs-(H) > (S) > (C) > (I). The physicochemical properties of a catalyst for structure sensitive reactions modulated by particle size and shape effects (quantum effect) depends highly on the preparation procedure. The effects of synthesis procedure are still unsettled matters in the art of chemical fabrication. Various preparation methods are discussed below.

2.9.1. Sol-gel method

In this method, reagents (metal precursors and alkoxides) are pre-mixed in suitable solvent such as H_2O or ethanol (EtOH). The mixture is then heated at appropriate temperature (~60 °C) to form a colloidal particle known as sol, upon hydrolysis and polycondensation, which is then dried to form a gel [111]. Aerogel, xerogel and cryogel are obtained from supercritical drying, ambient temperature drying and cold freeze drying, respectively. The gel is then calcined to form the active nanoparticle. The technique has advantage in effective fabrication of metal oxide such as silica, homogeneity of nanoparticle and low processing temperature. Afandi *et al.,* [109], have compared this method to other type of nanoparticle synthesis procedure such as impregnation, and found that metal active phase is well distributed on the support material, the functionalized carbon nanotubes (*f*CNTs).

Mesoporous (2-50 nm) SiO_2 have been used as a great inorganic incapsulating layer of metal oxide core, due to their high thermal stability and a simple sol-gel synthetic strategies [112]. The major limitations of sol-gel synthetic chemistry include several factors such as a high cost of metal alkoxide, residual carbon associated, toxic organic solvent involved, longer processing time [82-83]. For these and many other reasons, sol-gel method is rarely utilized in nanoparticle synthesis.

2.9.2. Impregnation method

Being one of the fasted and easy nanoparticle synthesis procedure, impregnation method is a straightforward nanoparticle synthesis technique. Incipient impregnation method, also known as dry or capillary impregnation, is highly used to fabricate heterogenous catalysts. In this method, a solution containing catalyst is introduced or impregnated into the pores of the support materials by capillary action followed by drying. For porous material such as SiO_2 and γ-Al_2O_3, the pores can be easily filled or impregnated by a dopants during synthesis, which can increase the size of the crystal due to agglomeration [109]. Blockage of the pores can lead to a reduced surface area, and this can be detrimental for catalysis. Rodrigues *et al.*, [68], impregnated CeO_2 with copper-oxide sourced from $Cu(NO_3)_2$ precursor in an excess solvent upon rotary evaporator. The catalyst exhibited small surface area (S.Area = 13 m^2/g) relative to its counterparts, such as that synthesised by co-precipitation (S.Area = 15 m^2/g). However, the catalyst managed to convert ~86 % CO at 100 ^oC during CO(PrOx) reaction. In addition to simplicity [32], impregnation is highly useful in sealing the pores of the support material, thus found vast application in electrode fabrication to consolidate the grain boundaries of polycrystalline nano material with the aim of enhancing the mobility and conductivity along this border [26, 86, 87]. Confinement of CoO inside the bimodal mesoporous carbon (BMS) framework to improve its cathodic activity through synergy in Li-O_2 rechargeable batteries, was carried out successfully using wet impregnation method by, Zhang *et al.,* [116]. The resulting CoO-(BMS) solid material had high initial capacity (4000 mA h g^{-1}), higher rate capability with low overpotential, and prove to be active towards system biproduct's (i.e., Li_2O_2 and carbonates) decomposition, with greater cycling stability. Nonetheless, impregnation method is not beneficial in designing highly porous materials thereby limiting its application in nano catalysis, even though the mobility benefits induced by grain boundaries resistant minimization by this technique, could be envied. The method also produces high amounts of waste due to concomitant 'evaporation' reaction during the technique, therefore not environmentally benign for large scale applications.

2.9.3. Urea combustion method

For highly porous small nanocrystalline material, inexpensive process such as combustion using low heat igniting fuels as urea could go a long way [117]. Here, a required amount of a metal salt precursor and urea are dissolved in distilled water and heated to ~60 – 90 °C. The resulting viscous gel is then calcined at high temperatures (~500 °C), were it ignites (combust) rapidly, realising large amounts of gases, which attributes to most of the textural properties of a material prepared by this technique [117]. For instance, Yin *et al.,* [91], noted an increase in pore size and surface area of nitrogen doped cobalt catalyst, N-Co_3O_4 (prepared in closed system), which were much greater than those of the pristine Co_3O_4 (prepared in an open system), due to the releases of large amount of NH_3 from pyrolysis of excess urea during synthesis. The catalysts demonstrated higher catalytic activity in CO(PrOx) owing to a highly porous material synthesised by this technique, as well as an increase in oxygen vacancies because of the impurity atom, the nitrogen, ascertaining an importance of composition during catalyst preparation.

2.9.4. Precipitation method

Nanoparticles can be synthesized by a precipitation technique, in which particles are accumulated by means of solidified material in a solution or on a solid material. The major steps driving this precipitation process include supersaturation, nucleation, and growth (i.e., aggregation into macroscopic crystals). The precipitates are usually formed as crystalline solids as the supersaturation of reaction intermediates increase (diminution of their equilibrium solubility), due to reduced transfer rate between suspended particles [118]. This slows down the Oswald ripening, a thermodynamically favoured crystal growth process by deposition of dissolved small particles onto larger ones. Metal-hydroxide and metal-carbonates are usually the preferred precipitates due to ease of decomposition to oxides (during calcination by air) with larger surface area without poisoning the catalysts (as by sulphur left when sulphates are used instead). They also have low solubility which implies easily accessible supersaturation level hence small precipitate particles [118]. Metallic and metal-sulphides crystalline solid precipitate are also possible. However, amorphous solids can be obtained at very high supersaturation, in which the aggregation rate exceeds the crystal lattice orientation rate. Two main types of precipitation method involve co-precipitation as well as deposition precipitation.

2.9.4.1. Co-precipitation method

The method is rendered as one of the most effective and reliable method to obtain well distributed homogeneous nanoparticles in metal-support systems. Co-precipitation techniques use a suitable base (NaOH, NH_4OH, TETA, Na_2CO_3) to solidify or precipitate metal particles in a mixture of solvated metal precursors solution at certain pH and simultaneously as a unified solid, hence 'co-precipitation'. Xu *et al.*, [82], prepared CuO_x-CeO_2 catalyst via co-precipitation method and managed to obtain finely distributed and uniformly dispersed CuO over CeO_2 support. This allowed strong Cu-Ce interaction, which supressed the formation of metallic copper (Cu^0) from an active phase, Cu^+, earning a remarkable catalytic property in CO(PrOx) reaction. It converted ~100% CO into CO_2, even at higher temperatures (235 ^oC). Malwadkar *et al.*, [8], had also found similar results in terms of homogenous distribution of cobalt species within the pores of ceria matrix containing copper, using co-precipitation approach. Javaid and Nanba [119], reported that high catalytic activity of MgO-CeO_2 supported Ru for NH_3 synthesis was attributed to the higher dispersion of Ce, selective precipitation of Ru (i.e. on CeO_2 not MgO) and large surface area when this catalyst was prepared by co-precipitation method (and impregnation), as compared to conventional physical mixing technique. Furthermore, their XRD profile demonstrated low peak intensity of MgO prepared by impregnation method, relative to the one executed by co-precipitation, which clearly indicates low exposure of such crystal planes in the former, and crystal planes or facets contain atoms and electrons needed for catalysis, which was the underlaying reason why co-precipitation fabricated Ru/MgO-CeO_2 catalyst demonstrated such high activity. Co-precipitation technique is usually the preferred method in nanoparticle synthesis and always ubiquitous in the fabrication of compounds at their nanoscale as a hyphenated technique (i.e., combined with other technique such as microemulsion, hydrothermal etc.,) to synthesise highly active catalysts.

The method is simple and time saving, easy to control particle distribution and composition, with various possibilities to modify the overall homogeneity and provide higher output yield of a solid product [120]. However, it has always been known that extreme care must be undertaken to avoid independent or consecutive solidification of NPs. The pH adjustment and standardization at the beginning of the reaction co-operatively and continuously with reactants using a suitable base can slightly adjust this slight limitation [118]. This slight limitation relative to other techniques makes co-precipitation the best method of catalysts preparation in the time of its history.

2.9.4.2. Deposition-precipitation (DP) method

Unlike co-precipitation procedure, DP involves precipitating nanoparticles from a solid material such as a support rather than solution as unity. The solid support is usually suspended in solution containing a substance to be deposited such as metal ions, which precipitates as in co-precipitation but 'banking' (deposited) on a solid support [121]. The various ways in which the precipitate is formed, classifies DP into either homogenous or heterogenous DP. The former involves precipitation of metal ion homogenously and slowly by urea hydrolysis, in which high dispersion and small sized particles of large surface area are expected and the latter involves precipitating quickly by an aqueous base [121]. Deposition precipitation has many advantages over other conventional methods (impregnation, sol-gel, physical mixing, combustion methods etc.,) in terms of creating pure and homogeneous solid nanoparticles. Higher distribution of active components within a support is highly possible with this method. Few years ago, Chang *et al.,* [122], synthesized Au-Ru/Fe_2O_3 catalysts by deposition and co-precipitation methods, and obtained a well dispersed Au and Ru on Fe_2O_3 surface, for sample prepared by deposition precipitation (TEM evident). These led to a strong metal-metal and metal-support interactions that facilitated the activation site, leading to enhanced oxygen mobility and subsequently increased catalytic activity for partial oxidation of methanol, in H_2 synthesis. The same group also demonstrated that the reduction of Au and Ru to their metallic state occurred at much low temperature for catalyst prepared by deposition precipitation method as compared to co-precipitation technique. However, depositing an active phase on a solid support could limit the entirety of the support phase to participate in chemical catalysis [6], since the support surface will be populated by metal phase and those atoms in the bulk of the support remains chemically inert. On the other hand, when the two phase (support-metal) are precipitated as one (co-precipitation), the resulting solid catalyst features a strong interaction between the support and the metal, and the new surface area is of both the metal and the support.

In real time experiments all these discussed techniques including co-precipitation as well as deposition precipitation methods can be modified or coupled with additional stages. Closed systems such as reflux as well as hydrothermal in a Teflon autoclave, are some additional experimental procedures that are coupled with various techniques to obtain maximum yield and unique physicochemical properties.

2.9.5. Reflux assisted nanoparticle synthesis method

In chemical synthesis, reflux refers to boiling a substance while simultaneously cooling the vapour by a condenser back into the reaction vessels [94-95]. During nanoparticles synthesis in an alkaline media (such as in Co_3O_4 preparation from alkaline $Co(OH)_2$ precursor) by reflux method, the constant influx of the solvent breaks the gel like cobalt-hydroxide structure into more energetically favoured small crystals, maintaining the total concentration of species present, thereby ensuring high product yield at low reaction temperatures (i.e., the temperature close to that of a boiling point of a solvent used) [113]. In nanomaterial fabrication, aqueous based reflux method provides precise control of morphology, particle size and crystallinity by varying the time of reflux, cooling rate, order of precursor introduction as well as the type of the solvent [81, 94]. In general, a faster cooling rate leads to increase in defects, and incomplete phase formation occurs when reaction is stopped too early with subsequent formation of bulk species when the reaction is refluxed for too long. The order of precursor introduction impacts ternary and quaternary system in which undesired separate phase favoured by formation of a more stable bimetallic exist [123].

The reflux stage is also important in preserving simple compounds with low boiling point such as organic substances (surfactants, polymers, capping agents etc) that are normally used in stabilization and shape/size control of nanoparticles during synthesis [96-98]. After precipitating a mixture of CNTs, surfactant polymers (composed of $PMEO_2MA_{84}$-b-P(St_{61}-co-tAA_5) and cobalt acetate tetrahydrate in ethanolic solution by ammonia hydroxide (27-30 vol.%), followed by reflux at 85 ^oC for 3 hours, Kuo *et al.*, [65], obtained a highly crystalline Co_3O_4@CNTs catalyst with abundant {111} and {220} planes, associated with the spinel Co_3O_4 nanostructure. The spherical (polymer/surfactant induced property) Co_3O_4 NPs were uniformly distributed along the CNTs and had average particle size 0.5-2 nm, which explained the remarkable catalytic activity towards CO oxidation exhibited by this catalyst (~100% CO conversion between 25 - 200 ^oC). The preservation of these organic structure directing agents and stabilizers by reflux, could’ve been the reason why such physicochemical behaviour accompanied by such high catalytic activity was obtained, and this attributes for the reflux stage are scarce in the paper. This minor gap suggests further investigations in reflux assisted nanoparticle synthesis. Nonetheless, the prepared Co_3O_4/CNTs catalyst reported by the same group of Kuo *et al.*, [65], was also promoted by fluorinated alkyl chains (XPS verified; F 1s peak at 688 eV) to modulate the surface hydrophobicity of CNTs, and the results demonstrated good catalytic activity in moisture-feed gas environment at T > 150 ^oC.

This work thus envisages a catalyst prepared by reflux assisted co-precipitation technique in an inert atmosphere such as N_2, to exhibit high catalytic performance and stability towards CO(PrOx) reaction not only in moisture but also in CO_2 environment.

2.9.6. Hydrothermal assisted nanoparticle synthesis method

In 1845, a German geologist, Karl Emil Franz von Schafhäutl (1803–1890), successfully grew microscopic SiO_2 crystals (quartz) in a pressure cooker, by simply simulating a geological processes of rock formation and crystal growth, under hot water vapour [128]. Three years later a German chemist, Robert Bunsen, independently grew strontium as well as barium carbonate (at ~200 ^oC and 15 atm) in a stainless glass and pioneered a simple, low costly and environmentally benign way of synthesising high yields solid-state materials. At that time of history such solid materials as barium carbonate formed a centre and milestone precursors of perovskites (specifically $BaTiO_3$), one of the most ubiquitous material in electro ceramics with diverse application e.g., in piezoelectric ceramics, multilayer capacitors and thermal sensors [104, 105].

The technique gained so much popularity and to date, known as the hydrothermal method, this method involves performing a chemical reaction in a solvent (water) contained in a sealed stainless-steel pressure vessel called an autoclave, in which the temperature of the solvent can be brought to around their critical point by heating synchronously with an autogenous pressure [98-99]. In this way, crystals that have higher vapor pressure close to their melting point are easily obtained, and the reaction's high pressures and temperatures further aid in one-step development for highly crystalline material without post annealing treatment. For example, metal oxide phase such as CeO_2-ZrO_2 structure could be obtained during hydrothermal treatment [27], and co-exist with the expected M-OH solid phase in an alkaline solution. Such pre-existing metal oxide phase before post annealing treatments could serve as a seed/substrate for epitaxial as well as topotactic type of growth mode, directing the resulting final structure as M-OH oxidizes in air during calcination, which could lead to a highly controlled nanoparticle, by simply controlling the size and shape of the seed during hydrothermal treatment [98–100]. A study by Adak *et al.*, [7], demonstrated a novel synthetic route using CTAB and PVP to control the morphology, particle size and distribution of CuO_x over CeO_2 nanoparticles in hydrothermal conditions, and obtained the best physicochemical properties that attributed to the remarkable catalytic activity in CO(PrOx) reaction in excess H_2.

Again, from a children's perspective, during hydrothermal treatment, particles acquire enough kinetic energy and become mobile. Generally, the mobility, reaction cooling rate as well as the complexity of the lattice structure dictate the degree of crystal formation [94, 99]. The accrued mobility as a function of hydrothermal temperatures (> 100 ^oC, [128]) catalysed by high pressure within the autoclave, allows nanoparticles to achieve a greater homogenised distribution and high dispersion. Afandi *et al.*, [109], developed Ni-Ce/fCNTs-(H), using hydrothermal technique, and obtained about ~92% CH_4 and 96% CO_2 conversion respectively, at 800 ^oC during CO_2 reforming of methane to syngas. The catalyst was highly stable, and its outstanding high activity is owed to well Ni and Ce distribution over f-CNTs. Hydrothermal technique has found vast application in many aspect of science from material digestion, crystal synthesis, chemical processing, hydrometallurgy, fabrication of building materials and hardening [128]. A natural occurring spinel compound, $MgAl_2O_4$ (gemstone), generated from MgO and Al_2O_3 at temperature > 1200 ^oC can be easily obtained in an autoclave, at temperature of just 300 ^oC and pressures of about 98 bar [128], making this technique monumental for synthesis of spinel (including Co_3O_4) based catalysts, as in this study. When organic solvent is used instead of water in hydrothermal treatment, the technique is called solvothermal.

Traditional dry methods of synthesizing nanoparticles of various dimensions and shapes such as chemical vapour deposition (~550 ^oC), thermal decomposition and evaporation (~210-815 ^oC), chemical spray pyrolysis (~350-400 ^oC) as well as vacuum-based techniques such as vacuum deposition, requires a huge amount of energy annihilation in the form of heat and ultra-high vacuum conditions, and for these reasons, they are rarely deployed in nano catalyst fabrication [82, 94]. Non vacuum techniques such as electrodeposition and solution processing, use toxic chemical substances and organic solvents that are detrimental to the environment [123].

Another important factor impacting the resulting material beside the technique used in preparation, is the strength of the acidity within the chemical environment. Different researchers have ploughed various strategies that helped to understand and control various textural properties of a material such as morphology, particularly by exploitation of pH during nanoparticle synthesis.

2.10. EFFECT OF pH DURING NANOPARTICLE SYNTHESIS

The pH of the environment at which the catalysts are prepared has a greatinfluence on the resulting material. For example, Ma *et al.*, [132], fabricated $SmMn_2O_5$ catalyst by tuneable hydrothermal technique, and noticed a peculiar anisotropic behaviour in which the catalyst changed morphology, from nanorod to nanoparticle when the pH was increased from 3 (acidic) to 9 (alkaline). The nanoparticles exhibited higher NO conversion to NO_2 than nanorod. Furthermore, the long-thick samarium hydroxide ($Sm(OH)_3$ nanorods as well as agglomerated lump-like $SmMn_2O_5$ were observed at relatively high pH ~12. The anisotropic nature of the paradoxical $SmMn_2O_5$ nanorods and nanoparticle at pH of 3 was due to irregular solution charge density, arising from proton adsorption in such acidic environments. This led to different growth rate and hence different morphology, which showed different catalytic activity.

Lee and co-workers [133], recently reported the same monotonical behaviour after noticing a perturbing change of irregular grain-like MoS_2 particles, to a flower-like morphology, upon increase in the pH value. The team deciphered that hydrothermal treatment of sample at pH ~9,5 increased the MoS_2 crystallinity by enhancing the packing of the (002) lattice planes. This catalyst together with its counterpart (obtained at pH ~7,0) had higher activity in CO methanation than catalyst treated hydrothermally at pH = 4.5. The enhanced methanation catalytic activity was facilitated by formation of sulphur vacancies resulting from complete decomposition of a precursor salt, ammonium tetrathiomolybdate (ATTM), to MoS_2 at those higher pH values (pH ~7.0 & 9.5). Such physicochemical properties do have similar impact in related reactions, including CO(PrOx).

2.11. STABILISATION OF METAL NANOPARTICLES

Nanoparticles follow the same laws of nature from their formation and sometimes throughout their lifespan and utilisation. As in most living organism, life begins by fertilization followed by growth whereas in the world of the nanoparticles, it begins by nucleation, and then growth. Nucleation of nanoparticles is the beginning of condensation of a supersaturated solution [134]. A highly ordered phase of high local density is obtained if the condensed phase is crystalline [134]. Aggregation and coagulation of metal nanoparticles (MNPs) as a result of their highly dispersed state during nanoparticle nucleation and crystal growth needs to be stabilized [108]. Excessive Ostwald ripening (OR), is a fundamental 'need stabilization' spontaneous process (thermodynamically favoured) of crystal growth that could impoverish small sized particles by forming larger ones, and that could severely deteriorate catalytic capabilities by reducing the surface area [60]. The reverse of Ostwald ripening is the digestive ripening, which is also a mode of a crystal growth but unlike OR, it is kinetically favoured and results in a uniform and narrow size distribution, which also needs to be stabilized during their development. Immobilization onto the support and encapsulation of these nanoparticles in an organic ligand shell, such as capping agents which includes simple molecules, polymers and surfactants are few remedies recommended by several authors to aid in MNPs stabilization, size and shape manipulation [26, 76, 96, 98, 101, 105-106].

2.11.1. Capping agents and their role in nanoparticle fabrication

In nano synthesis, capping agents (CAs) are binding molecules that are added and utilized in fraction of quantity for precise nanoparticle growth (i.e., size and shape) control and stabilization during synthesis [136]. They cover ("capping") a refined surface of metal nanoparticle and prevent them from coagulation and aggregation during a chemical reaction thus, inhibiting the growth along one direction while allowing other directions to facilitate crystal growth, thereby determining the shape (i.e., structure directing agents) [106, 107].

Capping agents such as polyvinylpyrrolidone (PVP) control the size and shape of nanoparticle by several modes. They ensure that agglomeration doesn't take place via the mentioned inevitable thermodynamic spontaneous processes of particle growth, the Oswald ripening [60], which leads to a narrow particle size distribution since most particles will exist in large size at equilibrium, thus resulting in low dispersion. Capping agents facilitate the metal-support anchoring, which dramatically increases their dispersion [108]. Capping agents that are normally utilized in nanoparticle synthesis include small organic molecules (ligands, such as citrate) and ligands of Mw ~50-150 Da, polymers (PVP, PVA, PEG), dendrimers (PAMAM), cyclodextrins, reducing agents ($NaBH_4$), surfactants (CTAB, ADBS, SDS), polysaccharides and proteins (e.g., bovine serum albumin) [76, 105-107]. They pave many applications in biomedical and pharmaceutical for biofunctionalization, in which they provide functional groups for attachments of drugs and biomolecules on a nanoparticle, for cancer as well as other chronic disease treatment including diabetes, for instance; Chitosan-Liposomes; antidiabetic, PVA-Ag and PEG-TiO_2; anticancer [136].

The mode of stabilization of nanoparticles by capping agents can involve various types of interaction including electrostatic, dipole-dipole, ion-dipole, hydration forces, van der Waals forces, steric hindrance, or combination of these interactions, which themselves depend highly on the zeta potential of the surface of the nanoparticle. For instance, PVP uses the negatively charged oxygen amide induced resonance through carbonyl group (i.e., $C\text{-}O^-$ group) in the pyrrolidone moiety to bind preferentially to Au {100} ions, via the electrostatic attraction, which kinetically prohibits them from growing, while simultaneously permitting growth along the <111> directions to obtain Ag nanowires [137]. Furthermore, PVP is a bulky, nontoxic, non-ionic polymer with diverse functional groups (C=O, C-N & CH_2) used in nanoparticle synthesis and the resulting nanoparticles have elongated distance that the PVP can be regarded as a nano dispersant. Another study had also reported that successful incorporation of the Au nanoparticle inside mesoporous Si-MCM-41 framework attributes to the electrostatic attraction between the positively charged CTAB head group within the porous silica 'Mobi' composite (i.e., positive Zeta potential) and the negative charge of the precursor salt, $[AuCl_4]^-$ [138], demonstrating the importance of a precursor salt. The study further recommended that exploring various method of surfactants removal rather than calcination would circumvent undesired crystal aggregation, and maintain the nanoparticles within the support, as was shown to coalesce on the surface of the Si-MCM-41 when calcined at 500 °C for 12 h. Again, a surfactant bound NPs can provide functionality for PVP molecule to bind and aid in stabilization (see Figure 2.3).

More studies are conducted each year to get full insight into the nature and chemistry induced by capping agents and how they affect physical and chemical properties of nanoparticle. Zhao *et al.,* [139], designed a highly ordered mesoporous architecture, Co_3O_4/Ce-ZrO_2 catalyst using CTAB surfactant as a capping agent, and achieved ~65% CO conversion at 125 °C in CO(PrOx). On the other hand, a relatively low CO conversion (~10%) was obtained when the anionic surfactant ammonium dodecylbenzene sulfonate (ADBS) was used instead. The low activity was corroborated to residual sulphur (NH_3-TPD and FTIR evident), which gave the acidic nature of the catalyst that was apt to break the equilibrium of the surface acidic and basic sites, resulting in very low catalytic activity. Zhao *et al.,* [139], suggests that, choosing an appropriate capping agent is also important in nanoparticle synthesis and this is still a challenge [108].

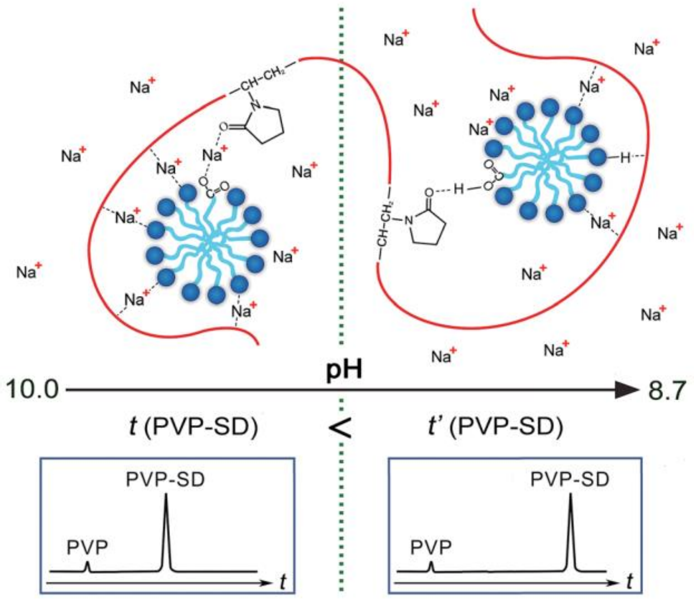

Figure 2.3 Metal cation (Na^+) PVP-SD (polymer/surfactant) pH dependent complexation in a basic water solution [140].

Using a small organic ligand, citric acid, rather than large molecules (polymers/surfactants) as a capping agent, Xu *et al.,* [82], obtained highly crystalline and spherically shaped CuO_x-CeO_2, that resulted in a quite strong Cu-Ce interaction, which supressed $Cu^+ \rightarrow Cu^0$ reaction by facile Ce^{3+}/Ce^{4+} redox couple, maintaining the active Cu^+ species. The catalyst showed 100% CO conversion, even at a higher temperature (>120-235 °C), whereas many reported catalysts in the literature impoverish, as a result of low selectivity at higher temperature in H_2 rich stream [24, 85, 120]. The team used a polydentate ligand, hexamethylenetetramine ($(CH_4)_6N_4$), as precipitating agent, and with its chelating effect, nanoparticle capping and stabilization was maximized, which could have been the reason behind a highly controlled spherical catalyst looking product, but such attributes are not deciphered in this paper.

Great understanding into role of capping agent in nano catalysis and recent advancements for these potential substances in nanomaterial synthesis was touched briefly by Campisi's *et al.,* [108]. Capping agents are widely reported as stabilizing agents and as enhancers, that facilitates anchoring of metal active phase onto the support, resulting in higher metal dispersion, but only limited studies touched on the chemistry and relation between these properties and effects linked to capping agents directly. On a catalytic point of view, many capping agents enclose a nanoparticle inside like a capsule, and these could hinder the active sites, especially when that capping agent is found in the final product of the catalyst [137]. Luo *et al.*, [141], reported that the strongly adsorbed PVP on the surface of Pt-Pd doped CdS photocatalyst had negative impact on the overall catalytic activity. The rate of H_2 yield was ~359 μmol/h when the catalyst had PVP adsorbed on its surface and 1583 μmol/h when the PVP was removed by $NaBH_4$/tert-butylamine (TBA), during partial oxidation of methanol. The increased activity was correlated to more available active site after PVP removal. Thus the concentration of PVP adsorbed on the surface of the catalyst determines the catalytic activity [141].

2.11.1.1. Interfaces as a function of capping agents in metal solution

Campisi's *et al.,* [108], elaborated the physical mechanism and chemistry associated with capping agents that give rise to such manifesting catalytic behaviour, which arise from interfaces. The composition, spatial arrangement, and specific interaction of the capping agent with metal surface and other chemical species (reactants/solvent) are function of metal-ligand interface (MLIc) and metal-solution interface (MSIc). The two interfaces are said to be introduced by capping agents [108]. The textural properties, morphology and the energetics of these interfaces govern the overall kinetics of catalytic reactions, by altering the local environment around the active sites (i.e., crystal plane, edge, corners). Moreover, MLIc affect the catalytic activity and selectivity via various mechanisms such as charge transfer, molecular recognition, selective blocking, adsorption geometries and as mentioned, the steric hinderance.

Since heterogeneous catalysis involves breaking and formation of bond between the catalysts and the reactants, which imply their electronic properties, the activity and selectivity of a catalyst can be enhanced by charge transfer or other type of electronic changes taking place at the MLIc. The border between this effect is very unstable and kinetically labile, and depends highly on the nature and the strength of metal-ligand interactions (MLIn) and kinetics depends on battle between the ligand and the reactant for an active site [26, 82]. Strong MLIn leads to catalyst deactivation [108]. Sometimes altered electronic density originated by charge transfer and polarization at MLIc can promote the activation of the adsorbed species and enhancing catalytic activity [82, 122].

2.11.1.2. Electronic induced character by surface capped nanoparticle

A study by Tsunoyama *et al.,* [143], revealed a remarkable catalytic property, owing to a special electronic mechanism induced by PVP coated gold (Au) nanoparticle. Electron donation by the PVP molecule adsorbed on the Au surface increase the electronic density on the Au core, which are then donated to the π* orbitals of molecular O_2 thus, activating it to superoxide (O_2^-) (see Figure 2.4). These enhanced the catalytic activity during aerobic oxidation of alcohols.

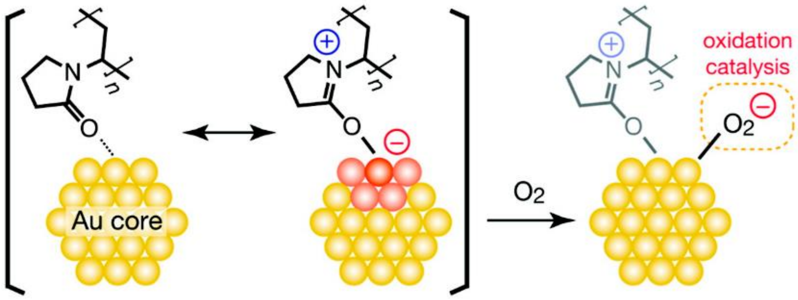

Figure 2.4 Induced charge transferer mechanism between PVP and Au nanocluster for activation of molecular oxygen [104].

In a more rational manner, such partially negative charged nanoparticles can be stabilized by pie acceptor ligands such as CO to relieve that excessive charge density, just like in Fischer carbenes. These can dramatically influence the catalytic activity by selectively adsorbing such reactant (CO), which could subsequently be beneficial for CO(PrOx) reactions, yet no study had ever considered such electronic induced plausible selectivity. The molecular weight and concentration of PVP dictates its fractional coverage on the surface of the nanoparticle, in turn determines its morphology, decomposition temperature and more importantly the redox potential of the resulting capped nanomaterial [137]. PVP is believed to lie flat on the nanoparticle surface and its high binding energy arising from direct carbonyl interaction or van der Waals forces [137]. Nevertheless, capping agents also have their own limitation ranging from difficulties and complexity of their removal from metal surface for catalysis applications, to their uncontrolled interactions (van der Waals, electrostatic forces, hydrogen bonding, adhesive forces etc.,) with the nanoparticles. The removal of capping agents such as PVP from the surface of the nanoparticle for specific application without altering the morphology, is also a challenge in the art of nanoparticle synthesis and engineering, as it requires specialized technique, cautious heat treatments or even the prescribed expensive chemicals such as $NaBH_4$/tert-butyl amine, H_2O_2/H_2SO_4 [137]. Therefore, studying capping agents adsorbed on the surface of the catalyst prior to CO(PrOx) reactions is of also great importance, and this is rarely done in the literature.

2.12. METHODS USED TO CHARACTERISE METAL OXIDES CATALYST FOR CO(PrOx)

In CO(PrOx) catalysis and related processes such as adsorption, structural properties plays and important role thus, catalyst materials must be characterised to link the catalytic performance to physicochemical properties.

2.12.1. SPECTROSCOPIC CHARACTERISATION

Atomic structure is unique for every element, which allows electromagnetic radiation to interact uniquely with such materials, forming a basis behind light characterisation and thus spectroscopy [111]. Spectroscopic techniques are utilised everywhere from biochemistry to material science, including catalysis such as in CO(PrOx) for structural elucidation and characterisation.

2.12.1.1. Fourier Transform Infrared (FTIR) Spectroscopy

Fourier transform infrared spectroscopy (FTIR) relies on the functional group of a substance to characterise a material and remain a powerful tool for structural elucidation [7-12]. A certain functional group would adsorb a specific frequency of [144]. As a result, information regarding the bond strength and the nature of the bond between two species can be identified [145]. A study reported by Sidi-yacoub *et al.,* [146], dedicated to identify lignocellulosic component during pyrolysis of exhausted sugar beet pulp (ESBP), relied exclusively on the FTIR technique to characterise the material. The instrument demonstrated the presents of lignin polysaccharide (cellulose and hemicellulose). These were characterised by the C-H vibrational mode at 2909 cm^{-1} with free and esterified carboxylic groups peaks, centred at 1730-1745 and 1630-1635 cm^{-1} respectively, assigned to the pectin structure. The antifungal nano material composing of polyol coated Zn and Cu (ZnO@PEG and CuZn@DEG) nanoflowers, synthesised by solvothermal technique have been confirmed via the FTIR spectroscopy by Tryfon and co-workers [147]. They reported the -OH mode of glycol (or H_2O adsorbed) was noticed ~3450 cm^{-1} and the strong peaks at around 1660 and 1600 cm^{-1}, attributed to the oxidized form of the DEG and PEG respectively. However, the team couldn't detect any M-O IR peak below 500 cm^{-1} in CuZn@DEG fungicide but ZnO@PEG had a distinctive peak at ~451 cm^{-1} due to the Zn-O bond. The FTIR spectroscopy is very powerful in studying surface capping agents coated nanomaterial, such as PVP-coated nanoparticle [12, 17].

2.12.1.2. Scanning Electron Microscopy (SEM)

After the revolution in wave-particle duality of light, people started to utilise electron wave to visualize samples and materials, simulating conventional low resolution (~0.2 μm) optical light microscopes [148]. Scanning electron microscope (SEM) uses a tungsten filament and or lanthanum hexaboride crystals as source of electrons (electron gun) for microstructural visualization (see Figure 2.5 (a)). Microstructures are directly linked to mechanical, electrical, magnetic and catalytic properties, and depends heavily on the preparation method. For instance , Guimarães *et al*., [149], witnessed a plaque like morphology on a hydrothermally prepared CuO/CeO_2 catalyst, with well distributed CuO species using SEM technique. The morphology was distinctive from a spongy like structure of a CuO/CeO_2 counter catalyst prepared by precipitation technique, which featured agglomerated CuO species. CO(PrOx) activity has been found to vary exclusively on different Co_3O_4 catalyst's morphology, increasing from nanoplate > nanorod > nano-cubes > nanosphere, in a study reported by Dey and Dhal [36]. These shows the importance of shows the importance of microstructures towards the reactivity properties of the developed material and emphasise the importance of preparation method.

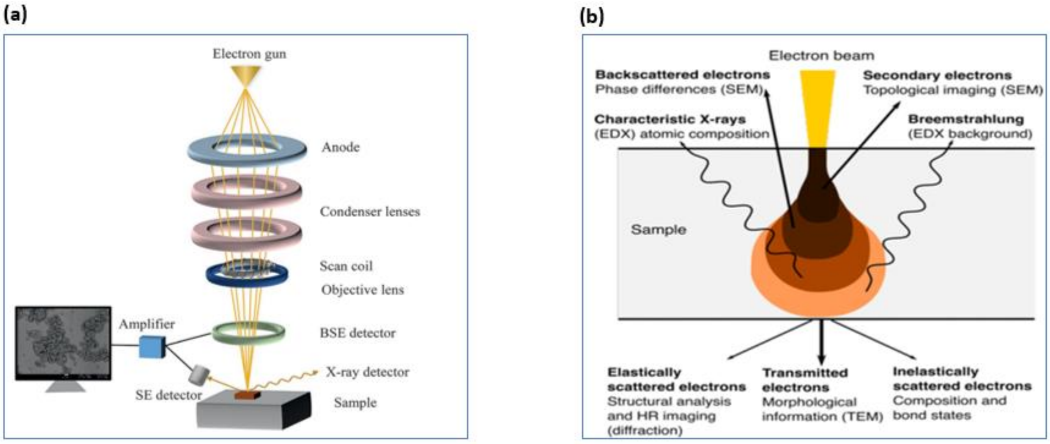

Figure 2.5 (a) depicts the main components of SEM instrument, [143], and a typical electron-sample interaction in electron microscopy (b), [145].

SEM samples are normally analysed in a vacuum chamber to minimize atmospheric gas-electron interaction, which could attenuate electron acceleration and thus temper with resolution [15, 17]. Non-conducting nanomaterial such as some metal oxides, CNTs as well as liquids or liquid forming substances (DNA, proteins, lipids, and other biological molecules) remain a challenge to conventional SEM analysis. For these reason, modern SEM instruments such as field emission electron microscope (FESEM) as well as environmental SEM are deployed [3, 15, 17]. Non-conducting limitations of SEM can be side-stepped by coating a sample with a conducting material such as gold or carbon, prior to imaging.

2.12.4. Transmission electron microscopy (TEM)

Transmission electron microscopy principles are similar to those of SEM [150]. However, as can be seen from the Figure 2.5 (b), TEM is based mainly on transmitted (or tunnelled) electrons, inelastic and elastic scattered electrons, in order to visualise the 2-D structure of a material and nanocomposite [148]. High resolution images obtain from TEM (HRTEM) allows crystal structure determination, and operated with conjunction of selected area electron diffraction (SAED) and energy dispersive x-ray spectroscopy (EDX), TEM can also provide crystallographic and elemental mapping of material in real time, allowing greater resolution in depth of inner structure of the synthesised nano materials and their elemental composition/dispersion [15, 20-22]. Motha *et al*., [151], has recently used TEM to confirmed that copper and manganese are incorporated into a crystal structure of CeO_2 (evident by HRTEM lattice fringes), and the resulting $Ce_{0.85}Cu_{0.10}Mn_{0.05}O_{2-\delta}$ catalyst, showed good performance in CO(PrOx) reaction (100% CO conversion, at T = 150 °C). By examining the SAED pattern, the polycrystalline nature and the dispersion of a catalyst can be identified, as was done in Cu-CeO_2 based catalysts, used for CO(PrOx) reaction [152].

2.12.1.3. Powder x-ray diffraction

X-ray spectroscopy remains one of the most vital characterisation techniques in most of the developed material. Atoms or molecules packed closely in a crystal can be thought of as planes, and these 'horizontal lattice grids or planes diffract x-ray light waves. Constructive interference happens when the diffracted wave is in phase with the next wave diffracted from the next crystal plane and this ' [111] happens only when the wavelength scattered is of the multiple integer value, as suggested by the Braggs law (see Figure. 2.6).

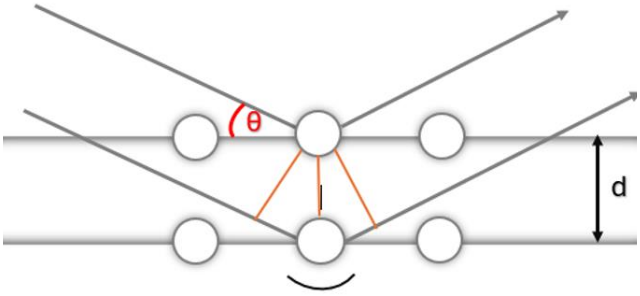

Braggs' law; $n\lambda = 2d\sin(\theta)$

Figure 2.6 Constructive interference between two x-ray waves scattered from adjacent atomic planes in a crystal in Braggs' experiment.

The angle at which the x-ray causes the atoms to diffract (e.g., as in constructive interference) gives the precise location of atoms in the planes, and crystal plane systematics can give a fingerprint about the lattice (or crystal) structure of the studied material [30, 112]. The intensity of the scattered beam depends on the overall structure factor of the crystal which relies on the atomic number as well as the positioning of the atoms. The x-ray spectrograph plots the intensity versus position (angle/2θ) and is itself a fingerprint of material's crystal structure. A stored diffraction database (JCPD) is useful to identify unknown solid sample from X-Ray data [27. 30]. Liu *et al.,* [144], developed a method of reconstructing the broken Si-O-Si bond iron ore tailings catalysts by $Ca(OH)_2$. The mechanism involved chemisorption of the broken Si-O-Si bond on the surface of calcium, forming calcium silicate phase evidenced by XRD spectroscopy ($2\theta = 29.5^{o}$). The XRD was also used to verify the Co_3O_4 [27, 28] and CeO_2 crystal structures [29, 30], both with catalytic value towards CO oxidation. The crystallite size can also be determined from the XRD pattern using Debey-Scherrer formular and it is strongly related to surface area of a material and thus, its adsorption properties and catalytic activity [111].

2.12.1.4. X-Ray photoelectron spectroscopy (XPS)

XPS also uses a form of x-ray radiation to photoemit electrons from the inner shells of the atoms on the surface of the materials, and record the emitted electron's energies [150]. These electron energies carry information about the atom emitting them as well as the local chemical and environmental state, since the binding energies (BE) of the electrons depends on the chemical bonding in the vicinity of an atom. Thus, the XPS spectrum is a mirror of the electronic structure of an atom in details, beside those electrons in the valence bands since their cross section is very much weaker, which gives less intensity in their spectral regions at low BE (<30 eV), and it is for this reason that core electrons are studied in XPS instead [14, 20]. XPS can also provide spin-orbital coupling information from energy state with higher azimuthal quantum number (l) greater than 1 such as ($l = 2,3,4$ in p, d, f orbitals respectively) resulting in peak splitting from same level with slightly different BE [20, 33]. XPS is so powerful in elucidating the oxidation state of metal oxide including catalysts. For example, Malwadkar *et al.,* [8] studied the effect of cobalt dopant in CuO/CeO_2 catalysts. Their

XPS data demonstrated surface enriched Co^{2+}, Co^{3+}, Cu^{2+}, Cu^{+}, Ce^{3+} and Ce^{4+} metal cation, which synergically carried out CO(PROX) activity.

2.12.2. THERMAL CHARACTERISATION

Materials can also be characterised by examining changes in some their properties of under a controlled temperature programme [154]. Characterising substance with temperature (thermal characterisation) involves the input of heat on a material and measurements in material's temperature susceptible changes, which depends highly on the material characteristic, such as the crystallinity, melting point, ignition characters, redox properties and more, making temperature a useful parameter in characterisations [149, 156].

2.12.2.1. Thermogravimetric analysis (TGA)

Thermogravimetric analysis is an analytical technique that measures the mass dynamics as a function of time during temperature variation [148–150]. In nanoparticle synthesis using organic reagents and stabilizers, the final product's purity and stability can be determined by TGA experiments [148, 149]. TGA usually plots weight loss (in %), with respect to either temperature or time (TGA curve) [38, 39]. The first derivative of the TGA curve is the differential thermogravimetric analysis (DTA) curve, which is often coupled with TGA to obtain in depth information such as melting points and transitional temperatures. Suresh *et al.*, [156], noticed the presence of organic residues on the FTIR spectrograph of CeO_2 nanoparticles (NPs) which was confirmed by the TGA analysis. The team noticed a major weight loss (~4%) of CeO_2 NPs at 400 °C due to adsorbed H_2O/organics decomposition. Furthermore, oxygen weight loss at higher temperature (~800 °C) was also noticed with a small percentage (~1%), due to ceria reduction, validating the strength of TGA to provide information about redox reactions. Sarruf *et al.,* [160], used TGA technique and observed a change in the stability of Co_3O_4 catalyst above 850 °C, due to oxygen mass loss of 7%, from $Co_3O_4 \rightarrow CoO$ reaction. Most polymers usually melt before decomposition, and TGA is also powerful in studying the thermal stability of such polymers [157] and useful in studying capping agents adsorbed on the surface of the NPs [36, 37].

2.12.2.2. Temperature programmed reduction (TPR)

Temperature programmed reduction (TPR) is another type of thermal characterising technique based on a programmed temperature control to induce a reduction reaction between a solid catalyst and a gaseous substance [11, 31, 41]. In heterogenous catalytic component consisting of a support and an active phase, TPR can be so powerful in elucidating the effect and nature of metal-support interaction [97]. When H_2 is used as a reducing agent, the technique is referred to as the H_2-TPR. Other reducing agents such as CO are also wonderful probes for TPR experiments. A typical H_2-TPR plot signal from a detector (e.g., TCD signal, effluent H_2O mole fraction and or H_2 consumption), as a function of temperature (or time). The crystalline phase formation of wuestite ($Fe_{1-x}O$) based catalysts during reduction has shown to strongly depends on the presence of the promoters, as confirmed by H_2-TPR in Folke's work [100]. The reduction temperature of various metal oxides such as Co_3O_4 [158], CuO_x [45, 46], CeO_2 [29, 47], MnO_x [41, 48] etc., depends highly on the oxidation state of the metal surface as well as the nature of the neighbouring substances such as the metal oxides support and metal dopants [8]. For example, it was found that Co_3O_4 and CuO_x reduces in two steps, with first reduction temperature at around 300 ^oC and the second one at around 500 ^oC assigned to transformation of various oxidation states in each metal oxide [160]. However, for multicomponent system, the H_2 peak signals can overlap, which makes it difficult to interpret H_2-TPR data without peak deconvolution [160]. Folke *et al.,* [100], suggested that peak asymmetry could indicate overlaying reduction steps or high order kinetics.

2.12.3. BET SURFACE AREA, VOLUME AND POROSITY CHARACTERISATION

Thermal characterisations and spectroscopic techniques cannot provide surface area measurements [150]. As reviewed, CO(PrOx) reaction is manly heterogenous catalysis, with gaseous CO molecules and a solid catalyst reacting together to facilitate oxidation reaction. A quantitative relationship between the pressure of gaseous molecules adsorbed on the surface of the catalysts and the concentration of the active sites at constant temperature, provide a useful representation of kinetics of surface catalysts reaction. This relationship is known as the adsorption isotherm [150]. Several types of adsorption isotherms exist, but in porous materials, the Brunauer-Emmett-Teller (BET) isotherms (Type I, II, III, IV & V) is the most encountered isotherms for solid-gas reaction [39, 49, 50]. BET measurements are performed under gaseous N_2 at its boiling point (77 K), and the adsorption and desorption dynamics of this gas are used to obtain textural information of solid material such as surface area, pore size and pore volume, which are all linked to catalytic activity [39, 49, 54]. Pandey *et al.,* [163], observed a mixture of dissimilar porosity characterised by the presence of both type IV and type II N_2 adsoprtion/desoprtion isotherms, on Fe_3O_4/PVP nanoparticles. The type IV isotherm is a characteristic of a mesoporous powdered sample and is vital for catalysis and adsorption reactions [163]. Specific pore volume (or surface area) and pore size distribution of a solid catalysts samples can be easily obtained by the Barrett-Joyner-Halenda (BJH) adsorption/desorption technique [159]. The high catalytic activity towards CO oxidation in moisture rich conditions was ascribed to the high dispersion of Pd nanoparticles within the mesoporous CeO_2 of a slit like pores in Pd/CeO_2 catalyst, studied by N_2 sorption isotherm [164].

2.13. REFERENCES

[1] H. Liu, D. Guo, W. Zhang, and R. Cao, “$Co(OH)_2$ hollow nanoflowers as highly efficient electrocatalysts for oxygen evolution reaction,” Journal of Materials Research, vol. 33, no. 5, pp. 568–580, 2018.

[2] X. Guo, J. Mao, and R. Zhou, “Influence of the copper coverage on the dispersion of copper oxide and the catalytic performance of CuO/CeO_2 (rod) catalysts in preferential oxidation of CO in excess hydrogen,” Journal of Power Sources, vol. 371, pp. 119–128, 2017.

[3] A. Shakoor, F. Ashraf, S. Shakoor, A. Mustafa, A. Rehman, and M. M. Altaf, “Biogeochemical transformation of greenhouse gas emissions from terrestrial to atmospheric environment and potential feedback to climate forcing,” Environmental Science Pollution Research, vol. 27, no. 31, pp. 38513–38536, 2020.

[4] N. Guerrero Moreno, M. Cisneros Molina, D. Gervasio, and J. F. Pérez Robles, “Approaches to polymer electrolyte membrane fuel cells (PEMFCs) and their cost,” Renew. Sustain. Energy Rev., vol. 52, pp. 897–906, 2015.

[5] C. Wang, Q. Cheng, X. Wang, K. Ma, X. Bai, S. Tan, Y. Tian, T. Ding, L. Zheng, J. Zhang, and X. Li, “Enhanced catalytic performance for CO preferential oxidation over CuO catalysts supported on highly defective CeO_2 nanocrystals,” Applied Surface Science, vol. 422, pp. 932–943, 2017.

[6] T. Cwele, N. Mahadevaiah, S. Singh, and H. B. Friedrich, “Applied Catalysis B : Environmental Effect of Cu additives on the performance of a cobalt substituted ceria ($Ce_{0.90}Co_{0.10}O_{2-\delta}$) catalyst in total and preferential CO oxidation,” Applied Catalysis B: Environmental, vol. 182, pp. 1–14, 2016.

[7] S. Adak, J. Rabeah, R. Ranjan, T.S. Khan, M.K. Poddar, R.K. Gupta, T. Sasaki, S. Kumar, A. Bordoloi, C.S. Gopinath, and A. Brückner. "In-situ experimental and computational approach to investigate the nature of active site in low-temperature CO-PROX over $CuOx-CeO_2$ catalyst". Applied Catalysis A: General, 624, p. 118305, 2021.

[8] S. Malwadkar, P. Bera, and C. V. V Satyanarayana, “In fl uence of cobalt on performance of $Cu-CeO_2$ catalysts for preferential oxidation of CO,” vol. 38, pp.

941–950, 2020.

[9] N. Bion, F. Epron, M. Moreno, F. Mariño, and D. Duprez, “Preferential oxidation of carbon monoxide in the presence of hydrogen (PROX) over noble metals and transition metal oxides: Advantages and drawbacks,” Topics in Catalysis, vol. 51, no. 1–4, pp. 76–88, 2008.

[10] A. Arango-Diaz, J. A. Cecilia, J. Marrero-Jerez, P. Nuñez, J. Jiménez-Jiménez, and E. Rodríguez-Castellón, “Freeze-dried Co_3O_4-CeO_2 catalysts for the preferential oxidation of CO with the presence of CO_2 and H_2O in the feed,” Ceramics International, vol. 42, no. 6, pp. 7462–7474, 2016.

[11] T. M. Nyathi, N. Fischer, A. P. E. York, and M. Claeys, “Environment-Dependent Catalytic Performance and Phase Stability of Co_3O_4 in the Preferential Oxidation of Carbon Monoxide Studied in Situ,” ACS Catalysis, vol. 10, no. 20, pp. 11892–11911, 2020.

[12] O.H. Laguna, M.I. Domínguez, S. Oraá, A. Navajas, G. Arzamendi, L.M. Gandía, M.A. Centeno, M. Montes and J.A. Odriozola, “Influence of the O_2/CO ratio and the presence of H_2O and CO_2 in the feed-stream during the preferential oxidation of CO (PROX) over a CuO_x/CeO_2-coated microchannel reactor,” Catalysis Today, vol. 203, pp. 182–187, 2013.

[13] E. D. Park, D. Lee, and H. C. Lee, “Recent progress in selective CO removal in a H2-rich stream,” Catalysis Today, vol. 139, no. 4, pp. 280–290, 2009.

[14] K. Liu, A. Wang, and T. Zhang, “Recent advances in preferential oxidation of co reaction over platinum group metal catalysts,” ACS Catal., vol. 2, no. 6, pp. 1165–1178, 2012.

[15] S. Xing, H. Su, M. Yang, H. Gong, S. Ban, C. Zhao, and H. Wang, “Experimental optimization analysis on operating conditions of CO removal process from hydrogen-rich reformate,” International Journal of Hydrogen Energy, vol. 48, no. 64, pp.25216-25230. 2022.

[16] L. Wolski, G. Nowaczyk, S. Jurga, and M. Ziolek, “Texture and Catalytic Activity of Au-CeO_2 Catalysts in Low-Temperature Oxidation of Benzyl Alcohol,” Catalysts, vol. 11, no. 5, p.641.2021.

[17] C. Pojanavaraphan, W. Nakaranuwattana, A. Luengnaruemitchai, and E. Gulari, “Effect of support composition and metal loading on Au/$Ce_{1-x}Zr_xO_2$ catalysts for the oxidative steam reforming of methanol,” Chemical Engineering Journal, vol. 240, pp. 99–108, 2014.

[18] J. Saavedra, T. Whittaker, Z. Chen, C. J. Pursell, R. M. Rioux, and B. D. Chandler, “Controlling activity and selectivity using water in the Au-catalysed preferential oxidation of CO in H_2,” Nat. Chem., vol. 8, no. 6, pp. 584–589, 2016.

[19] L. Du, W. Wang, H. Yan, X. Wang, Z. Jin, Q. Song, R. Si, and C. Jia, “Copper-ceria sheets catalysts: Effect of copper species on catalytic activity in CO oxidation reaction,” Journal of Rare Earths, vol. 35, no. 12, pp. 1186–1196, 2017.

[20] L. B. Ngema, M.D. Farahani, S. Raseale, N. Fischer, A.S. Mohamed, S. Singh, and H.B. Friedrich, “In situ construction of a highly active surface interface for a $Co_3O_4|ZrO_2$ catalyst enhancing the CO-PrOx activity,” Surfaces and Interfaces, vol. 38, p. 102826, 2023.

[21] Q. Guo and Y. Liu, “MnOx modified Co_3O_4-CeO_2 catalysts for the preferential oxidation of CO in H_2-rich gases,” Appl. Catalysis B: Environmental, vol. 82, no. 1–2, pp. 19–26, 2008.

[22] W. Huan, J. Li, J. Ji, and M. Xing, “In situ studies on ceria promoted cobalt oxide for CO oxidation,” Chinese journal of catalysis, vol. 40, no. 5, pp. 656–663, 2019.

[23] S. Dey, G. Chandra, D. Mohan, and R. Prasad, “Synthesis of highly active Cobalt catalysts for low temperature CO oxidation,” Chemical Data Collections, vol. 24, p. 100283, 2019.

[24] J. Zhen, X. Wang, D. Liu, S. Song, Z. Wang, Y. Wang, J. Li, F. Wang, and H. Zhang, “Co_3O_4@CeO_2 core@shell cubes: Designed synthesis and optimization of catalytic properties,” Chemistry–A European Journal, vol. 20, no. 15, pp. 4469–4473, 2014.

[25] M. Konsolakis, M. Sgourakis, and S. A. C. Carabineiro, “Applied Surface Science Surface and redox properties of cobalt–ceria binary oxides : On the effect of Co content and pretreatment conditions,” Applied Surface Science, vol. 341, pp. 48–54, 2015.

[26] M. V. Konishcheva, D. I. Potemkin, P. V. Snytnikov, O. A. Stonkus, V. D. Belyaev, and V. A. Sobyanin, “The insights into chlorine doping effect on performance of ceria supported nickel catalysts for selective CO methanation,” Appl. Catalysis B: Environmental, vol. 221, pp. 413–421, 2018.

[27] T. Tsoncheva, R. Ivanova, J. Henych, M. Dimitrov, M. Kormunda, D. Kovacheva, N. Scotti, V. Dal Santo and V. Štengl, “Effect of preparation procedure on the formation of nanostructured ceria-zirconia mixed oxide catalysts for ethyl acetate oxidation: Homogeneous precipitation with urea vs template-assisted hydrothermal synthesis,” Applied Catalysis A: General, vol. 502, pp. 418–432, 2015.

[28] R. Samal, B. Dash, C.K. Sarangi, K. Sanjay, T. Subbaiah, G. Senanayake and M. Minakshi, “Influence of synthesis temperature on the growth and surface morphology of Co_3O_4 nanocubes for supercapacitor applications,” Nanomaterials, vol. 7, no. 11, p.356, 2017.

[29] L. Nguyen, S. Zhang, S. J. Yoon, and F. F. Tao, “Preferential Oxidation of CO in H_2 on Pure Co_3O_{4-x} and Pt/Co_3O_{4-x},” ChemCatChem, vol. 7, no. 15, pp. 2346–2353, 2015.

[30] X. Guo, Z. Qiu, J. Mao, and R. Zhou, “Shape-controlled $Cu_xCe_{1-x}O_2$ nanorods catalyst and the active components functioned in selective oxidation of CO in hydrogen-rich stream,” Journal of Power Sources, vol. 451, p. 227757, 2020.

[31] J. Ding, L. Li, H. Zheng, Y. Zuo, X. Wang, H. Li, S. Chen, D. Zhang, X. Xu, and Li, G, “Co_3O_4-$CuCoO_2$ Nanomesh: An Interface-Enhanced Substrate that Simultaneously Promotes CO Adsorption and O_2 Activation in H_2 Purification,” ACS Applied Material Interfaces, vol. 11, no. 6, pp. 6042–6053, 2019.

[32] S. A. Chernyak, D.N. Stolbov, K.I. Maslakov, S.V. Maksimov, R.V. Kazantsev, O.L. Eliseev, D.O. Moskovskikh, and S.V. Savilov, “Consolidated Co- and Fe-based Fischer-Tropsch catalysts supported on jellyfish-like graphene nanoflake framework,” Catalysis Today, vol. 397–399, pp. 296–307, 2022.

[33] T. G. Vo, P. Y. Tsai, and C. Y. Chiang, “Tuning selectivity and activity of the electrochemical glycerol oxidation reaction by manipulating morphology and exposed facet of spinel cobalt oxides,” Jornal of Catalysis, vol. 424, pp. 64–73,

2023.

[34] F. Zasada, J. Janas, W. Piskorz, M. Gorczyńska, and Z. Sojka, “Total Oxidation of Lean Methane over Cobalt Spinel Nanocubes Controlled by the Self-Adjusted Redox State of the Catalyst: Experimental and Theoretical Account for Interplay between the Langmuir-Hinshelwood and Mars-Van Krevelen Mechanisms,” ACS Catalysis, vol. 7, no. 4, pp. 2853–2867, 2017.

[35] H. Park, E.J. Lee, H. Woo, D. Yoon, C.H. Kim, C.H. Jung, K.B. Lee and K.Y. Lee, “Enhanced hydrothermal durability of Co_3O_4@CuO–CeO_2 Core-Shell catalyst for carbon monoxide and propylene oxidation,” Applied Surface Science, vol. 606, p. 154916, 2022.

[36] S. Dey and G. C. Dhal, “The catalytic activity of cobalt nanoparticles for low-temperature oxidation of carbon monoxide,” Material Today Chemistry, vol. 14, p. 100198, 2019.

[37] H. Shang, X. Zhang, J. Xu, and Y. Han, “Effects of preparation methods on the activity of CuO/CeO_2 catalysts for CO oxidation,” Frontiers of Chemical Science and Engineering, vol. 11, no. 4, pp. 603–612, 2017.

[38] F. Gao, H. Yan, X. Tang, H. Yi, S. Zhao, Q. Yu, and S. Ni, “Simultaneous removal of gaseous CO and elemental mercury over Cu-Co modified activated coke at low temperature,” Journal of Environmental Science (China), vol. 101, pp. 36–48, 2021.

[39] R. U. I. Wang, C. Chen, S. Deng, P. A. N. Shen, L. E. I. Gong, and N. Zhang, “Improvement of preferential co oxidation activity over CuO/Co_3O_4-CeO_2 catalysts: effect of co / ce ratio,” Journal of the Chilean Chemical Society, vol. 59, no. 4, pp.2710-2716, 2014.

[40] D. Gu, C.J. Jia, H. Bongard, B. Spliethoff, C. Weidenthaler, W. Schmidt, and F. Schüth, “Applied Catalysis B : Environmental Ordered mesoporous Cu – Ce – O catalysts for CO preferential oxidation in H_2 -rich gases: Influence of copper content and pretreatment conditions,” "Applied Catalysis B: Environmental, vol. 152–153, pp. 11–18, 2014.

[41] P. Garbis, C. Kern, and A. Jess, “Kinetics and reactor design aspects of selective

methanation of CO over a Ru/γ-Al_2O_3 catalyst in CO_2/H_2 rich gases," Energies, vol. 12, no. 3, pp. 1–15, 2019.

[42] U. Lucia, "Overview on fuel cells," Renewable and Sustainable Energy Reviews, vol. 30, pp. 164–169, 2014.

[43] W. Chen, B. Chen, K. Meng, H. Zhou, and Z. Tu, "Experimental study on dynamic response characteristics and performance degradation mechanism of hydrogen-oxygen PEMFC during loading," International Journal of Hydrogen Energy, vol. 48, no. 12, pp. 4800–4811, 2023.

[44] T. V. Reshetenko, K. Bethune, M. A. Rubio, and R. Rocheleau, "Study of low concentration CO poisoning of Pt anode in a proton exchange membrane fuel cell using spatial electrochemical impedance spectroscopy," Jorunal of Power Sources, vol. 269, pp. 344–362, 2014.

[45] A. Papavasiliou, T. Van Everbroeck, C. Blonda, B. Oliani, E. Sakellis, P. Cool, P. Canu, and F.K. Katsaros, "Mesoporous CuO/TiO_2 catalysts prepared by the ammonia driven deposition precipitation method for CO preferential oxidation: Effect of metal loading," Fuel, vol. 311, p. 122491, 2022.

[46] W. H. Chen and C. Y. Chen, "Water gas shift reaction for hydrogen production and carbon dioxide capture: A review," Applied Energy, vol. 258, p. 114078, 2020.

[47] D. B. Pal, R. Chand, S. N. Upadhyay, and P. K. Mishra, "Performance of water gas shift reaction catalysts: A review," Renewable and Sustainable Energy Reviews, vol. 93, pp. 549–565, 2018.

[48] J. Cao, X. Zhang, X. Ou, T. Liu, T. Xing, Z. Li, X. Zhou, H. Yan, Y. Liu, X. Feng, and Y. Tuo, "Reactant adsorption modulation by Fe and K in Pt catalyst for highly effective CO preferential oxidation in practical conditions," Chemical Engineering Journal, vol. 444, p. 136661, 2022.

[49] L. Chikh, V. Delhorbe, and O. Fichet, "(Semi-)Interpenetrating polymer networks as fuel cell membranes," Journal of membrane science, vol. 368, no. 1–2, pp. 1–17, 2011.

[50] H. Ishaq and I. Dincer, "Investigation and optimization of a new hybrid natural

gas reforming system for cascaded hydrogen, ammonia and methanol synthesis," Computers & Chemical Engineering, vol. 148, p. 107234, 2021.

[51] S. Sahebdelfar and M. T. Ravanchi, "Carbon monoxide clean-up of the reformate gas for PEM fuel cell applications: A conceptual review," International Journal of Hydrogen Energy, vol. 48, no. 64, pp. 24709-24729, 2022.

[52] U. Surya, M. Ali, M. Rizwan, A. Al-yaseri, A. Keshavarz, and S. Iglauer, "ScienceDirect Current advances in syngas (CO and H_2) production through bi-reforming of methane using various catalysts : A review," International Journal of Hydrogen Energy, vol. 46, no. 65, pp. 32809–32845, 2021.

[53] Y. Chen, J. Lin, and X. Wang, "Noble-metal based single-atom catalysts for the water-gas shift reaction," Chemical Communication, vol. 58, no. 2, pp. 208–222, 2022.

[54] Q. I. Roode-Gutzmer, D. Kaiser, and M. Bertau, "Renewable Methanol Synthesis," ChemBioEng Reviews, vol. 6, no. 6, pp. 209–236, 2019.

[55] D. B. Bukur, B. Todic, and N. Elbashir, "Role of water-gas-shift reaction in Fischer–Tropsch synthesis on iron catalysts: A review," Catalysis Today, vol. 275, pp. 66–75, 2016.

[56] R. García, M. V. Gil, F. Rubiera, D. Chen, and C. Pevida, "Renewable hydrogen production from biogas by sorption enhanced steam reforming (SESR): A parametric study," Energy, vol. 218, p. 119491, 2021.

[57] L. Zhong, T. Kropp, W. Baaziz, O. Ersen, D. Teschner, R. Schlögl, M. Mavrikakis and S. Zafeiratos, "Correlation between Reactivity and Oxidation State of Cobalt Oxide Catalysts for CO Preferential Oxidation," ACS Catalysis, vol. 9, no. 9, pp. 8325–8336, 2019.

[58] I. A. Ivanin, I. N. Krotova, O. V Udalova, K. L. Zanaveskin, and M. I. Shilina, "Synergistic Catalytic Effect of Cobalt and Cerium in the Preferential Oxidation of Carbon Monoxide on Modified Co/Ce/ZSM-5 Zeolites," vol. 62, no. 6, pp. 798–811, 2021.

[59] J. Lu, J. Wang, Q. Zou, D. He, L. Zhang, Z. Xu, S. He and Y. Luo, "Unravelling the Nature of the Active Species as well as the Doping Effect over Cu/Ce-Based

Catalyst for Carbon Monoxide Preferential Oxidation," Acs Catalysis, 9(3), pp.2177-2195, 2019.

[60] K. Mingle and J. Lauterbach, "Synthesis-structure-activity relationships in Co_3O_4 catalyzed CO oxidation," Frontiers of Chemistry, vol. 6, pp. 1–12, 2018.

[61] A. Mishra and R. Prasad, "A Review on Preferential Oxidation of Carbon Monoxide in Hydrogen Rich Gases," vol. 6, no. 1, pp. 1–14, 2011.

[62] R. Alcala, A. DeLaRiva, E.J. Peterson, A. Benavidez, C.E. Garcia-Vargas, D. Jiang, X.I. Pereira-Hernández, H.H. Brongersma, R. ter Veen, J. Staněk and J.T. Miller, "Atomically Dispersed Dopants for Stabilizing Ceria Surface Area," Appl. Catal. B Environ., vol. 284, no. November 2020, pp. 1–9, 2021.

[63] B. Qiao, A. Wang, X. Yang, L.F. Allard, Z. Jiang, Y. Cui, J. Liu, J. Li, and T. Zhang, "Single-atom catalysis of CO oxidation using $Pt_1/FeOx$," Nature chemistry, vol. 3, no. 8, pp. 634–641, 2011.

[64] A. Elmhamdi, L. Pascual, K. Nahdi, and A. Martínez-arias, "Applied Catalysis B : Environmental Structure / redox / activity relationships in $CeO_2/CuMn_2O_4$ CO-PROX catalysts," "Applied Catalysis B: Environmental, vol. 217, pp. 1–11, 2017.

[65] C.H. Kuo, W. Li, W. Song, Z. Luo, A.S. Poyraz, Y. Guo, A.W. Ma, S.L. Suib, and J. He, "Facile synthesis of Co_3O_4@ CNT with high catalytic activity for CO oxidation under moisture-rich conditions," ACS applied materials & interfaces, vol. 6, no. 14, pp.11311-11317, 2014.

[66] G. Grzybek, K. Ciura, J. Gryboś, P. Indyka, A. Davó-Quiñonero, D. Lozano-Castelló, A. Bueno-Lopez, A. Kotarba and Z. Sojka, "CO-PROX Reaction over $Co_3O_4|Al_2O_3$ Catalysts - Impact of the Spinel Active Phase Faceting on the Catalytic Performance," The Journal of Physical Chemistry C, vol. 123, no. 33, pp. 20221–20232, 2019.

[67] X.U. Yan, X.H. DU, L.I. Jing, W.A.N.G. Peng, Z.H.U. Jie, F.J. GE, Z.H.O.U. Jun, S.O.N.G.Ming and W.Y. ZHU, "A comparison of Al_2O_3 and SiO_2 supported Ni-based catalysts in their performance for the dry reforming of methane," Ranliao Huaxue Xuebao/Journal Fuel Chemical Technology, vol. 47, no. 2, pp. 199–208, 2019.

[68] A. Rodrigues, M. Cruz, E. Moreira, J. Fernandes, and J. Mansur, “New insights about the effect of the synthesis method on the CuO-CeO_2 redox properties and catalytic performance towards CO-PROX reaction for fuel cell applications,” Journal of environmental management, vol. 242, pp. 272–278, 2019.

[69] F. Liu, C. Okolie, R.M. Ravenelle, J.C. Crittenden, C. Sievers, P.C. Bruijnincx and B.M. Weckhuysen, “Silica deposition as an approach for improving the hydrothermal stability of an alumina support during glycerol aqueous phase reforming,” Applied Catalysis A: General, vol. 551, pp. 13–22, 2018.

[70] F. Liu, C. Okolie, R.M. Ravenelle, J.C. Crittenden, C. Sievers, P.C. Bruijnincx and B.M. Weckhuysen, “Silica deposition as an approach for improving the hydrothermal stability of an alumina support during glycerol aqueous phase reforming,” Applied Catalysis A: General, vol. 551, pp. 13–22, 2018.

[71] M. Ma, R. Yang, C. He, Z. Jiang, J.W. Shi, R. Albilali, K. Fayaz and B. Liu, “Pd-based catalysts promoted by hierarchical porous Al_2O_3 and ZnO microsphere supports/coatings for ethyl acetate highly active and stable destruction,” Journal of Hazardous Materials, vol. 401, p. 123281, 2021.

[72] H. Shin, M. Choi, and H. Kim, “A mechanistic model for hydrogen activation, spillover, and its chemical reaction in a zeolite-encapsulated Pt catalyst,” Physical Chemistry Chemical Physics, vol. 18, no. 10, pp. 7035–7041, 2016.

[73] P. Jing, X. Gong, B. Liu, and J. Zhang, "Recent advances in synergistic effect promoted catalysts for preferential oxidation of carbon monoxide," Catalysis Science & Technology, vol. 10, no. 4, pp.919-934. 2020.

[74] S.A. Singh and G. Madras, "Sonochemical synthesis of Pt, Ru doped TiO_2 for methane reforming," Applied Catalysis A: General., vol. (518), pp.102-114. 2016.

[75] A. Davó-Quiñonero, E. Bailon-Garcia, S. Lopez-Rodriguez, J. Juan-Juan, D. Lozano-Castello, M. García-Melchor, F.C. Herrera, E. Pellegrin, C. Escudero, and A. Bueno-Lopez, "Insights into the oxygen vacancy filling mechanism in CuO/CeO_2 catalysts: a key step toward high selectivity in preferential CO oxidation," ACS Catalysis, vol. 10, no. 11, pp.6532-6545. 2020.

[76] X. Cui, J. Liu, X. Yan, Y. Yang, and B. Xiong, “Exploring reaction mechanism of CO oxidation over $SrCoO_3$ catalyst: A DFT study,” Applied Surface Science, vol. 570, p. 151234, 2021.

[77] R. Mu, Q. Fu, X. Guo, X. Xu, D. Tan, and X. Bao, “A comparative study in structure and reactivity of ‘FeO_x-on-Pt’ and ‘NiO_x-on-Pt’ catalysts,” Science China Chemistry, vol. 58, no. 1, pp. 162–168, 2015.

[78] S. Dey, S. Sun, and N. S. Mehta, “Carbon monoxide catalytic oxidation over various iron-based nanoparticles at ambient conditions: A Review,” Carbon Capture Science Technology, vol. 1, p. 100013, 2021.

[79] J. Yu, Y. Yang, M. Zhang, B. Song, Y. Han, S. Wang, Z. Ren, L. Wang, P. Yin, L. Zheng and X. Zhang, “Highly Active MnCoOx Catalyst toward CO Preferential Oxidation,” ACS Catalysis, vol. 14, no. 3, pp. 1281–1291, 2024.

[80] D. Gamarra, G. Munuera, A.B. Hungría, M. Fernández-García, J.C.Conesa, P.A. Midgley, X.Q. Wang, J.C. Hanson, J.A. Rodríguez, and A. Martínez-Arias, "Structure− activity relationship in nanostructured copper− ceria-based preferential CO oxidation catalysts," The Journal of Physical Chemistry C, 111(29), pp.11026-11038. 2007.

[81] M. K. Koh, Y. J. Wong, S. P. Chai, and A. R. Mohamed, “Carbon dioxide hydrogenation to methanol over multi-functional catalyst: Effects of reactants adsorption and metal-oxide(s) interfacial area,” ournal of industrial and engineering chemistry, vol. 62, pp. 156–165, 2018.

[82] C. Xu, S. Li, Y. Zhang, Y. Li, and J. Zhou, “ScienceDirect Synthesis of CuO_x-CeO_2 catalyst with high-density interfaces for selective oxidation of CO in H_2-rich stream,” International Journal of Hydrogen Energy, vol. 44, no. 8, pp. 4156–4166, 2018.

[83] G. Marbán and A. B. Fuertes, “Highly active and selective CuO_x/CeO_2 catalyst prepared by a single-step citrate method for preferential oxidation of carbon monoxide,” Applied Catalysis B: Environmental, vol. 57, no. 1, pp. 43–53, 2005.

[84] S. A. Singh, S. Mukherjee, and G. Madras, “Role of CO_2 methanation into the kinetics of preferential CO oxidation on Cu/Co_3O_4,” Molecular Catalysis, vol.

466, no. November 2018, pp. 167–180, 2019.

[85] Z. Zhang, Y. Tian, W. Zhao, P. Wu, J. Zhang, L. Zheng, T. Ding and X. Li, “Hydroxyl promoted preferential and total oxidation of CO over ε-MnO_2 catalyst,” Catalysis Today, vol. 355, pp. 214–221, 2020.

[86] Z. Zhao, T. Bao, Y. Li, X. Min, D. Zhao, and T. Muhammad, “The supported CeO_2/Co_3O_4-MnO_2/CeO_2 catalyst on activated carbon prepared by a successive-loading approach with superior catalytic activity and selectivity for CO preferential oxidation in H_2-rich stream,” Catalysis Communications, vol. 48, pp. 24–28, 2014.

[87] V. D. B. D. Dasireddy, and B. Likozar, “Cu-Mn-O nano-particle/nano-sheet spinel-type materials as catalysts in methanol steam reforming (MSR) and preferential oxidation (PROX) reaction for purified hydrogen production,” Renewable Energy, 182, pp.713-724, 2022.

[88] V. D. B. D. Dasireddy, J. Valand, and B. Likozar, “PROX reaction of CO in $H_2/H_2O/CO_2$ Water–Gas Shift (WGS) feedstocks over Cu–Mn/Al_2O_3 and Cu–Ni/Al_2O_3 catalysts for fuel cell applications,” Renewable Energy, vol. 116, pp. 75–87, 2018.

[89] P. Gawade, B. Bayram, A. C. Alexander, and U. S. Ozkan, “Applied Catalysis B : Environmental Preferential oxidation of CO (PROX) over CoO_x/CeO_2 in hydrogen-rich streams: Effect of cobalt loading,” "Applied Catalysis B: Environmental, vol. 128, pp. 21–30, 2012.

[90] R. Mhlaba, T. Mosuang, and T. Magadzu, “Effect of Hydrazine Pretreatment on the Activity , Stability and Active Sites of Cobalt Species for Preferential Oxidation (PROX) of CO in H_2 -Rich Stream,” Chemistry, vol. 1, no. 1. pp. 164–179, 2019.

[91] C. Yin, Y. Liu, Q. Xia, S. Kang, X. Li, Y. Wang, and L. Cui, “Journal of Colloid and Interface Science Oxygen vacancy-rich nitrogen-doped Co_3O_4 nanosheets as an efficient water-resistant catalyst for low temperature CO oxidation,” vol. 553, pp. 427–435, 2019.

[92] J. L. Zhang and G. Y. Hong, "Nonstoichiometric Compounds," In Modern

inorganic synthetic chemistry, pp. 329-354, Elsevier B.V, 2017.

[93] T. S. Cam, S. O. Omarov, M. I. Chebanenko, S. G. Izotova, and V. I. Popkov, “Recent progress in the synthesis of CeO_2-based nanocatalysts towards efficient oxidation of CO,” Journal of Science: Advanced Materials and Devices, vol. 7, no. 1, p. 100399, 2022.

[94] F. Parrino, F. R. Pomilla, G. Camera-roda, V. Loddo, and L. Palmisano, "Properties of titanium dioxide." In Titanium Dioxide (TiO_2) and Its Applications, pp. 13-66. Elsevier, 2021.

[95] P. Adamski, W. Czerwonko, and D. Moszyński, “Thermal Stability of Potassium-Promoted Cobalt Molybdenum Nitride Catalysts for Ammonia Synthesis,” Catalysts, vol. 12, no. 1, 2022.

[96] D. Martínez del Monte, A. J. Vizcaíno, J. Dufour, and C. Martos, “Effect of K, Co and Mo addition in Fe-based catalysts for aviation biofuels production by Fischer-Tropsch synthesis,” Fuel Process. Technol., vol. 194, p. 106102, 2019.

[97] J. L. Ayastuy, E. Fernández-Puertas, M. P. González-Marcos, and M. A. Gutiérrez-Ortiz, “Transition metal promoters in CuO/CeO_2 catalysts for CO removal from hydrogen streams,” Internationa Journal of Hydrogen Energy, vol. 37, no. 9, pp. 7385–7397, 2012.

[98] H. Ronduda, M. Zybert, W. Patkowski, D. Moszyński, A. Albrecht, K. Sobczak, A. Małolepszy and W. Raróg-Pilecka, “Co nanoparticles supported on mixed magnesium–lanthanum oxides: effect of calcium and barium addition on ammonia synthesis catalyst performance,” RSC Advances, vol. 13, no. 7, pp. 4787–4802, 2023.

[99] T.N. Ye, S.W. Park, Y. Lu, J. Li, M. Sasase, M. Kitano, T. Tada and H. Hosono, “Vacancy-enabled N_2 activation for ammonia synthesis on an Ni-loaded catalyst,” Nature, vol. 583, no. 7816, pp. 391–395, 2020.

[100] J. Folke, K. Dembélé, F. Girgsdies, H. Song, R. Eckert, S. Reitmeier, A. Reitzmann, R. Schlögl, T. Lunkenbein and H. Ruland, “Promoter effect on the reduction behavior of wuestite-based catalysts for ammonia synthesis,” vol. 387, no. March 2021, pp. 12–22, 2022.

[101] A. B. Dongil, B. Bachiller-Baeza, E. Castillejos, N. Escalona, A. Guerrero-Ruiz, and I. Rodríguez-Ramos, “Promoter effect of alkalis on CuO/CeO$_2$/carbon nanotubes systems for the PROx reaction,” Catalysis Today, vol. 301, pp. 141–146, 2018.

[102] J. Antonio, A. Arango-díaz, V. Rico-pérez, A. Bueno-lópez, and E. Rodríguez-castellón, “The influence of promoters (Zr , La , Tb , Pr) on the catalytic performance of CuO-CeO$_2$ systems for the preferential oxidation of CO in the presence of CO$_2$ and H$_2$O,” Catal. Today, vol. 253, pp. 115–125, 2015.

[103] G. Sedmak and S. Ho˘, “Kinetics of selective CO oxidation in excess of H 2 over the nanostructured Cu 0 . 1 Ce 0 . 9 O 2 − y catalyst,” vol. 213, pp. 135–150, 2003.

[104] F. Marin, “Supported base metal catalysts for the preferential oxidation of carbon monoxide in the presence of excess hydrogen (PROX),” Applied Catalysis B: Environmental, vol. 58, no. 3-4, pp.175-183, pp. 175–183, 2005.

[105] C. Hudy, J. Gryboś, K. Steenbakkers, K. Góra-Marek, F. Zasada, and Z. Sojka, “Isotopic evidence for the tangled mechanism of the CO-PROX reaction over mixed and bare cobalt spinel catalysts,” Catal. Sci. Technol., vol. 12, no. 18, pp. 5723–5741, 2022.

[106] M. P. Woods, P. Gawade, B. Tan, and U. S. Ozkan, “Applied Catalysis B : Environmental Preferential oxidation of carbon monoxide on Co/CeO$_2$ nanoparticles,” "Applied Catalysis B: Environmental, vol. 97, no. 1–2, pp. 28–35, 2010..

[107] J. W. H. Leow and E. C. Y. Chan, “Atypical Michaelis-Menten kinetics in cytochrome P450 enzymes: A focus on substrate inhibition,” Biochem. Pharmacol., vol. 169, p. 113615, 2019.

[108] S. Campisi, M. Schiavoni, C. E. Chan-thaw, and A. Villa, “Untangling the Role of the Capping Agent in Nanocatalysis : Recent Advances and Perspectives,” no. Figure 1, pp. 1–21, 2016.

[109] N. S. Afandi, M. Mohammadi, S. Ichikawa, and A. R. Mohamed, “CO$_2$ reforming of methane to syngas over multi-walled carbon nanotube supported Ni-Ce

nanoparticles: effect of different synthesis methods," Environmental Science Pollution Resource, vol. 27, no. 34, pp. 43011–43027, 2020.

[110] C. H. Tu, A. Q. Wang, M. Y. Zheng, X. D. Wang, and T. Zhang, "Factors influencing the catalytic activity of SBA-15-supported copper nanoparticles in CO oxidation," Applied Catalysis A: General, vol. 297, no. 1, pp. 40–47, 2006.

[111] A. Ahmad, I. Ahmad, S. Ramzan, M. Z. Kiyani, D. Dubal, and N. M. Mubarak, Nanomaterial synthesis protocols. Elsevier Inc., 2021.

[112] K. An and G. A. Somorjai, "Nanocatalysis I: Synthesis of Metal and Bimetallic Nanoparticles and Porous Oxides and Their Catalytic Reaction Studies," Catal. Lett. 2014 1451, vol. 145, no. 1, pp. 233–248, Dec. 2014, doi: 10.1007/S10562-014-1399-X.

[113] K. An and G. A. Somorjai, "Nanocatalysis I: Synthesis of Metal and Bimetallic Nanoparticles and Porous Oxides and Their Catalytic Reaction Studies," Catalysis Letter, vol. 145, no. 1, pp. 233–248, 2014.

[114] R. Jokar, S. M. Alavi, M. Rezaei, and E. Akbari, "CO preferential oxidation in H_2-rich stream over the CuO-MnOx mixed oxide catalysts prepared by a facile mechanochemical preparation method," International Journal of Hydrogen Energy, vol.48, no.64, pp.24833-24844, 2022.

[115] H. Xie, C. Li, W.H. Kan, M. Avdeev, C. Zhu, Z. Zhao, X. Chu, D. Mu, and F. Wu, "Consolidating the grain boundary of the garnet electrolyte LLZTO with Li_3BO_3 for high-performance $LiNi_{0.8}Co_{0.1}Mn_{0.1}O_2/LiFePO_4$ hybrid solid batteries," J. Mater. Chem. A, vol. 7, no. 36, pp. 20633–20639, 2019.

[116] X. Zhang, R. Gao, Z. Li, Z. Hu, H. Liu, and X. Liu, "Electrochimica Acta Enhancing the Performance of CoO as Cathode Catalyst for Li-O_2 Batteries through Confinement into Bimodal Mesoporous Carbon," Electrochemical Acta, vol. 201, pp. 134–141, 2016.

[117] B. Abu-zied and A. M. Asiri, "Urea-Based Combustion Process for the Synthesis of Nanocrystalline Ni-La-Fe-O Catalysts," Journal of Nanomaterials, pp.126-126, 2012.

[118] C. Perego and P. Villa, "Catalyst preparation methods," Catalysis Today, vol. 34,

no. 3–4, pp. 281–305, 1997.

[119] R. Javaid and T. Nanba, “Efficient Ru/MgO–CeO_2 catalyst for ammonia synthesis as a hydrogen and energy carrier,” Int. J. Hydrogen Energy, vol. 48, no. 30, pp. 11214–11224, 2023.

[120] A. Noor Azeerah, A. A. Haliza, A. M. Zulina, and I. Zainab, “Co-precipitation technology for preparation of solid catalyst in oleochemical processes,” vol. 524, 2012.

[121] Z. Huang, F. Cui, J. Xue, J. Zuo, J. Chen, and C. Xia, “Cu/SiO_2 catalysts prepared by hom- and heterogeneous deposition-precipitation methods: Texture, structure, and catalytic performance in the hydrogenolysis of glycerol to 1,2-propanediol,” Catalysis Today, vol. 183, no. 1, pp. 42–51, 2012.

[122] F. W. Chang, L. S. Roselin, and T. C. Ou, “Hydrogen production by partial oxidation of methanol over bimetallic Au–Ru/Fe_2O_3 catalysts,” Applied Catalysis A: General, vol. 334, no. 1–2, pp. 147–155, 2008.

[123] S. K. Aditha, A. D. Kurdekar, L. A. A. Chunduri, S. Patnaik, and V. Kamisetti, “Aqueous based reflux method for green synthesis of nanostructures: Application in CZTS synthesis,” MethodsX, vol. 3, p. 35, 2016.

[124] H.C. Genuino, Y. Meng, D.T. Horvath, C.H. Kuo, M.S. Seraji, A.M. Morey, R.L. Joesten and S.L. Suib, “Enhancement of Catalytic Activities of Octahedral Molecular Sieve Manganese Oxide for Total and Preferential CO Oxidation through Vanadium Ion Framework Substitution,” ChemCatChem, vol. 5, no. 8, pp. 2306–2317, 2013.

[125] P. Zhan, “Large scale hydrothermal synthesis of β-$Co(OH)_2$ hexagonal nanoplates and their conversion into porous Co_3O_4 nanoplates,” Journal of alloys and compounds, vol. 478, no. 1–2, pp. 823–826, 2009.

[126] S. M. Lam, M. W. Kee, and J. C. Sin, “Influence of PVP surfactant on the morphology and properties of ZnO micro/nanoflowers for dye mixtures and textile wastewater degradation,” Materials Chemistry and Physics, vol. 212, pp. 35–43, 2018.

[127] Y. Chen, Y. Chen, P. Hu, S. Ma, and Y. Li, “The effects of PVP surfactant in the

direct and indirect hydrothermal synthesis processes of ceria nanostructures," Ceramics International, vol. 42, no. 16, pp. 18516–18520, 2016.

[128] N. Mertzsch, "Hydrothermal processes in industry," ChemTexts, vol. 6, no. 4, pp. 1–12, 2020.

[129] S. Xiong, J. S. Chen, X. W. Lou, and H. C. Zeng, "Mesoporous Co_3O_4 and CoO@C topotactically transformed from chrysanthemum-like $Co(CO_3)_{0.5}(OH)·0.11H_2O$ and their lithium-storage properties," Advanced Functional Materials, vol. 22, no. 4, pp. 861–871, 2012.

[130] J. Nai, J. Zhang, and X. W. (David) Lou, "Construction of Single-Crystalline Prussian Blue Analog Hollow Nanostructures with Tailorable Topologies," Chem, vol. 4, no. 8, pp. 1967–1982, 2018.

[131] Z. Zhang, Y. Song, and J. Sun, "Self-stacked $Co(OH)_2/Co_3O_4$ nanosheets for high-selectivity gas sensor to n-butyl alcohol," Applied Surface Science, vol. 610, p. 155438, 2023.

[132] S. jing Ma, X. wei Wang, T. Chen, and Z. hao Yuan, "Effect of surface morphology on catalytic activity for NO oxidation of $SmMn_2O_5$ nanocrystals," Chemical Engineering Jorunal, vol. 354, pp. 191–196, 2018.

[133] S. J. Lee, Y. S. Son, J. H. Choi, S. S. Kim, and S. Y. Park, "Morphology and catalytic performance of MoS_2 hydrothermally synthesized at various ph values," Catalysts, vol. 11, no. 10, pp. 1–12, 2021..

[134] S.J. Lee, S.S. Shin, Y.C. Kim, D. Kim, T.K. Ahn, J.H. Noh, J. Seo and S.I. Seok , "Fabrication of efficient formamidinium tin iodide perovskite solar cells through SnF_2–pyrazine complex," Journal of the American Chemical Society, vol. 138, no. 12, pp.3974-3977. 2016.

[135] I. A. Safo, M. Werheid, C. Dosche, and M. Oezaslan, "The role of polyvinylpyrrolidone (PVP) as a capping and structure-directing agent in the formation of Pt nanocubes," Nanoscale Adv., vol. 1, no. 8, pp. 3095–3106, 2019.

[136] R. Javed, M. Zia, S. Naz, S. O. Aisida, N. ul Ain, and Q. Ao, "Role of capping agents in the application of nanoparticles in biomedicine and environmental remediation: recent trends and future prospects," Journal of Nanobiotechnology,

vol. 18, no. 1, p. 172, 2020.

[137] K. M. Koczkur, S. Mourdikoudis, L. Polavarapu, and S. E. Skrabalak, “Polyvinylpyrrolidone (PVP) in nanoparticle synthesis,” Dalton transactions, vol. 44, no. 41, pp. 17883–17905. 2015.

[138] M. P. Mokhonoana, N. J. Coville, and A. K. Datye, “Small Au Nanoparticles Supported on MCM-41 Containing a Surfactant,” Catalysis letters, vol.135, pp. 1–9, 2010.

[139] Z. Zhao, R. Jin, T. Bao, X. Lin, and G. Wang, “Applied Catalysis B : Environmental Mesoporous ceria-zirconia supported cobalt oxide catalysts for CO preferential oxidation reaction in excess H_2,” "Applied Catalysis B: Environmental, vol. 110, pp. 154–163, 2011.

[140] Y. Wu, M. Chen, Y. Fang, and W. Wang, “Investigation of pseudo-polyanion formation between polyvinylpyrrolidone and sodium dodecanoate in aqueous solution by capillary electrophoresis, conductometry, tensiometry and calcium stability,” RSC Adv., vol. 7, no. 15, pp. 9338–9346, 2017.

[141] M. Luo, Y. Hong, W. Yao, and C. Huang, C., Xu, Q. and Wu, Q., "Facile removal of polyvinylpyrrolidone (PVP) adsorbates from Pt alloy nanoparticles," Journal of Materials Chemistry A, vol. 3, no. 6, pp.2770-2775, 2015.

[142] K. Deori, S. K. Ujjain, R. K. Sharma, and S. Deka, “Morphology controlled synthesis of nanoporous Co_3O_4 nanostructures and their charge storage characteristics in supercapacitors,” ACS Applied Material Interfaces, vol. 5, no. 21, pp. 10665–10672, 2013.

[143] H. Tsunoyama, N. Ichikuni, H. Sakurai, and T. Tsukuda, “Effect of electronic structures of au clusters stabilized by poly(N-vinyl-2-pyrrolidone) on aerobic oxidation catalysis,” Journal of the American Chemical Society, vol. 131, no. 20, pp. 7086–7093, 2009..

[144] J. hong Liu, Y. cheng Zhou, A. xiang Wu, and H. jiang Wang, “Reconstruction of broken Si-O-Si bonds in iron ore tailings (IOTs) in concrete,” International Journal of Minerals, Metallurgy, and Materials, vol. 26, no. 10, pp. 1329–1336, 2019.

[145] S. K. Paswan, S. Kumari, M. Kar, A. Singh, H. Pathak, J. P. Borah, and L. Kumar, “Optimization of structure-property relationships in nickel ferrite nanoparticles annealed at different temperature,” Journal of Physics and Chemistry of Solids, vol. 151, p. 109928, 2021.

[146] B. Sidi-yacoub, F. Oudghiri, and M. Belkadi, “Characterization of lignocellulosic components in exhausted sugar beet pulp waste by TG/FTIR analysis,” vol. 8, pp. 1801–1809, 2019.

[147] P. Tryfon, N.N. Kamou, S. Mourdikoudis, K. Karamanoli, U. Menkissoglu-Spiroudi, and C. Dendrinou-Samara, "CuZn and ZnO nanoflowers as nano-fungicides against Botrytis cinerea and Sclerotinia sclerotiorum: Phytoprotection, translocation, and impact after foliar application", Materials, vol. 14, no. 24, p.7600. 2021.

[148] J. Zhao and X. Liu, Electron microscopic methods (TEM, SEM and energy dispersal spectroscopy), 2nd ed. Elsevier Ltd., 2022.

[149] C. Guimarães, T. De Freitas, M. Iuki, M. Naceur, and J. Mansur, “Effect of nature of ceria support in CuO/CeO_2 catalyst for PROX-CO reaction,” vol. 97, pp. 245–252, 2012.

[150] J. Ekspong, Electrocatalysts for Sustainable Hydrogen Energy Disordered and Heterogeneous. 2021.

[151] S. Motha, A. S. Mahomed, S. Singh, and H. B. Friedrich, “Highly Active Cerium Oxide Supported Solution Combustion Cu/Mn Catalysts for CO-PrOx in a Hydrogen-Rich Stream,” Catalysts, vol. 14, no. 9, p. 603, 2024.

[152] O. M. Zhigalina, O.S. Morozova, D.N. Khmelenin, A.A. Firsova, O.V. Silchenkova, G.A. Vorobieva, A.V. Bukhtiyarov, E.N. Cherkovskiy and V.G. Basu, “Effect of Copper Particle Size on the Surface Structure and Catalytic Activity of Cu–CeO_2 Nanocomposites Prepared by Mechanochemical Synthesis in the Preferential CO Oxidation in a H_2-Rich Stream (CO-PROX),” Catalysts, vol. 14, no. 4, 2024.

[153] A. Elmhamdi, L. Pascual, K. Nahdi, and A. Martínez-arias, “Applied Catalysis B : Environmental Structure/redox/activity relationships in CeO_2/$CuMn_2O_4$ CO-

PROX catalysts," "Applied Catal. B, Environ., vol. 217, pp. 1–11, 2017.

[154] M. F. Gazulla, M. J. Ventura, and C. Andreu, "Characterization of Cobalt Oxides Transformations with Temperature at Different Atmospheres," Int J Chem Sci Res, vol. 17, no. 3, p. 312, 2019

[155] G. C. Egan, K. T. Sullivan, T. Y. Olson, T. Y. J. Yong-Jin Han, M. A. Worsley, and M. R. Zachariah, "Ignition and Combustion Characteristics of Nanoaluminum with Copper Oxide Nanoparticles of Differing Oxidation State," The Journal of Physical Chemistry C, vol. 120, no. 51, pp. 29023–29029, 2016.

[156] R. Suresh, V. Ponnuswamy, and R. Mariappan, "Applied Surface Science Effect of annealing temperature on the microstructural , optical and electrical properties of CeO_2 nanoparticles by chemical precipitation method," Applied Surface Science, vol. 273, pp. 457–464, 2013.

[157] J. P. Mofokeng and A. S. Luyt, "Morphology and thermal degradation studies of melt-mixed poly(lactic acid) (PLA)/poly(ε-caprolactone) (PCL) biodegradable polymer blend nanocomposites with TiO_2 as filler," Polymer Testing, vol. 45, pp. 93–100, 2015.

[158] M. T. Makhlouf, B. M. Abu-Zied, and T. H. Mansoure, "Direct Fabrication of Cobalt Oxide Nanoparticles Employing Sucrose as a Combustion Fuel," Journal of Nanoparticles, vol. 2013, pp. 1–7, 2013.

[159] Y. H. Tan, J. A. Davis, K. Fujikawa, N. V. Ganesh, A. V. Demchenko, and K. J. Stine, "Surface area and pore size characteristics of nanoporous gold subjected to thermal, mechanical, or surface modification studied using gas adsorption isotherms, cyclic voltammetry, thermogravimetric analysis, and scanning electron microscopy," Journal of materials chemistry, vol. 22, no. 14, pp. 6733–6745, 2012.

[160] B. J. M. Sarruf, J. E. Hong, R. Steinberger-Wilckens, and P. E. V. de Miranda, "$CeO_2Co_3O_4CuO$ anode for direct utilisation of methane or ethanol in solid oxide fuel cells," International Journal of Hydrogen Energy, vol. 43, no. 12, pp. 6340–6351, 2018.

[161] G. Hitkari, S. Sandhya, P. Gajanan, M. K. Shrivash, and D. Kumar, "Synthesis

of Chromium Doped Cobalt Oxide (Cr:Co_3O_4) Nanoparticles by Co-Precipitation Method and Enhanced Photocatalytic Properties in the Visible Region," J. Mater. Sci. Eng, vol. 07, no. 01, pp. 3–9, 2018.

[162] G. Ertl, S. B. Lee, and M. Weiss, "Kinetics of nitrogen adsorption on Fe(111)," Surface Science, vol. 114, no. 2–3, pp. 515–526, 1982.

[163] G. Pandey, S. Singh, and G. Hitkari, "Synthesis and characterization of polyvinyl pyrrolidone (PVP)-coated Fe_3O_4 nanoparticles by chemical co-precipitation method and removal of Congo red dye by adsorption process," International Nano Letters, vol. 8, no. 2, pp. 111–121, 2018.

[164] G. Li, L. Li, Y. Yuan, J. Shi, Y. Yuan, Y. Li, W. Zhao and J. Shi, "Highly efficient mesoporous Pd/CeO_2 catalyst for low temperature CO oxidation especially under moisture condition," Applied Catalysis B: Environmental, vol. 158–159, pp. 341–347, 2014.

CHAPTER 3

---

3. EXPERIMENTAL

3. 1. INTRODUCTION

As described in chapter 2, the method of catalysts preparation has a great influence on the resulting chemical and physical state of the catalysts. Designing the best synthesis method makes chemistry the centre in catalysis field [1-3]. Complex and highly non-spontaneous reaction characterised by high activation energy could be established at low temperatures using a catalyst, which imply low energy cost, and at high output/production. This chapter covers the detailed experimental methodology, based on the preparation and characterisations of Co_3O_4 supported CuO_x and CeO_2 catalysts; that were used for removal of CO in excess H_2 rich stream. All the solution and chemical reagents utilised in these experiments are explicitly listed for reference, with the names of chemical companies in the parenthesis and their corresponding % purity.

3.1. CHEMICAL REAGENTS AND SOLUTIONS

Chemical reagents and analytical salts were utilised as received, throughout the progress of this study. Analytical grade salts used as metal precursors include $Cu(NO)_3.3H_2O$ (ACE chemicals, purity ~98 %), $Co(NO)_3.6H_2O$ (Rochelle Chemicals (RC), ~ 97% purity) and $Ce(NO)_3.6H_2O$ from Sigma Aldrich (purity ~ 99%). Chemical ingredients such as cetyltrimethylammonium bromide (CTAB) together with polyvinyl pyrrolidone (PVP) were purchased from Sigma Aldrich (assay: min. ≥ 98%). Ethanolic solution (ratio, CH_3OH:H_2O; 50:50) was prepared in the laboratory from distilled-deionized water (d-H_2O) on the house, and 99.99 vol.% ethanol (CH_3OH) from GLASSWORLD company. Ammonium hydroxide (NH_4OH) or ammonia (NH_3) solution (25%), came from Rochelle Chemicals (RC). All gas cylinders which were used, containing 1% CO/He, 1% O_2/He and 15% CO_2/He mixtures, were purchased from African oxygen limited (AFROX). Pure nitrogen (N_2) and hydrogen (H_2) cylinder gases, as well as Helium's (He) also came from AFROX.

3.2. CATALYSTS SYNTHESIS METHODS

The chemical reagents and suitable preparation techniques chosen for this study were utilised in a concise and appropriate manner, to ensure precise control of nanoparticles during synthesis, which determined the resulting catalytic product.

3.2.1. Hydrothermal assisted precipitation method in Co_3O_4(Hyd) catalyst synthesis

Simulation of the catalyst preparation method reported by Adak *et al.,* [4], with slight modifications to synthesize Co_3O_4 catalyst involved the following details: A suitable amount of $Co(NO_3)_3.6H_2O$ salt was dissolved in 150 mL distilled water and stirred (at 4000 rpm) for 15 minutes, to ensure complete dissolution and homogeneity. Thereafter, 25% NH_4OH aqueous solution was introduced to the cobaltous solution dropwise while stirring, until a pH of ~8.0 was reached. Subsequently, a 50% ethanolic solution containing 0.2 g of CTAB, was added to the reaction mixture and further stirred for 1 h at room temperature. After 1 h of vigorous stirring, another 50% of ethanolic solution mixed with 0,099 g PVP was added, and the mixture was stirred for a further 2 h. A bluish-green dense blend was obtained and transferred into a Teflon autoclave. The Teflon autoclave was sealed within a stainless-steel pressure vessel and the solution was digested at 180 °C for 24 h. After allowing the vessel to cool down to ambient temperature, the pinkish liquid layer was decanted of the residual $Co(OH)_2$ precipitates. The precipitates were then washed carefully for several times with d-H_2O and collected by suction filtration. The wet solid brucite $Co(OH)_2$ precipitate was dried in the oven at 100 °C overnight. This sample was denoted as U-Co_3O_4(Hyd) (where U represents uncalcined). A small portion of this solid compound was calcined at 300 °C for 3 h in air, to obtained Co_3O_4 catalyst, which was denoted as Co_3O_4(Hyd). The preparation of Co_3O_4(Hyd) catalyst is depicted in Figure 3.1.

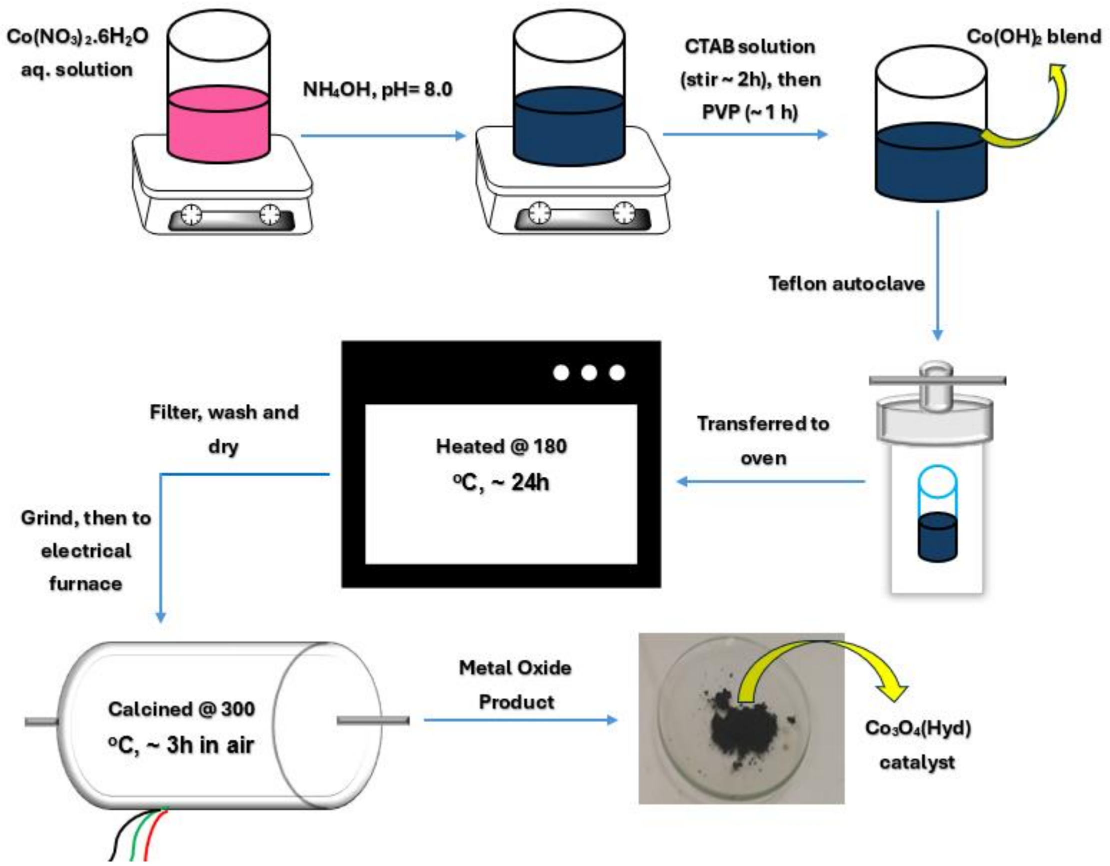

Figure 3.1 Schematic illustration of hydrothermal synthesis of Co_3O_4(Hyd) catalyst.

3.2.2. Preparation of μ-CuO_x/Co_3O_4(Hyd) catalysts by co-precipitation under hydrothermal method

Different amounts of CuO_x species in weight percentage (wt.%) were varied over Co_3O_4 support. Typically, an appropriated amounts (in g) of $Cu(NO)_3.3H_2O$ and $Co(NO)_3.6H_2O$ salts were pre-dissolved at once, in 150 mL d-H_2O. Thereafter, a similar procedure as described in section 3.2.1 was followed. The resulting catalysts were denoted μ-CuO_X/Co_3O_4(Hyd) (where μ = 3, 5, 10, 15 wt.%).

3.2.3. Synthesis of Co_3O_4(Hyd) supported CeO_2 catalysts by hydrothermal method

On the other hand, different wt.% of CeO_2 catalysts were also varied on Co_3O_4 catalysts, following a similar procedure used to prepare μ-CuO_X/Co_3O_4(Hyd) catalysts, and were named as β-CeO_2/Co_3O_4 (where β = 1, 3, 5 wt.%).

3.2.4 Preparation of ternary composites 5 wt.% CuO_X-βCeO_2/Co_3O_4(Hyd) catalysts under hydrothermal technique

A three metal (ternary) system composing of 5 wt.% CuO_X and various amount of β-CeO_2 (β = 0, 1, 3, 5 wt.%) supported on Co_3O_4 catalyst, were fabricated by similar preparation method. However, a required amount of $Cu(NO)_3.3H_2O$ and $Ce(NO)_3.6H_2O$ were dissolved in 50 mL d-H_2O, and another calculated amount of $Co(NO)_3.6H_2O$ salt was also dissolved separately in 100 mL d-H_2O. The mixtures were stirred for 30 minutes at room temperature. The copper-ceria nitrate aqueous solution was then transferred into the 100 mL solution of cobalt nitrate, under vigorous stirring. The resulting mixture was allowed to stir for 30 minutes before NH_4OH addition, upon which further steps were carried out likewise, as in other catalysts preparation (section 3.2.1-3.2.3). The final products were denoted as 5Cu-βCe/Co (β = 1, 3, 5 wt.%).

3.2.5. Reflux assisted precipitation method for Co_3O_4(Ref) preparation

Another Co_3O_4 support catalyst was also prepared by similar method reported by Adak *et al.*, [4], but with slight alterations. The procedure was carried out the same way as in section 3.2.1 (preparation of Co_3O_4(Hyd) catalyst); but the hydrothermal stage was replaced by a reflux stage (at 180 °C, for ~24 h), under N_2 environment (~1 atm, and 10 mL/min). Figure 3.2 represents a typical reflux setup. All the preparation conditions and composition were kept the same as in the previously developed pure Co_3O_4(Hyd) catalysts and was therefore denoted as (Co_3O_4(Ref)) (where Ref represents reflux). Calcination was also performed at 300 °C for 3 h in air.

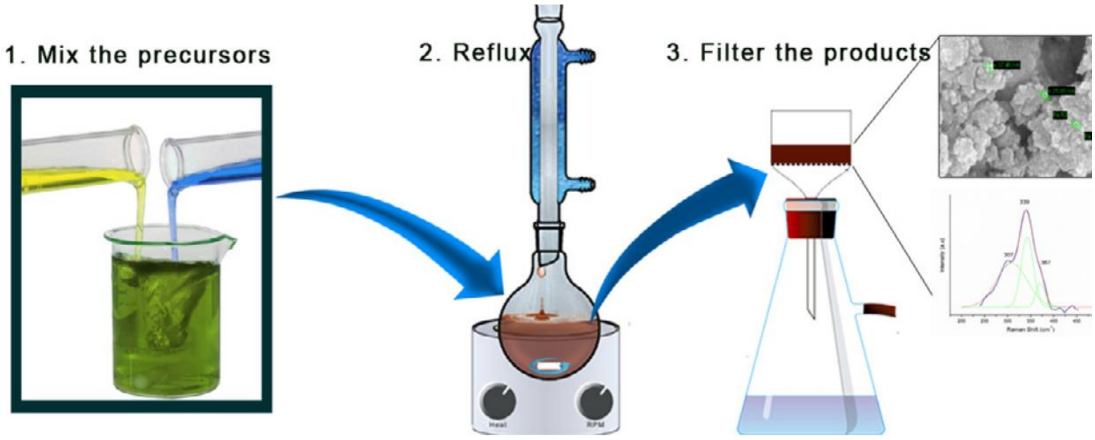

Figure 3.2 Graphical representation of a reflux setup and general procedure [5].

3.2.6. Preparation of μ-CuO_x/Co_3O_4(Ref) catalysts co-precipitation under reflux method

Likewise, another series of CuO_x/Co_3O_4 catalysts with varying CuO_x load were developed by reflux assisted co-precipitation method, following similar method used to develop μ-CuO_X/Co_3O_4(Hyd) (section 3.2.2) but replacing the hydrothermal treatment with reflux. These series of catalysts were denoted μ-CuO_x/Co_3O_4(Ref) (μ = 3, 5, 10, 15 wt.%).

3.2.7. Synthesis of Co_3O_4(Ref) supported CeO_2 catalysts via reflux method

The β-CeO_2/Co_3O_4(Ref) catalysts (β = 1, 3, 5 wt.%) were prepared similarly as β-CeO_2/Co_3O_4(Hyd) catalysts (section 3.2.3), although under reflux method.

3.2.8. Preparation of ternary 5 wt.% CuO_X-βCeO_2/Co_3O_4(Ref) catalysts by co-precipitation/reflux method

Likewise, a ternary catalytic system as 5 wt.% CuO_X-βCeO_2/Co_3O_4(Hyd) **was** also developed by N_2/reflux instead of hydrothermal treatment, following the same procedure as in section 3.2.4 and the catalysts were denoted 5Cu-βCe/Co(Ref) (β = 0, 1, 3, 5 wt.%).

3.3. CATALYSTS CHARACTERISATION

3.3.1. Fourier transform infrared (FTIR) spectroscopy

The FTIR spectra of all post-synthesised catalysts were recorded using a well-equipped Alpha II BRUKER FTIR spectrometer, at 10 cm^{-1} resolution per 100 scan measurements. On a crystal metal plate with pivotal 'pressing' clamp of the instrument, a small-powdered catalyst sample was mounted and then compressed. The IR frequency in wavenumber (cm^{-1}) interacting with these samples were allowed to range from 400-4000 cm^{-1}, and the transmitted light was then plotted as a function of the wavenumbers to obtain an IR spectrum. The Debey temperatures were also obtained from the FTIR spectra using equation (7), as per [6].

$$T_D = \frac{hcV_{12}}{k_B} \tag{7}$$

Here, $V_{12} = \frac{v1+v2}{2}$ is an average frequency of IR vibrations ($v1$ and $v2$ represent the frequency arising from either the A site or the B site cationic oxide in spinel catalyst, i.e., Co_3O_4), h represents the Planck constant (6.626 x 10^{-34} J.s), k_B is the Boltzmann constant (1.381 x 10^{-21} J/K) and c represents the velocity of light (3.0 x 10^{8} m/s).

3.3.2. Scanning electron microscopy (SEM)

SEM microstructures of all samples were recorded using Gemin Sigma 500 VP, ZEISS spectrometer, at 20 KX magnification and an optimum kV value of EHT = 3 kV. All powdered metal oxide samples were pre-mounted on a sticky circular black metal chip and coated with a sputter 'carbon' coater in an inert argon (Ar) environment, to prevent carbon oxides formation (coater's deterioration). The coating allows electrical conduction for imaging and prevent sample charging during SEM scan of NPs. The coated samples were stored in a vacuum sample chamber overnight to maximize air loss, that would have otherwise tempered with the electron's mean free path and thus image resolutions. Photomicrographs were obtained using the SEM spectrometer coupled to a computer monitor for image digitalization and microstructure conceptional processing.

3.3.3. Catalysts analysis by tunnelling electron microscopy (TEM)

Low resolution TEM images, Phase-contrast high-resolution TEM (HRTEM), energy dispersive spectroscopy (EDS/EDX), and selected area electron diffraction (SAED) measurements were captured by using Joel JEM-2100F transmission electron microscope, operated at 200 Kv. The instrument was equipped with Lanthanum hexaboride (LaB_6) electron source and charged coupled device (CCD) digital camera. Before TEM imaging, a small amount of catalyst sample was dispersed onto a 200-mesh sized Cu-grid, coated with a thin film made of lacy carbon material. Sample's average particle size (D) were estimated from the TEM images and the provided scale bar [6].

3.3.4. X-ray powdered diffraction (XRD) analysis

Crystal structures as well as phase transformation and compositional purity for all post-synthesised catalysts were elucidated using Bruker D8 small angle X-Ray scattering (SAXS) powder diffractometer, equipped with a monochromatic Cu-K_α radiation (λ = 0.15406 nm, 40 KV, 40 mA). The XRD patterns were collected from 15-75° of 2θ, at a scanning rate of 0.02°/s. The crystallite size was determined from Debey-Scherrer (equation 8) [7, 8].

$$D_{x.tal} = \frac{k\lambda}{\beta Cos\theta} \tag{8}$$

Here, $D_{x.tal}$ is the crystallite size, k is the Scherrer's constant (~0.9), λ is the wavelength of incident X-Ray radiation (for Cu Kα radiation, λ = 0.15406 nm) and diffraction pattern parameter, β, is the full width at half maximum (FWHM) height of the most intense diffraction peak.

3.3.5. Thermogravimetric analysis (TGA)

The phase transformation of the metal-hydroxide precursors obtained from either hydrothermal or reflux fabricated samples as well as the stability of the final metal-oxide catalysts, were investigated from the thermal reactions provided by the thermogravimetric analyser. The presence of organic capping agents (PVP/CTAB) as well as H_2O molecules adsorbed on the surface of the catalysts were also inspected to gauge the sample purity. Catalysts analysis by TGA was performed using TGA 4000: Perkin Elmer instrument. Approximately 10 mg of the catalyst sample was degassed upon heating at 100 °C in an oven (~1 h), then loaded into the sample pan and annealed from 35 °C, with a heating ramp of 10 °C/min to 700 °C under N_2 environment

(20 mL/min). The weight loss (in %) was plotted against temperature to obtain the TGA curves, from which the corresponding derivative curves were obtained.

3.3.6. Hydrogen temperature programmed reduction (H_2-TPR) analysis

Hydrogen temperature-programmed reduction (H_2-TPR) was used to study the redox properties and electronic behaviour of the as prepared catalysts. The H_2-TPR of the samples were carried out on an AutoChem II 2920 V4.06 TPR analyser, fitted with a thermal conductivity detector (TCD). In typical analysis, about 0.20 g of the metal oxide catalyst sample was first conditioned under 10 vol.% O_2/He mixture, for ~1–2 h at ambient temperature. TPR analysis was performed by flowing a H_2 gas in Ar rich stream (10 vol. % H_2/Ar) over the sample, while the temperature was increased linearly up to 900 ^oC at a heating rate of 10 ^oC/min. The H_2 consumption by the catalysts was monitored using a TCD detector.

3.3.7. Surface area and porosity studies

The specific surface area (S_{BET}) of the calcined catalysts was determined by the Brunauer-Emmett-Teller (BET) method and the pore features were analysed by the Barrett-Joyner-Halenda model. N_2 adsorption/desorption isotherms were recorded with a Nova 800 Physisorption Analyser, at the boiling point of liquid nitrogen (-196 ^oC or 77 K). Prior to the measurements, the samples were evacuated at 200 ^oC for 2 h to remove any pre adsorbed gases or contaminants. This was done by heating the catalysts at a heating rate of 5 ^oC/min, while soaking for 120 min towards the target temperature (200 ^oC). The final mass of the degassed catalyst samples varied between 0.12 – 0.15g.

3.4. CATALYTIC ACTIVITY TEST

The catalytic activity tests in CO(PrOX) reaction were carried out in a continuous flow fixed bed U-shape borosilicate glass reactor (inner diameter = 5 mm) system, situated inside a temperature programmable incinerator. In a typical analysis, a 100 mg of the powdered solid catalyst sample was weighed and supported on a cotton wool, to form a catalyst bed inside the U-shaped glass. The reactor bed was fitted inside the temperature programmer and degassed by helium gas (flow rate, 50 mL/min) at 60 ^{o}C. The flow rate of the overall gas mixture (CO, H_2 and O_2) after degasification, was kept at 100 mL/min (Total GHSV = 60000 mg/L.h), in which H_2 flow rate was 50 mL/min; CO and O_2 stoichiometrically shared the other 50 mL/min according to equation 16. H_2O tests was carried by bubbling He gas through a moisture containing saturator at a flow rate of 10 mL/min, giving 10 vol.% H_2O. CO_2 tests was carried out under 15 vol.% CO_2 gas. The resulting gaseous products were identified using an online GINI gas chromatography (GC), equipped with a Porapak Q and the molecular sieve column for separation of products as well as a thermal conductive detector (TCD). The feed gas comprised of 1% CO, 1% O_2 and 50% H_2 balance helium (He). The copper sulphate desiccant was used to trap water downstream of the reactor before GC analysis.

The catalytic activity was investigated from 40 to 200 ^{o}C at atmospheric pressure. The % CO conversion and CO_2 selectivity were calculated from equation 9 and 10, respectively.

$$\%\, CO\ Conversion = \frac{[CO]^{in} - [CO]^{out}}{[CO]^{in}} \text{ x } 100\ \% \qquad (9)$$

$$\%\, CO_2\ Selectivity = \frac{([CO]^{in} - [CO]^{out})}{2\,([O_2]^{in} - [O_2]^{out})} \text{ x } 100\ \% \qquad (10)$$

Where $[CO]^{in}$, represents the standard (or stoichiometric) concentration of CO entering a catalyst bed, and leaving as unreacted, $[CO]^{out}$. The $[O_2]^{in}$ is also the standard concentration of O_2 entering the reactor and leaving as $[O_2]^{out}$, after the heterogeneously catalysed chemical reaction (equation 11). The overall CO(PrOx) schematic diagram/setup used for analysis in this work is shown in figure 4.

$$2CO + O_2 \rightarrow 2CO_2 \qquad (11)$$

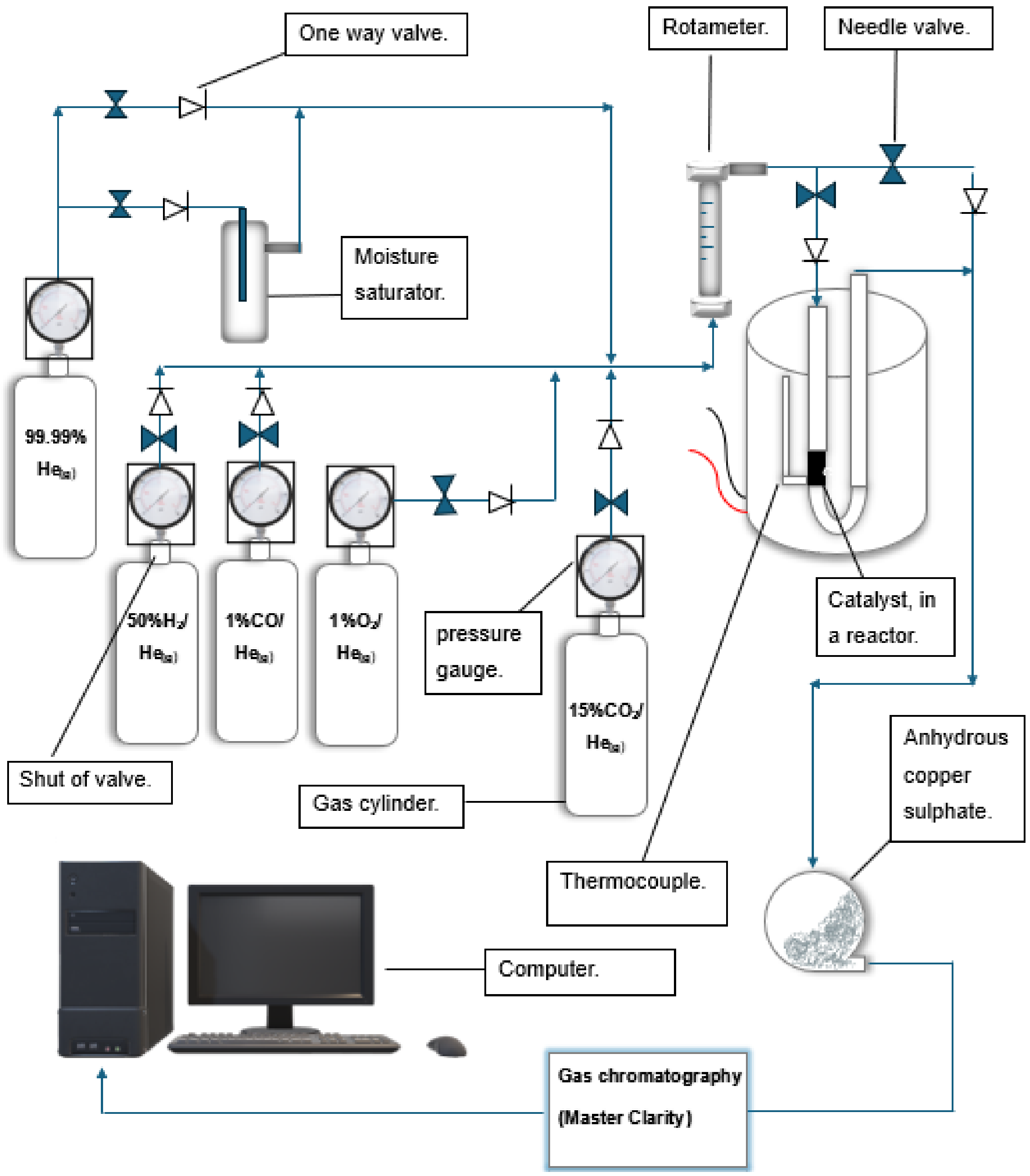

Figure 3.3 A typical CO(PrOx) U-shaped glass reactor system (coupled with GC) used on CO oxidation in hydrogen rich stream over the prepared catalyst materials.

3.5. REFERENCES

[1] N. S. Afandi, M. Mohammadi, S. Ichikawa, and A. R. Mohamed, “CO_2 reforming of methane to syngas over multi-walled carbon nanotube supported Ni-Ce nanoparticles: effect of different synthesis methods,” Environmental Science and Pollution Research, vol. 27, no. 34, pp. 43011–43027, 2020.

[2] L. Li, Y. Yao, Z. Tang, W. Ji, Y. Dai, and X. Shen, “Size effect of Co_3O_4 nanoparticles as catalysts for CO oxidation,” Journal of Nanoscience and Nanotechnology, vol. 16, no. 7, pp. 7573–7578, 2016.

[3] M. A. Mohamed, J. Jaafar, A. F. Ismail, M. H. D. Othman, and M. A. Rahman, Fourier Transform Infrared (FTIR) Spectroscopy. In Membrane characterization (pp. 3-29). Elsevier B.V., 2017.

[4] S. Adak, J. Rabeah, R. Ranjan, T.S. Khan, M.K. Poddar, R.K. Gupta, T. Sasaki, S. Kumar, A. Bordoloi, C.S. Gopinath, and A. Brückner. "In-situ experimental and computational approach to investigate the nature of active site in low-temperature CO-PROX over CuOx-CeO_2 catalyst". Applied Catalysis A: General, 624, p. 118305, 2021.

[5] S. K. Aditha, A. D. Kurdekar, L. A. A. Chunduri, S. Patnaik, and V. Kamisetti, “Aqueous based reflux method for green synthesis of nanostructures: Application in CZTS synthesis,” MethodsX, vol. 3, p. 35, 2016.

[6] S. K. Paswan, S. Kumari, M. Kar, A. Singh, H. Pathak, J. P. Borah, and L. Kumar, “Optimization of structure-property relationships in nickel ferrite nanoparticles annealed at different temperature,” Journal of Physics and Chemistry of Solids, vol. 151, p. 109928, 2021.

[7] G. Chai, W. Zhang, L. F. Liotta, M. Li, Y. Guo, and A. Giroir-Fendler, “Total oxidation of propane over Co_3O_4-based catalysts: Elucidating the influence of Zr dopant,” Applied Catalysis B: Environmental, vol. 298, p. 120606, 2021.

[8] A. B. Dongil, B. Bachiller-Baeza, E. Castillejos, N. Escalona, A. Guerrero-Ruiz, and I. Rodríguez-Ramos, “Promoter effect of alkalis on CuO/CeO_2/carbon nanotubes systems for the PROx reaction,” Catalysis Today, vol. 301, pp. 141–146, 2018.

CHAPTER 4

---

4. RESULTS AND DISCUSSION

4.1. INTRODUCTION

This chapter presents, the preparation, characterisation and catalytic activity tests of Co_3O_4 based catalysts, towards preferential oxidation of carbon monoxide (CO(PrOx)) in H_2-rich stream. All the pre-calcined catalysts (i.e., $Co(OH)_2$, $Ce(OH)_4/Co(OH)_2$ and $Cu(OH)_2/Co(OH)_2$) prepared by precipitation (for bare catalysts) and or co-precipitation (for doped) under both hydrothermal (Hyd) and reflux (Ref) method, were converted to their oxide's phases (i.e., Co_3O_4, CeO_2/Co_3O_4 and CuO_x/Co_3O_4) upon calcination in air for 3 h, at 300 ^{o}C. The as prepared metal oxide catalysts were characterised by various techniques and evaluated for their catalytic activity and stability in CO(PrOx) reaction. CuO_x species promoted Co_3O_4 catalysts more than CeO_2, when investigated at varying content, with the reflux obtained 5 wt.% CuO_x/Co_3O_4(Ref) catalyst showing the best catalytic performance than all the prepared catalysts, followed by its hydrothermal 5 wt.% CuO_x/Co_3O_4(Hyd) counterpart. The 5 wt.% CuO_x/Co_3O_4(Ref) catalyst also showed a good stability in CO_2 co-fed CO(PrOx) environment with less moisture tolerant.

The chapter also focused on the ternary metal-oxide catalysts based on ceria, copper and cobalt prepared by varying ceria content (1, 3, 5 wt.%) on the optimized 5 wt.% CuO_x/Co_3O_4 catalysts, following similar methods used to prepare the bimetallic oxides. Although the catalytic performance in CO(PrOx) reaction decreased after the addition of a third metal-oxide (CeO_2) in both cases, the 3 wt.% CeO_2 was found to be an optimum load for 5 wt.% CuO_x/Co_3O_4 under reflux. As a result, the characterisation techniques in relation to CO(PrOx) performances were narrowed to this sample in comparison to its hydrothermal counterpart. The as prepared ternary 3 wt.% CeO_2-5 wt.% CuO_x/Co_3O_4(hyd) and 3 wt.% CeO_2-5 wt.% CuO_x/Co_3O_4(Ref) catalysts, were denoted as 3Ce-5Cu/Co(Hyd) and 3Ce-5Cu/Co(Ref) respectively, throughout the chapter for simplicity.

4.2. CHARACTERISATION OF THE CATALYST SAMPLES

4.2.1. X-ray powder diffraction (XRD) analysis

4.2.1.1. Effect of CuO_x and CeO_2 species on the crystal structure of Co_3O_4(Hyd) catalyst, prepared by hydrothermal (hyd) method

The XRD patterns of polycrystalline Co_3O_4(Hyd), 5 wt.% CuO_x/Co_3O_4(Hyd) and 5 wt.% CeO_2/Co_3O_4(Hyd) catalysts, prepared by hydrothermal method and calcined at 300 °C are shown in Figure 4.1. Pure Co_3O_4(Hyd) and 5 wt.% CuO_x/Co_3O_4(Hyd) catalysts (Figure 4.1(a) and (b)), shows diffraction lines at similar glancing angle, $2\theta = 19.3$, 31.2, 36.8, 39.7, 44.9, 56.1, 59.8, 65.9 and 69.3°, emerging from Cu radiation (K_α, $\lambda = 0.15406$ nm) scattered by (111), (220), (311), (222), (400), (422), (511), (440) and (531) crystal planes at those angles, respectively [11, 12]. Such systematics are fingerprint accession of a face centred cubic (FCC) spinel structure (Co_3O_4), JCPDs card no. 42-1467 [1]. Some of these signals are also detected in 5 wt.% CeO_2 doped Co_3O_4(Hyd) catalyst (Figure 4.1 (c)).

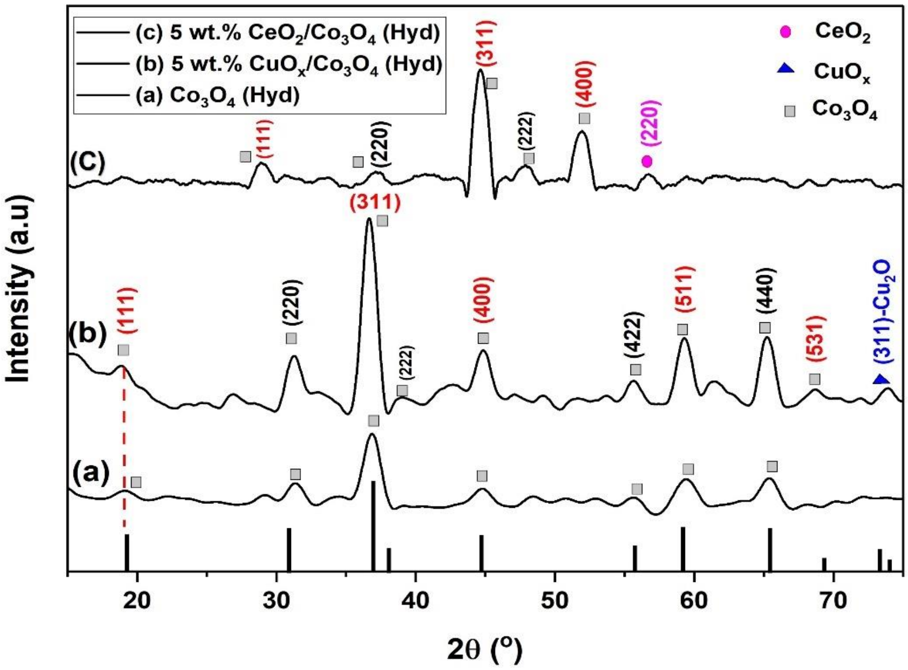

Figure 4.1 The XRD patterns of (a) Co_3O_4(Hyd), (b) 5 wt.% CuO_x/Co_3O_4(Hyd), (c) 5 wt.% CeO_2/Co_3O_4(Hyd) catalysts prepared by hydrothermal method and calcined at 300 °C, for 3 h.

The XRD profiles thus, suggest the existence of Co_3O_4 phase in all the prepared catalysts. Furthermore, doping with both CuO_x and CeO_2 catalyst increase the crystallinity of bare Co_3O_4(Hyd) catalyst (Figure (a)), as shown by their relatively intensified diffraction peaks in Figure 4.1 (b) and (c), respectively.

It is clearly observed that most CuO_x species exists as cuprous oxide (Cu_2O) phase, as distinguished by the (311) crystal plane at 73.8° (Figure 4.1 (b)) [1, 35]. These Cu_2O crystals were generated during calcination and deposited on Co_3O_4 catalyst, generating a high density CuO_x-Co_3O_4 interfacial regions rather than a solid solution, as shown by a relatively constant lattice parameter (Table 4.1) [5]. Similar results were reported by Gao *et al*. [3]. The crystallite size ($D_{(X.al)}$) of Co_3O_4(Hyd) catalyst also remain unchanged (at ~7.2 nm) after 5 wt.% CuO_x introduction, due to inability of the deposited CuO_x species to form part of Co_3O_4 structure and restrict its crystal growth during calcination at 300 °C [30-32].

The XRD profile of pure Co_3O_4(Hyd) catalyst moved towards high 2θ angles after CeO_2 introduction, suggesting a decrease in the lattice parameter (Figure 4.1 (c)). This results when Co_3O_4(Hyd) lattice contract, due to high degree of oxygen vacancies (O_v) caused by ceria, in order to maintain the spinel structure [9]. These observations were complimented by the H_2-TPR analysis. The cubic fluorite CeO_2 phase could be distinguished by the (220) crystal plane (JCPDS 43-1002) [28]. Crystallite size of bare Co_3O_4(Hyd) catalyst decreased after 5 wt.% CeO_2 introduction (see Table 4.1) and most of the Co_3O_4 diffraction lines disappeared, which emphasise a spinel phase transformation to a new symmetry, perhaps CoO phase (has high O_v). Other researchers have reported on similar results [41-43].

4.2.1.2. Effect of CuO_x and CeO_2 species on the crystal structure of Co_3O_4(Ref) catalyst, prepared by reflux/co-precipitation (Ref) method

Figure 4.2 shows the XRD profiles of Co_3O_4(Ref), 5 wt.% CuO_x/Co_3O_4(Ref) and 5 wt.% CeO_2/Co_3O_4(Ref) catalysts prepared by reflux assisted co-precipitation method. As expected, bare Co_3O_4(Ref) catalyst (Figure 4.2 (b)) shows similar diffraction lines as Co_3O_4(Hyd) catalyst (Figure 4.1 (a)), assigned to Co_3O_4 spinel structure (see section 4.2.1.1). As in hydrothermal method (Figure 4.1), CuO_x addition also increased the crystallinity of bare Co_3O_4(Ref) catalyst, as shown in Figure 4.2 (b). Interestingly, the

(111) peak of bare Co_3O_4(Ref) catalyst (Figure 4.2 (a)), vanished after the addition of 5 wt.% CuO_x dopant (Figure 4.2 (b)).

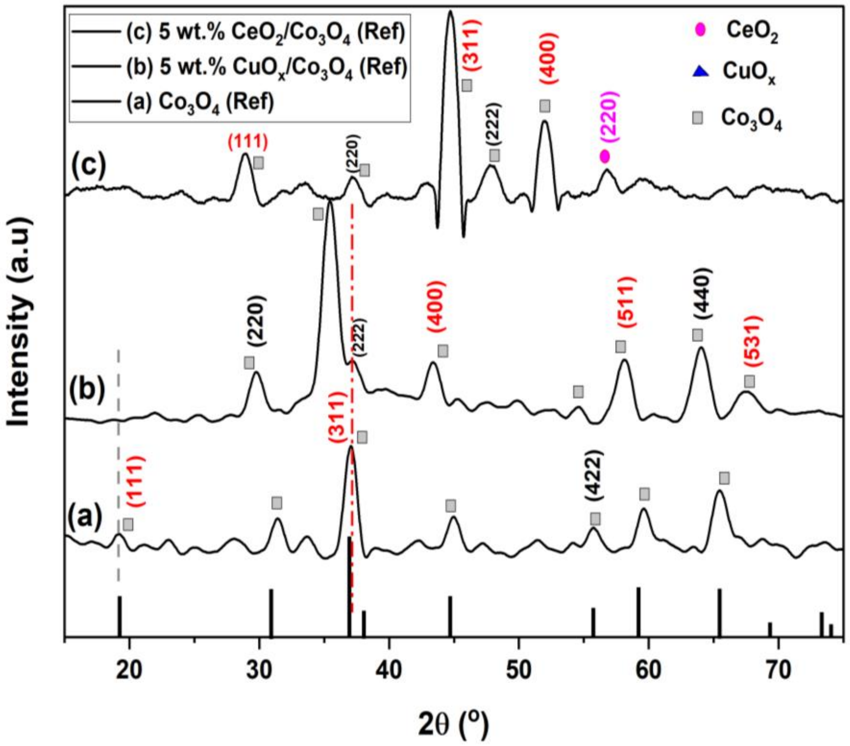

Figure 4.2 The XRD profiles of (a) Co_3O_4(Ref), (b) 5 wt.% CuO_x/Co_3O_4(Ref), (c) 5 wt.% CeO_2/Co_3O_4(Ref) catalysts prepared by reflux method.

This (111) crystal planes are rich in tetrahedrally coordinated Co^{2+} cations [1]. Therefore, the peak disappearance suggests the replacement of most Co^{2+} cations by ions of different scattering factor (i.e., obviously CuO_x cations), thereby creating a solid solution [13-15]. The absence of CuO_x phase in the as prepared 5 wt.% CuO_x/Co_3O_4(Ref) catalyst further confirms the formation of a solid solution, which strengthens CuO_x-Co_3O_4 interactions [3, 30, 36]. By using Inert N_2-environmnet as done in the reflux method, oxidation of metal ions precursors prior to calcination could be prevented, which conserves their ionic radii and allows facile substitution. It could also be observed that the XRD pattern of bare Co_3O_4(Ref) catalyst (Figure 4.2 (a), (red lines)), slightly shifts towards lower 2θ values followed by partial line broadening, as 5 wt.% CuO_x is introduced (Figure 4.2 (b)). The former implies a minor lattice expansion and the latter suggest a decrease in Co_3O_4(Ref) crystallite size from ~7.2 – 5.0 nm [21-23].

Since the ionic radii (r_+), ((Co^{2+}) ~79 pm and (Cu^{2+}) ~87 pm), valence state (i.e., 2+) and the electronegativity (Co^{2+} ~1.90 and Cu^{2+} ~1.88) of copper and cobalt divalent cations are closer to one another, a perfect copper-cobaltite crystal will exhibit a pure Co_3O_4 XRD pattern [14, 23-26]. Therefore, the lattice expansion must have caused by free Co_3O_4 interstitial sites occupancy by a relatively large ion, probably Cu^+ species (r_+ ~96 pm) generated during calcination [4, 26-28], or via Cu^{2+} reduction by oxygen vacancies of Co_3O_4(Ref) crystals [20]. Chen and co-workers [9], reported on similar results. Such defects produces high energy configurations, which enhances local molecular interactions [26], and are beneficial for CO(PrOx) catalysis [14].

Table 4.1 Summarises the identified crystal phases, crystallite sizes and lattice parameters estimated from the XRD data of the prepared catalysts.

Catalysts	Identified crystal phase	Crystallite size ($D_{x.tal}$) (nm)	Lattice parameter, a, (Å)	interplanar distance, d_s (311), (Å)
Co_3O_4(Hyd)	Co_3O_4	7.2	8.070	2.433
5wt.%CuO_x/Co_3O_4(Hyd)	Co_3O_4, Cu_2O	7.2	8.100	2.442
5wt.%CeO_2/Co_3O_4(Hyd)	Co_3O_4, CeO_2	6.5	6.570	1.981
3Ce-5Cu/Co(Hyd)	Co_3O_4, CeO_2, Cu_2O	6.5	8.001	2.412
Co_3O_4(Ref)	Co_3O_4	7.2	8.050	2.427
5wt.%CuO_x/Co_3O_4(Ref)	Co_3O_4	5.0	8.313	2.506
5wt.%CeO_2/Co_3O_4(Ref)	Co_3O_4, CeO_2	4.2	6.521	1.965
3Ce-5Cu/Co(Ref)	Co_3O_4	5.8	7.880	2.376

The theoretical lattice constant, a = 8.08 Å, for pure Co_3O_4 spinel crystal [27].

The XRD pattern of 5 wt.% CeO_2/Co_3O_4(Ref) catalyst in Figure 4.2 (c) also revealed a fluorite-type CeO_2 cubic structure. Although reflux method might have also favoured

CeO_2-Co_3O_4 solid solution as in the CuO_x case, the relatively large ionic radius of CeO_2 cation (Ce^{4+}, r_+ ~101 pm) impedes it from entering the small sized spinel's (Co_3O_4) interstitial voids [10, 38, 41]. Therefore, solidifies as fluorite nanocrystals on the surface of Co_3O_4(Ref) catalyst. It was further observed by an increase peak intensity and the broadening of (311) signal, that CeO_2 addition by reflux method also results in an increase in the crystallinity and a decrease in crystallite size of bare Co_3O_4(Ref) catalyst (see Figure 4.2 (a) and (c)). Ceria is known to prevent extensive sintering of Co_3O_4 crystals during growth and reduce their grain size [28], which is consistent with these observations.

Cooling rate can also affect the crystallite size [30], which could have also been an important 'neglected' factor, because borosilicate glass (reflux media), with a low thermal capacity than stainless steel (hydrothermal media), would cool at a different rate. For faster cooling rate such as in reflux, small crystallite size are most probable [33, 34]. These could explain why all catalysts (doped) prepared under reflux method have small crystallite size as compared to their hydrothermal counterparts (Table 4.1).

4.2.1.3. X-ray powder diffraction (XRD) patterns of 3 wt.% CeO_2 doped 5 wt.% CuO_x/Co_3O_4(Hyd) and 5 wt.% CuO_x/Co_3O_4(Ref) catalysts under hydrothermal and reflux method

Figure 4.3 compared the XRD patterns of the hydrothermally and reflux prepared 3Ce-5Cu/Co(Hyd) and 3Ce-5Cu/Co(Ref) ternary catalysts, to their bimetallic counterparts. In addition to the fluorite phase at $2\theta = 56.6^o$, the diffraction peaks of Co_3O_4 spinel in 5 wt.% CuO_x/Co_3O_4(Hyd) catalyst (Figure 4.3 (a)), were still identified after the addition of 3 wt.% CeO_2 under hydrothermal method (Figure 4.3 (b)). Moreover, the lattice parameter and the crystallite size decreased slightly after 3 wt.% CeO_2 addition (see Table 4.1), followed by a small decrease in (311) peak intensity, again, indicating low crystallinity. The Cu_2O diffraction peak was still identified in the ternary 3Ce-5Cu/Co(Hyd) catalyst, although less intense (Figure 4.3 (b)), perhaps due to the oxidation of Cu_2O to a highly dispersed amorphous CuO species by CeO_2, as evidenced by the absence of CuO signal(s) (Figure 4.3 (b)) [1, 9, 10], and supported by the H_2-TPR and TEM data. Elmhamdi *et al*., [15], has reported on similar results for CeO_2 modified $CuMn_2O_4$ catalyst, prepared by reverse microemulsion method.

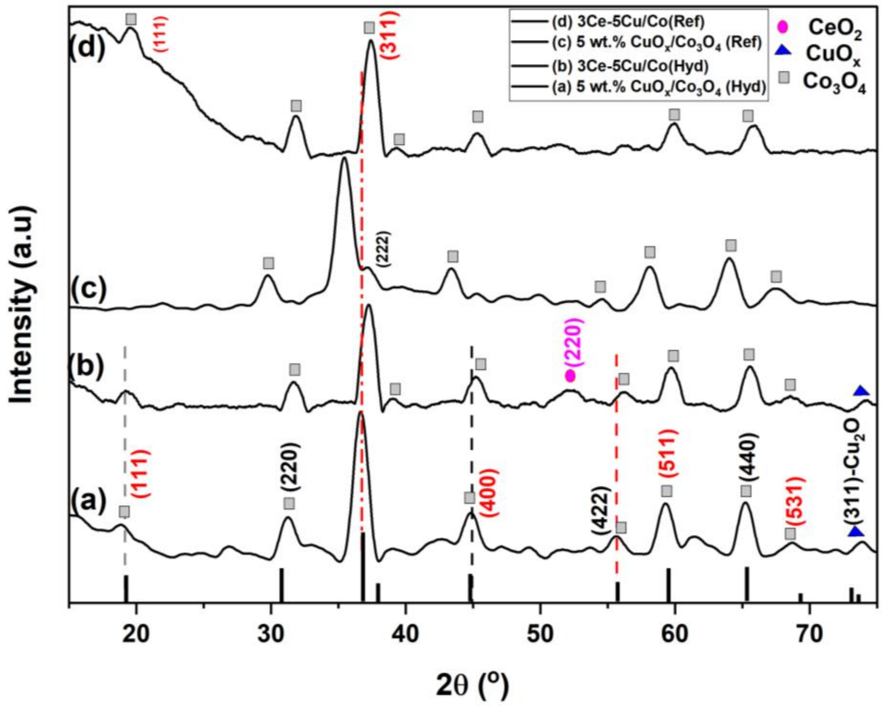

Figure 4.3 XRD pattern of (a) 5 wt.% CuO_x /Co_3O_4(Hyd), (b) 3Ce-5Cu/Co(Hyd), (c) 5 wt.% CuO_x /Co_3O_4(Ref) and (d) 3Ce-5Cu/Co(Ref) catalysts.

In contrast, the addition of 3 wt.% CeO_2 ceria under reflux method increased the crystallite size from ~5.0 to 5.8 nm (reduced the surface area) due to agglomeration of ceria-copper nanocrystals, in agreement with TEM and BET results. The lattice parameter also decreased after CeO_2 introduction (see Table 4.1). Interestingly, the (111) peak that had disappear in 5 wt.% CuO_x/Co_3O_4(Ref) catalyst (Figure 4.3 (c)), has remerged after 3 wt.% CeO_2 addition (Figure 4. 3 (d)). This suggest that CuO_x and CeO_2 interact more strongly than CuO_x was with Co_3O_4 in the solid solution, also confirmed by the H_2-TPR data. No CeO_2 and and CuO_x phase were detected in reflux fabricated ternary sample (Figure 4.3 (d)), suggesting that the strongly interacting CeO_2 and CuO_x nanoparticles form an amorphous clusters on the surface of Co_3O_4(Ref) catalyst [35, 36]. The XRD data is consistent with the previous reports [14–16].

4.2.2. Brunauer-Emmet-Teller (BET) analysis

4.2.2.1. Influence of hydrothermal and reflux method towards the textural properties of Co_3O_4(Hyd) and Co_3O_4(Ref) catalysts in the presence of CuO_x and or CeO_2 species

Textural properties of the as prepared catalyst samples were investigated by N_2 adsorption/desorption isotherm shown in Figure 4.4. The measured surface area as well as the porosity data by BET analysis and Barett-Joyner-Halenda (BJH) model (Figure 4.4, insets) respectively, are listed in Table 4.2.

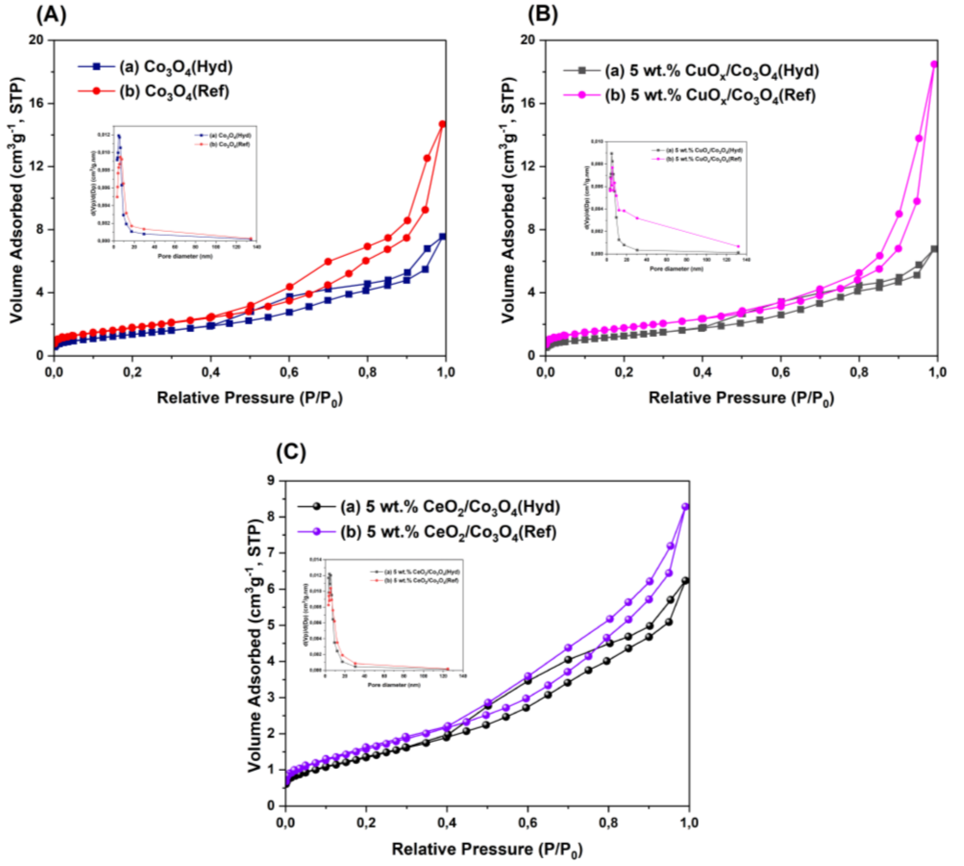

Figure 4.4 N_2 adsorption-desorption isotherms of the as prepared Co_3O_4(Hyd) and Co_3O_4(Ref) (A), 5 wt.% CuO_x/Co_3O_4 (B) and 5 wt.% CeO_2/Co_3O_4 (C), catalysts and their BJH pore size distribution curves (insets).

All catalysts indicated a type IV isotherm (Figure 4.4 (A) - (C)), associated with mesoporous features according to IUPAC classifications [36, 47], also corresponding with their average pore size range reported in Table 4.2. However, the isotherms differs in term of the shapes of their hysteresis loop, indicating different pore architecture [36, 48]. Nonetheless, both the bare Co_3O_4(Hyd) and Co_3O_4(Ref) catalysts (Figure 4.2 (A) (a)-(b)) demonstrate a mixture of H1 and H3 type of hysteresis loop, consistent with complex pore system of various shape and greater size distribution [47, 49, 50]. The surface area of Co_3O_4(Hyd) is larger than that prepared by reflux (Co_3O_4(Ref), (Table 4.2). The discrepancy in the surface area between these two materials regardless of their similar crystallite sizes could be associated with agglomerated Co_3O_4(Ref) nanoparticles observed from the SEM and TEM micrographs. Co_3O_4(Ref) catalyst possess the largest pore diameter (6.55 nm), which are formed between the inter-linked agglomerated particles [35].

Table 4.2. The BET surface area (S_{BET}), pore size, pore volume and crystallite sizes (from XRD results) of the prepared catalyst samples.

Catalysts	BET surface area (m^2/g)	Average pore diameter (nm)	Pore volume (cm^3/g)	Crystallite size (nm)
Co_3O_4(Hyd)	57.6	4.88	0.122	7.2
5wt.%CuO_x/Co_3O_4(Hyd)	39.8	4.88	0.0826	7.2
5wt.%CeO_2/Co_3O_4(Hyd)	64.0	4.28	0.106	6.5
3Ce-5Cu/Co(Hyd)	40.9	5.59	0.0849	6.3
Co_3O_4(Ref)	50.8	6.55	0.171	7.2
5wt.%CuO_x/Co_3O_4(Ref)	64.9	5.60	0.278	5.0
5wt.%CeO_2/Co_3O_4(Ref)	67.6	5.60	0.132	4.2
3Ce-5Cu/Co(Ref)	55.8	4.30	0.108	5.8

When 5 wt.% CuO_x was introduced in Co_3O_4(Hyd) catalyst by hydrothermal method, the shape of the hysteresis loop did not change much (Figure 4.4 (C) (a)) however, a significant decrease in the specific surface area (S_{BET}) from 57.6 m^2/g to 39.8 m^2/g was observed, due to pore filling (decrease in pore size, Table 4.2) [50], probably by the deposited Cu_2O species detected in the XRD analysis (Figure 4.1 (a)). Although occupation of Co_3O_4(Hyd) mesopores reduces the S_{BET}, the interaction between copper and cobalt at the interphase is enhanced, as probed by the H_2-TPR data [34]. On the other hand, Hitkari *et al.*, [38], reported an increase in surface area with diminution in pore volume of Co_3O_4 catalyst after 5 wt.% Cr addition. This odd behaviour is strongly affected by the preparation method [36, 52].

An increase in surface area was observed when 5 wt.% CuO_x species was introduced by reflux (Table 4.2). Similar results were reported on 5 wt.% Cr:Co_3O_4 catalyst prepared by reflux (at 180 °C, for 2 h) [38]. Nevertheless, the study [38], reported a relatively high surface area (99.12 m^2/g) than the one measured on 5 wt.% CuO_x/Co_3O_4(Ref) catalyst (64.9 m^2/g). This could be related to the prolonged reflux (180 °C, 24 h) carried out in this work, which increase the particle size and compromise the surface area [33, 53]. Furthermore, Co_3O_4(Ref) catalyst resulted in a well-defined type IV H3 type hysteresis loop (Slit-shaped mesopore features), after 5 wt.% CuO_x addition by reflux method (Figure 4.4 (B) (b)), denoting porous channels of a high mesoscopic periodicity [50, 55, 56]. In such pore geometry, condensation (adsorption) of gases occurs via multi-layer adsorption and the desorption occurs via capillary evaporation from all sites of the slit's meniscuses, and this textural property plays a crucial role in CO(PrOx) reaction, especially in sever environment (like moisture/CO_2 stream) [50, 56, 57].

To further gain more sight into the effects of the two-preparation method on the textural properties of bare Co_3O_4(Hyd) and Co_3O_4(Ref) catalysts, CeO_2 loaded at similar content of 5 wt.% was also studied by BET analysis. The S_{BET} of Co_3O_4(Hyd) increased from 57.6 m^2/g to 64.0 m^2/g after 5 wt.% CeO_2 addition via hydrothermal method. Introducing ceria by reflux method also increased the surface area of Co_3O_4(Ref) catalyst (Table 4.2). These increase in surface area is of course associated with small crystallite size obtained after CeO_2 addition (Table 4. 2) [18]. Interestingly, pore volume decreased marginally when ceria was added under reflux method, as compared to hydrothermal, which was reflected by the relatively high Debey temperature (T_D), calculated from the FTIR data. Material with small pore volume are relatively rigid therefore, exhibit high T_D [45]. The adsorption and desorption branches of both 5 wt.% CeO_2/Co_3O_4(Hyd) (Figure 4.4 (C); (a)) and 5 wt.% CeO_2/Co_3O_4(Ref) (Figure 4.4 (C); (b)) catalysts, also created a type IV isotherm. Nonetheless, the results shows that the introduction of either species (5 wt.% CuO_x and or 5 wt.% CeO_2) by reflux method yields catalyst materials of high S_{BET} than their hydrothermal counterparts, which stimulates CO(PrOx) catalysis [46].

4.2.2.2. BET analysis of ternary catalyst samples: Effects of 3 wt.% CeO_2 on 5 wt.% CuO_x/Co_3O_4 (Hyd) and 5 wt.% CuO_x/Co_3O_4 (Ref) catalyst

The BET surface area and porosity data of the three metal-oxide catalysts are also shown in Table 4.2, and their N_2 sorption isotherm are compared to their bimetallic counterparts (without 3 wt.% CeO_2) in Figure 4.5. Addition of 3 wt.% CeO_2 to 5 wt.% CuO_x/Co_3O_4(Hyd) catalyst via hydrothermal method slightly increased the S_{BET} from 39.8 m^2/g to 40.9 m^2/g. The 3Ce-5Cu/Co(Hyd) catalyst also indicated a type IV isotherm for mesoporous features (Figure 4.5 (B); (a)), with similar H1 and H3 mixed hysteresis loop, as in bare 5 wt. % CuO_x/Co_3O_4(Hyd) catalyst (Figure 4.5 (A); (a)), although had a relatively large pore size distribution (Table 4.2) [20, 22].

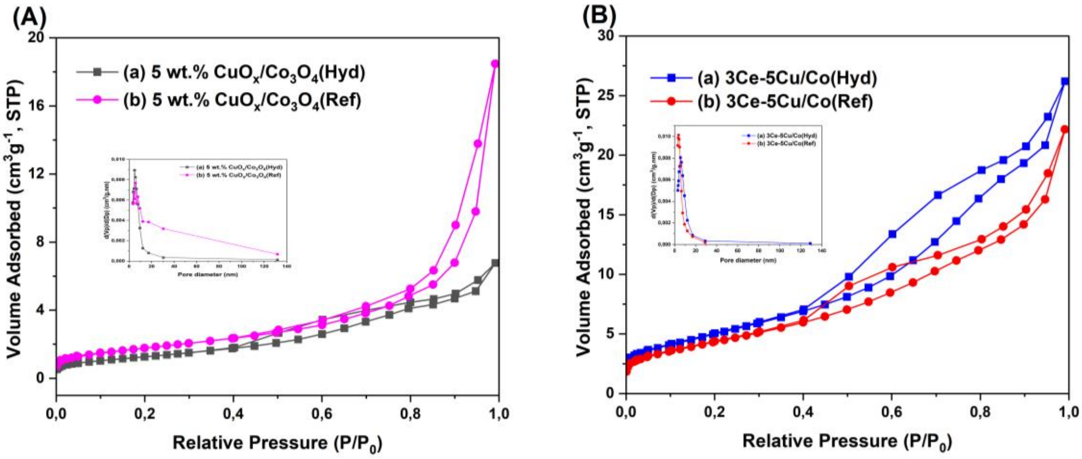

Figure 4.5 The N_2-sorption curves (A) of (a) 5 wt.% CuO_x/Co_3O_4(Hyd) and (b) 5 wt.% CuO_x/Co_3O_4(Ref) catalysts, and the N_2-sorption curves (B) of (a) 3Ce-5Cu/Co(Hyd) and (b) 3Ce-5Cu/Co(Ref) catalysts.

An improved surface area of 55.8 m^2/g was observed over the ternary catalyst prepared by reflux method. However, the addition of 3 wt.% CeO_2 to 5 wt.%CuO_x/Co_3O_4(Ref) catalyst drastically decreased the pore diameter and pore volume, so was the surface area (Table 4.2). These was caused by the occluded CeO_2-CuO_x nanocrystals withing the Co_3O_4(Ref) support's mesopores according to the TEM data [12, 20]. Lacoste *et al.,* [39], has reported on similar results. It was also observed that the addition of ceria changed the shape of the hysterisis loop of bare 5wt.% CuO_x/Co_3O_4(Ref) catalyst (Figure 4.5 (A); (b)), which implies porosity shape transformation to a new geometry.

4.2.3. Fourier Transform Infrared (FTIR) spectroscopy

Fourier transform infrared (FTIR) spectroscopy was performed to investigate the surface functional groups associated with the prepared catalysts as well as the pre-calcined catalysts. The results are presented in the following subsections.

4.2.3.1. Fourier Transform Infrared (FTIR) spectroscopy of CeO_2 doped Co_3O_4(Hyd) and Co_3O_4(Ref) catalysts, at varying content (β, wt.%)

The FTIR spectra of hydrothermally and reflux prepared βCeO_2/Co_3O_4(Hyd) and βCeO_2/Co_3O_4(Ref) catalysts (β = 0, 1, 3, 5 wt.%), are depicted in Figure 4.6. Both pure Co_3O_4(Hyd) and Co_3O_4(Ref) demonstrates some vibrational frequency bands at around 652 and 542 cm^{-1}, arising from Co^{2-} and Co^{3+}-O^{2-} bond vibrations respectively (Figure 4.6 (A); (a) and Figure 4. 6 (B); (a)), within the identified Co_3O_4 crystal structure (see XRD analysis (Figure 4.1 (a) and 4.2 (b)) [63, 64]. Doping both Co_3O_4(Hyd) and Co_3O_4(Ref) catalysts with 1 wt.% CeO_2 resulted in a shift of both Co^{2+}-O^{2-} vibrational and Co^{3+}-O^{2-} to higher frequencies and remained constant upon further increase in CeO_2 content to a maximum load of 5 wt.% (Figure 4.6 (A) and (B); (b)-(d)). These shortening of Co-O bond order arise from surface atomic hybridization between Co_3O_4 and CeO_2 nanocrystals, obviously complementing the reduced lattice parameter, as ceria was introduced by either method (Table 4.1) [50].

The temperatures at which the crystal lattice of Co_3O_4(Hyd) and Co_3O_4(Ref) catalysts exhibit maximum vibrations i.e., the Debey Temperature (T_D) [45], are relatively similar (~859.3 K), due to the same frequencies of vibrations (see equation (8), section 3.3.1). However, 5 wt.% CeO_2/Co_3O_4(Ref) catalyst prepared by reflux showed a higher T_D value of 904.1 K, as compared to its hydrothermal 5 wt.% CeO_2/Co_3O_4(Hyd) catalyst counterpart (T_D ~901.7 K). An increase in the T_D value is attributed to the increase in the rigidity of a material according to Paswan *et al.*, [45], and improves the mechanical stability of the catalyst during operation [51].

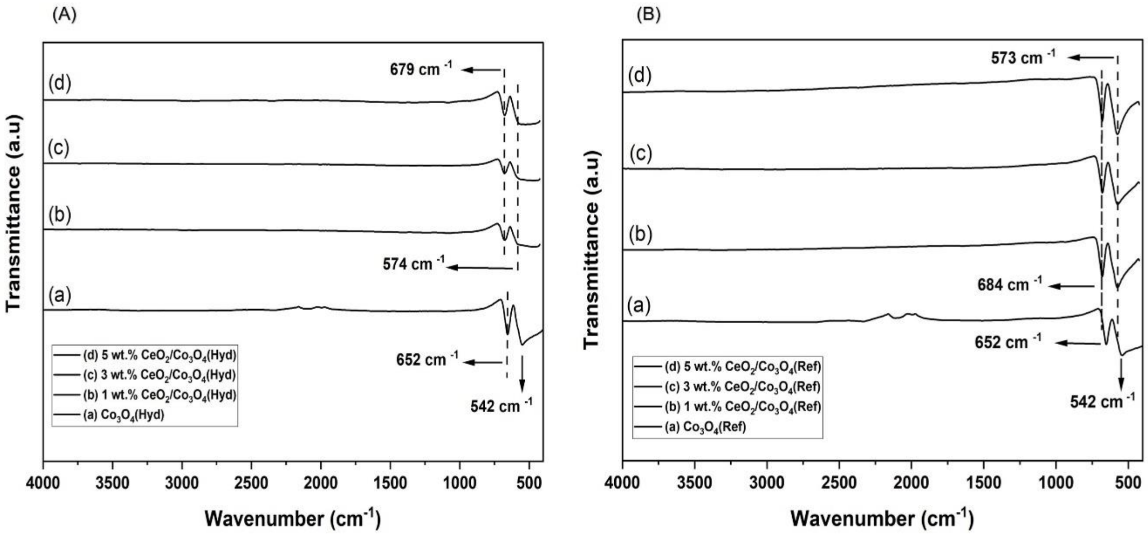

Figure 4.6 FTIR Spectra of (A) hydrothermal: (a) Co_3O_4(Hyd), (b) 1 wt.% CeO_2/Co_3O_4(Hyd), (c) 3 wt.% CeO_2/Co_3O_4(Hyd), (c) 5 wt.% CeO_2/Co_3O_4(Hyd) and (B) reflux: (a) Co_3O_4(Ref), (b) 1 wt.% CeO_2/Co_3O_4(Ref), (c) 3 wt.% CeO_2/Co_3O_4(Ref), (d) 5 wt.% CeO_2/Co_3O_4(Ref) catalysts.

4.2.3.2. Fourier Transform Infrared (FTIR) spectroscopy of CuO_x doped Co_3O_4(Hyd) and Co_3O_4(Ref) catalysts, at various amounts (μ, wt.%)

Figure 4.7 (A) and (B) shows the FTIR spectra of μCuO_x (μ = 0, 3, 5, 10, 15 wt.%) doped Co_3O_4(Hyd) and Co_3O_4(Ref) catalysts under both hydrothermal and reflux method, respectively. All samples showed characteristic vibrational frequencies of Co^{2+}-O^{2-} and Co^{3+}-O^{2-} metal oxide bonds (Figure 4.7 (A) and (B); (a)-(e)), arising from Co_3O_4 structure, also in accordance with the XRD data of the analysed samples, i.e., bare and 5 wt.% CuO_x/Co_3O_4(Hyd) and Co_3O_4(ref) catalysts (see Figure 4.1). However, the transmittance intensity of the Co^{2+}-O^{2-} characteristic peak decrease as the amount of CuO_x increase in reflux fabricated samples (Figure 4.7 (B)). Thus, the concentration of Co^{2+} species decreases with CuO_x content [62, 67, 68], complementing the isomorphous substitution happening, as probed by the XRD data of 5 wt.% CuO_x/Co_3O_4(Ref) catalyst (Figure 4.2 (b)).

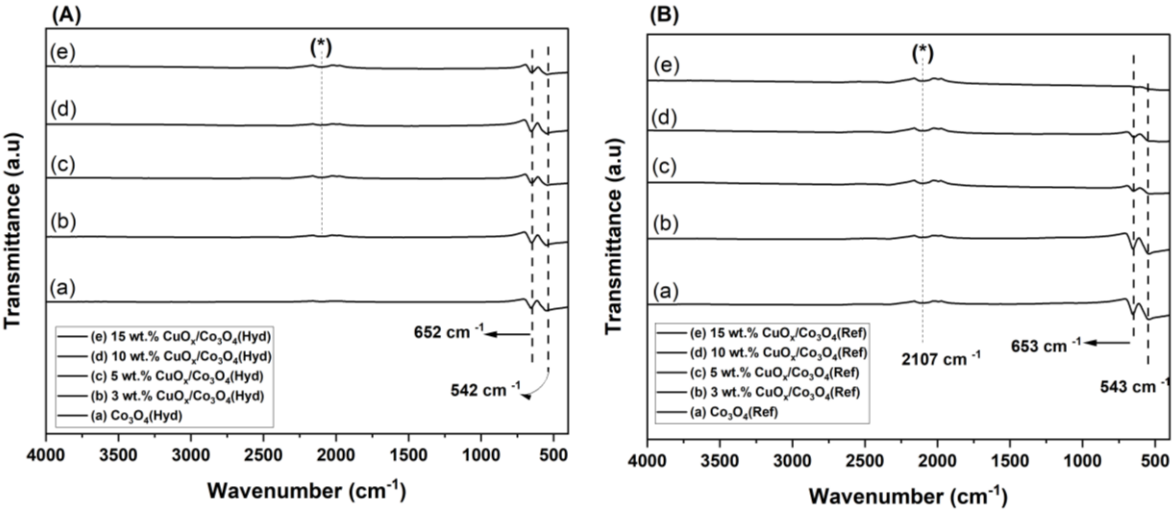

Figure 4.7 FTIR Spectra (A) Hydrothermal: (a) Co_3O_4(Hyd), (b) 3 wt.% CuO_x/Co_3O_4(Hyd), (c) 5 wt.% CuO_x/Co_3O_4(Hyd), (d) 10 wt.% CuO_x/Co_3O_4(Hyd), (e) CuO_x/Co_3O_4(Hyd) and (B) Reflux: (a) Co_3O_4(Ref), (b) 3 wt.% CuO_x/Co_3O_4(Ref), (c) 5 wt.% CuO_x/Co_3O_4(Ref), (d) 10 wt.% CuO_x/Co_3O_4(Ref), (e) 15 wt.% CuO_x/Co_3O_4(Ref) catalysts.

It could also be observed in Figure 4.7 that all CuOx doped Co_3O_4 catalysts showed relatively the same vibrational frequencies as that of their bare Co_3O_4(Hyd) and Co_3O_4(Ref) catalysts, regardless of the preparation method thus, had no effect on the resulting Debey temperature (T_D). Therefore, CuO_x doesn't alter the rigidity of Co_3O_4 as much as CeO_2 is concerned (structural modifying promoter). The doublet positive bands (asterisks) observed at ~2107 cm^{-1} are associated with CO_2 present on the catalyst surface (Figure 4.7 (A) and (B)) [69, 70], usually when collecting the FTIR background spectrum [57], and they could easily be degassed prior to catalyst tests [56].

4.2.3.3. Fourier transform infrared (FTIR) Spectroscopy of 3 wt.% CeO_2 doped 5 wt.% CuO_x/Co_3O_4 catalysts under both hydrothermal and reflux method

The Co-O bond vibrations of spinel were also observed in Figure 4.8 (b) and (d) for both 3Ce-5Cu/Co(Hyd) and 3Ce-5Cu/Co(Ref) ternary catalysts, respectively. Intrestingly, an increase in the transmittance strength of Co^{2+}-O band at ~654 cm^{-1} was observed after 3 wt.% CeO_2 addition, under reflux method (Figure 4.8 (d)). These confirms the notion that CeO_2 interact with CuO_x species, preventing it from removing

Co^{2+} cations in the Co_3O_4(Ref) spinel framework as evidenced by the reappearance of the (111) peak on the XRD profile (Figure 4.3 (d)).

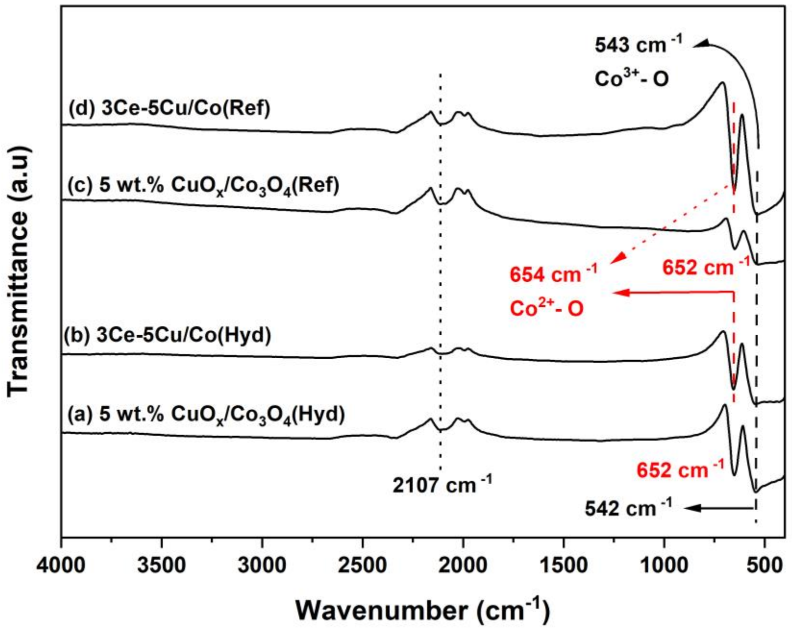

Figure 4.8 The FTIR spectra of hydrothermally prepared (a) 5 wt.% CuO_x/Co_3O_4(Hyd) and (b) 3Ce-5Cu/Co(Hyd), and of reflux prepared (a) 5 wt.% CuO_x/Co_3O_4(Ref) and (b) 3Ce-5Cu/Co(Ref) catalysts.

4.2.3.4. Investigation of polymer/surfactant capped nanoparticles: FTIR spectroscopy of the pre-calcined and calcined catalysts

It was visualised from the SEM images that the incorporation of CTAB and PVP capping agents plays a significant role in the morphology of the final catalyst (See appendix (A), as also reported elsewhere [31, 62]. Therefore, to confirm the presence of CTAB and PVP on the surface of the catalysts prior to calcination, FTIR spectra of pre calcined bare Co_3O_4(Hyd), Co_3O_4(Ref), 5 wt.% CuO_x/Co_3O_4(Hyd) and 5 wt.% CuO_x/Co_3O_4(Ref) catalysts, were recorded and compared to their calcined polymorphs. The FTIR spectra of pure CTAB and PVP powders were also recorded for reference (Figure 4.9).

The carbonyl peaks of the povidone moiety in the PVP polymer, could clearly be observed at ~1647 cm^{-1} in the uncalcined Co_3O_4(Ref) and Co_3O_4(Hyd) catalysts (Figure 4.9 (A); (a) and (b)) [58]. The peak at ~1308 cm^{-1} could be ascribed to the C-

N stretching mode of a bi-substituted amide group of N-vinyl pyrrolidone [58], and that ~1019 cm^{-1} is ascribed to the quaternary amide-carbon bond (C-N$^+$) of CTAB functional group [76, 78, 79]. This peak is visible in all the uncalcined catalyst samples (Figure 4.9 (A); (a)-(d)) but less intense in U-Co_3O_4(Hyd) catalyst (Figure 4.9 (A); (b)).

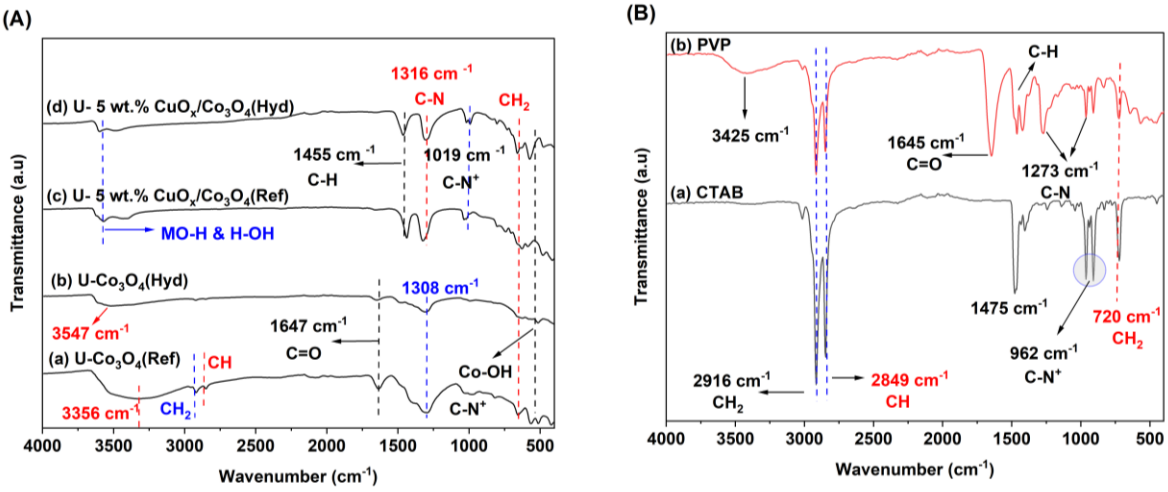

Figure 4.9 The FTIR spectra of uncalcined (shown as, U) catalysts and their calcined counter forms (without 'U') (A) and the FTIR spectra of pure CTAB and PVP powders (B).

The C-N$^+$ band of the U-Co_3O_4(Hyd) catalyst becomes visible after the addition of 5 wt.% CuO_x by hydrothermal method (Figure 4.9 (A); (d)), suggesting that $Cu(OH)_2$ helps in binding the CTAB surfactant. On the other hand, the was already present C-N$^+$ peak in bear U-Co_3O_4(Ref) catalyst (Figure 4.9 (A); (a)), became sharper after the introduction of 5 wt.% CuO_x by reflux route (Figure 4.9 (A); (d)), indicating a more ordered CTAB methylene chains on the surface [80, 81]. It could be the decomposition of these ordered CTAB structures from the pre-calcined (uncalcined) catalyst, that gave rise to the highly ordered slit-like mesopores of the final 5 wt.% CuO_x/Co_3O_4(Ref) sample, as understood from the N_2 sorption isotherm (Figure 4.4 (B); (b)). Interestingly, the C-N peaks (~1308 cm^{-1}) intensify and shifts towards higher frequencies (~1316 cm^{-1}) in the presence of 5 wt.% CuO_x species (Figure 4.9 (A); (c) and (d)). This is due to $Cu(OH)_2$ interactions with the lone pairs of the nitrogen in PVP [58], showing that the polymer binds more stronger in the presence of CuO_x species [68, 80], regardless of the preparation method.

All the uncalcined catalysts showed vibrational peak frequencies related to those observed on the pure CTAB and PVP spectra (Figure 4. 9 (B)), including the -OH bands of the surface adsorbed H_2O molecules ~3356-3547 cm^{-1} [63]. The broad nature of these -OH bands in the bare Co_3O_4(Ref) and Co_3O_4(Hyd) catalysts (Figure 4.9 (A), (a) and (b)), is a powerful indication of an immense hydrogen bonding of water molecules. Otherwise if the peaks originated from the -OH vibrations of the metal hydroxide (i.e., $Cu(OH)_2$ or $Co(OH)_2$), they would've been relatively sharper [64], as slightly adopted by 5 wt.% CuO_x doped U-Co_3O_4(Ref) and U-Co_3O_4(Hyd) catalysts (i.e., Figure 4.9 (A); (c) and (d), respectively). These could suggest the presence of $Cu(OH)_2$ species. Moreover, Co-OH bands could also be identified at lower vibrational frequencies (~ 500 cm^{-1}) in all the uncalcined catalyst samples (Figure 4. 9 (A); (a)-(d)) [65]. No capping agents (PVP/CTAB) or surface adsorbed H_2O characteristic peaks were detected in the final catalyst samples (see Figure 4.7 (a) and (c) of (A) and (B)), likely because they were removed at high calcination temperature (300 ^oC).

The FTIR data showed that the structure directing agents (PVP and CTAB) were successfully coated on the surface of the catalysts before they underwent solid-state reaction (i.e., calcination). The interaction between the adsorbed capping agents and the M-$(OH)_x$ (oxide precursors) leads to small sized particles during crystal growth [54]. This was reported by Pandey's group [60], on PVP coated magnetite (Fe_3O_4) catalyst.

4.2.4. Thermogravimetric (TGA) analysis

The decomposition of surface adsorbed species on the pre-calcined catalysts and the thermal stability of the final catalyst's samples were monitored by TGA analysis, as shown in Figure 4.10. The thermogram (TGA) of all the uncalcined (U) hydrothermally U-Co_3O_4(Hyd) and reflux fabricated U-Co_3O_4(Ref) catalysts as well as their CuO_x doped counterparts show a two-stage weight loss (Figure 4.10 (A); (a)-(d)). The first steps start from 150 to around 300 ^oC and is ascribed to the decomposition of surface adsorbed capping agents (PVP/CTAB) as well as the evolution H_2O molecules detected by the FTIR spectroscopy (see Figure 4.9). The PVP/CTAB and H_2O removal superimposed with the decomposition of the Co_3O_4 precursor (i.e., $Co(OH)_2 \rightarrow Co_3O_4$) [12, 84], and showed a corresponding weight loss of 21, 15, 20 and 19%, endothermically signalling at 255, 228, 247, 277 ^oC as shown by their DTG curves

(Figure 4.10 (B); (a)-(d)) for U-Co_3O_4(Hyd), U-Co_3O_4(Ref), U-5 wt.% CuO_x/Co_3O_4(Hyd) and U-5 wt.% CuO_x/Co_3O_4(Ref) catalysts, respectively.

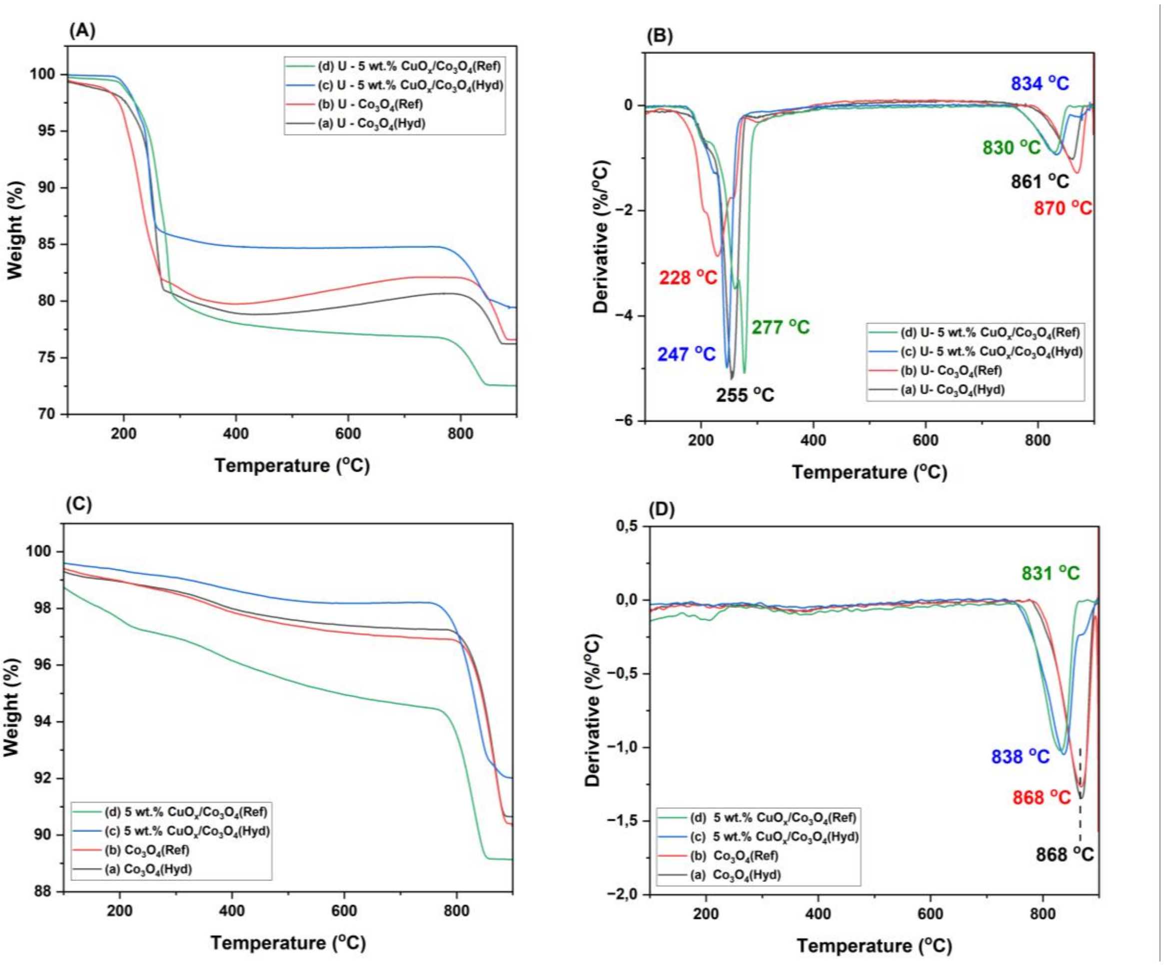

Figure 4.10 TGA (A and C) and the corresponding derivative (DTG) (B and D) curves of the pre-calcined and calcined catalysts, annealed at a heating ramp of 10 °C min^{-1} in Argon/air (20 mL/min) environment.

According to Zasada *et al.,* [67], the release of CO_2 and H_2O during thermal decomposition of the organic substances (PVP and CTAB in this case) generates a large amount of vacancies/voids, thereby creating a porous structure. This compliments the BET data and other similar claims [31, 77, 79]. For instance, Li *et al.,* [43], ascribed a mesoporous character of Pd/CeO_2 nanoparticles to the voids created when oxalate decompose during thermal processing. At temperatures above 300 °C, the $Co(OH)_2$ transform into a thermally stable Co_3O_4 structure, and no weight loss was detected up to ~800 °C (Figure 4.10 (A); (a)-(d)). The formation of Co_3O_4 structure is believed to occur via $Co(OH)_2$ dihydroxylation between 200-400 °C temperature range [69]. The last endothermic steps peaked at 861, 870, 834, 830 °C on DTG (Figure 4.10

(B); (a)-(d)) corresponds to a total WLs of 5, 6, 5, 5% (TGA curve, Figure 4. 10 (A); (a)-(d)). These peaks are redox in nature and are ascribed to the thermal reduction of $Co^{3+} \rightarrow Co^{2+}$ due to the decomposition of $Co_3O_4 \rightarrow CoO$ i.e., the collapse of the spinel structure. This kind of behaviour was also reported by Makhlouf's group [2].

As expected, the calcined catalysts product illustrates only the $Co_3O_4 \rightarrow CoO$ thermal reduction behaviour at around 700 – 800 °C (Figure 4. 9 (C)), which shows the high thermal stability of the produced metal oxide. Thus 300 °C was the appropriate minimum calcination temperature to obtain the final catalyst, as also supported by the FTIR and XRD analysis. This low temperature and less time required to obtain a final catalyst is economically feasible for large scale applications. The Co_3O_4(Hyd), Co_3O_4(Ref), 5 wt.% CuO_x/Co_3O_4(Hyd) and 5 wt.% CuO_x/Co_3O_4(Ref) catalysts remain stable up to 868, 868, 838 and 831 °C (Figure 4.10 (D); (a)-(d)), which corresponds to a total weight loss of 7, 7, 6, 6 %, respectively (Figure 4.10 (C); (a)-(d)). Noticeably, the temperatures are much lower in CuO_x containing catalysts, which suggesting that CuO_x dopant lowers the thermal stability of Co_3O_4(Hyd) and Co_3O_4(Ref) catalysts. No weight loss corresponding to thermal decomposition of CTAB and PVP was detected on the final catalysts (Figure 4.10 (C), because they were completely removed from the surface upon calcination, according to FTIR data (see Figure 4.9). The removal of CTAB and PVP on the catalyst ensures that more active sites are exposed to the reactants during catalysis [62, 68, 82, 86].

4.2.5. Scanning electron microscopy (SEM)

4.2.5.1. Scanning electron microscopy (SEM) of bare and CuO_x doped Co_3O_4(Hyd) and Co_3O_4(Ref) catalysts

The SEM images of the prepared catalyst samples are depicted in Figure 4.11. Pure Co_3O_4(Hyd) catalyst obtained by hydrothermal technique consists of a hemi octahedral-like (pyramidal shape) Co_3O_4 clusters with an average edge length in micron scale (~1.5 – 2.0 μm), coarsened by spherical like particles (in nm scale) (Figure 4.11 (a)). This pyramidal shape differs from the pure octahedral type of Co_3O_4 morphology obtained by Vo *et al.* [1], by hydrothermal method (180 °C, 5 h), although both morphologies are promoted by the crystal grow along the <111> direction [1]. Doping Co_3O_4(Hyd) with 5 wt.% CuO_x under hydrothermal method resulted in morphology transformation to well-defined cubes with sharp vertices and a relatively smaller edge length (~0.60 μm) (Figure 4.11 (b)).

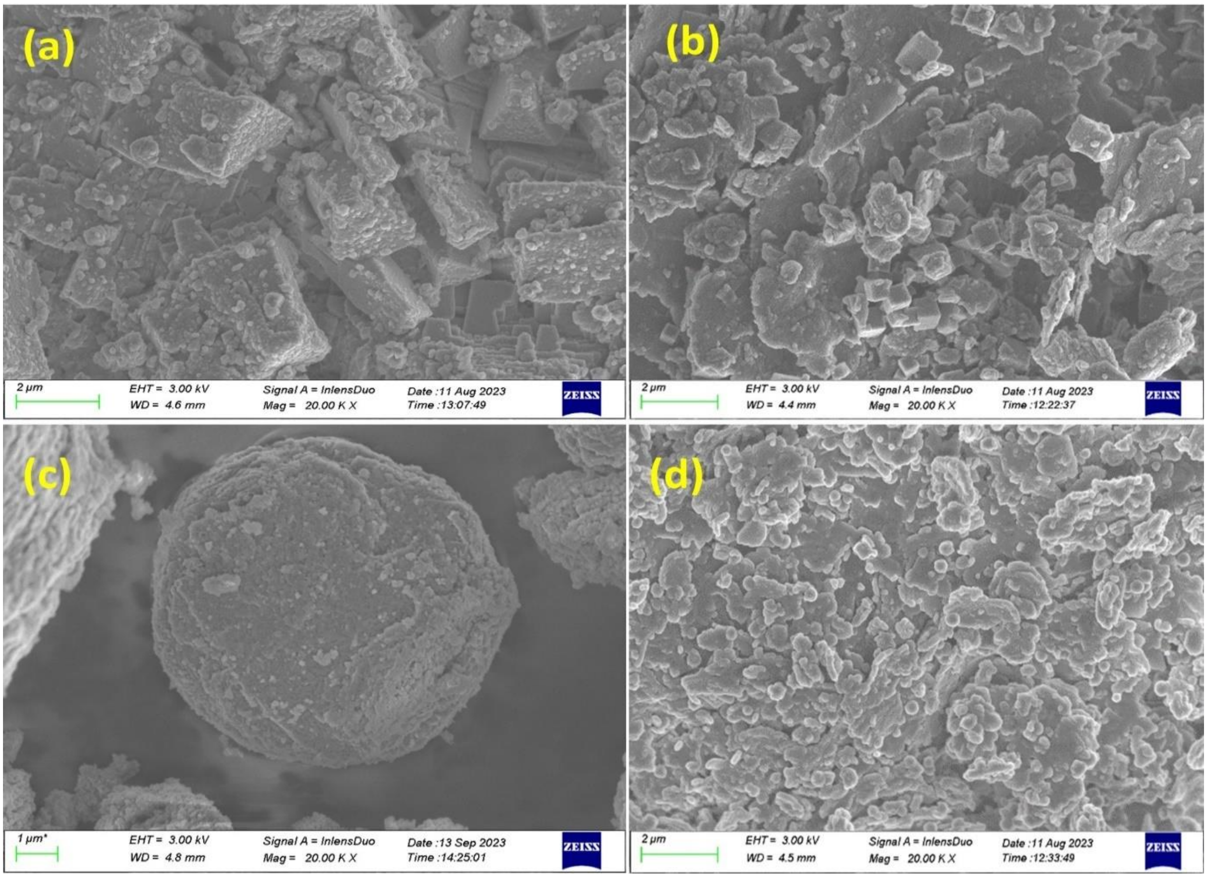

Figure 4.11 SEM micrograph of (a) Co_3O_4(Hyd), (b) 5 wt.% CuO_x/Co_3O_4(Hyd), (c) Co_3O_4(Ref) and (d) 5 wt.% CuO_x/Co_3O_4(Ref) catalysts.

The cubic morphology is a consequence of CuO_x dopant and not a "surface wrapping mechanism" suggested by Samal *et al*., [65]. The CuO_x played an important role in the interaction with the structure directing agents (CTAB and PVP), as supported by the FTIR spectroscopy (Figure 4.9). These kinetically hinders crystal growth along the <111> directions and promotes the crystal growth along the <100> vectors, to give 5 wt.% CuO_x/Co_3O_4(Hyd) catalyst with a cubic morphology. Using hydrothermal method, Xia *et al*., [72], noticed a transition from truncated cubes of Co_3O_4 nanocrystals (without PVP) to a well-defined cubes in the presence of PVP, driven by PVP binding to cobalt ions in (111) crystal planes. Zhen *et al*., [29], reported a good catalytic CO oxidation over Co_3O_4-CeO_2 core shell catalyst with cubic morphology, prepared by hydrothermal (180 °C, 5h). When 5 wt.% CuO_x/Co_3O_4(Hyd) catalyst was prepared without CTAB and PVP, the morphology featured agglomerated and truncated cubes, deposited over a ‘covert bird feather-like’ structure and with relatively low catalytic CO(PrOx) performance (See Appendix (A)). On the other hand, when calcination was performed at 550 °C (Similar to Adak *et al*’s work [11]) instead of 300 °C, the cubes segregated over a porous plate-like rods, lowering the catalytic performance of 5 wt.% CuO_x/Co_3O_4(Hyd) (Appendix B (b)).

Pure Co_3O_4(Ref) catalyst obtained by reflux method consists of a large and rough sphere-like structure of ~5.0 μm in diameter (Figure 4.11 (c)). Agglomerations of Co_3O_4(Ref) crystals is a consequences of Ostwald ripening due to their small sized nanoparticles (See TEM, Figure 4.13 (d)), which could lower their Tamman-Hüttig temperatures [19, 27, 90]. The large spherical shape might have resulted from the tiny nanoparticles nucleating from an already growing spherical-shaped crystal via, topotactical/topochemical growth process [84, 91]. The Co_3O_4(Ref) agglomeration was circumvented by 5 wt.% CuO_x dopants (Figure 4.11 (d)), which stabilized this tiny unstable Co_3O_4 crystals by cooperating with the CTAB and PVP capping agents (see Figure 4. 9) and or through ‘sacrificial templating’ phenomena [7]. This resulted in a highly distributed nano spheres over a well-developed Ulva-like structure (Figure. 4.11 (d)). Similar morphology was also reported by Xue *et al.,* [20], on $CuCo_2O_4$ photocatalyst, prepared by reflux method (100 °C, 1.5 h). Methylene blue has been degraded by Cr:Co_3O_4 photocatalysts [38], and CO gas has been oxidized efficiently in moisture conditions (without H_2) by Co_3O_4@CNT catalyst [76].

When 5 wt.% CuO_x/Co_3O_4(Ref) catalyst was obtained by annealing at 550 °C, the morphology transformed into a porous hexagonal like plates with spherical-like particles accumulated on their surface, resulting in low catalytic CO(PrOx) performance (Appendix B (d)). Such macroscopic pores can trap the reactants and increase particle-particle interactions [77].

4.2.5.2. Effect of 3 wt.% CeO_2 on the morphology of 5 wt.% CuO_x/Co_3O_4(Hyd) and 5 wt.% CuO_x/Co_3O_4(Ref) catalysts

The SEM micrographs of 5 wt.% CuO_x /Co_3O_4 bimetallic catalysts are compared with their ternary counterparts in Figure 4.12. Introduction of 3 wt.% CeO_2 on bare 5 wt.% CuO_x/Co_3O_4(Hyd) catalyst by hydrothermal method (Figure 4.12 (b)), has led to surface coarsensness and the new size of the cubes are roughly twice the size of those of observed in undoped 5 wt.% CuO_x/Co_3O_4(Hyd) catalyst (Figure 4.12 (a)). This could suggest that CeO_2 expands those cubes, which in turn raptures them, collapsing the morphology of 5 wt.% CuO_x/Co_3O_4(Hyd) catalyst, leading to a high degree of surface roughness and relatively large pore size and pore volume (see Table 4.2, BET analysis). Similar effects of CeO_2 species on the morphology of Co_3O_4 based catalyst has been reported in the literature [28, 29].

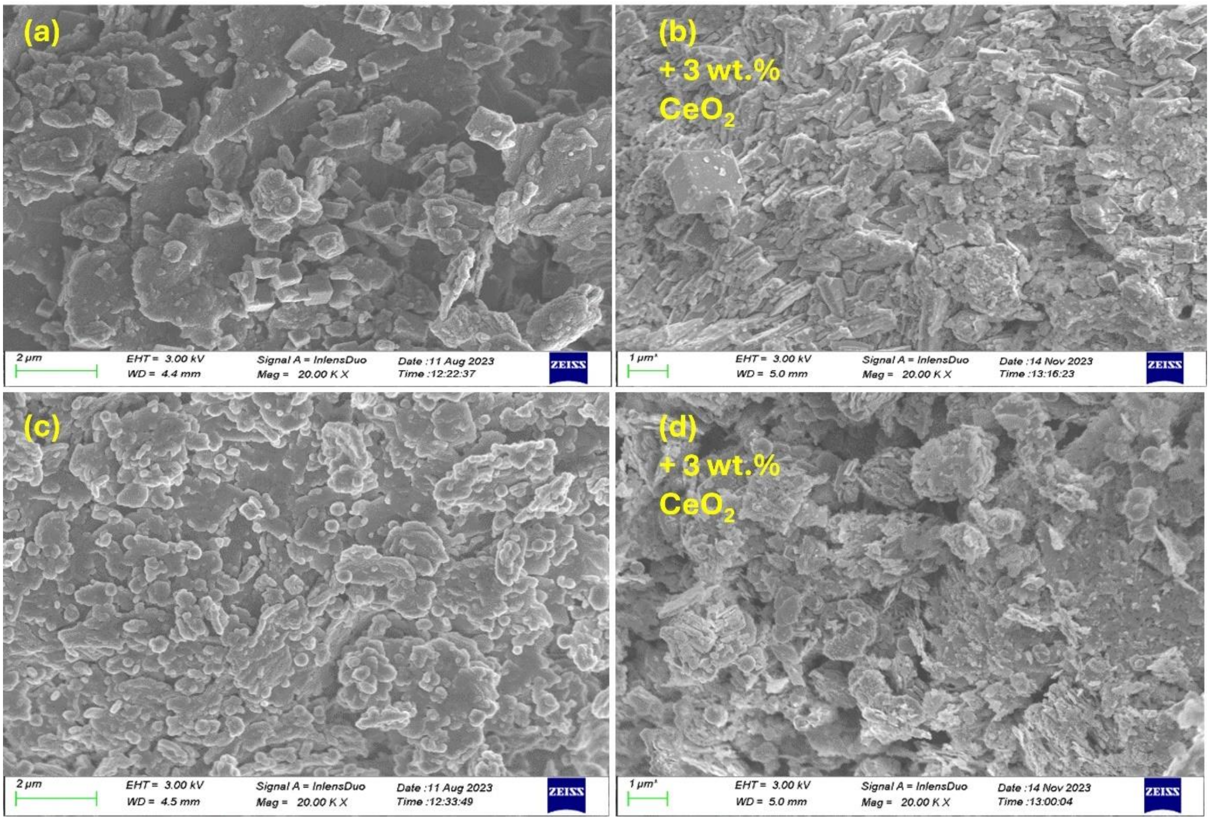

Figure 4.12 SEM micrographs of (a) 5 wt.% CuO_x /Co_3O_4Hyd, (b) 3Ce-5Cu/Co(Hyd), (c) 5 wt.% CuO_x/Co_3O_4(Ref), and (d) 3Ce-5Cu/Co(Ref) catalysts.

The spherical like particles dispersed over the Ulva-like aggregates in pure 5 wt.% CuO_x /Co_3O_4(Ref) catalyst (Figure 4.12 (c)) seems to be destructed after the addition of of 3 wt.% CeO_2 by reflux method, also showing some surface roughness and morphology transformation to an irregular mesh-like porous clusters (Figure 4.12 (d)).

4.2.6. Tunnelling electron microscopy (TEM) analysis

4.2.6.1. Tunnelling electron microscopy (TEM) analysis of bare Co_3O_4(Hyd) and Co_3O_4(Ref) catalyst and their bimetallic counterparts (i.e., with CuO_x and CeO_2)

Since CuO_x species couldn't be identified by the XRD analysis and in conjunction with verifying the crystal structure of the prepared nano catalysts, elemental composition and surface morphology, TEM analysis was performed (see Figure 4.13). All the prepared catalysts show concentric ring-like SAED patterns, (Figure 4.13 a_4, b_5, c_5 d_4, e_5, f_5)), which confirms their polycrystalline nature, as probed by the XRD analysis (see Figure 4.1 and 4.2) [69]. The Co_3O_4(Hyd) and Co_3O_4(Ref) catalysts (Figure 4.9 (a) and (d), respectively) shows a nanoporous structure with large number of spherical nanoparticles of uniform size distribution (~7 – 23 nm). However, these nanoparticles are highly sintered in the latter, in agreement with the SEM analysis (see Figure 4.11 (c)).

The Co_3O_4 lattice fringes could clearly be observed on bare Co_3O_4(Hyd) and Co_3O_4(Ref) catalysts in Figure 4.13 (a_1) and (d_1) respectively, with high cobalt and oxygen dispersion, as shown in the EDX images (Figure 4.13 (a_2)-(a_3) and (d_2)-(d_3)) [3, 83]. The surface of Co_3O_4(Hyd) catalyst is predominantly exposed by the (220) planes, with a d-spacing (d_s) of 0.29-0.30 nm, whereas that of Co_3O_4(Ref) is terminated by the (311) (d_s = 0.25), (111) (d_s = 0.47 nm) and (220) (d_s = 0.29) crystal planes [3, 18, 29]. These confirms the characteristic spinel (Co_3O_4) structure of Co_3O_4(Hyd) and Co_3O_4(Ref) catalysts and correlates well with the XRD and the H_2-TPR data.

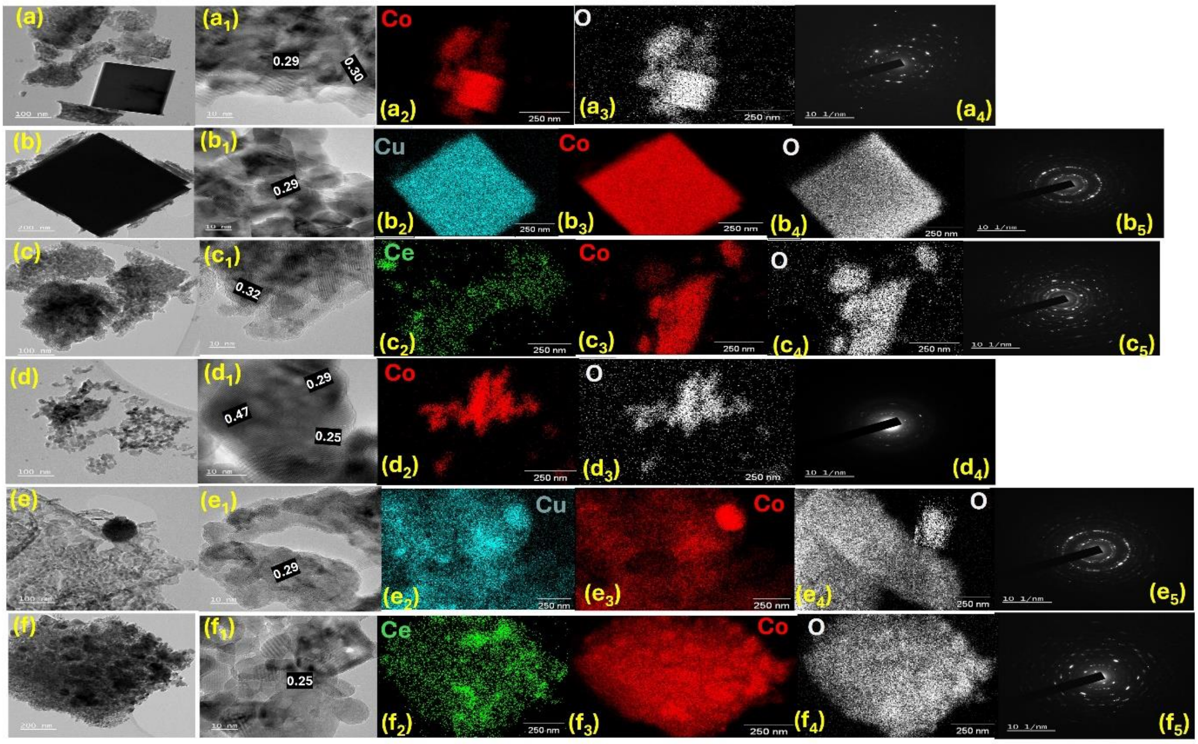

Figure 4.13 The TEM images of catalysts prepared by hydrothermal method (a) Co_3O_4(Hyd), (b) 5 wt.% CuO_x/Co_3O_4(Hyd), (c) 5 wt.% CeO_2/Co_3O_4(Hyd) and (B) reflux method (d) Co_3O_4(Ref), (e) 5 wt.% CuO_x/Co_3O_4(Ref), (f) 5 wt.% CeO_2/Co_3O_4(Ref). The HRTEM (a_1-f_1), EDX elemental mapping (a_2-a_3, b_2-b_4, d_2-d_3, e_2-e_5, f_2-f_5) and SAED (a_4, b_5, c_5 d_4, e_5, f_5) analysis images of these samples are also illustrated.

The sharp corners of 5 wt.% CuO_x/Co_3O_4(Hyd) catalyst's cubes observed from the SEM micrograph (Figure 4.12 (b)) can also be seen on the low-resolution TEM image and seems to be dispersed by a structure of porous nano cubes with an average edge length of 7 - 19 nm (Figure 4.13 (b)). The phase-contrast HRTEM micrograph of this sample (5 wt.% CuO_x/Co_3O_4(Hyd)) also showed lattice-border intersections spaced similarly (d_s = 0.29 nm) as in bear Co_3O_4(Hyd) catalyst (Figure 4.13 (a_1)), with (220) preferential surface exposure (Figure 4.13 (b_1)). These implies that the addition of 5 wt.% CuO_x species under hydrothermal method did not change the exposed crystal planes rather the morphology of Co_3O_4(Hyd) catalyst, as observed from the SEM images (see Figure 4.12 (a) and (b)). Therefore, the exposed crystal planes were not the major factor contributing to the outstanding CO(PrOx) performance over 5 wt.% CuO_x /Co_3O_4(Hyd) catalyst [13].

Addition of 5 wt.% CuO_x dopant under reflux method prevented the sintering of Co_3O_4(Ref) nanocrystals (Figure 4.13 (d_1)), resulting in a highly porous structure made up of ultra-small sized nanoparticles (Figure 4.13 (e_1)) (5-16 nm), in agreement with the BET and XRD analysis (Table 4.2). Small sized nanoparticles are formed when bulk network structures are chopped down by cooled influx droplets, during reflux method [81]. Moreover, CuO_x is evenly distributed in Co_3O_4 spinel matrix as shown by the HRTEM and EDX images in Figure 4.13 (e_1) and (e_2), respectively. Interestingly, the (111) facets and (311) of Co_3O_4(Ref) catalyst (Figure 4.13 (d_1)), could not be detected after 5 wt.% CuO_x addition under reflux method (Figure 4.13 (e_1)). These confirms the lattice distortion caused by incorporation of CuO_x species within the Co_3O_4(Ref) matrix, in agreement with the XRD data (see Figure 4.2) [57, 84, 85]. Nonetheless, CuO_x lattice fringes (or d spacing) could not be identified from the HRTEM images of all CuO_x doped catalysts (Figure 4.13 (b_1) and (e_1)), as was resistant in [13]'s work. This makes it difficult to conclude on the nature of CuO_x species hence, the formular CuO_x/Co_3O_4.

Figure 4.13 (c) shows that the addition of 5 wt.% CeO_2 onto Co_3O_4(Hyd) catalyst under hydrothermal method results in relatively small sized (6-10 nm) nanoparticles, as compared to CuO_x doped counterpart which confirms the improved surface area (see Table 4.2). However, the Co_3O_4(Hyd) nanoparticles are coated with a dense layer of CeO_2 nanoparticles (Figure 4.13 (c)) [29], which could explain the difficulties in their reducibility as probed by the H_2-TPR data. The crystal surface of 5 wt.% CeO_2/Co_3O_4(Hyd) catalyst is dominated by the fluorite (CeO_2) facets, terminated by (111) planes, with lattice spacing of 0.32 nm (Figure 4.13 (c_1)) [29, 86].

The introduction of 5 wt.% CeO_2 on Co_3O_4(Ref) catalyst (Figure 4.13 (d)), under reflux method also resulted in the agglomeration of CeO_2 nanocrystals on the support surface (Figure 4.13 (f)). However, the eclipsing effects of Co_3O_4 nanoparticles by CeO_2 shadows is reduced by reflux method (Figure 4.13 (f)), as compared to the hydrothermal counterpart (Figure 4.13 (c)). As a result, the surface of 5 wt.% CeO_2/Co_3O_4(Ref) catalyst is terminated by (311) crystal planes of Co_3O_4 crystallite as indicated by the HRTEM lattice fringes, with d_s = 0.25 nm (Figure 4. 8 (f_1)). Moreover, the less intensified ring pattern in the SAED profiles of CeO_2 doped Co_3O_4(Hyd) and Co_3O_4(Ref) catalysts (Figure 4.13 (c_5) and (f_5)), agrees well with the XRD peak disappearance of bare Co_3O_4(Hyd) and Co_3O_4(Ref) catalyst (Figure 4.1 (c) and 4.2 (c)), after 5 wt.% CeO_2 addition [83, 86].

4.2.6.2. TEM analysis of ternary catalysts: Effect of 3 wt.% CeO_2 on the structure of 5 wt.% CuO_x/Co_3O_4(Hyd) and 5 wt.% CuO_x/Co_3O_4(Hyd) catalysts.

Figure 4.14 compares the TEM, HRTEM and the corresponding EDX/SAED mapping analysis images of the prepared polycrystalline ternary catalyst to their bimetallic counterpart. The addition of 3 wt.% CeO_2 on 5 wt.% CuO_x/Co_3O_4 (Figure 4.14 (a)) under hydrothermal method reduced the size of Co_3O_4 cube from the micron scale (see SEM. Figure 4.11 (b)) to a nanometer scale (~70-92 nm) (Figure 4.14 (b)). This is consistent with the decrease in the crystallite size and imroved surface area of 3Ce-Cu/Co(Hyd) catalyst as compared to its bimetallic 5 wt.% CuO_x/Co_3O_4(Hyd) counterpart (see Table 4.4). According to the EDX (Figure 4.19 (b_2)-(b_5)) and the SAED pattern (Figure 4.14 (b_6)) of 3Ce-5Cu/Co(Hyd) catalyst, the Co_3O_4 crystals are dispersed by an amorphous cluster of CeO_2-CuO_x, creating a core-shell like cubic structure (Figure 4.14 (b)) [114, 152].

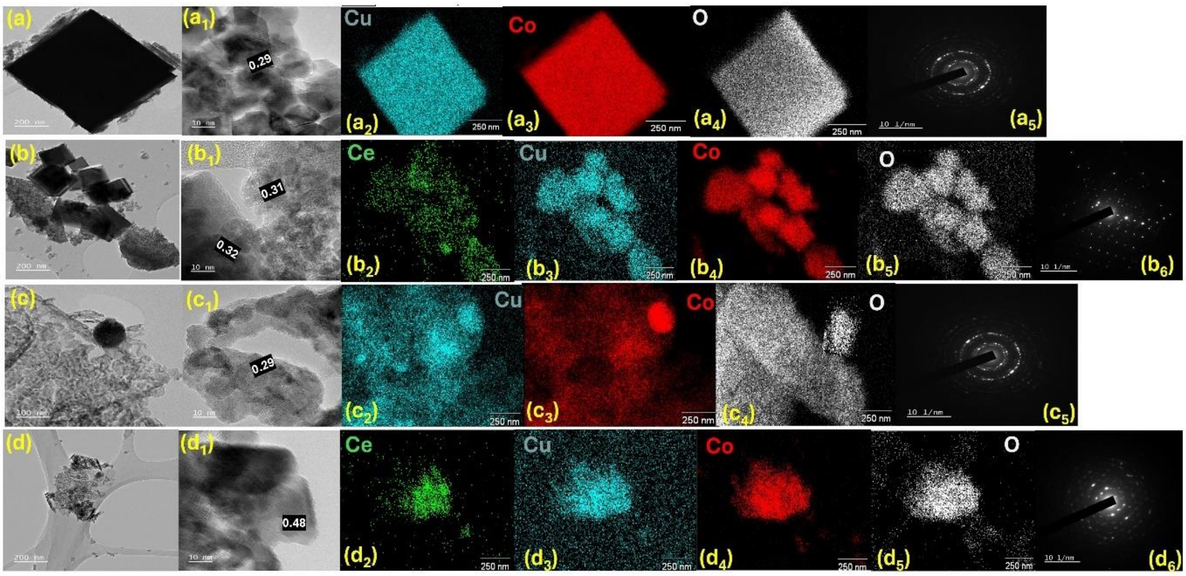

Figure 4.14 The TEM images of (a) 5 wt.% CuO_x /Co_3O_4(Hyd), (b) 3Ce-5Cu/Co(Hyd), (c) 5 wt.% CuO_x /Co_3O_4(Ref) and (d) 3Ce-5Cu/Co(Ref) catalysts. The HRTEM (a_1-d_1), EDX elemental mapping (a_2-a_3, b_2-b_5, c_2-c_4, d_2-d_5) and SAED (a_5, b_6, c_5, d_6) analysis images of the corresponding samples.

The HRTEM images of this catalyst showed the lattice fringes with interplana spacing of 0.31 nm and 0.32 nm, which confirms the surface exposure of (111) crystal facets of CeO_2 fluorite structure (Figure 4.14 (b_1)) [78]. On the other hand, the addition of 3 wt.% CeO_2 on 5 wt.% CuO_x/Co_3O_4(Ref) by reflux method changed the spherical nanoparticles (Figure 4.14 (c)), to clustred rod-like nano material, with diameter of ~4 nm and length of 20 – 40 nm (Figure 4. 14 (d)). Qiu *et al.*, [47], has observed similar results. It is also clear that the nanopores of 5 wt.% CuO_x /Co_3O_4(Ref) catalyst (Fugure 4.14 (c)) are blocked by aggregates after ceria addition under reflux method, consistant with the N_2 adsortpion/dsoprtion isotherm data (Table 4. 2). The HRTEM image of 3Ce-5Cu/Co(Ref) catalyst shows crystal plane and lattice fringes with d_s = 0.48, ascribed to (111) crystal facets of Co_3O_4 spinel structure, approving the XRD results of this material (Figure 4.14 (d)) [84, 152]. It was also observed that some diffraction ring patterns of bear bimetallic catalysts (Figure 4.14 (a_5) and (a_6)) diffuse after ceria addition under both hydrothermal and reflux method (Figure 4.14 (b_6) and (d_6), respectively). These confirms the existence of an amorphous phase on the catalysts' surface, in agrrement with XRD data (Figure 4. 3) [83, 86].

4.2.7. Hydrogen Temperature program reduction (H_2-TPR) analysis

4.2.7.1. Effect of hydrothermal method towards the reducibility of Co_3O_4(Hyd) catalyst in the presence of 5 wt.%, CuO_x and CeO_2 species

The redox properties of Co_3O_4(Hyd) catalyst prepared by hydrothermal method, and the nature of its interaction with CuO_x and CeO_2 nanocrystals was investigated by H_2-TPR analysis, as revealed in Figure 4.15. The reduction of bare Co_3O_4(Hyd) catalyst starts at ~140 ^oC and shows a small peak maximum at 150 ^oC, followed by two main reduction peaks at 284 and 467 ^oC (Figure 4.15 (A); (a)). The peak at 150 ^oC belongs to the reduction of surface adsorbed oxygen species [37, 95], and the two large main peaks correspond to the stepwise reduction of a spinel crystallite to metallic cobalt, via Co_3O_4 (Co^{3+}) → CoO and CoO (Co^{2+}) → Co (Co^0) process, sequentially [13, 42, 95]. The peak at 467 ^oC can be separated into two components, which clearly shows the reduction of surface and bulk CoO species to metallic form at 417 ^oC and 558 ^oC, respectively (Figure 4.15 (B)).

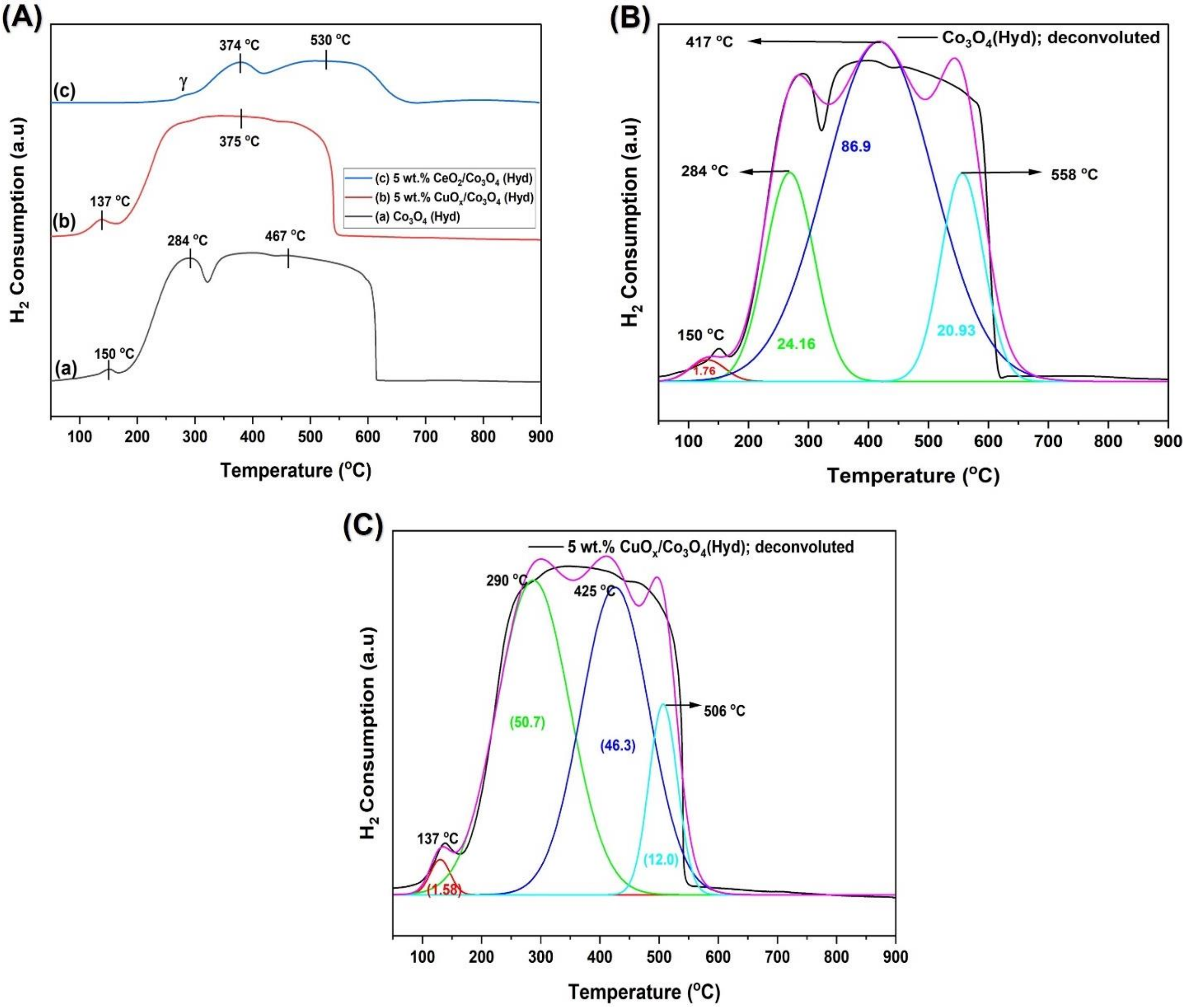

Figure 4.15 H_2-TPR profiles (A) of (a) Co_3O_4(Hyd), (b) 5 wt.% CuO_x/Co_3O_4(Hyd), (c) 5 wt.% CeO_2/Co_3O_4(Hyd) catalysts. (B) and (C) illustrates the deconvoluted components of (a) Co_3O_4(Hyd) and (b) 5 wt.% CuO_x/Co_3O_4(Hyd) catalyst.

After the addition of 5 wt.% CuOx species, the Co_3O_4(Hyd) reduction begins at a very low temperature of 120 °C, with a peak maximum at 137 °C (Figure 4.15 (A); (b)). This peak is ascribed to the reduction of highly dispersed CuO_x species on Co_3O_4(Hyd) surfaces, certainly the Cu_2O island probed by the XRD (Figure 4.1 (b)) [13]. It could also be observed that the reduction temperatures of Co_3O_4 → Co two-step process overlap into a single broad peak at ~375 °C after 5 wt.% CuO_x addition, due to relative high cobalt content [46]. According to Lukashuk *et al.,* [86], the overlap of Co_3O_4 reduction peaks could be due to the transformation of Co_3O_4 directly to metallic Co, without passing through CoO intermediate, which is thermodynamically unstable at low reduction temperatures (< 291 °C). The merging of Co_3O_4 reduction peaks as a result of copper oxide dopant were also reported elsewhere [23, 28]. This makes it difficult to conclude on the redox properties of the supported catalysts and it's a serious limitation of H_2-TPR technique [12]. However, such issues could be resolved experimentally by lowering the heating rate or statistically by data deconvolution, as shown in Figure 4.15 (C). As a results, the Co_3O_4 reduction peaks in 5 wt.% CuO_x/Co_3O_4(Hyd) catalyst could easily be distinguished at around 290 and 425 ^oC, and that of bulk Co_3O_4 reduction isolated from CuO_x dopant at ~506 ^oC [26, 37].

On the other hand, introduction of 5 wt.% CeO_2 increase the reduction temperatures and the first reduction peak, represented as 'γ' begins at around 267 ^oC, followed by the two main reduction signals for spinel transition to zero valent cobalt at around 374 and 530 ^oC (Figure 4.15 (A); (c)). The XRD data (Table 4.1) showed a significant lattice contraction after 5 wt.% CeO_2 addition, as a results of high oxygen vacancies. This can explain the relatively small total reduction peak area under 5 wt.% CeO_2/Co_3O_4(Hyd) catalyst, as compared to that of bare Co_3O_4(Hyd) catalyst (Figure 4.15 (A); (a)). Furthermore, due to limited surface oxygen in 5 wt.% CeO_2/Co_3O_4(Hyd) catalyst, the reduction of Co_3O_4(Hyd) support could also be occurring by electron donation from CeO_2, and not via H_2 consumption. This notion is supported by the absence of $Ce^{4+} \rightarrow Ce^{3+}$ reduction peak(s), which occurs at around ~500 ^oC [3, 21, 105]. Similar results has been reported by Niu *et al.*, [88]. The H_2-TPR data shows that the strong synergistic interaction between CuO_x and Co_3O_4(Hyd) catalyst at the interphase promotes Cu^{2+}/Cu^{+} and Co^{2+}/Co^{3+} redox shuttle, which stimulates the release of oxygen from the support and could benefit CO(PrOx) reaction [1, 37, 41]. Meanwhile ceria addition steals the oxygen from Co_3O_4 support, and the resulting metal-support interaction decreases the Co_3O_4(Hyd) catalyst's reduction temperature, despite the improved surface area (see BET analysis, Table 4.2).

4.2.7.2. Effect of reflux method towards the reducibility of Co_3O_4(Ref) catalyst in the presence of 5 wt.%, CuO_x and CeO_2 species

Figure 4.16 shows the H_2-TPR data of Co_3O_4(Ref), 5 wt.% CuO_x/Co_3O_4(Ref) and 5 wt.% CeO_2/Co_3O_4(Ref) catalysts prepared by reflux method. Bare Co_3O_4(Ref) catalyst shows a weak reduction peak at around 293 ^oC, followed by large two peaks, one beginning at around 350 ^oC with a maximum at ~577 ^oC. The other one start at ~650 ^oC and levels from 716 ^oC up to a maximum scanning temperature of 900 ^oC (Figure

4.16 (A); (a)). Just like in Co_3O_4(Hyd) catalyst (Figure 4.15 (A); (a)), the 293 °C peak belongs to the reduction of surface adsorbed oxygen species and the last two main peaks (577 °C and 716 °C) represents Co_3O_4(Ref) transition to metallic cobalt. Such difficulties in the reducibility of Co_3O_4(Ref) catalyst could be ascribed to agglomerated Co_3O_4 nanoparticles as observed from the SEM (Figure 4.11 (c)) and TEM data (Figure 4.13 (d)).

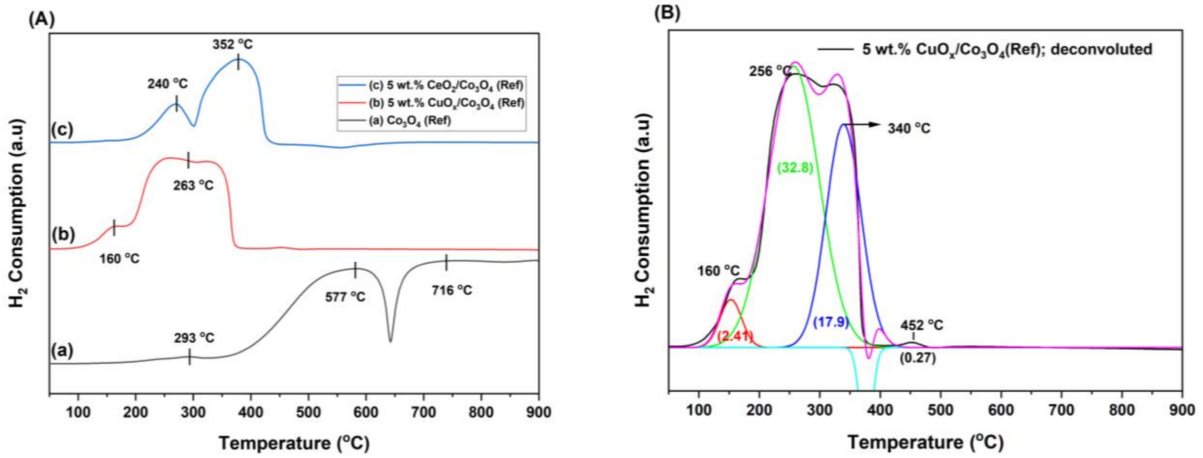

Figure 4.16 The H_2-TPR profiles (A) of (a) Co_3O_4(Hyd), (b) 5 wt.% CuO_x/Co_3O_4(Hyd), (c) 5 wt.% CeO_2/Co_3O_4(Hyd) catalysts. (B) is the deconvoluted components of (b) 5 wt.% CuO_x/Co_3O_4(Ref) catalyst.

However, after the addition of 5 wt.% CuO_x species, the reduction behaviour of Co_3O_4(Ref) catalyst (Figure 4.16 (A); (a)), was tremendously improved and the resulting 5 wt.% CuO_x/Co_3O_4(Ref) catalyst starts to reduce earlier at ~130 °C, with a peak maximum at 160 °C (Figure 4.9 (A); (b)). This peak belongs to the reduction of CuO_x nanoparticles interacting with Co_3O_4 support, whose overlapping peaks (~263 °C) could also be observed clearly in the deconvoluted H_2-TPR profile (Figure 4.16 (B)). In addition to increased surface area and high nanoparticle dispersion, the good reducibility of 5 wt.% CuO_x/Co_3O_4(Ref) catalyst is also associated with the strong interaction between CuO_x and Co_3O_4(Ref) withing the solid solution (see XRD analysis, Figure 4.2) [20]. This alters the electronic structure of the support and increase oxygen mobility for H_2 consumption [1, 17, 23, 41]. The small reduction peak located at higher temperatures (452 °C) (Figure 4.16 (B)) is ascribed to the reduction of bulk copper-cobaltite crystals [90], due to the stabilized spinel cations [26, 27, 100]. This lone peak is a fingerprint assertion towards CuO_x enhanced bulk Co_3O_4(Ref) reducibility [57], a characteristic that 5wt.% CuO_x/Co_3O_4(Hyd) catalyst don't inherit (Figure 4.15 (A); (a)).

Hence the reducibility of bulk Co_3O_4 support catalyst was improved significantly by CuO_x addition under, reflux method.

Notice that the area under the curves corresponding to the main reduction peaks of $Co_3O_4 \rightarrow CoO \rightarrow Co$ transformation in 5 wt.% CuO_x/Co_3O_4(Ref) catalyst (256 °C; area 32.8 and 340 °C; area = 17.9) (Figure 4.16 (B)), are all smaller than those of 5 wt.% CuO_x/Co_3O_4(Hyd) catalyst (290 °C; area = 50,7 and 420 °C; area = 46.3) (Figure 4.16 (B)). This implies that the substitution of Co^{2+} by Cu^{2+} in the former (see XRD, Figure 4.2 (b)), decreases the total consumption of H_2 by spinel phase (Co_3O_4), due to the reduced cobalt concentration [99, 100]. A similar behaviour was reported by Souza *et al.,* [91], on Mg modified Co-Al spinel catalyst prepared by co-precipitation method. Furthermore, the CuO_x reduction peak of 5 wt.% CuO_x/Co_3O_4(Ref) catalyst has large area of ~2.41 (at 160 °C, Figure 4.16 (B)) as compared to just 1.58 of 5 wt.% CuO_x/Co_3O_4(Hyd) catalyst (at 137 °C, Figure 4.15 (B)), despite the same CuO_x content. This is because most of Cu^{2+} cations in CuO_x have already been reduced to to Cu^+ (Cu_2O) species in 5wt.% CuO_x/Co_3O_4(Hyd) catalyst (see XRD analysis, Figure 4.1 (b)), thus also assisting in total reducibility of CuO_x species as shown by the relatively low reduction temperature (137 °C) [17, 45, 48].

The 5 wt.% CeO_2/Co_3O_4(Ref) shows only two reduction temperatures starting at around 152 °C and peaking at 240 °C and the second reduction peak begins from 298 °C with a corresponding maximum at 352 °C (Figure 4.16 (A); (c)). These two peaks belong to a two staged spinel reduction to cobalt metals. This is an improvement on bare Co_3O_4(Ref) catalyst's reducibility, previously requiring 577 and 716 °C for a similar two staged processes, accordingly (Figure 4.16 (A); (a)). Such ease in the reduction of 5 wt.% CeO_2/Co_3O_4(Ref) catalyst could be brought upon by its relatively high surface area and large pore size distribution (see Table 4.2) [37, 52, 66]. The Hydrogen spill-over process from Co_3O_4(Ref) to CeO_2 (or verse versa), can also increase the catalyst's reducibility, and textural properties (such as pore volume and surface area) plays a crucial role during this process [21, 38, 66]. The H_2-TPR is in well agreement with the literature findings [42, 60, 106, 107].

4.2.7.3. Effect of 3 wt.% CeO_2 on the reducibility of 5 wt.% CuO_x/Co_3O_4(Hyd) and 5 wt.% CuO_x/Co_3O_4(Ref) catalysts

The reducibility of the prepared ternary catalysts was also studied by H_2-TPR analysis, as shown in Figure 4.17. It could be observed that the reduction peak of highly dispersed CuO_x species at ~137 °C in 5 wt.% CuO_x/Co_3O_4(hyd) catalyst (Figure 4.17 (A); (a)), shifts towards high reduction temperatures (~163 °C) after the addition of 3 wt.% CeO_2 by co-precipitation under hydrothermal method (Figure 4.17 (A); (b)). Similarly, transition from Co_3O_4 to metallic Co has shifted from 367 to 439 °C peak maxima. The slight shifts to higher reduction temperatures could be explained by the hindered Co_3O_4(Hyd) crystallite, by highly dispersed CeO_2 flurorite phase (see HRTEM, Figure 4.14 (b_1)). Addition of rare earth elements has also been shown to increase the reduction temperatures of Cu/Co oxide composite [94]. Interestingly, two new peaks are observed in 3Ce-5Cu/Co(Hyd) sample (Figure 4.17 (A); (b)), peak 'α' (200 °C) and peak 'β' (284 °C), and Figure 4.17 (B) shows the deconvoluted component of this catalyst sample.

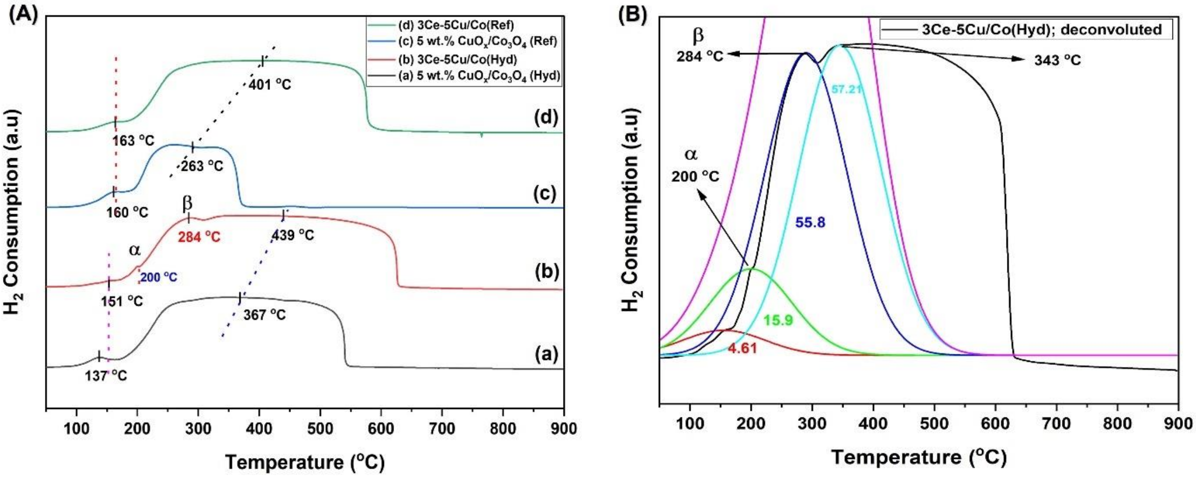

Figure 4.17 The H_2-TPR curves (A) of (a) 5 wt.% CuO_x/Co_3O_4 (Hyd)), (b) 3Ce-5Cu (Hyd), (c) 5 wt.% CuO_x/Co_3O_4 (Ref) and 3Ce-5Cu/Co(Ref) catalysts, and the decomvoluted component (B) of (b) 3Ce-5Cu (Hyd) catalyst.

According to [2, 32], peak α is attributed to CuO_x species, strongly interacting with ceria, which complements the XRD (see Figure 4.3) and the TEM data (Figure 4.14). It was observed that the overlap of Co_3O_4 to CoO peak shoulder with that of CoO to Co transition was due to the addition of copper species (Figure 4.17 (A); (a)). The emergence of peak β, clearly suggest the existence of disseminated Co_3O_4

nanoparticles, definitely those that were interacting with CuO_x species. This results confirms nothing else but strong CuO_x-CeO_2 interactions in 3Ce-5Cu/Co(Hyd) catalyst.

Under reflux conditions, the CuO_x peak maximum at 160 ^oC in pure 5 wt.% CuO_x/Co_3O_4(Ref) catalyst (Figure 4.17 (c)), shifts only by 3 ^oC towards higher reduction temperatures after the introduction of 3 wt.% CeO_2, in addition to the peak broadening of superimposed Co_3O_4 to Co reduction at 401 ^oC (Figure 4.17 (d)). This implies that CuO_x-CeO_2 interactions stimulates the oxygen storage capacity and mobility of 3Ce-5Cu/Co(Ref) catalyst. The broad nature of this profile (Figure 4.17 (d)), without any humbs makes its hard to deconvolute and as discussed these could be due to Co_3O_4 reduction directly to metallic Co [86].

The shapes and the reduction temperatures of the H_2-TPR curves for samples obtained by hydrothermal differs significantly from their counter samples obtained by reflux method. This concludes that the reduction behaviour of the prepared catalysts depends significantly on the preparation method, particularly the treatments of metal salt's precoursor solution, prior to calcination. These has a direct influence on the catalytic perfomance of the nanomaterials.

4.3. CATALYTIC ACTIVITY TESTS OF THE PREPARED SAMPLES IN CO(PrOx) REACTION

Carbon monoxide oxidation in hydrogen rich stream was carried out in a continuous reactor bed (U shape borosilicate glass with inner diameter of 5 mm), containing 100 mg of the catalyst. The feed gas comprised of 1 vol.% CO, 1 vol.% O_2 and 50 vol.% H_2 balanced He (48 vol.%), at a total flow rate of 100 mL/min and 60 000 mL/h.g gas hourly space velocity (GHSV). The outlet gaseous mixture was monitor by an online GC chromatography and the % CO conversion was measured as a function of temperature, ranging from 40 – 200 ^oC (at 1 atm). Effects of CeO_2 and CuO_x load (in wt.%) in CO(PrOx) reaction over Co_3O_4 catalyst were evaluated to find the optimum load, under both hydrothermal (Hyd) and or reflux (Ref) method. An optimum load of the best Co_3O_4 dopants prepared by each method was further investigated towards CO(PrOx) in moisture saturated feed gas. The stability of the as prepared catalysts was also evaluated under dry, moisture (10 vol.% H_2O) and 15 vol.% CO_2 in the feed stream. The CO(PrOx) results are discussed in the following subsections.

4.3.1. Effects of ceria load on CO(PrOx) reaction over Co_3O_4(Hyd) and Co_3O_4(Ref) catalysts

Various amounts of CeO_2 (1, 3, and 5 wt.%) were introduced on Co_3O_4(Hyd) and Co_3O_4(Ref) catalyst, under hydrothermal and reflux method respectively and tested towards CO(PrOx) reaction as shown in Figure 4.18.

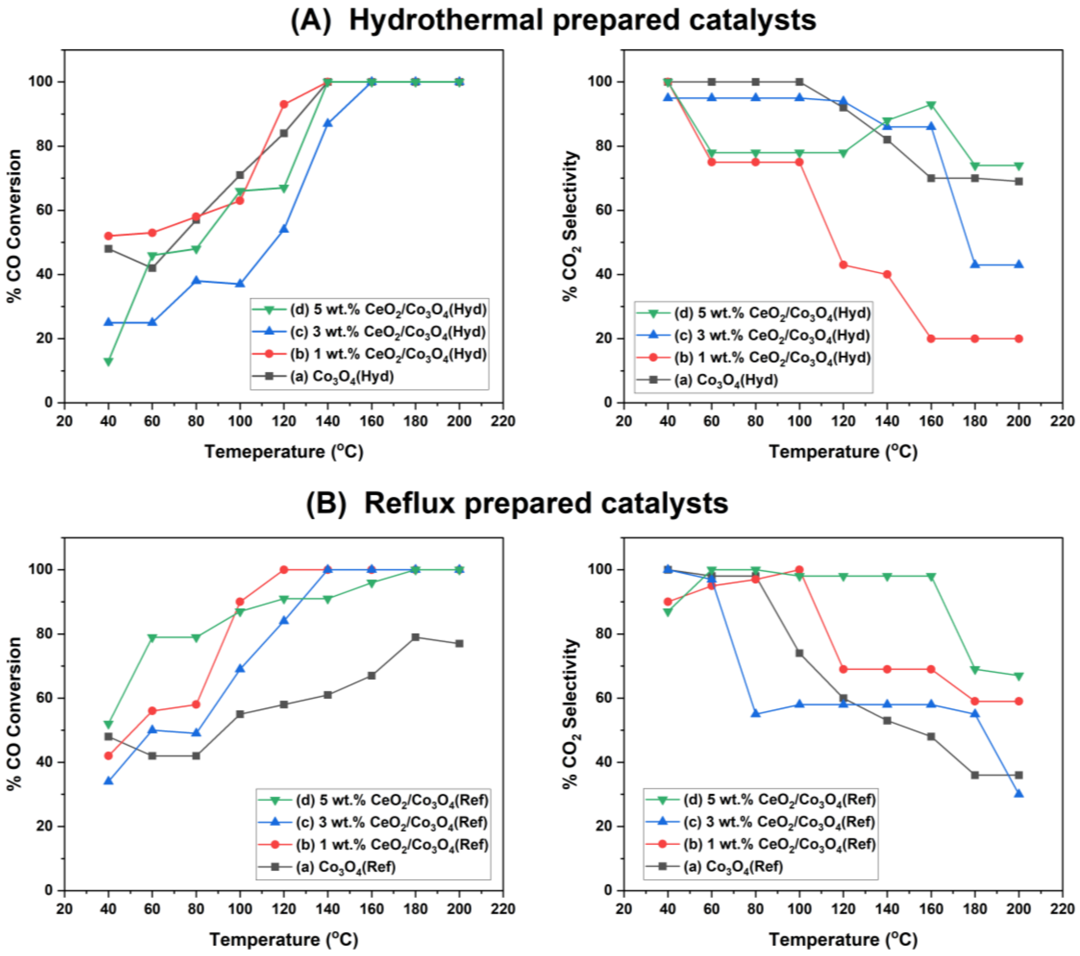

Figure 4.18 CO conversion and CO_2 selectivity of (A) hydrothermally prepared (a) Co_3O_4, (b) 1 wt.% CeO_2/Co_3O_4(Hyd), (c) 3 wt.% CeO_2/Co_3O_4(Hyd), (d) 5 wt.% CeO_2/Co_3O_4(Hyd) and of (B) reflux prepared (a) Co_3O_4(Ref), 1 wt.% CeO_2/Co_3O_4(Ref), (c) 3 wt.% CeO_2/Co_3O_4(Ref), (d) 5 wt.% CeO_2/Co_3O_4(Ref) catalysts.

The hydrothermally prepared bare Co_3O_4(Hyd) catalyst converted 40% CO gas at 60 °C, which increased linearly with temperature, reaching complete CO oxidation (100%) at 140 °C (Figure 4.18 (A); (a)). Introduction of 1 wt.% CeO_2 slightly improves the CO oxidation and the resulting 1 wt.% CeO_2/Co_3O_4(Hyd) catalyst realizes CO conversion of 52% at 60 °C, and outcompetes its counterparts i.e., 3 and 5 wt.% CeO_2 load (Figure 4.18 (A); (c) and (d)), anywhere below 140 °C. However, the 1 wt.% CeO_2/Co_3O_4(Hyd) catalyst showed the worst CO_2 selectivity (Figure 4.18 (A); (a)), as compared to all the catalysts prepared under this method. At temperature range 60 – 140 °C, the catalytic activity of bare Co_3O_4(Hyd) is greater than that of maximum CeO_2 load, i.e., 5 wt.% CeO_2/Co_3O_4 catalyst (Figure 4.10 (A); (d)). This could be ascribed to the high reduction temperatures required to reduce 5 wt.% CeO_2/Co_3O_4 catalyst, as compared to bare Co_3O_4(Hyd) catalyst (see H_2-TPR data (Figure 4.15 (A)), regardless of the improved surface area (Table 4.1). This shows that the addition of ceria doesn't always enhances CO(PrOx) performance of the catalyst. Zhao *et al.,* [34], observed similar effects on CeO_2/Co_3O_4–MnO_2/CeO_2 catalyst supported on activated carbon. The author [34], suggested that appreciable methods for CeO_2 introduction are essential.

Under reflux method as shown in Figure 4.18 (B), the data indicates a slight increase in CO conversion with the addition of 1% CeO_2 on Co_3O_4(Ref) catalyst ((Figure 4.18 (B); (b)). However, when the concentration is raised to 3 wt.% CeO_2 (Figure 4.18 B; (c)), a decrease in activity was observed. Interestingly, when the concentration is raised to 5 wt.% CeO_2 ((Figure 4.18 (B)1(d)), an increase in activity to 80% conversion was obtain at 60 °C as compared to 41% of Co_3O_4(Ref) ((Figure B(a)). Furthermore, the activity of 5 wt.% CeO_2/Co_3O_4 catalyst seems to show an increase in CO(PrOx) as temperature increases and these is accompanied by good selectivity (which remain stable up to 160 °C) ((Figure 4.18 (B); (d)). This increase in CO(PrOx) performance could be brough upon by improved reducibility of Co_3O_4(Ref) catalyst and an increase in its surface area, pore size and pore volume after 5 wt.% CeO_2 addition (see Figure 4. 16 and Table 4.2) [51, 63, 116]. In addition to temperature sensitivity of H_2 oxidation reaction [114, 115], a low selectivity in all 5 wt.% CeO_2 doped counterparts (Figure 4.18 (A) and (B); (a)-(c)) could be ascribed to lowered oxygen storage capacity, as a results of low CeO_2 content [98].

The H_2-TPR data showed that the catalytic activity of bare Co_3O_4(Hyd) and Co_3O_4(Ref) catalysts at low temperatures depends on the surface adsorbed electrophilic oxygen species (such as O_2^-, O_2^{2-}, O^-) thus, imply Eley-Ridel's mechanism [18, 95, 96]. These species were difficult to reduce in the latter, which explain its relatively low CO(PrOx) activity (Figure 4.18 (A); (a)) as compared to Co_3O_4(Hyd) catalyst (Figure 4.18 (B);

(a)). Moreover, the hydrothermally prepared 5 wt.% CeO_2/Co_3O_4(Hyd) catalyst demonstrates a lowest catalytic performance anywhere below 140 °C in CO(PrOx) (Figure 4.18 (A); (d)), as compared to its reflux counterpart (Figure 4.10 (A); (d)). The discrepancies in CO(PrOx) performance over 5 wt.% CeO_2/Co_3O_4(Hyd) and 5 wt.% CeO_2/Co_3O_4(Ref) catalysts could be directly linked to the different S_{BET} of 64.0 m^2/g and 67.6 m^2/g, respectively [45, 131]. The hydrothermal loading of CeO_2 showed agglomeration of cerium oxide clusters, (see TEM, Figure 4.13 (c)). which could hinder the Co_3O_4(Hyd) active sites [84], and decrease the reduction temperature of 5 wt.% CeO_2/Co_3O_4(Hyd) catalyst (H_2-TPR evident, Figure 4.15), which could explain its relatively low activity [123, 128].

4.3.2. Effects of copper oxide load on CO(PrOx) reaction over Co_3O_4(Hyd) and Co_3O_4(Ref) catalysts

Copper oxide (CuO_x) was also introduced at varying content (3, 5, 10, 15 wt.%) on Co_3O_4(Hyd) and Co_3O_4(Ref) catalysts under hydrothermal and reflux method and tested for CO(PrOx) reaction as shown in Figure 4.19. Introduction of 3 wt.% CuO_x on Co_3O_4(Hyd) catalyst (Figure 4.19 (A); (a)) by hydrothermal method, supressed the catalytic activity below 100 °C (Figure 4.19 (A); (b)). When CuO_x content increase to 5 wt.%, 74% CO conversion at 40 °C with good and stable CO_2 selectivity (~100%) below 160 °C, was observed (Figure 4.19 (A); (c)). The high CO conversion and selectivity of 5 wt.% CuO_x/Co_3O_4(Hyd) catalyst as compared to bare Co_3O_4(Hyd) regardless of its relatively small surface area (Table 4.2), could be attributed to the easily reducible and highly dispersed CuO_x nano cubes over Co_3O_4(Hyd) catalyst, as probed by the XRD, TEM and H_2-TPR data. Zhao *et al*., [34], observed similar results. At these CuO_x-Co_3O_4(Hyd) heterojunctions, CO forms a Cu^+-CO complex, which is readily oxidized to CO_2 by lattice oxygen of the support [39, 116]. As the amount of copper increase further to 10 and 15 wt.%, the CO conversion decreased (Figure 4.19 (A); (c) and (e)), perhaps due to agglomeration of CuO_x particles, as claimed in the literature [3, 57, 105, 117]. On contrary, the introduction of 3 wt.% CuO_x species under reflux method as shown in Figure 4.19 (B); (b), improved the catalytic performance of Co_3O_4(Ref) catalyst (Figure 4.19 (B); (a)), at all temperatures. As in hydrothermal method, the performance of bare Co_3O_4(Ref) catalyst was enhanced drastically when

5 wt.% CuO_x was introduced (Figure 4.19(B);(c)). The 5 wt.% CuO_x/Co_3O_4(Ref) catalyst oxidize 94% CO gas at 40 °C.

(A) Hydrothermal prepared catalysts

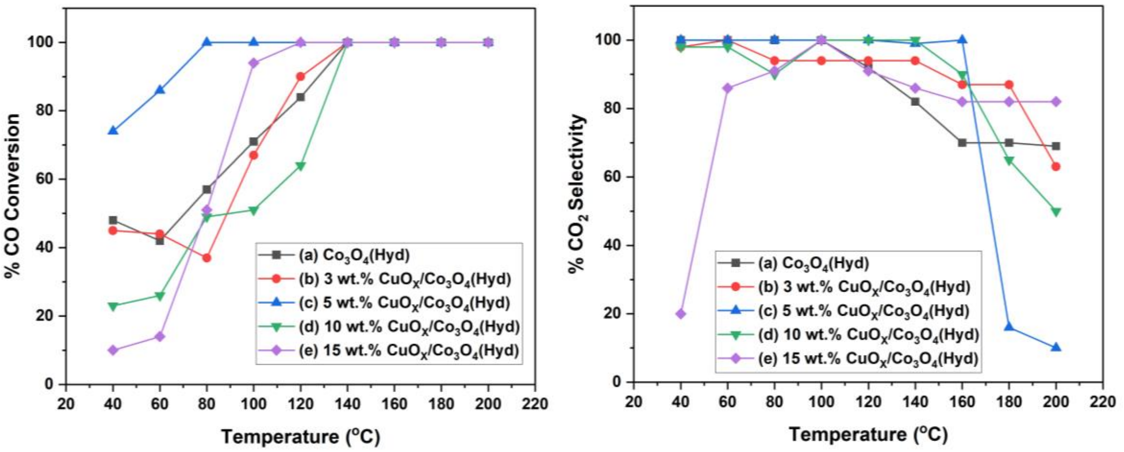

(B) Reflux prepared catalysts

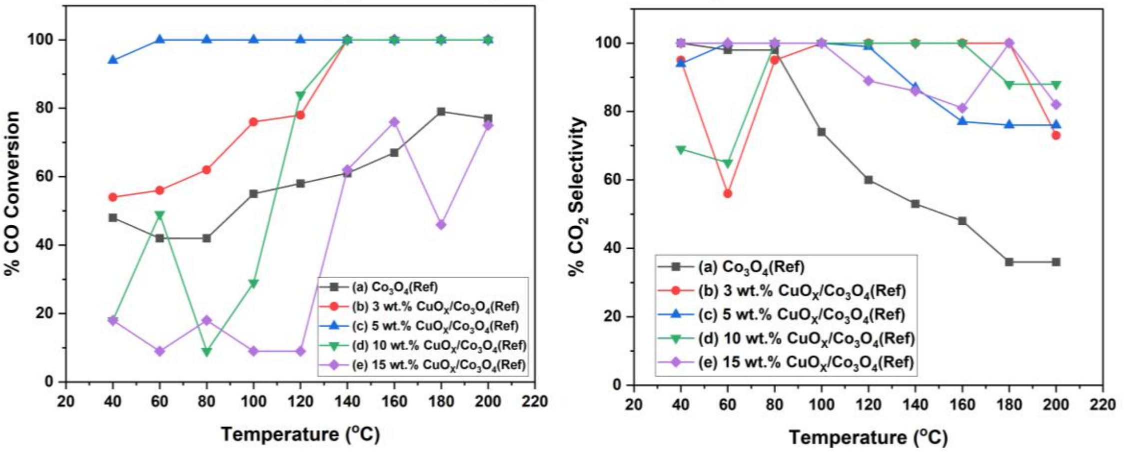

Figure 4.19 CO conversion and CO_2 selectivity of (A) hydrothermal prepared (a) Co_3O_4(Hyd), (b) 3 wt.% CuO_x/Co_3O_4(Hyd), (c) 5 wt.% CuO_x/Co_3O_4(Hyd), (d) 10 wt.% CuO_x/Co_3O_4(Hyd)and (e) 15 wt.% CuO_x/Co_3O_4(Hyd), and the CO conversion and CO_2 selectivity of (B) reflux synthesised (a) Co_3O_4(Ref), (b) 3 wt.% CuO_x/Co_3O_4(Ref), (c) 5 wt.% CuO_x/Co_3O_4(Ref), (d) 10 wt.% CuO_x/Co_3O_4(Ref) and (e) 15 wt.% CuO_x/Co_3O_4(Ref) catalysts.

The good catalytic performance of 5 wt.% CuO_x/Co_3O_4(Ref) catalyst as compared to bare Co_3O_4(Ref) catalyst could be ascribed to the relatively high S_{BET} (see Table 4.2) [50, 54] and easily reducible surface oxygens (Figure 4.16) [45, 96, 128]. The strong CuO_x-Co_3O_4(Ref) interactions in the solid solution revealed by the XRD (Figure 4.2) and H_2-TPR (Figure 4.15) in 5 wt.% CuO_x/Co_3O_4(Ref) catalyst, leads to abundant active Co^{3+} sites, which are conducive to CO adsorption [20]. Cwele's group [104], found that CO oxidize selectively on the copper site in copper-cobalt bimetallic catalyst, whereas H_2 oxidation to H_2O takes place on the cobalt vicinities. However, the selectivity seems to drop from 100 % as soon as the temperature surpasses 120 °C to almost 76% at 200 °C, showing the sensitivity of H_2 oxidation to temperature (Figure 4.19 (B); (c)). Likewise, the CO(prOx) performance decreased as the load of CuO_x was increased further to 10 and 15 wt.%, with the latter showing the worst CO(PrOx) performance than all the catalysts prepared by reflux method (Figure 4.19 (B)).

For the effects of preparation method, close inspection of the CO(PrOx) performance revealed a higher CO conversion over 5 wt.% CuO_x/Co_3O_4(Ref) catalyst (Figure 4.19 (B); (c)), as compared to 5 wt.% CuO_x/Co_3O_4(Hyd) catalyst (Figure 4.19 (A); (c)) at temperatures below 80 °C. The relatively good CO(PrOx) performance of CuOx/Co_3O_4(Ref) can be ascribed to the strong interaction between CuO_x-Co_3O_4 in the solid solution (See XRD analysis (Figure 4.1)) and high surface area (see Table 4. 2) [1, 22, 26, 41]. However, the two catalyst samples show a complete (100%) CO oxidation from 80 °C – 200 °C. Therefore, low temperature CO(PrOx) is catalysed by CuO_x species (regardless of the preparation method), as also reported by other researchers [3, 36]. Adak *et al.*, [11], has reported that large antiferromagnetic CuO clusters favours competitive H_2 oxidation to H_2O over CuO_x-CeO_2 catalyst, prepared by similar hydrothermal method. Such CuO_x clusters could be avoided by refluxing the primary solution and lowering the calcination temperature (to that below 550 °C, [11]) as was done in this work. This have shown to remarkably improve the catalytic performance of copper-based catalysts as compared to previous reports (See Table 2.1). The 5 wt.% CuO_x/Co_3O_4(Hyd) and 5 wt.% CuO_x/Co_3O_4(Ref) catalysts converts all CO molecules within the required temperature window of CO(PrOx) catalyst to be accepted for PEMFCs application, which is 80 – 100 °C [57].

4.3.3. Effects of CeO_2 load on CO(PrOx) performance over 5 wt.% CuO_x/Co_3O_4 catalysts prepared under hydrothermal and reflux method

Figure 4.20 shows the CO(PrOx) performance over ternary catalysts obtained by varying CeO_2 content (1, 3, 5 wt.%) on 5 wt.% CuO_x/Co_3O_4(Hyd) and 5 wt.% CuO_x/Co_3O_4(Ref) catalyst, under hydrothermal and reflux conditions. The catalytic activity curves demonstrate a suppression in CO(PrOx) performance of 5 wt.% CuO_x /Co_3O_4(Hyd) catalyst (Figure 4.20 (A); (a)), as ceria is introduced (Figure 4.20 (A); (b)-(d)), with 3 wt.% CeO_2 showing the lowest CO conversion anywhere below 80 ^oC. Such drop in the catalytic activity over 3Ce-5Cu/Co catalyst can be related to the poor reducibility and weak interaction between CuO_x and the support component (Co_3O_4) as shown by the H_2-TPR data (Figure 4.17) [12, 27, 28]. The % CO_2 selectivity is somehow improved at higher temperatures (>160 ^oC) over 3Ce-5Cu/Co(Hyd) catalyst (Figure 4.20 (A); (c)), relative to the undoped 5 wt.% CuO_x/Co_3O_4(Hyd) bimetallic oxide (Figure 4.20 (A); (a)). This could be ascribed to the stabilized Co^{3+} centre by CeO_2, as suggested by the H_2-TPR (Figure 4.17 (b), peak 'β'). Park *et al*., [84], has reported on similar results over a ternary cobalt-copper-ceria catalyst prepared by hydrothermal method. The same team [84], have also observed that reactive copper sites were hindered as ceria content increase CeO_2, which could also explain the low catalytic activity of these samples, as compared to their bimetallic CuO_x/Co_3O_4(Hyd) catalyst.

Similaraly, the CO(PrOx) performance over 5 wt.% CuO_x/Co_3O_4(Ref) catalyst (Figure 4.20 (B); (a)), have also decreased marginally after the addition of CeO_2 under reflux method (Figure 4.20 (B); (b)-(d)). the negative influence of ceria on the CO(PrOx) performance of 5 wt.% CuO_x/Co_3O_4(Ref) catalyst can be associated with the relatively low surface area (See Table 4.2), poor reducibility, morphological alterations (see SEM, Figure 4.12 (d)) and overshadowing of CuO_x/Co_3O_4(Ref) catalyst's active sites by agglomerated fluorite (CeO_2) nanocrystals, as observed from the HRTEM (Figure 4.14 (d_1)) [15, 24, 38, 39]. Intrestingly, 88% CO conversion was observed over 3Ce-5Cu/Co(Ref) catalyst, at 80 ^oC with 97% CO_2 selectivity (Figure 4.20 (B); (c)). As temperature continue to rise (>80 ^oC), the 3Ce-5Cu/Co(Ref) catalyst demonstrates a complete CO conversion.

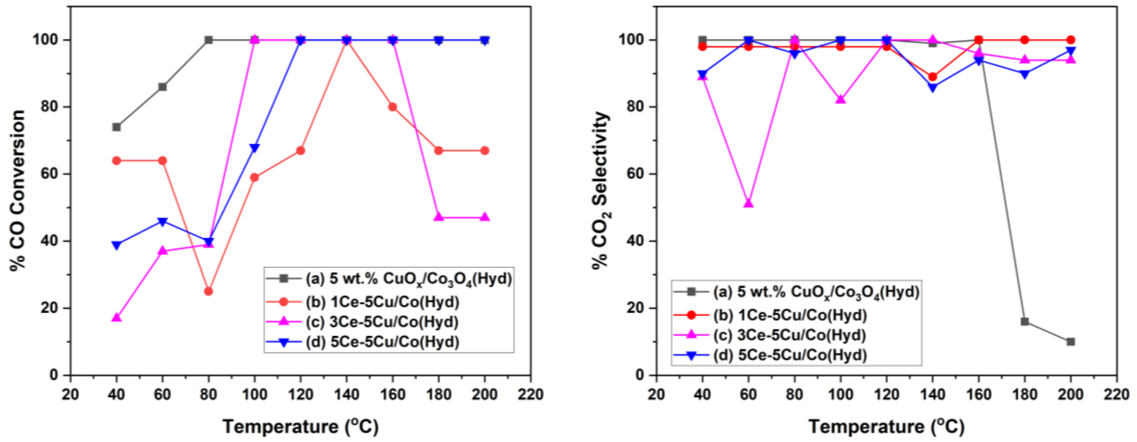
(A) Hydrothermal prepared catalysts

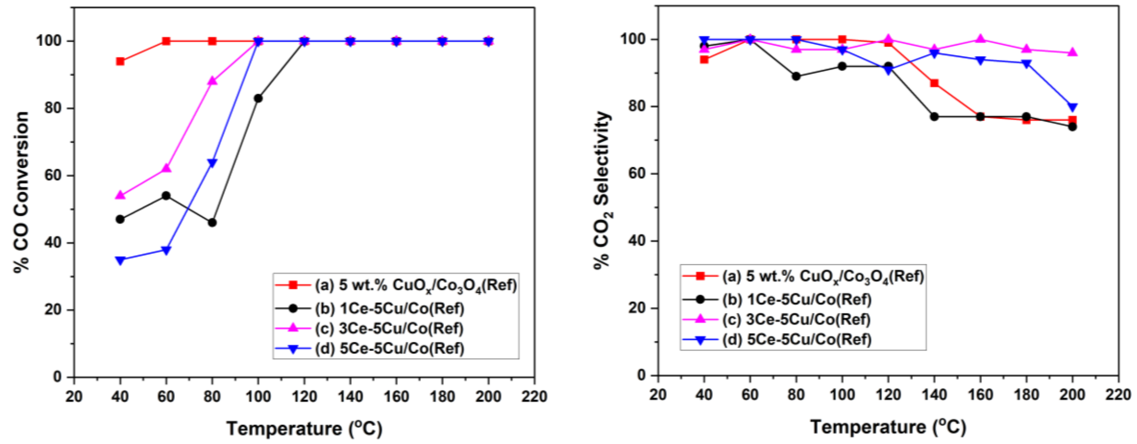
(B) Reflux prepared catalysts

Figure 4.20 The CO conversion and CO_2 selectivity of (A) Hydrothermal prepared (a) 5 wt.% CuO_x/Co_3O_4(Hyd), (b) 1Ce-5Cu/Co(Hyd), (c) 3Ce-5Cu/Co(Hyd)and (d) 5Ce-5Cu/Co(Hyd), and the CO conversion and CO_2 selectivity of Reflux prepared (a) 5 wt.% CuO_x/Co_3O_4(Ref), (b) 3Ce-5Cu/Co(Ref), (c) 3Ce-5Cu/Co(Ref)and (d) 5Ce-5Cu/Co(Ref) catalysts.

The catalytic activity data suggests that CuO_x-Co_3O_4 phase are responsible for low temperature CO(PrOx) and their interactions (synergy) gets compromised by the third metal (CeO_2). Inability of CuO_x to receive electrons from the facile redox autotuning Co_3O_4 support catalyst due to its relation with CeO_2 leads to an inactive CuO_x species. A new induced co-operation between CeO_2 and CuO_x is responsible for the observed catalytic activity suppression over Co_3O_4 support catalyst, and this depends highly on ceria content as well as the method of preparation, as also reported elsewhere [5, 19].

4.3.4. Catalytic activity tests in moisture saturated CO(PrOx) feed gas over 5 wt.% CuO_x/Co_3O_4(Hyd) and 5 wt.% CuO_x/Co_3O_4(Ref) catalysts.

The effects of moisture on the CO(PrOx) activity over 5 wt.% CuO_x/Co_3O_4 was studied by bubbling liquid water with He gas, at a constant flow rate of 10 mL/min in a saturator, at room temperature. The % CO conversion, as a function of temperature in dry and moisture conditions are depicted in Figure 4.21. The CO conversion over 5 wt.% CuO_x/Co_3O_4(Hyd) catalyst decreased from 74% in dry CO(PrOx) (Figure 4.21 (a)) to 13% at 40 °C, in the presence of moisture (Figure 4.21 (A); (c)). However, the % CO_2 selectivity is surprisingly improved (> 80%) above 160 °C in moisture (Figure 4.21 (B); (c)). The catalytic deactivation of the catalysts in moisture could be ascribed to the surface mesopore blockage by capillary condensed H_2O molecules at low temperatures (< 100 °C) [56, 134, 135], as well as the hindrance of the metal active sites by the surface adsorbed water molecules [5, 18, 19, 41, 121]. As temperature rise above 100 °C, the CO(PrOx) activity rise drastically, and a 100% CO conversion was regained (Figure 4.21 (A); (c)), in which most water molecules could have evaporated from the surface of 5 wt.% $CuO_x/$ Co_3O_4(Hyd) catalyst. Similar results were observed by other researchers [18, 56].

Similarly, the 5 wt.% CuO_x/Co_3O_4(Ref) catalyst prepared by reflux method also suffered prematurely in the presence of H_2O on stream. The % CO conversion drops from 94% in dry (Figure 4.21 (c)) to 40% in moisture (Figure 4.21 (A); (d) at 40 °C, over 5 wt.% $CuO_x/$ Co_3O_4(Ref) catalyst, with CO_2 selectivity of 36% (Figure 4.21 (B); (d)). The CO conversion of 100% was regained at 120 °C, as in 5 wt.% $CuO_x/$ Co_3O_4(Hyd) catalyst (Figure 4.21 (A) (c)).

Interestingly, due too relatively high surface area of reflux prepared 5 wt.% $CuO_x/$ Co_3O_4(Ref) catalyst (Table 4.2), a relatively high CO(PrOx) performance in moisture was observed at temperatures below 120 °C, as compared to 5 wt.% $CuO_x/$ Co_3O_4(Hyd) counter catalyst, in the presence of moisture (Figure 4.21 (A); (c) and (d)). The Cu_2O phase deposited on the surface of 5 wt.% $CuO_x/$ Co_3O_4(Hyd) catalyst (see XRD, Figure 4.1 (b)), could be highly prone to oxidation by water H_2O molecules to inactive cupric ions (Cu^{2+}) (i.e., $Cu(OH)_2$) [4, 136], as compared to the stabilized CuO_x

species in 5 wt.% CuO_x/Co_3O_4(Ref) catalyst's solid solution (also see XRD, Figure 4.2 (b)) [1, 32]. These could also explain their discrepancies in CO(PrOx) activity in humid conditions.

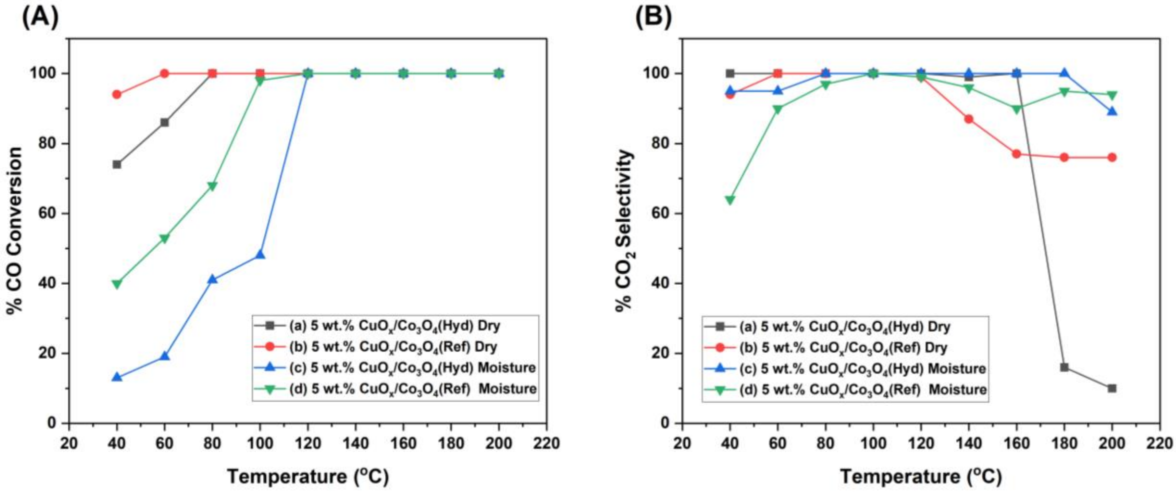

Figure 4.21 CO conversion (A), and CO_2 selectivity (B), of 5wt.% CuO_x/Co_3O_4(Hyd) and (b) 5wt.% CuO_x/Co_3O_4(Ref) catalyst under dry ((a)-(b)) and moisture conditions ((c)-(d)).

Moreover, blockage of metal active site by H_2O molecules generates a metal ligand interface (MLI) during CO(PrOx) reaction [71, 103]. MLI controls the catalytic activity and selectivity dynamics via charge transferer mechanisms, molecular recognitions, selective blocking, adsorption geometries, steric hindrance etc., and a strong metal ligand interactions lead to catalyst deactivation [113]. Thus, we can deduce that H_2O (ligand) interact more strongly with CuO_x species (active metal) in both the 5 wt.% CuO_x/Co_3O_4(Hyd) and 5 wt.% CuO_x/Co_3O_4(Ref) catalysts, since CuO_x was responsible for the enhanced low temperatures activity of the pristine Co_3O_4(Hyd) and Co_3O_4(Ref) catalysts (See Figure 4.19 (A) and (B); (c)).

4.3.5. Stability of the prepared mesoporous catalysts in CO(PrOx) reaction under moisture and CO_2 stream

The existed of moisture and CO_2 in a CO(PrOx) reactor is inevitable in practical applications [101]. This is because H_2O (~10 vol.%) and CO_2 (~15- 20 vol.%) are always present in a gaseous mixture derived from upstream steam reforming (SR) and water gas shift reaction (WGSR) used to produce H_2 [73, 126, 140]. Cobalt based catalysts can have low CO_2 selectivity or even deactivates with time on stream during

CO(PrOx), especially when moisture and CO_2 are present [43, 97, 133, 141]. For an industrial purposes (both domestic and economic) of fuel cell's applications, the stability of CO(PrOx) catalysts plays a key role [126, 142]. Thus, the stability of Co_3O_4(Hyd) and Co_3O_4(Ref) catalysts doped with 5 wt.% CuO_x species under hydrothermal and reflux was investigated towards CO(PrOx) reaction at a maximum PEMFCs operating temperature (i.e., 100 °C) [57], in a continuous run on stream for a prolonged time (26 hours). The catalyst' stability was also tested in humid (H_2O) and CO_2 conditions as discussed in the following subsections.

4.3.5.1. The stability of Co_3O_4(Hyd) and Co_3O_4(Ref) catalysts prepared by hydrothermal and reflux method in the presence of 5 wt.% CuO_x species in various CO(PrOx) environment

The CO conversion as a function of time on stream at 100 °C over Co_3O_4(Hyd) and 5 wt.% CuO_x/Co_3O_4(Hyd) are illustrated in Figure 4.13. Bare Co_3O_4(Hyd) catalyst shows a stable CO conversion of 40% anywhere from 100 to 280 min, above which CO conversion decreased to 28%, with CO_2 selectivity of just 38% in dry CO(PrOx) conditions after 26 h (Figure 4.22 (A); (a)). The CO conversion increase from 28% at 100 min to 67% at 220 min over the as prepared 5 wt.% CuO_x/Co_3O_4(Hyd) catalyst, with good CO_2 selectivity (Figure 4.22 (A); (b)). However, deactivation was noticed immediately when time progressed above 220 min, realizing less than 67% CO conversion anywhere up to maximum time of operation (26 h) (Figure 4.22 (A); (b)). The stability of 5 wt.% CuO_x/Co_3O_4(Hyd) catalyst deactivates also in the presence of moisture (Figure 4.22 (A); (c)), but to a lesser extend as compared to in dry conditions (Figure 4.22 (A); (b)). Such improvements in moisture saturated feed gas are ascribed to the positive effects of H_2O towards CO(PrOx) reaction by several authors [18, 138].

In the presence of 15 vol.% CO_2 gas on stream, the catalytic performance over 5 wt. % CuO_x/Co_3O_4(Hyd) catalyst is surprisingly the highest for the entire 24 h (1440 min) (Figure 4.22 (A); (d)), as compared to other conditions (Figure 4.22 (A); (b) and (c)). However, the CO conversion decreased as time progressed (above 24 h), achieving a stable CO conversion of 62% ((Figure 4.22 (A); (c)), which was 5% less than in moisture condition (Figure 4.22 (A); (c)). According to the literature, deactivation in a CO_2 environment in a catalyst with high density interphase such as the 5 wt. % CuO_x/Co_3O_4(Hyd) catalyst, manly arise due to formation of slowly desorbing carbonate species [139, 149]. However, no carbonates species were detected on the G.C chromatogram, which left out the suppression of interface redox process by CO_2 species the main reason for the deactivation [18, 139].

(A) Hydrothermal prepared

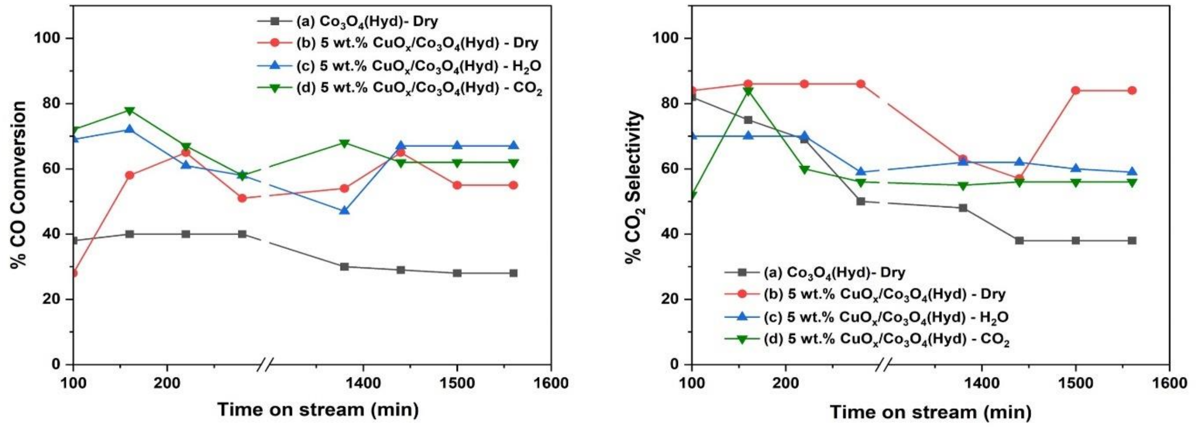

(B) Reflux prepared

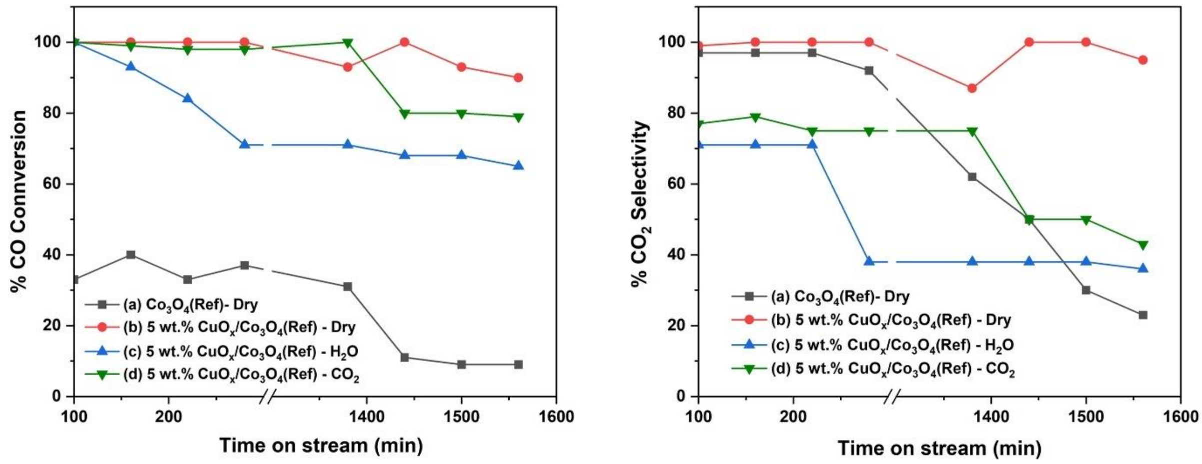

Figure 4.22 The CO conversion and CO_2 selectivity of (A) hydrothermal prepared, Co_3O_4(Hyd) catalyst in (a) dry and 5 wt.% CuO_x/Co_3O_4(Hyd) catalyst in (b) dry, (c) moisture (d) CO_2 environment, and the CO conversion and CO_2 selectivity of (B) reflux prepared, Co_3O_4(Ref) catalyst in (a) dry and 5 wt.% CuO_x/Co_3O_4(Ref) catalyst in (b) dry, (c) moisture (d) CO_2 environment.

Under reflux method as shown in Figure 4.22 (B), the Co_3O_4(Ref) catalyst shows a decreasing CO conversion profile from 40% (above 100 min), to 9% after total run of 26 hours on stream in dry feed stream (Figure 4.22 (B); (a)). The as prepared 5 wt.% CuO_x/Co_3O_4(Ref) catalyst, shows a complete CO conversion (100%) in dry conditions, which remain stable for almost 4 h on stream (Figure 4.22 (B); (b)). After 26 h of operation, the catalytic conversion over this sample drops by only 10%, with good selectivity (95%). The presence of moisture in the reactor feed decreased the CO conversion over 5 wt.% CuO_x/Co_3O_4(Ref) catalyst, and less than 71% CO conversion was observed from 280 min, throughout the run (Figure 4.22 (B); (c)). Nonetheless, the 5 wt.% CuO_x/Co_3O_4(Ref) catalyst outperforms its 5 wt.% CuO_x/Co_3O_4(Hyd) counterpart (Figure 4.22 (A); (c)), in this condition. The unique slit like mesoporous feature of 5 wt.% CuO_x/Co_3O_4(Ref) catalyst (see Figure 4.4 (B); (b)), allows water to evaporate easily from all sites of the slit's meniscus, exposing the active sites, and improve the catalyst's stability in moisture conditions [56, 156].

In the presence of CO_2, the as prepared 5 wt. % CuO_x/Co_3O_4(Ref) catalyst showed a CO conversion of 100% at 100 min, above which it decreased slightly (Figure 4.22 (B); (d)). These shows the role of CuO_x species in resisting deactivation against CO_2. CO_2 was also shown to be tolerated as copper was loaded in cobalt substituted ceria catalyst [104]. However, the catalyst's selectivity decreased by almost 20% as compared to in dry conditions anywhere between 100 to 280 (Figure 4.22 (B); (d)). At maximum time of operation (26 h), the 5 wt.% CuO_x/Co_3O_4(Ref) catalyst can still convert 79% of CO molecules, in CO_2 environment. Nonetheless, the slight catalysts deactivation can be linked to CO_2 adsorption on the copper sites [124], or onto Co^{2+} cations , which prevents their reverse oxidation to active Co^{3+} centre by O_2 in the feed stream [117]. CO_2 inhibition effects on the catalytic performance of 5 wt.% CuO_x/Co_3O_4(Ref) catalyst seem to be less pronounced than H_2O effects. Similar results were observed by Cwele *et al.,* [104], who noticed a much detrimental effects of H_2O than CO_2 on $Ce_{0.90}Co_{0.10}O_{2-\delta}$ catalyst. On the other hand, carbon dioxide and hydrogen can partake in two side reaction, i.e., CO_2 methanation as well as reverse water gas shift reaction (RWGSR) during CO(PrOx), which could counteract the CO(PrOx) mission [6, 145, 158].

4.3.5.2 Effect of 3 wt.% CeO_2 on the stability of of 5 wt.% CuO_x/Co_3O_4(Hyd) and 5 wt.% CuO_x/Co_3O_4(Ref) catalysts in various CO(PrOx) environments.

Carbon dioxide has shown to adsorb selectively on CeO_2 support and CuO/CeO_2 catalyst [107]. Ceria (CeO_2) is also known to adsorb large amounts of water molecules when acting as a catalyst in CO(PrOx) [10], and in three-way catalytic conversion, for reducing automotive exhaust emissions [40, 41]. Thus, the following section aimed at improving the catalytic stability of 5 wt.% CuO_x/Co_3O_4(Hyd) and 5 wt.% CuO_x/Co_3O_4(Ref) catalyst in moisture and CO_2 environmnet by re-introducing 3 wt.% CeO_2 species on 5 wt.% CuO_x/Co_3O_4 catalysts.

Figure 4.23 shows the % CO conversion as a function of time on stream over 3 wt.% CeO_2 doped 5 wt.% CuO_x /Co_3O_4 (Hyd) and 5 wt.% CuO_x /Co_3O_4 (Ref) catalysts. The stability of 5 wt.% CuO_x /Co_3O_4 (Hyd) catayst (Figure 4.23 (A); (a)) was tremendously improved in dry conditions after the addition of 3 wt.% CeO_2 (Figure 4.23 (A); (b)). A % conversion of > 98% was achieved over 3Ce-5Cu/Co(Hyd) catalyst anywhere between 100 to 280 min, which could be linked directly to the improved surface area (Table 4.2). In moisture on the stream, the CO conversion over 3Ce-5Cu/Co(Hyd) catalyst decreased substantially to 68% at 280 min, and increase slightly to a stable CO conversion of 70% towards maximum time of operation (26 h) on stream (Figure 4.23 (A); (c)). However, no H_2O species were detected on the FTIR spectrum of the spent 3Ce-5Cu/Co(Hyd) catalyst (Appendix (C); (c)). The selectivity has also improved remarkably in moisture stream over 3Ce-5Cu/Co(Hyd) catalyst (89% at t = 26 h) (Figure 4.23 (A); (c)) as compared to dry conditions (Figure 4.23 (A); (b)) (59 % at t = 26 h). Selective adsorption of moisture on CeO_2 and not on the active CuO_x/Co_3O_4 sites could be an underlying reason behind good CO_2 selectivity over 3Ce-5Cu/Co(Hyd) ternary catalyst in moisture environment [43].

The 3Ce-5Cu/Co(Hyd) catalyst shows the worst stability in CO(PrOx) reaction in the presence of CO_2 on stream (Figure 4.23 (A); (d)). The CO conversion over this sample decrease from 78% at 100 min to 56% at 280 min and then reach 55% CO conversion between 24 and 26 h (Figure 4.23 (A); (d)). Nonetheless, the CO_2 selectivity is somehow improved in CO_2 environment over 3Ce-5Cu/Co(Hyd) catalyst, as compared to pure 5 wt.% CuO_x/Co_3O_4(Hyd) catalyst (see Figure 4.22 (A); (d)). This illustrates the importance of ceria towards selective CO(PrOx) catalysis, as reported eleshwere [19, 33]. CO_2 can stimulate the reverse water gas shift reaction (RWGSr), which could also decrease the CO conversion [4,39]. A tiny fraction of water molecules were detected from the FTIR spectrum of the spent 3Ce-5Cu/Co(Hyd) catalyst in CO_2 environmnet, which could suggest RWGSr (Appendix C (e)).

(A) Hydrothermal prepared

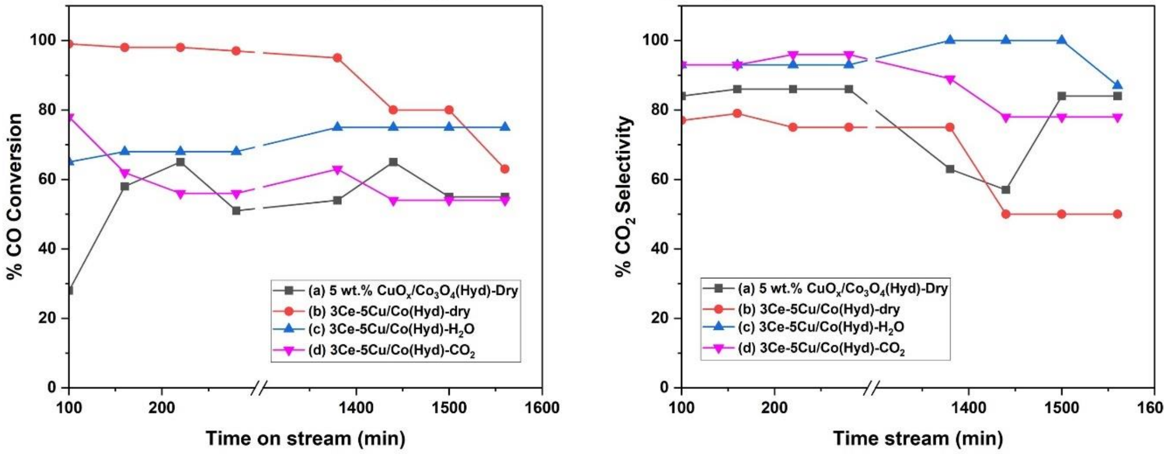

(B) Reflux prepared

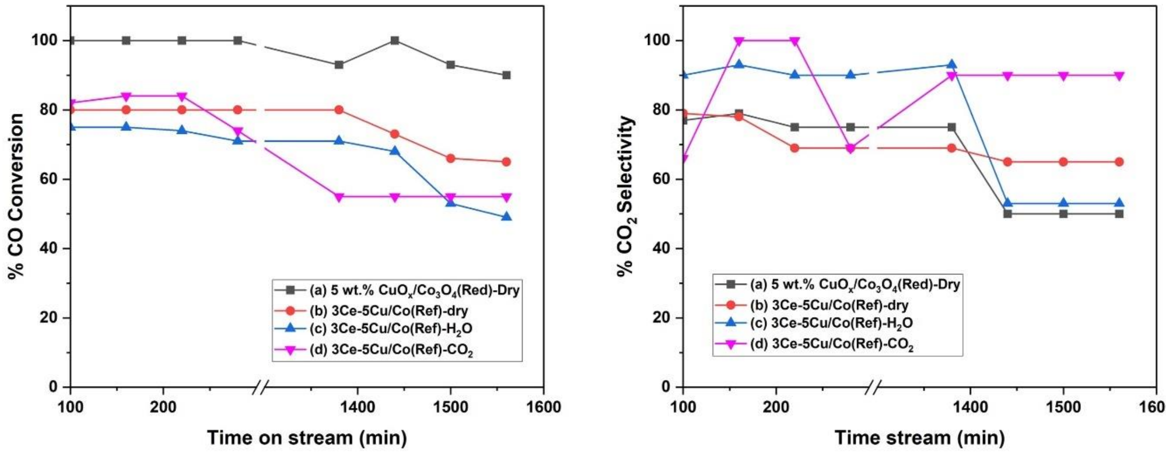

Figure 4.23 The CO conversion and CO_2 selectivity of (A) hydrothermal prepared, 5 wt.% CuO_x/Co_3O_4(Hyd) catalyst in (a) dry and 3Ce-5Cu/Co(Hyd) catalyst in (b) dry, (c) moisture (d) CO_2 environment, and the CO conversion and CO_2 selectivity of (B) reflux prepared, (a) dry and 5 wt.% CuO_x/Co_3O_4(Ref) catalyst in (a) dry and 3Ce-5Cu/Co(Ref) catalyst in (b) dry, (c) moisture and (d) CO_2 environment.

The CO(PrOx) stability results over the as prepared 3Ce-5Cu/Co(Ref) catalyst under reflux method, is shown in Figure 4.23 (B). The 3Ce-5Cu/Co(Ref) catalyst in dry conditions shows CO conversion of 80% as from 100 min, and remain constant for up to 280 min (Figure 4.23 (A) (b)). However, this is 20% lower than that achieved on the undoped 5 wt.% CuO_x/Co_3O_4(Ref) catalyst (Figure 4.23 (A); (a)). The textural properties (Table 4.5) have shown that CeO_2 blocked the mesopores and reduced the surface area of the 5 wt.% CuO_x/Co_3O_4(Ref) catalyst thus, preventing reactant uptake by the 3Ce-5Cu/Co(Ref) catalyst, lowering its CO conversion and stability [18, 30]. The H_2-TPR have also demonstrated that ceria lowers the reduction temperature of

3Ce-5Cu/Co(Ref) catalyst (see Figure 4.17), which could also explain the deactivation of this catalyst. After a maximum operation time of 26 h on stream in dry CO(PrOx), the 3Ce-5Cu/Co(Ref) catalyst (Figure 4.23 (B); (b)), still shows low CO(PrOx) performance as compared to 5 wt.% CuO_x/Co_3O_4(Ref) catalyst (Figure 4.23 (B); (a)).

The 3Ce-5Cu/Co(Ref) catalyst demonstrated a relatively poor CO conversion in moisture (Figure 4.23 (B); (b)), as compared to dry condition (Figure 4.23 (B); (b)), at all times, perhaps due to active sites blockage by water molecules or decresed surface area after ceria addition (64.9 m^2/g to 55.8 m^2/g) [23, 49, 50]. Howerver, unlike in 3Ce-5Cu/Co(Hyd) catalyst, the H_2O functional group (-OH) was observed from the FTIR spectrum of spent 3Ce-5Cu/Co(Ref) catalyst (Appendix (C); (c) and (d)). This imply that the latter is good at adsorbing water, perhaps due to the relatively large surface area (see Table 4.2).

When tested for CO_2 deactivation resistances, the 3Ce-5Cu/Co(Ref) catalyst showed CO conversion above 80% (below 220 min), which then deactivated with time on stream (Figure 4.23 (C); (d)). At maximum hours of operation (26 h), only 55% of CO could be oxidized over this sample. The spent 3Ce-5Cu/Co(Ref) catalyst in CO_2 environment showed the existence of moisture and carbon species (formate and CO_2) in the FTIR spectrum (Appendix (C) (f)). The detection of H_2O species in a moisture free environment suggest a RWGSr, which could explain the catalyst deactivation in CO_2 stream [32, 39]. Formates are usually generated by the reaction of CO with the hydroxylated metal oxide surface [57]. Other researchers claim that the deactivation of metal oxide catalysts (e.g., copper oxide and ceria), in CO_2 (and or moisture) modified CO(PrOx) is only related to physicochemical interaction with the catalyst and not RWGSr (and or WGS) reaction, due to narrow CO(PrOx) temperature window [5, 47]. Nonetheless, the improved CO_2 selectivity over the as prepared ternary catalysts relative to their bimetallic counterparts shows the importance of CeO_2 and CuO_x/Co_3O_4 synegistic interactions in developing highly stable CO(PrOx) catalysts for H_2O and CO_2 tolerance, as also ascribed by [34]. These suggests the needs for further investigations into these ternary catalyst materials.

4.4. CONCLUSION

The preparation of Co_3O_4(Hyd) and Co_3O_4(Ref) by precipitation method and the co-precipitation of various loads of CeO_2 and CuO_x species was achieved successfully under hydrothermal (Hyd) and reflux (Ref) method, at 300 °C calcination. The obtained mesoporous Co_3O_4(Hyd) and Co_3O_4(Ref) catalysts, demonstrated CO(PrOx) activity in H_2-rich stream but to a lesser extent. Based on the experimental and characterisation results involving H_2-TPR and XRD analysis, the catalytic activity of both Co_3O_4(Hyd) and Co_3O_4(Ref)) arose from surface adsorbed electrophilic oxygen species. However, the Co_3O_4(Ref) catalyst was less active, due to agglomerated Co_3O_4 nanocrystals visualized from the TEM and SEM data.

The addition of various amounts of CeO_2 under hydrothermal method demonstrated an increase in CO(PrOx) performance of Co_3O_4(Hyd) catalyst, only for miniscule amounts of ceria load (1 wt.%). Under reflux method, the trend was reversed, and the good activity was observed over maximum ceria load (5 wt.%) with good and stable CO_2 Selectivity below 160 °C. The XRD data revealed that 5 wt.% CeO_2 causes lattice expansion of either Co_3O_4 (Hyd) and Co_3O_4(Ref) catalysts, regardless of the method, which decreased their crystallite size, lattice parameter and improved the surface area. However, low activity of 5 wt.% CeO_2/Co_3O_4(Hyd) as compared to 5 wt.% CeO_2/Co_3O_4(Ref) was found to be associated with its relatively low surface area. Loading CuO_x species on Co_3O_4(Hyd) and Co_3O_4(Ref) catalysts, under hydrothermal and reflux method respectively, showed a positive result in terms of CO(PrOx) performance. However, as the content of CuO_x was increased to high loads, the catalytic activity was shown to be reduced, probing just 5 wt.% as appropriate amount, in either case (hydrothermal or reflux). Both the 5 wt.% CuO_x/Co_3O_4(Hyd) and 5 wt.% CuO_x/Co_3O_4(Ref) catalysts required a minimum temperature of just 60 and 80 °C respectively, to completely oxidize CO gas, with good selectivity. Introduction of 10 vol. % H_2O to the gas feed negatively impaired the propensity of the prepared catalyst to oxidize CO, with hydrothermal prepared 5 wt.% CuO_x/Co_3O_4(Hyd) catalyst being less tolerant than its reflux counterpart. The CO conversion as a function of time profiles indicated that the 5 wt.% CuO_x/Co_3O_4(Ref) catalyst was stable in dry, moisture and CO_2 feed gas, as compared to all other samples prepared in this work. From the XRD, H_2-TPR and TEM, these was made possible by the strongly interacting CuO_x-

Co_3O_4(Ref) in the solid solution, which decreased the crystallite size and the reduction temperature of the support catalyst and improved its nanoparticle dispersion.

In an attemps to stabilize both 5 wt.% CuO_x/Co_3O_4(Hyd) and 5 wt.% CuO_x/Co_3O_4(Ref) catalysts, in various CO(PrOx) environment, we found that the CO(PrOx) perfomance declines significantly after the introduction of the third metal oxide(CeO_2), regardless of the preparation route. Upon inspection of the CO(PrOx) performance and the stability in relation to the physiochemical properties of 3 wt.% CeO_2 modified 5 wt.% CuO_x/Co_3O_4(Hyd) and 5 wt.% CuO_x/Co_3O_4(Ref) (i.e., 3Ce-5Cu/Co(Hyd) and 3Ce-5Cu/Co(Ref), respecitvely) catalysts, the deactivations were associated with the morphological and textural property changes of the undoped catalysts catalysts. After 3 wt.% CeO_2 introduction, both 3Ce-5Cu/Co(Hyd) and 3Ce-5Cu/Co(Ref) ternary catalysts showed low surface area, surface transformation to a higher degree of roughness and low reducibilityas evident by the BET, SEM and H_2-TPR data. Pore size and pore volume of pure 5 wt.% CuO_x /Co_3O_4(Ref) catalyst diminished substantially after ceria addtion and showed relatively less CO_2 and H_2O tolerance in CO(PrOx) reaction, over time on stream. Surprisingly, addition of 3 wt.% CeO_2 showed to be crucial for H_2O tolerance in 5 wt.% CuO_x/Co_3O_4(Hyd) catalyst as a function of time but was less resistant to CO_2 deactivation. The results shows that CuO_x-Co_3O_4 synergy is responsible for enhanced CO(PrOx) perfomance of the prepared samples and ceria addition compromises these relationship. The stability tests in CO_2 and moisture conditions showed that CeO_2 improves only the CO_2 selectivity of the 5 wt. % CuO_x/Co_3O_4 catalysts with time on stream, at an expense of CO conversion. It was also found that the catalyst materials synthesised by under reflux method are easily reducible and have relatively high surface area (S_{BET}) as compared to their hydrothermally prepared counterparts, all of which were in favour of CO(PrOx) reaction. The study provides an economically valuable and a highly environmentally benign route (reflux) of synthesising efficient and stable nano-sized CO(PrOx) catalysts, for delivering high purity H_2 for use in PEMFCs.

4.5. REFERENCES

[1] T. G. Vo, P. Y. Tsai, and C. Y. Chiang, “Tuning selectivity and activity of the electrochemical glycerol oxidation reaction by manipulating morphology and exposed facet of spinel cobalt oxides,” Journal of Catalysis, vol. 424, pp. 64–73, 2023.

[2] M. T. Makhlouf, B. M. Abu-Zied, and T. H. Mansoure, “Direct Fabrication of Cobalt Oxide Nanoparticles Employing Sucrose as a Combustion Fuel,” Journal of Nanoparticles, vol. 2013, pp. 1–7, 2013.

[3] F. Gao, H. Yan, X. Tang, H. Yi, S. Zhao, Q. Yu, and S. Ni, “Simultaneous removal of gaseous CO and elemental mercury over Cu-Co modified activated coke at low temperature,” Journal of Environmental Science (China), vol. 101, pp. 36–48, 2021.

[4] M. Mallik, S. Monia, M. Gupta, A. Ghosh, M. P. Toppo, and H. Roy, “Synthesis and characterization of Cu_2O nanoparticles,” Journal of Alloys and Compound., vol. 829, p. 154623, 2020.

[5] Y. Chen, D. Liu, L. Yang, M. Meng, J. Zhang, L. Zheng, S. Chu, and T. Hu, “Ternary composite oxide catalysts CuO/Co_3O_4-CeO_2 with wide temperature-window for the preferential oxidation of CO in H_2-rich stream,” Chemical Engineering Journal, vol. 234, pp. 88–98, 2013.

[6] G. Marbán and A. B. Fuertes, “Highly active and selective $CuOx/CeO_2$ catalyst prepared by a single-step citrate method for preferential oxidation of carbon monoxide,” Applied Catalysis B: Environmental, vol. 57, no. 1, pp. 43–53, 2005.

[7] K. An and G. A. Somorjai, “Nanocatalysis I: Synthesis of Metal and Bimetallic Nanoparticles and Porous Oxides and Their Catalytic Reaction Studies,” Catalysis Letters, vol. 145, no. 1, pp. 233–248, 2014.

[8] H. Shang, X. Zhang, J. Xu, and Y. Han, “Effects of preparation methods on the activity of CuO/CeO_2 catalysts for CO oxidation,” Frontiers of Chemical Science and Engineering, vol. 11, no. 4, pp. 603–612, 2017.

[9] Z. Chen, A. Zhou, S. Lin, Q. Kang, D. Jin, M. Fan, X. Guo and T. Ma, "Photothermal CO-PROX reaction over ternary $CuCoMnO_x$ spinel oxide

catalysts: the effect of the copper dopant and thermal treatment," Physical Chemistry Chemical Physics., vol. 25, no. 11, pp.8064-8073, 2023.

[10] S. Malwadkar, P. Bera, and C. V. V Satyanarayana, “Influence of cobalt on performance of Cu-CeO_2 catalysts for preferential oxidation of CO,” vol. 38, pp. 941–950, 2020.

[11] S. Adak, J. Rabeah, R. Ranjan, and T. Suvra, “In-situ Experimental and Computational Approach to Investigate the Nature of Active Site in Low-temperature CO-PROX over CuO_x-CeO_2 Catalyst Applied Catalysis A , General In-situ experimental and computational approach to investigate the nature of active s,” Applied Catalysis A: General, vol. 624, no. August, p. 118305, 2021.

[12] W. Huan, J. Li, J. Ji, and M. Xing, “In situ studies on ceria promoted cobalt oxide for CO oxidation,” Chinese Journal of Catalysis, vol. 40, no. 5, pp. 656–663, May 2019.

[13] J. Ding, L. Li, H. Zheng, Y. Zuo, X. Wang, H. Li, S. Chen, D. Zhang, X. Xu, and Li, G, “Co_3O_4-$CuCoO_2$ Nanomesh: An Interface-Enhanced Substrate that Simultaneously Promotes CO Adsorption and O_2 Activation in H_2 Purification,” ACS Applied Material Interfaces, vol. 11, no. 6, pp. 6042–6053, 2019.

[14] S. Dey, G. Chandra, D. Mohan, R. Prasad, and R. Nayan, “Applied Surface Science Cobalt doped $CuMnO_x$ catalysts for the preferential oxidation of carbon monoxide,” Applied Surface Science, vol. 441, pp. 303–316, 2018.

[15] A. Elmhamdi, L. Pascual, K. Nahdi and A. Martínez-Arias, “Structure/redox/activity relationships in CeO_2/$CuMn_2O_4$ CO-PROX catalysts,” Applied Catalysis B: Environmental, vol. 217, pp. 1–11, 2017.

[16] A. Papavasiliou, T. Van Everbroeck, C. Blonda, B. Oliani, E. Sakellis, P. Cool, P. Canu and F.K. Katsaros, 2022. Mesoporous CuO/TiO_2 catalysts prepared by the ammonia driven deposition precipitation method for CO preferential oxidation: Effect of metal loading. Fuel, 311, p.122491. 2022.

[17] L. Du, W. Wang, H. Yan, X. Wang, Z. Jin, Q. Song, R. Si and C. Jia, "Copper-ceria sheets catalysts: Effect of copper species on catalytic activity in CO oxidation reaction,” Journal of Rare Earths, vol. 35, no. 12, pp. 1186–1196,

2017.

[18] S. Lu, F. Wang, C. Chen, F. Huang, and K. Li, “Catalytic oxidation of formaldehyde over CeO_2-Co_3O_4 catalysts,” Journal of Rare Earths, vol. 35, no. 9, pp. 867–874, 2017.

[19] S. A. Singh, S. Mukherjee, and G. Madras, “Role of CO_2 methanation into the kinetics of preferential CO oxidation on,” Molecular Catalysis, vol. 466, no. November 2018, pp. 167–180, 2019.

[20] W. Xue, W. Chang, X. Hu, J. Fan, X. Bai, and E. Liu, “Journal of Colloid and Interface Science Highly dispersed copper cobalt oxide nanoclusters decorated carbon nitride with efficient heterogeneous interfaces for enhanced H_2 evolution,” Jornal of Colloid and Interface Science, vol. 576, pp. 203–216, 2020.

[21] W. Xu, X. Chen, J. Chen, and H. Jia, “Bimetal oxide CuO/Co_3O_4 derived from Cu ions partly-substituted framework of ZIF-67 for toluene catalytic oxidation,” Journal of Hazardous Materials, vol. 403, no. July 2020, p. 123869, 2021.

[22] J. H. Zhong, A. L. Wang, G. R. Li, J. W. Wang, Y. N. Ou, and Y. X. Tong, “Co $_3O_4$/Ni$(OH)_2$ composite mesoporous nanosheet networks as a promising electrode for supercapacitor applications,” Journal of Materials Chemistry, vol. 22, no. 12, pp. 5656–5665, 2012.

[23] H. Chen, C. Fang, X. Gao, G. Jiang, X. Wang, S.P. Sun, W.D. Wu, and Z. Wu, “Sintering- and oxidation-resistant ultrasmall Cu(I)/(II) oxides supported on defect-rich mesoporous alumina microspheres boosting catalytic ozonation,” Journal of Colloid and Interface Science, vol. 581, pp. 964–978, 2021.

[24] J. Ding, L. Li, H. Zheng, Y. Zuo, X. Wang, H. Li, S. Chen, D. Zhang, X. Xu, and Li, G, “Co_3O_4-$CuCoO_2$ Nanomesh: An Interface-Enhanced Substrate that Simultaneously Promotes CO Adsorption and O_2 Activation in H_2 Purification,” ACS Applied Materials and Interfaces, vol. 11, no. 6, pp. 6042–6053, 2019.

[25] G. Marbán, A. López, I. López, and T. Valdés-solís, “A highly active , selective and stable copper/cobalt-structured nanocatalyst for methanol decomposition,” Applied Catalysis B: Environmenta., vol. 99, pp. 257–264, 2010.

[26] F. Parrino, F. R. Pomilla, G. Camera-roda, V. Loddo, and L. Palmisano, "Properties of titanium dioxide", pp. 13-66. Elsevier, 2021.

[27] D. Su, S. Dou, and G. Wang, “Single crystalline Co_3O_4 nanocrystals exposed with different crystal planes for Li-O_2 batteries,” Scientific Reports, vol. 4, 2014.

[28] B. Liu, Y. Liu, H. Hou, Y. Liu, Q. Wang, and J. Zhang, “Variation of redox activity and synergistic effect for improving the preferential oxidation of CO in H_2-rich gases in porous Pt/CeO_2-Co_3O_4 catalysts,” Catalysis Science and Technology, vol. 5, no. 12, pp. 5139–5152, 2015.

[29] J. Zhen, X. Wang, D. Liu, S. Song, Z. Wang, Y. Wang, J. Li, F. Wang, and H. Zhang, “Co_3O_4@CeO_2 core@shell cubes: Designed synthesis and optimization of catalytic properties,” Chemistry-A European Journal, vol. 20, no. 15, pp. 4469–4473, 2014.

[30] S. K. Aditha, A. D. Kurdekar, L. A. A. Chunduri, S. Patnaik, and V. Kamisetti, “Aqueous based reflux method for green synthesis of nanostructures: Application in CZTS synthesis,” MethodsX, vol. 3, p. 35, 2016.

[31] J. L. Zhang and G. Y. Hong, "Nonstoichiometric Compounds," In Modern inorganic synthetic chemistry, pp. 329-354, Elsevier B.V, 2017.

[32] C. Pojanavaraphan, W. Nakaranuwattana, A. Luengnaruemitchai, and E. Gulari, “Effect of support composition and metal loading on Au/$Ce_{1-x}Zr_xO_2$ catalysts for the oxidative steam reforming of methanol,” Chemical Engineering Journal, vol. 240, pp. 99–108, 2014.

[33] L. Ilieva, P. Petrova, A.M. Venezia, E.M. Anghel, R. State, G. Avdeev and T. Tabakova, “Mechanochemically prepared Co_3O_4-CeO_2 catalysts for complete benzene oxidation,” Catalysts, vol. 11, no. 11, pp. 1–19, 2021.

[34] Z. Zhao, T. Bao, Y. Li, X. Min, D. Zhao, and T. Muhammad, “The supported CeO_2/Co_3O_4-MnO_2/CeO_2 catalyst on activated carbon prepared by a successive-loading approach with superior catalytic activity and selectivity for CO preferential oxidation in H_2-rich stream,” Catalysis Communication, vol. 48, pp. 24–28, 2014.

[35] X. Guo, J. Mao, and R. Zhou, “Influence of the copper coverage on the

dispersion of copper oxide and the catalytic performance of CuO/CeO_2 (rod) catalysts in preferential oxidation of CO in excess hydrogen," Journal of Power Sources, vol. 371, no. August, pp. 119–128, 2017.

[36] K. A. Cychosz and M. Thommes, "Progress in the Physisorption Characterization of Nanoporous Gas Storage Materials," Engineering, vol. 4, no. 4, pp. 559–566, 2018.

[37] Z. Zhao, R. Jin, T. Bao, H. Yang, X. Lin, and G. Wang, "Mesoporous $Ce_xMn_{1-x}O_2$ composites as novel alternative carriers of supported Co_3O_4 catalysts for CO preferential oxidation in H_2 stream," International Jornal of Hydrogen Energy, vol. 37, no. 6, pp. 4774–4786, 2012.

[38] G. Hitkari, S. Sandhya, P. Gajanan, M.K. Shrivash and K. Deepak, "Synthesis of Chromium Doped Cobalt Oxide ($Cr:Co_3O_4$) Nanoparticles by Co-Precipitation Method and Enhanced Photocatalytic Properties in the Visible Region," J. Mater. Sci. Eng., vol. 07, no. 01, pp. 3–9, 2018.

[39] A. M. Lacoste, I. S. Tiscornia, M. Bonne, L. Michelin, B. Lebeau, and A. V. Boix, "Study of $CuO–CeO_2$ catalysts supported on ordered porous silica with different mesostructure and morphology. Influence on CO preferential oxidation," Microporous Mesoporous Mater., vol. 320, 2021.

[40] T. Tsoncheva, R. Ivanova, J. Henych, M. Dimitrov, M. Kormunda, D. Kovacheva, N. Scotti, V. Dal Santo and V. Štengl, "Effect of preparation procedure on the formation of nanostructured ceria-zirconia mixed oxide catalysts for ethyl acetate oxidation: Homogeneous precipitation with urea vs template-assisted hydrothermal synthesis," Applied Catalysis A: General vol. 502, pp. 418–432, 2015.

[41] H.C. Genuino, Y. Meng, D.T. Horvath, C.H. Kuo, M.S. Seraji, A.M. Morey, R.L. Joesten and S.L. Suib, "Enhancement of Catalytic Activities of Octahedral Molecular Sieve Manganese Oxide for Total and Preferential CO Oxidation through Vanadium Ion Framework Substitution," ChemCatChem, vol. 5, no. 8, pp. 2306–2317, 2013.

[42] Y. H. Tan, J. A. Davis, K. Fujikawa, N. V. Ganesh, A. V. Demchenko, and K. J. Stine, "Surface area and pore size characteristics of nanoporous gold subjected

to thermal, mechanical, or surface modification studied using gas adsorption isotherms, cyclic voltammetry, thermogravimetric analysis, and scanning electron microscopy," Journal of Materials and Chemistry, vol. 22, no. 14, pp. 6733–6745, 2012.

[43] G. Li, L. Li, Y. Yuan, J. Shi, Y. Yuan, Y. Li, W. Zhao, and J. Shi, "Highly efficient mesoporous Pd/CeO_2 catalyst for low temperature CO oxidation especially under moisture condition," Applied Catalysis B: Environmental, vol. 158–159, pp. 341–347, 2014.

[44] X. Guo, Z. Qiu, J. Mao, and R. Zhou, "Shape-controlled $Cu_xCe_{1-x}O_2$ nanorods catalyst and the active components functioned in selective oxidation of CO in hydrogen-rich stream," Journal of Power Sources, vol. 451, no. December 2019, p. 227757, 2020.

[45] S. K. Paswan, S. Kumari, M. Kar, A. Singh, H. Pathak, J. P. Borah, and L. Kumar, "Optimization of structure-property relationships in nickel ferrite nanoparticles annealed at different temperature," Journal of Physics and Chemistry Solids, vol. 151, p. 109928, 2021.

[46] R. U. I. Wang, C. Chen, S. Deng, P. A. N. Shen, L. E. I. Gong, and N. Zhang, "Improvement of preferential co oxidation activity over CuO/Co_3O_4-CeO_2 catalysts: effect of Co/Ce ratio," Journal of the Chilean Chemical Society, vol. 59, no. 4, pp.2710-2716, 2014.

[47] Z. Qiu, X. Guo, J. Mao, and R. Zhou, "Trace CO elimination in H_2 -rich streams with a wide operation temperature window : Co deposited CuO–CeO_2 catalysts. Physical Chemistry Chemical Physics, vol. 24, no. 4," pp. 2070–2079, 2022.

[48] G. Chai, W. Zhang, L. F. Liotta, M. Li, Y. Guo, and A. Giroir-Fendler, "Total oxidation of propane over Co_3O_4-based catalysts: Elucidating the influence of Zr dopant," Applied Catalysis B: Environmental, vol. 298, p. 120606, 2021.

[49] Z. Fan, W. Fang, Z. Zhang, M. Chen, and W. Shangguan, "Highly active rod-like Co_3O_4 catalyst for the formaldehyde oxidation reaction," Catalysis Communications, vol. 103, 2017, pp. 10–14, 2018.

[50] J. Luo, M. Meng, Y. Zha, and L. Guo, “Identification of the Active Sites for CO and C_3H_8 Total Oxidation over Nanostructured CuO-CeO_2 and Co_3O_4-CeO_2 Catalysts,” pp. 8694–8701, 2008.

[51] S. Dey and G. C. Dhal, “The catalytic activity of cobalt nanoparticles for low-temperature oxidation of carbon monoxide,” Materials Today Chemistry, vol. 14, p. 100198, 2019.

[52] L. Shen, M. Chen, L. Hu, X. Chen, and J. Wang, “Growth and stabilization of silver nanoparticles on carbon dots and sensing application,” Langmuir, vol. 29, no. 52, pp. 16135–16140, 2013.

[53] M. Luo, Y. Hong, W. Yao, and C. Huang, “Facile removal of polyvinylpyrrolidone (PVP) adsorbates from Pt alloy nanoparticles,” journal of Materials Chemistry A, vol. 3, no. 6, pp. 2770–2775, 2015.

[54] K. M. Koczkur, S. Mourdikoudis, L. Polavarapu, and S. E. Skrabalak, “Polyvinylpyrrolidone (PVP) in nanoparticle synthesis,” pp. 17883–17905, 2015.

[55] Y. Wang, L. R. Winter, J. G. Chen, and B. Yan, “CO_2 hydrogenation over heterogeneous catalysts at atmospheric pressure: from electronic properties to product selectivity,” Green Chemistry, vol. 23, no. 1, pp. 249–267, Jan. 2021.

[56] S.A. Singh and G. Madras, "Sonochemical synthesis of Pt, Ru doped TiO_2 for methane reforming," Applied Catalysis A: General., vol. (518), pp.102-114. 2016.

[57] P. Gawade, B. Bayram, A. C. Alexander, and U. S. Ozkan, “Applied Catalysis B : Environmental Preferential oxidation of CO (PROX) over CoO_x/CeO_2 in hydrogen-rich streams : Effect of cobalt loading,” "Applied Catalysis B: Environmental, vol. 128, pp. 21–30, 2012.

[58] I. A. Safo, M. Werheid, C. Dosche, and M. Oezaslan, “The role of polyvinylpyrrolidone (PVP) as a capping and structure-directing agent in the formation of Pt nanocubes,” Nanoscale Advances, vol. 1, no. 8, pp. 3095–3106, 2019.

[59] M. A. Mohamed, J. Jaafar, A. F. Ismail, M. H. D. Othman, and M. A. Rahman, Fourier Transform Infrared (FTIR) Spectroscopy. Elsevier B.V., 2017.

[60] G. Pandey, S. Singh, and G. Hitkari, “Synthesis and characterization of polyvinyl pyrrolidone (PVP)-coated Fe_3O_4 nanoparticles by chemical co-precipitation method and removal of Congo red dye by adsorption process,” International Nano Letters, vol. 8, no. 2, pp. 111–121, 2018.

[61] Z. M. Sui, X. Chen, L.Y. Wang, L.M. Xu, W.C. Zhuang, Y.C. Chai, and C.J. Yang, 2006. Capping effect of CTAB on positively charged Ag nanoparticles. Physica E: Low-dimensional systems and nanostructures, vol. 33, no. 2, pp.308-314, 2006.

[62] T. Munawar, M. Shahid Nadeem, F. Mukhtar, S. Manzoor, M. Naeem Ashiq, and F. Iqbal, “Surfactant-assisted facile synthesis of petal-nanoparticle interconnected nanoflower like NiO nanostructure for supercapacitor electrodes material,” Materials Science Engineering B, vol. 284, no. July, p. 115900, 2022.

[63] R. Chen, Y. Tan, Z. Zhang, Z. Lei, W. Wu, N. Cheng and S. Mu, “Hydrazine Hydrate Induced Two-Dimensional Porous Co^{3+} Enriched Co_3O_4 Nanosheets for Enhanced Water Oxidation Catalysis,” ACS Sustainable Chemistry Engineering, vol. 8, no. 26, pp. 9813–9821, 2020.

[64] P. Zhan, “Large scale hydrothermal synthesis of β-$Co(OH)_2$ hexagonal nanoplates and their conversion into porous Co_3O_4 nanoplates,” Journal of Alloys and Compounds, vol. 478, no. 1–2, pp. 823–826, 2009.

[65] R. Samal, B. Dash, C.K. Sarangi, K. Sanjay, T. Subbaiah, G. Senanayake, and M. Minakshi, “Influence of synthesis temperature on the growth and surface morphology of Co_3O_4 nanocubes for supercapacitor applications,” Nanomaterials, vol. 7, no. 11, 2017.

[66] J. S. Chen, T. Zhu, Q.H. Hu, J. Gao, F. Su, S.Z. Qiao and X.W. Lou, “Shape-controlled synthesis of cobalt-based nanocubes, nanodiscs, and nanoflowers and their comparative lithium-storage properties,” ACS Appl. Mater. Interfaces, vol. 2, no. 12, pp. 3628–3635, 2010.

[67] F. Zasada, J. Janas, W. Piskorz, M. Gorczyńska, and Z. Sojka, “Total Oxidation of Lean Methane over Cobalt Spinel Nanocubes Controlled by the Self-Adjusted Redox State of the Catalyst: Experimental and Theoretical Account for Interplay between the Langmuir-Hinshelwood and Mars-Van Krevelen Mechanisms,”

ACS Catalysis, vol. 7, no. 4, pp. 2853–2867, 2017.

[68] N. El Amri and K. Roger, “Polyvinylpyrrolidone (PVP) impurities drastically impact the outcome of nanoparticle syntheses,” Journal of Colloid and Interface Science, vol. 576, pp. 435–443, 2020.

[69] K. Deori, S. K. Ujjain, R. K. Sharma, and S. Deka, “Morphology controlled synthesis of nanoporous Co_3O_4 nanostructures and their charge storage characteristics in supercapacitors,” ACS Applied Materials Interfaces, vol. 5, no. 21, pp. 10665–10672, 2013.

[70] S. M. Lam, M. W. Kee, and J. C. Sin, “Influence of PVP surfactant on the morphology and properties of ZnO micro/nanoflowers for dye mixtures and textile wastewater degradation,” Materials Chemistry and Physics, vol. 212, pp. 35–43, 2018.

[71] Y. Chen, Y. Chen, P. Hu, S. Ma, and Y. Li, “The effects of PVP surfactant in the direct and indirect hydrothermal synthesis processes of ceria nanostructures,” Ceramics International, vol. 42, no. 16, pp. 18516–18520, 2016.

[72] X. Xia, Z. Qiang, G. Bass, M. L. Becker, and B. D. Vogt, “Morphological control of hydrothermally synthesized cobalt oxide particles using poly(vinyl pyrrolidone),” Colloid Polymer Science, vol. 297, no. 1, pp. 59–67, 2019.

[73] K. Mingle and J. Lauterbach, “Synthesis-structure-activity relationships in Co_3O_4 catalyzed CO oxidation,” Frontiers in Chemistry, vol. 6, no. MAY, pp. 1–12, 2018.

[74] Y. Dai, P. Lu, Z. Cao, C. T. Campbell, and Y. Xia, “The physical chemistry and materials science behind sinter-resistant catalysts,” Chemical Society Review, vol. 47, no. 12, pp. 4314–4331, 2018.

[75] S. Xiong, J. S. Chen, X. W. Lou, and H. C. Zeng, “Mesoporous Co_3O_4 and CoO@C topotactically transformed from chrysanthemum-like $Co(CO_3)_{0.5}(OH)\cdot 0.11H_2O$ and their lithium-storage properties,” Advanced Functional Materials, vol. 22, no. 4, pp. 861–871, 2012.

[76] C.H. Kuo, W. Li, W. Song, Z. Luo, A.S. Poyraz, Y. Guo, A.W. Ma, S.L. Suib, and J. He, "Facile synthesis of Co_3O_4@CNT with high catalytic activity for CO

oxidation under moisture-rich conditions," ACS applied materials and interfaces, vol. 6, no. 14, pp.11311-11317, 2014.

[77] A. Akhgar, B. Khalili, B. Moa, M. Rahnama, and N. Djilali, "Lattice-Boltzmann simulation of multi-phase phenomena related to fuel cells," In AIP Conference Proceedings., vol. 1863, no. 1, 2017.

[78] B. Wu, C. Shan, X. Zhang, H. Zhao, S. Ma, Y. Shi, J. Yang, H. Bai and Q. Liu, "CeO_2/Co_3O_4 porous nanosheet prepared using rose petal as biotemplate for photo-catalytic degradation of organic contaminants," Applied Surface Science, vol. 543, 2020.

[79] Y. Zheng, Q. Zhao, C. Shan, S. Lu, Y. Su, R. Han, C. Song, N. Ji, D. Ma, and Q. Liu, "Enhanced Acetone Oxidation over the CeO_2/Co_3O_4 Catalyst Derived from Metal-Organic Frameworks," ACS Applied Materials Interfaces, vol. 12, no. 25, pp. 28139–28147, 2020.

[80] T. Baidya, T. Murayama, S. Nellaiappan, N.K. Katiyar, P. Bera, O. Safonova, M. Lin, K.R. Priolkar, S. Kundu, B. Srinivasa Rao and P. Steiger, "Ultra-Low-Temperature CO Oxidation Activity of Octahedral Site Cobalt Species in Co_3O_4 Based Catalysts: Unravelling the Origin of the Unique Catalytic Property," Journal of Physics and Chemistry C, vol. 123, no. 32, pp. 19557–19571, 2019.

[81] T. Ozkaya, A. Baykal, M. S. Toprak, Y. Koseoğlu, and Z. Durmuş, "Reflux synthesis of Co_3O_4 nanoparticles and its magnetic characterization," Journal of Magnetism and Magnetic Materials, vol. 321, no. 14, pp. 2145–2149, 2009.

[82] Z. Han, H. Zhang, B. Dong, Y. Ni, A. Kong, and Y. Shan, "High Efficient Mesoporous Co_3O_4 Nanocatalysts For Methane Combustion at Low Temperature," ChemistrySelect, vol. 1, no. 5, pp. 979–983, 2016.

[83] L. B. Ngema, M.D. Farahani, S. Raseale, N. Fischer, A.S. Mohamed, S. Singh, and H.B. Friedrich, "In situ construction of a highly active surface interface for a $Co_3O_4|ZrO_2$ catalyst enhancing the CO-PrOx activity," Surfaces and Interfaces, vol. 38, p. 102826, 2023.

[84] H. Park, E.J. Lee, H. Woo, D. Yoon, C.H. Kim, C.H. Jung, K.B. Lee and K.Y. Lee, "Enhanced hydrothermal durability of Co_3O_4@$CuO–CeO_2$ Core-Shell

catalyst for carbon monoxide and propylene oxidation," Applied Surface Science, vol. 606, p. 154916, 2022.

[85] A. Arango-Diaz, J. A. Cecilia, J. Marrero-Jerez, P. Nuñez, J. Jiménez-Jiménez, and E. Rodríguez-Castellón, "Freeze-dried Co_3O_4-CeO_2 catalysts for the preferential oxidation of CO with the presence of CO_2 and H_2O in the feed," Ceramics International, vol. 42, no. 6, pp. 7462–7474, 2016.

[86] L. Lukashuk, K. Föttinger, E. Kolar, C. Rameshan, D. Teschner, M. Hävecker, A. Knop-Gericke, N. Yigit, H. Li, E. McDermott and M. Stöger-Pollach,. "Operando XAS and NAP-XPS studies of preferential CO oxidation on Co_3O_4 and CeO_2-Co_3O_4 catalysts," Journal of Catalysis, vol. 344, pp. 1–15, 2016.

[87] A. B. Dongil, B. Bachiller-Baeza, E. Castillejos, N. Escalona, A. Guerrero-Ruiz, and I. Rodríguez-Ramos, "Promoter effect of alkalis on CuO/CeO_2/carbon nanotubes systems for the PROx reaction," Catalysis Today, vol. 301, pp. 141–146, Mar. 2018.

[88] X. Niu, Z. Lei and C. Yang, "Catalytic NO reduction by CO over ceria–cobalt oxide catalysts," New Journal of Chemistry, vol. 43, no. 47, pp.18611-18618, 2019.

[89] D. Gu, C.J. Jia, H. Bongard, B. Spliethoff, C. Weidenthaler, W. Schmidt and F. Schüth, "Applied Catalysis B : Environmental Ordered mesoporous Cu – Ce – O catalysts for CO preferential oxidation in H_2-rich gases : Influence of copper content and pretreatment conditions," "Applied Catalysis B: Environmental, vol. 152–153, pp. 11–18, 2014.

[90] D. Li, X. Liu, Q. Zhang, Y. Wang, and H. Wan, "Cobalt and Copper Composite Oxides as Efficient Catalysts for Preferential Oxidation of CO in H_2-Rich Stream," Catalysis letters, vol. 127, pp. 377–385, 2009.

[91] G. De Souza, N. R. Marcilio, and O. W. Perez-lopez, "Dry Reforming of Methane at Moderate Temperatures Over Modified Co-Al Co-precipitated Catalysts," vol. 17, no. 4, pp. 1047–1055, 2014.

[92] B. J. M. Sarruf, J. E. Hong, R. Steinberger-Wilckens, and P. E. V. de Miranda, "$CeO_2Co_3O_4CuO$ anode for direct utilisation of methane or ethanol in solid oxide

fuel cells," International Journal of Hydrogen Energy, vol. 43, no. 12, pp. 6340–6351, 2018.

[93] Y. Du, F. Gao, Y. Zhou, H. Yi, X. Tang, and Z. Qi, "Recent advance of CuO-CeO_2 catalysts for catalytic elimination of CO and NO," Journal of Environmental Chemical Engineering, vol. 9, no. 6, p. 106372, 2021.

[94] B. Ivanov, I. Spassova, M. Milanova, G. Tyuliev, and M. Khristova, "Effect of the addition of rare earths on the activity of alumina supported copper cobaltite in CO oxidation, CH_4 oxidation and NO decomposition," Journal of Rare Earths, vol. 33, no. 4, pp. 382–390, 2015.

[95] W. Wang, W.Z. Yu, P.P. Du, H. Xu, Z. Jin, R. Si, C. Ma, S. Shi, C.J. Jia, and C.H. Yan, "Crystal Plane Effect of Ceria on Supported Copper Oxide Cluster Catalyst for CO Oxidation : Importance of Metal − Support Interaction," . ACS Catalysis, vol. 7, no. 2, pp.1313-1329, 2017.

[96] G. Sedmak and S. Hoˇ, "Kinetics of selective CO oxidation in excess of H_2 over the nanostructured $Cu_{0.1}Ce_{0.9}O_{2-y}$ catalyst," vol. 213, pp. 135–150, 2003.

[97] J. L. Ayastuy, E. Fernández-Puertas, M. P. González-Marcos, and M. A. Gutiérrez-Ortiz, "Transition metal promoters in CuO/CeO_2 catalysts for CO removal from hydrogen streams," International Journal of Hydrogen Energy, vol. 37, no. 9, pp. 7385–7397, 2012.

[98] P. Aunbamrung and A. Wongkaew, "Effect of Cu Loading to Catalytic Selective CO Oxidation of CuO/CeO_2–Co_3O_4," . Advance in Chemical Engineering Science, vol. 3, pp. 15–19, 2013.

[99] C. X. Liu, Q. Liu, X. G. Huang, X. L. Nie, and Z. Huang, "Identification of the active sites for low temperature CO oxidation over nanocrystalline Co_3O_4 catalysts," Journal of Chinese Chemical Society, vol. 61, no. 4, pp. 490–494, 2014.

[100] Z. Li, L. Liu, Z. Wang, P. Gao, and G. K. Li, "Synthesis and Application of Mesoporous Materials: Process Status, Technical Problems, and Development Prospects: A Mini-Review," Energy and Fuels, vol. 37, no. 5, pp. 3413–3427, 2023.

[101] T. M. Nyathi, N. Fischer, A. P. E. York, and M. Claeys, “Environment-Dependent Catalytic Performance and Phase Stability of Co_3O_4 in the Preferential Oxidation of Carbon Monoxide Studied in Situ,” ACS Catalysis, vol. 10, no. 20, pp. 11892–11911, 2020.

[102] M. Meng, Y. Liu, Z. Sun, L. Zhang, and X. Wang, “Synthesis of highly-dispersed CuO–CeO_2 catalyst through a chemisorption-hydrolysis route for CO preferential oxidation in H_2-rich stream,” International Journal of Hydrogen Energy, vol. 37, no. 19, pp. 14133–14142, 2012.

[103] R. Jokar, S. M. Alavi, M. Rezaei, and E. Akbari, “CO preferential oxidation in H_2-rich stream over the CuO-MnOx mixed oxide catalysts prepared by a facile mechanochemical preparation method,” International Journal of Hydrogen Energy, 2022.

[104] T. Cwele, N. Mahadevaiah, S. Singh, and H. B. Friedrich, “Applied Catalysis B : Environmental Effect of Cu additives on the performance of a cobalt substituted ceria ($Ce_{0.90}Co_{0.10}O_{2-\delta}$) catalyst in total and preferential CO oxidation,” "Applied Catalysis B: Environmental, vol. 182, pp. 1–14, 2016.

[105] T. E. Rodrigues Fiuza, D. Santos Gonçalves, and D. Zanchet, “The Impact of Ceria Loading on the CuOx−CeO_2 Interaction and Performance of AuCu/CeO_2−SiO_2 Catalysts in CO-PROX Reaction,” European Journal of Inorganic Chemistry, vol. 2021, no. 40, pp. 4222–4229, 2021.

[106] C. Wang, Q. Cheng, X. Wang, K. Ma, X. Bai, S. Tan, Y. Tian, T. Ding, L. Zheng, J. Zhang and X. Li, “Enhanced catalytic performance for CO preferential oxidation over CuO catalysts supported on highly defective CeO_2 nanocrystals,” Applied Surface Science, vol. 422, pp. 932–943, 2017.

[107] A. Di Benedetto, G. L and i, L. Lisi, and G. Russo, “Role of CO_2 on CO preferential oxidation over CuO/CeO_2 catalyst,” Applied Catalysis B: Environmental, vol. 142–143, pp. 169–177, 2013.

[108] S. Sahebdelfar and M. T. Ravanchi, “Carbon monoxide clean-up of the reformate gas for PEM fuel cell applications: A conceptual review,” International Journal of Hydrogen Energy, vol. 48, no. 64, pp.24709-24729, 2022.

[109] A. F. Zedan and A. S. Aljaber, “Surface & Coatings Technology Cu-Ce-O catalyst revisited for exceptional activity at low temperature CO oxidation reaction,” Surface Coating Technology, vol. 354, pp. 313–323, 2018.

[110] J. Saavedra, T. Whittaker, Z. Chen, C. J. Pursell, R. M. Rioux, and B. D. Chandler, “Controlling activity and selectivity using water in the Au-catalysed preferential oxidation of CO in H_2,” National Chemistry, vol. 8, no. 6, pp. 584–589, 2016.

[111] R. Mhlaba, T. Mosuang, and T. Magadzu, “E ff ect of Hydrazine Pretreatment on the Activity , Stability and Active Sites of Cobalt Species for Preferential Oxidation (PROX) of CO in H_2-Rich Stream,” Chemistry, vol. 1, no. 1, pp.164-179, 2019.

[112] R. Alcala, A. DeLaRiva, E.J. Peterson, A. Benavidez, C.E. Garcia-Vargas, D. Jiang, X.I. Pereira-Hernández, H.H. Brongersma, R. ter Veen, J. Staněk and J.T. Miller, “Atomically Dispersed Dopants for Stabilizing Ceria Surface Area,” Applied Catalysis B: Environmental, vol. 284, 2020.

[113] S. Campisi, M. Schiavoni, C. E. Chan-thaw, and A. Villa, “Untangling the Role of the Capping Agent in Nanocatalysis : Recent Advances and Perspectives,” Catalysts, vol. 6, no. 12, p.185, 2016.

[114] A. Elmhamdi, L. Pascual, K. Nahdi, and A. Martínez-arias, “Applied Catalysis B : Environmental Structure/redox/activity relationships in CeO_2/$CuMn_2O_4$CO-PROX catalysts,” Applied Catalysis B, Environmental, vol. 217, pp. 1–11, 2017.

[115] J. Cao, X. Zhang, X. Ou, T. Liu, T. Xing, Z. Li, X. Zhou, H. Yan, Y. Liu, X. Feng and Y. Tuo, “Reactant adsorption modulation by Fe and K in Pt catalyst for highly effective CO preferential oxidation in practical conditions,” Chemical Engineering Journal, vol. 444, p. 136661, 2022.

[116] C. Xu, S. Li, Y. Zhang, Y. Li, and J. Zhou, “ScienceDirect Synthesis of CuOx-CeO_2 catalyst with high-density interfaces for selective oxidation of CO in H_2-rich stream,” International Journal of Hydrogen Energy, vol. 44, no. 8, pp. 4156–4166, 2018.

[117] I. A. Ivanin, I. N. Krotova, O. V Udalova, K. L. Zanaveskin, and M. I. Shilina,

"Synergistic Catalytic Effect of Cobalt and Cerium in the Preferential Oxidation of Carbon Monoxide on Modified Co/Ce/ZSM-5 Zeolites," vol. 62, no. 6, pp. 798–811, 2021.

[118] Y. Xie, J. Wu, G. Jing, H. Zhang, S. Zeng, and X. Tian, "Applied Catalysis B : Environmental Structural origin of high catalytic activity for preferential CO oxidation over CuO / CeO_2 nanocatalysts with di ff erent shapes," Applied Catalysis B: Environmental, vol. 239, no. July, pp. 665–676, 2018.

[119] C. Hudy, J. Gryboś, K. Steenbakkers, K. Góra-Marek, F. Zasada, and Z. Sojka, "Isotopic evidence for the tangled mechanism of the CO-PROX reaction over mixed and bare cobalt spinel catalysts," Catalysis Science and Technolgy, vol. 12, no. 18, pp. 5723–5741, 2022.

[120] G. Xiang, J. Huo, and Z. Liu, "Understanding and application of metal – support interactions in catalysts for CO-PROX," Physical Chemistry Chemical Physics, vol. 24, no. 31, pp.18454-18468, 2022.

[121] J. Lu, J. Wang, Q. Zou, D. He, L. Zhang, Z. Xu, S. He, and Y. Luo , "Unravelling the Nature of the Active Species as well as the Doping Effect over Cu/Ce-Based Catalyst for Carbon Monoxide Preferential Oxidation," 2019.

[122] O. H. Laguna, M.I. Domínguez, S. Oraá, A. Navajas, G. Arzamendi, L.M. Gandía, M.A. Centeno, M. Montes and J.A. Odriozola, "Influence of the O_2/CO ratio and the presence of H_2O and CO_2 in the feed-stream during the preferential oxidation of CO (PROX) over a CuO_x/CeO_2-coated microchannel reactor," Catalysis Today, vol. 203, pp. 182–187, 2013.

[123] E. Moretti, M. Lenarda, L. Storaro, A. Talon, R. Frattini, and S. Polizzi, "Catalytic purification of hydrogen streams by PROX on Cu supported on an organized mesoporous ceria-modified alumina," vol. 72, pp. 149–156, 2007.

[124] F. Marin, "Supported base metal catalysts for the preferential oxidation of carbon monoxide in the presence of excess hydrogen (PROX)," vol. 58, pp. 175–183, 2005.

[125] E. D. Park, D. Lee, and H. C. Lee, "Recent progress in selective CO removal in a H_2-rich stream," Catal. Today, vol. 139, no. 4, pp. 280–290, 2009.

[126] P. Garbis, C. Kern, and A. Jess, “Kinetics and reactor design aspects of selective methanation of CO over a Ru/γ-Al_2O_3 catalyst in CO_2/H_2 rich gases,” Energies, vol. 12, no. 3, pp. 1–15, 2019.

[127] T. L. Levalley, A. R. Richard, and M. Fan, “ScienceDirect The progress in water gas shift and steam reforming hydrogen production technologies e A review,” Int. J. Hydrogen Energy, vol. 39, no. 30, pp. 16983–17000, 2014.

[128] C. Guimarães, T. De Freitas, M. Iuki, M. Naceur, and J. Mansur, “Effect of nature of ceria support in CuO/CeO_2 catalyst for PROX-CO reaction,” vol. 97, pp. 245–252, 2012.

[129] V. D. Dasireddy, J. Valand, and B. Likozar, “PROX reaction of CO in $H_2/H_2O/CO_2$ Water–Gas Shift (WGS) feedstocks over Cu–Mn/Al_2O_3 and Cu–Ni/Al_2O_3 catalysts for fuel cell applications,” Renewable Energy, vol. 116, pp. 75–87, Feb. 2018.

CHAPTER 5

GENERAL CONCLUSION

This chapter concludes on the general effects of the preparation method (hydrothermal and or reflux), catalysts characterisation and their relation to the overall CO(PrOx) performance in H_2-rich stream. The findings of this research are also used to recommend plausible scientific hypothesis for future work in CO(PrOx) catalyst's design.

6.1. CATALYSTS SYNTHESIS, CHARACTERISATION AND THEIR CO(PrOx) PERFORMANCE

Mesoporous Cobalt oxide support catalysts (Co_3O_4(Hyd) and Co_3O_4(Ref)) based on a spinel crystal structure (Co_3O_4) were successfully prepared under reflux (Ref) and hydrothermal (Hyd) assisted precipitation method in a surfactants/polymer (CTAB/PVP) mixture. The XRD not only, confirmed the Co_3O_4 phase existence but also showed that the as prepared Co_3O_4 support catalysts (Co_3O_4(Ref) and Co_3O_4(Hyd)) were polycrystalline, in agreement with the TEM (SAED) data of the catalysts.

The selection of a specific promoter as well as the appropriate amount of a dopant for Co_3O_4 catalyst, plays a key role in the development of highly active and stable bimetallic oxide catalysts. Introduction of various amounts (in wt.%) of CeO_2 over Co_3O_4 support by co-precipitation under both hydrothermal and reflux led to a CeO_2/Co_3O_4 catalysts, which were not so active in CO(PrOx) reactions. Using 5 wt.% CeO_2 oxide as a standard characterisation for CeO_2 doped Co_3O_4 catalysts, we observed that introduction of cerium oxide (CeO_2) leads to a high Co_3O_4 lattice contraction, due to reduced surface oxygen species, regardless of the synthesis method. Phase transformations of Co_3O_4(Ref) and Co_3O_4(Hyd) to a new symmetry was also observed from the XRD profiles (peak disappearance), after 5 wt.% CeO_2 addition. These increased the reduction temperatures of Co_3O_4(Hyd) catalyst, despite its improved surface area (small crystallite sizes). On the other hand, ceria addition by reflux on Co_3O_4(Ref) catalyst improved the reducibility. Nonetheless, CO(PrOx) activity decreased with increase in CeO_2 content under hydrothermal method, but the reverse was observed under reflux method.

Addition of various amounts of copper species by similar synthesis procedures as in CeO_2/Co_3O_4 preparation, have demonstrated good effects over Co_3O_4(Hyd) and Co_3O_4(Ref) catalyst towards CO(PrOx) reaction. The catalytic activity in CO(PrOx) over Co_3O_4 catalysts increased with CuO_x content but switched to an inactive form of an oxide at the limits of high % loads. It was observed that an appropriate amount of CuO_x to dope Co_3O_4 support catalyst is 5 wt.%, under both reflux and the hydrothermal. These was probed by an outstanding CO conversion of 74% and 94% at low temperature (T = 40 ^oC) over 5 wt.% CuO_x/Co_3O_4(Hyd) and 5 wt.% CuO_x /Co_3O_4(Ref) catalysts, respectively. The high CO(PrOx) activity in the latter, was due to a relatively high surface area, high pore-size distribution and small crystallites of smooth reducibility. Nonetheless, the two catalysts have shown good CO(PrOx) performance at all temperature (40 – 200 ^oC), as compared to their 5 wt.% CeO_2 doped Co_3O_4 counterparts, because CuO_x is more active for CO adsorption and activation than CeO_2. Unlike 5 wt.% CeO_2, the optimum load of 5 wt.% CuO_x did not alter the crystal structure of Co_3O_4(Hyd) and Co_3O_4(Ref) catalysts as much as CeO_2 have. The H_2-TPR analysis concluded that the addition of 5 wt.% CuO_x species significantly improves the reducibility of Co_3O_4(Hyd) and Co_3O_4(Ref) catalysts, regardless of the preparation method. Nonetheless, the 5 wt.% CuO_x /Co_3O_4(Hyd) catalyst deactivated within the first few minutes of operation on stream in dry CO(PrOx) conditions and suffered even prematurely in moisture and CO_2 environment. On the other hand, 5 wt.% CuO_x /Co_3O_4(Ref) catalyst showed a stable CO conversion in the dry and CO_2 saturated CO(PrOx) co-fed gas for more than 23 h of operation on stream. Unfortunately, the 5 wt.% CuO_x/Co_3O_4(Ref) catalyst deactivated in moisture atmosphere, in less than 100 min of operation, to a % CO conversion less than that of a CO_2 condition as time progressed.

The study have also found that the CO(PrOx) perfomance declines substantially after the introduction of various amounts of CeO_2 on bimetallic oxides catalyst and this was method independent. It was revealed that the deactivations were associated with the morphological and textural property changes of the undoped catalysts. After 3 wt.% CeO_2 addition, both 3Ce-5Cu/Co(Hyd) and 3Ce-5Cu/Co(Ref) ternary catalysts showed low surface area and the catalyst texture aquired a rough surface, as was indicated by the BET and data SEM. The pore size and pore volume of pure 5 wt.% CuO_x/Co_3O_4(Ref) also decreased substantially after ceria addtion and showed relatively less tolerance to both CO_2 and H_2O in CO(PrOx) reaction over time on stream. However, the data showed that the addition of 3 wt.% CeO_2 is crucial for 5 wt.% CuO_x/Co_3O_4(Hyd) catalyst's stability in moisture conditions but was less resistant to CO_2 deactivation. The results therefore concludes that CuO_x-Co_3O_4 synergy is responsible for enhanced CO(PrOx) perfomance of the prepared samples and ceria addition compromises these relationship. Nonetheless, all catalysts synthesised via reflux method had enormous surface area and were easily reducible, as compared to their hydrothermal polymorphs. These resulted in highly active catalysts for CO(PrOx) performance, with the 5 wt.% CuO_x/Co_3O_4(Ref) catalyst being the superior candidate amongst all the prepared catalysts in this work. We revealed a cheap, non-hazardous and environmentally friendly method (reflux) of synthesising efficient CO(PrOx) catalysts.

6.2. FUTURE WORK/RECOMMENDATIONS

We have shown that CuO_x species doped at an appropriate amount of 5 wt.% under reflux media, can dramatically enhance CO(PrOx) activity of Co_3O_4 catalyst in H_2-rich stream. However, the catalyst showed low CO(PrOx) stability in moisture saturated feed gas. Addition of CeO_2 nanoparticle by co-precipitation under similar method resulted in a low catalytic activity in CO(PrOx) reaction. Thus, we recommend other synthesis procedures such as impregnation and or mechanical mixing method to be utilized when introducing a third dopant, on an already active bimetallic catalyst (i.e., 5 wt.% CuO_x/Co_3O_4(Ref) catalyst in our case). The selectivity of the catalysts improved over the ternary catalysts in various CO(PrOx) environments. Thus, three-metal oxide-based catalysts are promising candidates for highly stable CO(PrOx) functioning catalysts. Therefore, other rear-earth elements such as Lanthanum and transitional metal oxide catalysts such as manganese, zirconia, vanadium etc., could be investigated in future for their effects on the stability of 5 wt.% CuO_x/Co_3O_4 based catalysts in H_2O and CO_2 CO(PrOx) conditions. The effective oxidation states of CuO_x species that played a remarkable role in low temperature CO oxidation over 5 wt.% CuO_x/Co_3O_4(Ref) catalyst, could also be evaluated by X-Ray photoelectron spectroscopy (XPS) in future. The hypothetical model (mechanism) depicted in appendix D holds a core to CO(PrOx) catalysis over Co_3O_4 based catalysts and their design.

APPENDIXES SECTION

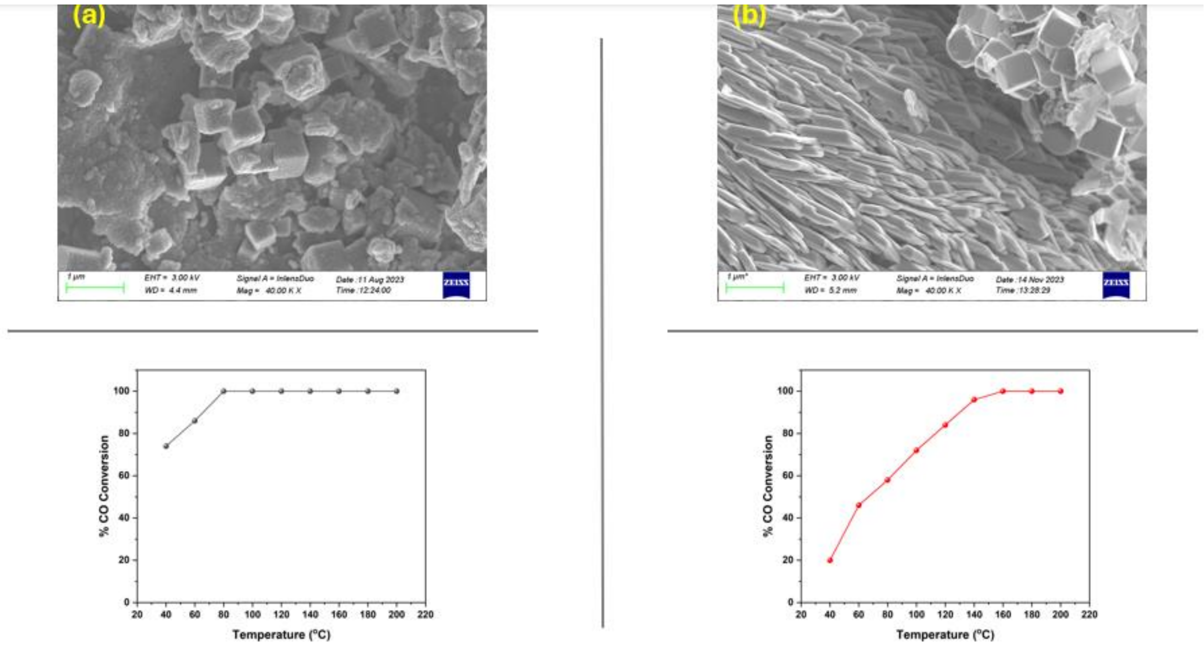

Appendix A The SEM micrograph of 5 wt.% CuO_x /Co_3O_4(Hyd) prepared with (a) CTAB/PVP and (b) without CTAB/PVP, and their CO(PrOx) performance (below).

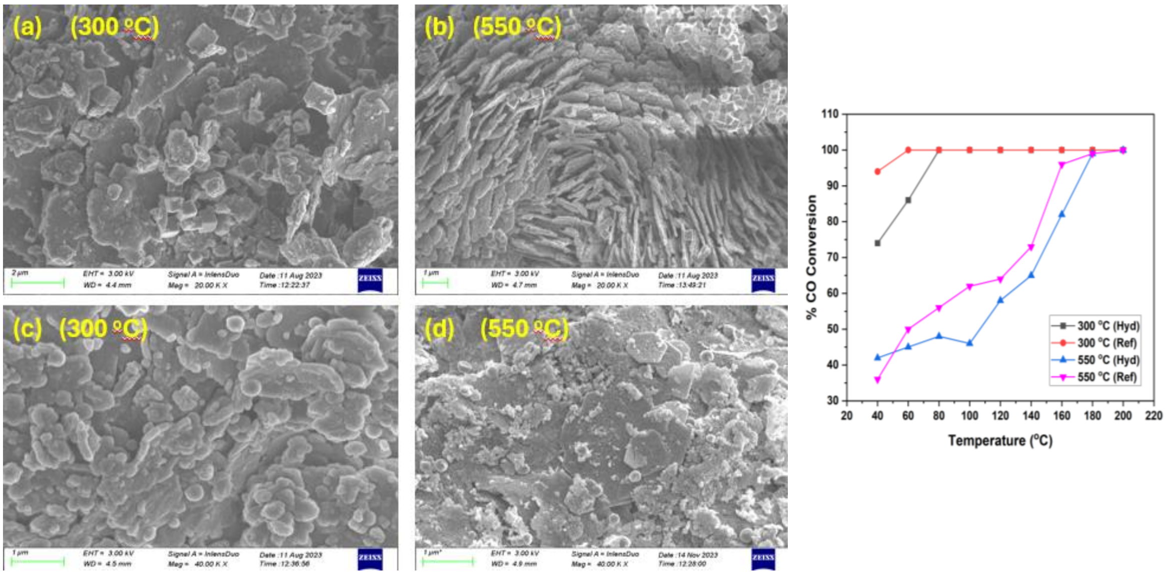

Appendix B Effects of morphology as a function of calcination temperature of 5 wt.% CuO_x/Co_3O_4 catalysts on CO(PrOx) performance, prepared under (a)-(b) hydrothermal and (c)-(d) reflux method.

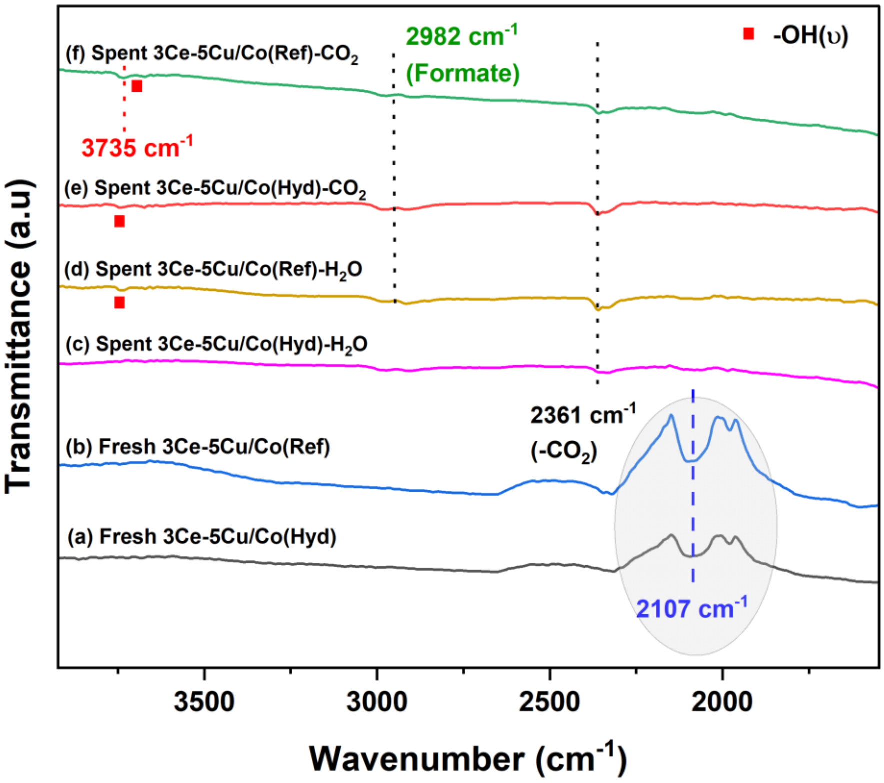

Appendix C FTIR spectra of Fresh (a) 3Ce-5Cu/Co(Hyd) and (c) 3Ce-5Cu/Co(Ref) catalysts, and of spent catalysts in H_2O ((c)-(d)) and CO_2 ((e)-(f)) saturated CO(PrOx) environment over time on stream.

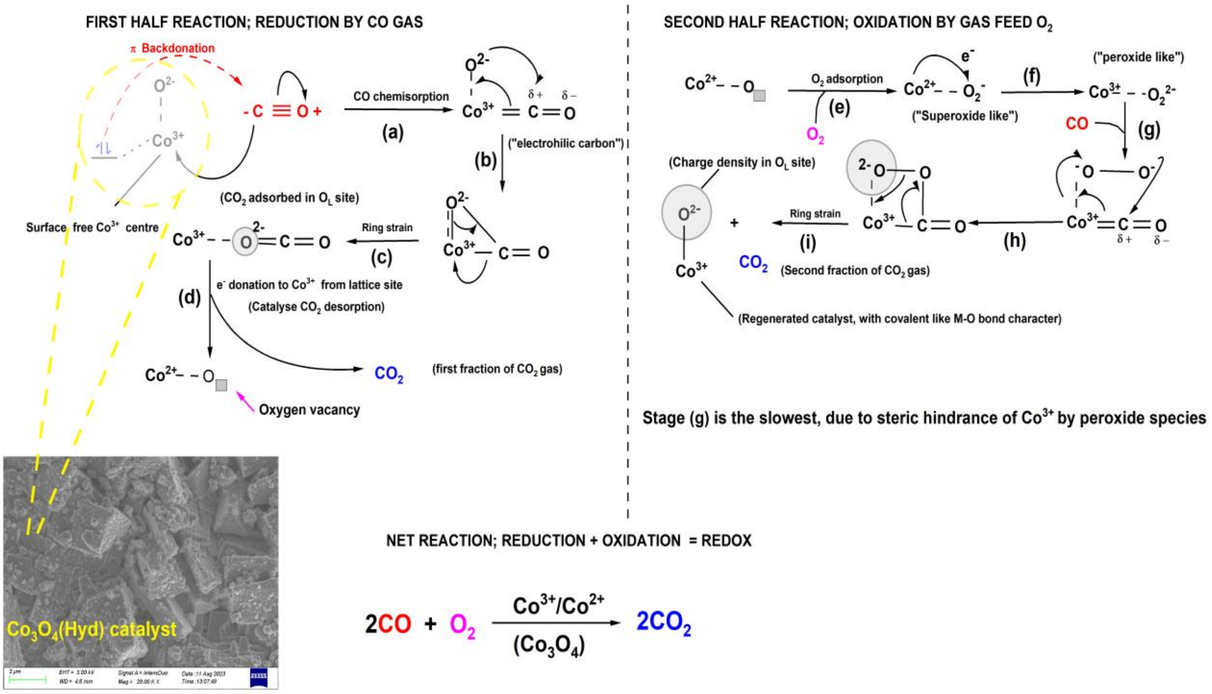

Appendix D A proposed ‘organic type’ of CO(PrOx) reaction mechanism over Co_3O_4(Hyd) catalyst. The doted bonds are ionic in character. Most intermediates and the chemistry are supported by the literature.